Vol. 61 FEBRUARY, 1957 No. 2

THE JOURNAL OF PHYSICAL CHEMISTRY

(Registered in U. S. Patent Office)

CONTENTS

30TH NATIONAL COLLOID SYMPOSIUM, PART II, MADISON, WISCONSIN, June 18–20, 1956

THE JOURNAL OF PHYSICAL CHEMISTRY

(Registered in U. S. Patent Office)

Published monthly by the American Chemical Society at 20th and Northampton Sts., Easton, Pa.

Entered as second-class matter at the Post Office at Easton, Pennsylvania.

The *Journal of Physical Chemistry* is devoted to the publication of selected symposia in the broad field of physical chemistry and to other contributed papers.

Manuscripts originating in the British Isles, Europe and Africa should be sent to F. C. Tompkins, The Faraday Society, 6 Gray's Inn Square, London W. C. 1, England.

Manuscripts originating elsewhere should be sent to W. Albert Noyes, Jr., Department of Chemistry, University of Rochester, Rochester 20, N. Y.

Correspondence regarding accepted copy, proofs and reprints should be directed to Assistant Editor, Allen D. Bliss, Department of Chemistry, Simmons College, 300 The Fenway, Boston 15, Mass.

Business Office: Alden H. Emery, Executive Secretary, American Chemical Society, 1155 Sixteenth St., N. W., Washington 6, D. C.

Advertising Office: Reinhold Publishing Corporation, 430 Park Avenue, New York 22, N. Y.

Articles must be submitted in duplicate, typed and double spaced. They should have at the beginning a brief Abstract, in no case exceeding 300 words. Original drawings should accompany the manuscript. Lettering at the sides of graphs (black on white or blue) may be pencilled in and will be typeset. Figures and tables should be held to a minimum consistent with adequate presentation of information. Photographs will not be printed on glossy paper except by special arrangement. All footnotes and references to the literature should be numbered consecutively and placed in the manuscript at the proper places. Initials of authors referred to in citations should be given. Nomenclature should conform to that used in *Chemical Abstracts*, mathematical characters marked for italic, Greek letters carefully made or annotated, and subscripts and superscripts clearly shown. Articles should be written as briefly as possible consistent with clarity and should avoid historical background unnecessary for specialists.

Notes describe fragmentary or less complete studies but do not otherwise differ fundamentally from Articles. They are subjected to the same editorial appraisal as are Articles. In their preparation particular attention should be paid to brevity and conciseness.

Communications to the Editor are designed to afford prompt preliminary publication of observations or discoveries whose value to science is so great that immediate publication is imperative. The appearance of related work from other laboratories is in itself not considered sufficient justification for the publication of a Communication, which must in addition meet special requirements of timeliness and significance. Their total length may in no case exceed 500 words or their equivalent. They differ from Articles and Notes in that their subject matter may be republished.

Symposium papers should be sent in all cases to Secretaries of Divisions sponsoring the symposium, who will be responsible for their transmittal to the Editor. The Secretary of the Division by agreement with the Editor will specify a time after which symposium papers cannot be accepted. The Editor reserves the right to refuse to publish symposium articles, for valid scientific reasons. Each symposium paper may not exceed four printed pages (about sixteen double spaced typewritten pages) in length except by prior arrangement with the Editor.

Remittances and orders for subscriptions and for single copies, notices of changes of address and new professional connections, and claims for missing numbers should be sent to the American Chemical Society, 1155 Sixteenth St., N. W., Washington 6, D. C. Changes of address for the *Journal of Physical Chemistry* must be received on or before the 30th of the preceding month.

Claims for missing numbers will not be allowed (1) if received more than sixty days from date of issue (because of delivery hazards, no claims can be honored from subscribers in Central Europe, Asia, or Pacific Islands other than Hawaii), (2) if loss was due to failure of notice of change of address to be received before the date specified in the preceding paragraph, or (3) if the reason for the claim is "missing from files."

Subscription Rates (1957): members of American Chemical Society, $8.00 for 1 year; to non-members, $16.00 for 1 year. Postage free to countries in the Pan American Union; Canada, $0.40; all other countries, $1.20. $12.50 per volume, foreign postage $1.20, Canadian postage $0.40; special rates for A.C.S. members supplied on request. Single copies, current volume, $1.35; foreign postage, $0.15; Canadian postage $0.05. Back issue rates (starting with Vol. 56): $15.00 per volume, foreign postage $1.20, Canadian, $0.40; $1.50 per issue, foreign postage $0.15, Canadian postage $0.05.

The American Chemical Society and the Editors of the *Journal of Physical Chemistry* assume no responsibility for the statements and opinions advanced by contributors to THIS JOURNAL.

The American Chemical Society also publishes *Journal of the American Chemical Society, Chemical Abstracts, Industrial and Engineering Chemistry, Chemical and Engineering News, Analytical Chemistry, Journal of Agricultural and Food Chemistry* and *Journal of Organic Chemistry*. Rates on request.

THE JOURNAL OF
PHYSICAL CHEMISTRY

VOLUME 61 FEBRUARY 21, 1957 NUMBER 2

γ-IRRADIATION OF POLYMETHYL METHACRYLATE AND POLYSTYRENE

BY L. A. WALL AND D. W. BROWN

National Bureau of Standards, Washington 25, D. C.

Received July 19, 1956

The number of scissions produced in polymethyl methacrylate for a given dose of γ-irradiation is decreased measurably by the presence of air, small amounts of benzene, and by lowering the temperature to −196°. Irradiation in air produced labile structures in the polymer, probably peroxides, which decompose and cause further scissions. The decomposition of these structures is accelerated by traces of *t*-butylcatechol, hydroquinone and dimethylaniline. The cross-linking reaction in polystyrene caused by γ-irradiation is also decreased when temperatures are lowered to −196°. Studies of partially-deuterated styrenes show little correlation between cross-link formation and site of deuteration. This observation, plus the fact that cross-links exceed the number of hydrogen molecules produced, suggests that the phenyl ring is involved in cross-linking. Comparison of the results with deuterated polystyrene and deuterated polyethylene indicates a difference between the two materials in the mechanisms of irradiation-induced processes.

Introduction

In recent years the effects of high-energy radiation on polymers have been investigated by a number of workers.[1] Due to the nature of these materials scissions and cross-links are most easily determined, and polymers have been catalogued as to whether they undergo one or the other of the two processes.[2,3] In reality both processes always occur simultaneously, at least to some extent, and studies have been made to determine the relative amounts of both processes.[4,5] Other processes are also occurring, such as the formation of certain types of double bonds in polyethylene along with the removal of vinylidene groups.[6]

In the present work polymethyl methacrylate and polystyrene were chosen for study because one undergoes scission while the other undergoes cross-linking, and in each case the alternative process is nearly absent. A comparison of the changes in the two processes produced by varying the conditions may give helpful information as to similarities and dissimilarities in the mechanisms involved and perhaps offer a clue as to the determining factors. Certain deuterated polystyrenes were available and were studied in order to determine to what extent different positions contributed to the cross-linking process and gas evolution.

(1) F. A. Pecjak and K. H. Sun give a comprehensive bibliography in Nuclear Engineering and Science Congress, Dec. 12–16, 1955 (Cleveland, Ohio).

(2) A. A. Miller, E. J. Lawton and J. S. Balwit, *J. Polymer Sci.*, **14**, 503 (1954).

(3) E. J. Lawton, H. M. Bueche and J. S. Balwit, *Nature*, **172**, 76 (1953).

(4) A. R. Schultz, Nuclear Engineering and Science Congress, Dec. 12–16, 1955 (Cleveland, Ohio).

(5) A. Charlesby, *Proc. Roy. Soc.* (*London*), **222**, 60 (1954).

(6) M. Dole and C. D. Keeling, *J. Am. Chem. Soc.*, **76**, 6082 (1953).

Experimental

The polymethyl methacrylate used for irradiation was prepared in 12% conversion from distilled, twice-degassed methyl methacrylate, polymerized at 60°, using 0.0082 mole per liter of benzoyl peroxide as catalyst. It was precipitated with methanol and dissolved in benzene three times. The third benzene solution contained about 5 weight % of polymer; it was frozen, and the benzene was sublimed off *in vacuo*. The residue was heated for 10 days at 60° in a vacuum oven. Its intrinsic viscosity in benzene at 29.3° was 1.66. This material is called polymethyl methacrylate sample FB-1.

A more disperse material was prepared by making a 0.5% solution of sample FB-1, freezing it and recovering the polymer as described above. This is called sample FB-2.

Films 0.2 mm. thick were prepared by dissolving the polymer in benzene and letting the solvent evaporate from a sheet of unplasticized cellophane.

Some experiments which are reported in Table III were performed with a biaxially stretched polymethyl methacrylate and with the original unstretched material, which was unplasticized.

For the data in Figs. 1 to 4, inclusive, and Table II each irradiation was performed in a tube that contained about 0.2 g. of one of the above materials. Before exposure, each specimen was heat-treated *in vacuo*, as outlined in the figures. After cooling, the samples that were to be irradiated *in vacuo* were sealed off; the others were removed and stoppered.

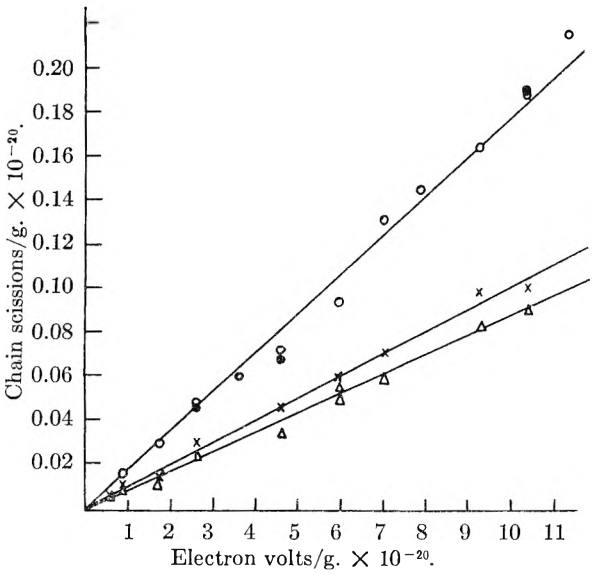

Fig. 1.—Scissions produced in polymethyl methacrylate sample FB-1 by γ-rays. Preheated at 100° for 20 hours: ○, irradiated *in vacuo*, viscosity determined in benzene; △, irradiated in air, viscosity determined in benzene; ●, irradiated *in vacuo*, viscosity determined in benzene containing 0.1% *t*-butylcatechol; X, irradiated in air, viscosity determined in benzene containing 0.1% *t*-butylcatechol.

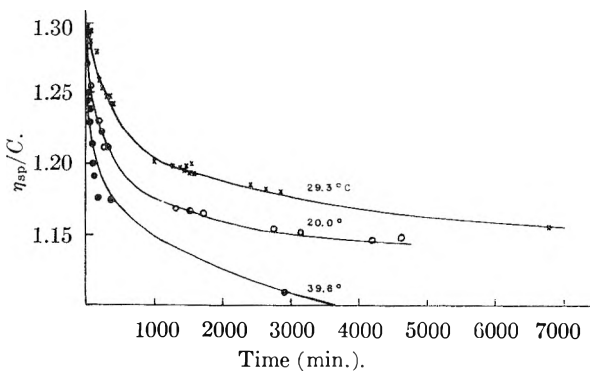

Fig. 2.—Change of viscosity with time. Polymethyl methacrylate sample FB-1 irradiated in air, in benzene solution containing 0.02% *t*-butylcatechol (4.796 g. of polymer per liter). Preheated at 100° for 20 hours.

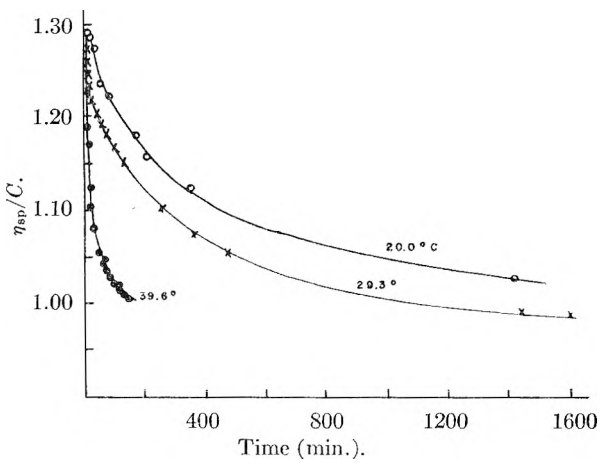

Fig. 3.—Change of viscosity with time. Polymethyl methacrylate sample FB-1, irradiated in air, in chloroform solution containing 0.02% *t*-butylcatechol (4.796 g. of polymer per liter). Preheated at 100° for 20 hours.

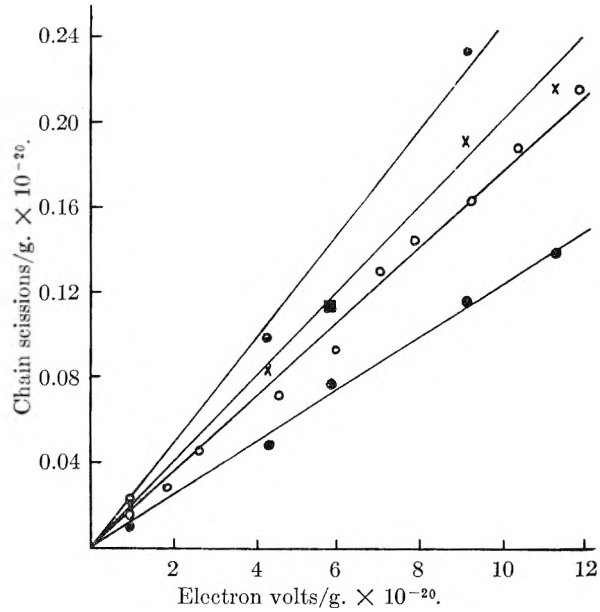

Fig. 4.—Scissions produced in various samples of solid polymethyl methacrylate by γ-rays; all samples irradiated *in vacuo*. ◒, sample FB-2, preheated 20 hours at 120° *in vacuo;* X, sample FB-1, preheated 20 hours at 120° *in vacuo;* ■, sample FB-2, preheated 20 hours at 100° *in vacuo;* ○, sample FB-1, preheated 20 hours at 100° *in vacuo;* ●, film, preheated 20 hours at 100° *in vacuo*.

The irradiations of polymethyl methacrylate at room temperature were performed at the Naval Research Laboratory, Washington, D. C. The NRL Source has been described.[7] The tubes were exposed in the inner cell in a holder that kept them in an annular arrangement within the cell. The polymer samples were each distributed through a cylindrical volume 0.8 cm. diameter by 1.5 ± 0.2 cm. high. The dose rates calculated were those at the center of each tube at the average height of the centers of the polymer samples. Individual polymer samples received doses different from those calculated because of variations in the height of the sample and variations in the dose rate around each annular ring. It is estimated, however, that such variations amounted to only about 5%. For all polymers studied with the exception of polyethylene-d_4, where a correction based on electron density was applied, it was assumed that one gram absorbed 58×10^{18} e.v. when given 1 megaroentgen.

The irradiations at liquid nitrogen temperature were performed with a 200-curie cobalt-60 source at the National Bureau of Standards. In order to get high dose rates a Dewar flask was made that could be positioned close to the source, and the film was irradiated in sealed glass ampules surrounded by liquid nitrogen at the bottom of the Dewar. Blanks were run at room temperature in the Dewar because the double thickness of glass and silver materially reduced the field.

After irradiation, the intrinsic viscosities of the polymers in benzene solution at 29.3° were determined. *t*-Butylcatechol was added (1 g. per liter) to solutions of the specimens irradiated in air, and after at least 20 hours the intrinsic viscosities were redetermined.

The intrinsic viscosity was converted to molecular weight by the relation[8]

$$M_n = 2 \times 10^5 [\eta]^{1.46}$$

This relation is for whole polymer, presumably one with a broad distribution in molecular weight. The quantity $(1/M_n - 1/M_\infty)$ gives the moles of breaks per gram, and it is converted into scissions per gram by multiplying with Avogadro's number.

The drop in viscosity with time after addition of *t*-butylcatechol was studied. Catechol was added to a solution of

(7) H. Rabin and W. E. Price, *Nucleonics* **13**, 33 (1955).

(8) J. Baxendale, S. Bywater and M. G. Evans, *J. Polymer Sci.*, **1**, 237 (1946).

the polymer that had been irradiated in air. The viscosity of the solution was then measured at various times with an Ubbelohde viscometer.

t-Butylcatechol was shown to decompose benzoyl peroxide in solution by determining the peroxide remaining in a standard solution by the iodine method of Siggia,[9] 24 hours after the addition of the catechol. The technique was modified to include a vacuum distillation of the liberated iodine because strong titratable color develops when *t*-butylcatechol and a solution of benzoyl peroxide are mixed. The distillation significantly reduces the observed titer of the standard solution, but the effect is small compared with that of the *t*-butylcatechol.

The deuterated styrene monomers were prepared by the reactions outlined below

α,β,β-Trideuterostyrene

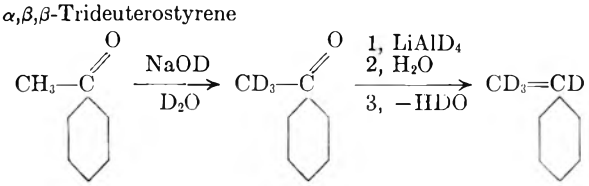

β,β-Dideuterostyrene

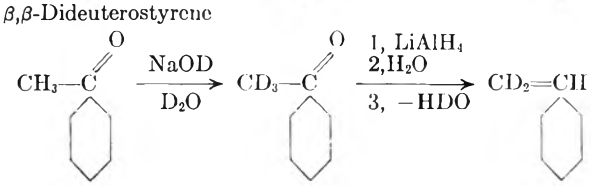

α-Deuterostyrene

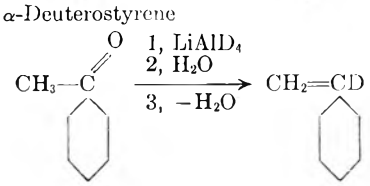

β-Deuterostyrene

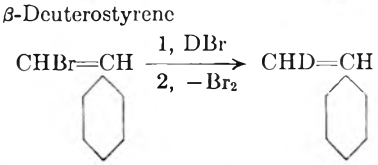

p-Deuterostyrene

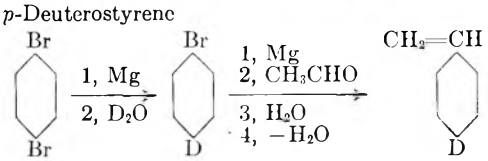

The numbers beside the compounds listed, above and below the arrows, indicate the sequence of reactions and reagents added. Their analyses by mass spectrometry are given in Table I.

TABLE I

MASS SPECTROMETRIC ANALYSIS OF DEUTERATED STYRENES

	IN %				
Components	*α,β,β*	*β,β*	*α*	*β*	*p*
Styrene	0.5	0.6	2	5.0	1.2
Styrene-d_1	0.4	3.4	98	94.0	98.5
Styrene-d_2	5.4	95.8	..	<1	0.2
Styrene-d_3	93.7	tr	..	<1	..

The polymers were prepared by thermal polymerization at 70° of carefully-degassed monomer samples. After preparation the polymer was freed from monomer, and films were prepared by the methods described above for polymethyl methacrylate.

The irradiation for all the polystyrene experiments was obtained from the NBS source. This is a single piece of cobalt that was calibrated by irradiating films of polymethyl methacrylate *in vacuo* at room temperature and then determining the dose from the film line in Fig. 4. A curve representing dose rate *versus* distance from the source was constructed for use with polystyrene.

Tubes containing disks of the polystyrene separated by wafers of polyethylene were heated for 20 hours *in vacuo* at 100°, cooled and sealed off. They were placed above the NBS source and irradiated for known times. The dose was determined from the calibration described above.

After irradiation the polystyrene films were dissolved, and single-point viscosity determinations were made at the same concentration for all films of the same polymer. Plots of relative viscosity *versus* dose were made; the one for non-deuterated 70° polystyrene is shown in Fig. 6. The dose at the gel point was assumed to be that value midway between the highest dose which gave a reproducible finite viscosity and the lowest dose which gave a material which would not flow through the viscometer. The reported tolerances indicate the magnitude of this spread when converted into electron volts absorbed per cross-link (see Table III).

The intrinsic viscosities of non-irradiated samples were converted into viscosity-average molecular weights by the relation[10]

$$[\eta] = 0.97 \times 10^{-4} M_v^{0.74}$$

The ratio of weight-average to viscosity-average molecular weight was calculated to be 1.07 from the relation of Flory.[11] The number of moles of cross-links per gram at the gel point is the reciprocal of twice the initial weight-average molecular weight.[12]

The hydrogen yield was obtained by irradiating a single film, preheated as above, of each of the polystyrenes with the NBS source and analyzing the resulting gases by the mass spectrometer. These gases were hydrogen and benzene, the latter being from the solvent left in the film since no deuterated benzene was found when *p*-deuterated polystyrene was irradiated. The yields of hydrogen and deuterium were calculated from the analysis and from the pressure and volume of the inlet system of the mass spectrometer.

Results

Polymethyl Methacrylate

Production of Scission.—In Fig. 1 are plotted the number of scissions produced for a given amount of energy absorbed. When the irradiations are carried out with the sample sealed in a highly evacuated tube the upper line is obtained. The lowest line was obtained when unevacuated tubes were used. In this case fewer scissions occurred, presumably because oxygen interfered with the process which produces scission.

Earlier work[13] had shown a small lowering of intrinsic viscosity when irradiated polymers were dissolved in solvents containing *t*-butylcatechol. The purpose of measuring intrinsic viscosity of polymers dissolved in such solutions was to see if immobilized free radicals could be detected. Provided that a high percentage of radicals combine on solution, the presence of a monofunctional inhibitor, or one that effectively terminates all radicals by a disproportionation process, would produce a lower viscosity than that observed in the absence of the inhibitor. Of course, if the radicals ordinarily terminate by disproportionation, no effect due to the inhibitor would be observed. For detection in this manner, a concentration of recombining radicals greater than 10^{-4} mole per liter would be necessary.

(9) S. Siggia, "Quantitative Organic Analysis Via Functional Groups," John Wiley and Sons, Inc., New York, N. Y., 1949, p. 100.

(10) Q. H. Ewart and H. C. Tingey, unpublished work referred to in "Styrene" Monograph, Reinhold Publ. Corp., New York, N. Y., 1952, p. 334.

(11) P. J. Flory, "Principles of Polymer Chemistry," Cornell University Press, Ithaca, N. Y., 1953, p. 373.

(12) Ref. 11, p. 359.

(13) L. A. Wall and M. Magat, *J. chim. phys.*, **50**, 308 (1953).

When the polymer was irradiated *in vacuo*, *t*-butylcatechol had no effect on the intrinsic viscosity and hence on the number of scissions (see solid circles in Fig. 1). However, when the polymer was irradiated in air the catechol produced a definite increase in the number of scissions (see intermediate line in Fig. 1). This result evidently is due to some peroxide structure formed during irradiation, that is decomposed by the catechol and simultaneously produced scission. Addition of catechol after the polymer was in solution produced the same ultimate decrease in viscosity over a period of time. In the absence of the catechol several weeks time is required before a slight decrease in the viscosity of a solution is observed.

Further study of the decrease in viscosity produced by *t*-butylcatechol showed that there is an increase in the rate of producing scissions with an increase in concentration of catechol. With benzene as solvent a puzzling change with temperature was observed. This is shown in Fig. 2, where it is seen that the viscosity drops at 20.0 and 39.6° are both faster than the one at 29.3°. Changing the solvent to chloroform gave a more normal result with changes in temperature as can be seen in Fig. 3. The difference of behavior with the solvents suggests that the mechanism involve a sensitive intermediate complex or possibly other solvent effects. No simple treatment could be applied to the data.

It is quite likely that peroxide structures at the ends of chains are present and produce no observable scissions on decomposition. The magnitude of the effect is too small for direct analysis of peroxide, and hence no attempt in this direction was made.

Volatile Products.—An investigation of the volatile products obtained from γ-irradiated polymethyl methacrylate has been reported elsewhere.[14] No monomer was produced during irradiation at room temperature and the observed products were similar to those reported by earlier workers.[15] Heating to 125° for three hours after irradiation, however, produced considerably more monomer than that obtained from the unirradiated material. This indicates the presence of long-lived free radicals which is in agreement with studies of polymerization induced by γ-irradiated polymethyl methacrylate[14] and of the paramagnetic resonance of γ-irradiated polymers.[16] Hence the foaming[17] effects observed in polymethyl methacrylate may be due in part at least to the formation of monomer by the depropagation of radicals.

Effect of Solvent.—The number of scissions observed for a given dose was found to vary with the method of treating or preparing the polymer. Since benzene was the only solvent used and should be the only appreciable impurity in our polymer, the possibility of "protection"[18] by this compound was explored. In Fig. 4, the results for several materials tested are presented so as to show the effect of the aromatic solvent (see also Table II). It is estimated by weighing experiments that the film contained 5% benzene by weight while the FB-2 sample contained less than one per cent. The intermediate points were in the range of 2–3% benzene. Thus it is seen that about 5% benzene decreases the scission rate by 50%.

The numbers of scissions per 100 electron volts of absorbed energy for various samples of polymethyl methacrylate are listed in Table II. It is seen that irradiation in air leads to a decrease in scissions for all samples for which data are available. Percentagewise the more benzene-free samples are slightly less protected by air. Also in Table II data on the biaxially-stretched polymer are compared with those on unstretched material. No significant changes in the number of scissions were observed with the stretched materials as compared with the unstretched. Also these materials, which should be free of aromatic impurities, gave results close to the other samples which were almost free of solvent.

TABLE II

G-VALUES[a] FOR SCISSIONS PRODUCED IN VARIOUS SAMPLES OF POLYMETHYL METHACRYLATE BY γ-RAYS

Sample	Treatment before irradiation	After irradiation *In vacuo*	After irradiation In air
Film	100° for 20 hr. *in vacuo*	1.23	0.645
FB-1	100° for 20 hr. *in vacuo*	1.70	0.894
FB-2	100° for 20 hr. *in vacuo*	1.99	1.37
FB-1	120° for 20 hr. *in vacuo*	2.00	1.25
FB-2	120° for 20 hr. *in vacuo*	2.48	1.52
Commercial Plexiglas, biaxially-stretched 150%	None	2.28	
	100° for 20 hr. *in vacuo*	2.31	
	120° for 20 hr. *in vacuo*	2.23	
Commercial Plexiglas, unstretched	None	2.23	
	100° for 20 hr. *in vacuo*	2.16	
	120° for 20 hr. *in vacuo*	2.16	

[a] *G*-value is number of scissions per 100 electron volts of absorbed energy.

Effect of Temperature.—Investigation of the degradation at liquid nitrogen temperature, −196°, revealed a considerable decrease in the number of scissions (see Fig. 5) as compared to those obtained at room temperature. For the film material irradiated *in vacuo*, *G* (scissions) was found to be 0.50 at −196°, compared with 1.23 at 25°. In Fig. 5 the results for film under different conditions are plotted for both temperatures. For the low temperature work it was not convenient to give samples high doses. At −196° irradiation in air appears to increase the number of scissions slightly rather than produce a large decrease. Addition in this case of *t*-butylcatechol did not produce more scissions. Exposure to air at −196° after irradiation and then allowing the sample to come to room temperature showed no effect.

Polystyrene

Formation of Cross-links.—The cross-linking of polystyrene and the various deuterated polystyrenes required quite long periods of irradiation. Fortunately the molecular weights were fairly large, otherwise the periods would have been inconven-

(14) L. A. Wall and D. W. Brown, *J. Res. Natl. Bureau of Standards*, **57**, 131 (1956).

(15) P. Alexander, A. Charlesby and M. Ross, *Proc. Roy. Soc. (London)*, **223A**, 392 (1954).

(16) E. E. Schneider, *Disc. Faraday Soc.*, **19**, 158 (1955).

(17) A. Charlesby and M. Ross, *Nature*, **171**, 1153 (1953).

(18) S. Gordon and M. Burton, *Disc. Faraday Soc.*, **12**, 88 (1952).

iently long. A typical curve is shown in Fig. 6 where the increase in the relative viscosity of ordinary polystyrene is plotted against energy absorbed. It is seen that just prior to gelation the viscosity rises sharply. The dashed vertical lines represent the erratic results obtained with samples that were definitely gelled and only incompletely soluble. The gel point is thus rather well-defined. In this manner the gel points of several ordinary polystyrenes and the five deuterated polymers were obtained.

In Table III the energy absorbed during the formation of a cross-link is listed for these polymers. It was observed that old samples of polystyrene gave higher values than freshly prepared material. The two polymers at the bottom of the table were several years old. The other ordinary polystyrene was prepared at the same time as the deutero polymers. It is reasonable to expect that slightly-oxidized polystyrenes will show less tendency to cross-link. Samples irradiated in air in a finely-divided state have always shown degradation. Other investigators[19] also have observed this behavior in the presence of air.

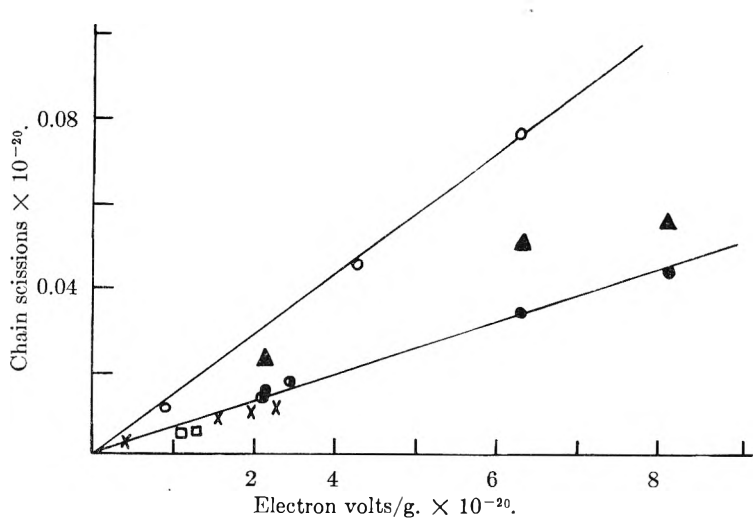

Fig. 5.—Scissions produced in various polymethyl methacrylate films by γ-rays. Preheated at 100° for 20 hours. ○, irradiated *in vacuo* at room temperature; ●, irradiated in air at room temperature; ▲, irradiated in air at room temperature, with *t*-butylcatechol added to solution; X, irradiated *in vacuo* at −196°; □, irradiated *in vacuo* at −196°, exposed to air before warming to room temperature; ◑, irradiated in air at −196°.

TABLE III

ENERGY DISSIPATED IN γ-IRRADIATED STYRENE AND DEUTEROSTYRENE POLYMERS DURING THE FORMATION OF CROSS-LINKS AND THE PRODUCTION OF HYDROGEN

Polymer	Initial mol. wt. (vis. av.)	E_c[a] (e.v.)	$E_{b(H_2+HD+D_2)}$[b] (e.v.)
α,β,β-d_3-Styrene	973,000	2370 ± 150	7650
β,β-d_2-Styrene	793,000	2970 ± 500	5450
α-d_1-Styrene	1,118,000	2550 ± 150	5240
β-d_1-Styrene	1,148,000	2150 ± 100	3830
p-d_1-Styrene	1,032,000	3300 ± 550	4730
d_0-Styrene	1,176,000	1860 ± 20	4490
d_0-Styrene	1,252,000	2050 ± 200	3910
d_0-Styrene	326,000	2200 ± 250	..

[a] Energy dissipated per cross-link formed. [b] Energy dissipated per molecule formed.

The effect of the deuteration on the cross-linking is not as large or as specific as might have been expected. If the cross-linking process involves the abstraction of a hydrogen in a specific position which had been deuterated, one would anticipate at least 1.4 times the energy required for a cross-link in ordinary styrene.[20] Hence one or more of the deuterated substances would have shown high values, and the others would show values close to that for the ordinary polymer.

In general the results in Table III show, as far as cross-linking is concerned, a lower probability for the deuterated species. However, no particular position or site would appear to be pre-eminently involved.

In Fig. 6 there are also shown some data obtained at −196° on the cross-linking reaction in polystyrene. Although the irradiations were not carried to the gel point at this temperature it is seen that the process is reduced to about 0.65 of the rate of cross-link production at room temperature. This is the same magnitude as the reduction in the scissioning process in polymethyl methacrylate, which was about 0.4 of that at room temperature.

Hydrogen Formation.—In polyethylene it is clear[6,21] that the number of hydrogen molecules formed is several times the number of cross-links. The formation of double bonds accounts for the excess hydrogen.

In Table III we see that for polystyrene the energy dissipated during hydrogen formation is much larger than that for cross-links. Apparently considerably more cross-links are formed than hydrogen molecules. This is the opposite of the behavior of polyethylene.

With hydrogen formation the effect of the deuteration is qualitatively more consistent. With the exception of the β-deuterated species, increasing deuteration leads to greater energy requirements, *i.e.*, lower yields. Deuteration in the α-position is also more effective than when in the *para* or β-position.

The composition of the evolved hydrogen is compared with that of the polymer in Table IV. The hydrogen, as measured, was always an equilibrium mixture of H_2, HD and D_2. The atom per cent. of deuterium is therefore listed in the table with that for the polymer. The third column is the uncorrected atom per cent. in polymer. The fourth column is the latter corrected for the lack of perfect deuteration in the monomer unit and for the contamination of the benzene solvent used for film preparation. The results indicate a variation in preference for hydrogen production over deuterium. The fifth column in Table IV is a meas-

(19) P. Y. Feng and J. W. Kennedy, *J. Am. Chem. Soc.*, **77**, 847 (1955).

(20) K. B. Wiberg, *Chem. Revs.*, **55**, 713 (1955).

(21) M. Dole, C. D. Keeling and D. G. Rose, *J. Am. Chem. Soc.*, **76**, 4304 (1954).

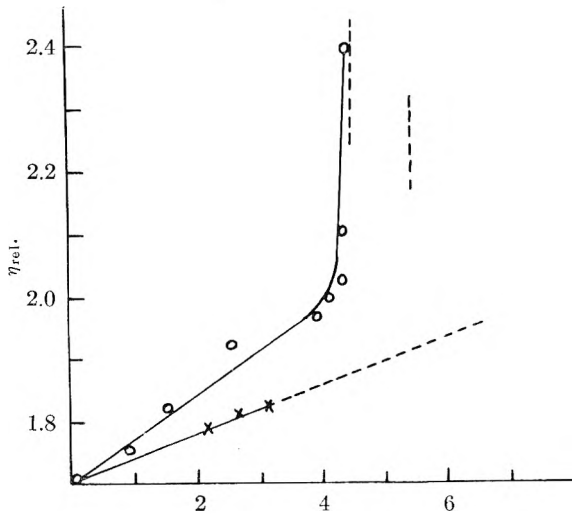

Fig. 6.—Relative viscosity of γ-irradiated polystyrene solution *versus* energy absorbed by polymer. O, irradiated *in vacuo* at room temperature, vertical dashed lines refer to samples incompletely soluble; X, irradiated *in vacuo* at −196°.

ure of the discrepancy between atom per cent. of D in gas *versus* that in polymer. It is seen that a more statistical result occurs as more deuterium is substituted for the less strongly-bonded hydrogens, *i.e.*, the α and β, in polystyrene.

TABLE IV

COMPARISON OF DEUTERIUM IN GASEOUS PRODUCTS WITH DEUTERIUM IN POLYMER

Polymer	Gas, atom %	Polymer, atom %	Polymer (cor.), atom %	Comparison[a]
α,β,β-d_3	34.4	37.5	35.0	0.02
β,β-d_2	19.3	25.0	23.8	.19
α-d_1	9.2	12.5	11.9	.23
β-d_1	9.0	12.5	11.9	.24
p-d_1	3.9	12.5	11.9	.67

[a] (Polymer (cor.) − gas)/polymer (cor.).

In Table V are listed the *G*-values, *i.e.*, number per 100 e.v., for the production of hydrogen and deuterium atoms. The second column shows that the total H plus D yield decreases with increased deuterium content, again with the exception of the β-d_1 polymer. For 1.5 m.v. electrons the *G*(H) for benzene-d_0 was 72 × 10^{-3}, and the *G*(D) for benzene-d_6 was 23.4 × 10^{-3}.[18] Recently, an almost identical value has been reported for the yield of hydrogen from γ-irradiated benzene,[22] as that from the electron irradiated. All these values compared favorably with those in Table V, and indicate that polystyrene is at least as stable, if not more so, than liquid benzene.

TABLE V

G-VALUES[a] FOR HYDROGEN AND DEUTERIUM ATOMS PRODUCED BY γ-IRRADIATION OF DEUTEROPOLYSTYRENES

Styrene polymer	*G*(H + D)	*G*(H)	*G*(D)
α,β,β-d_3	26.2	17.2	9.0
β,β-d_2	33.6	27.1	6.5
α-d_1	38.1	34.6	3.5
β-d_1	52.2	47.0	5.2
p-d_1	42.2	40.6	1.6
d_0	44.6	44.6	..

[a] Number of atoms per 100 e.v., values in table multiplied by 10^3.

The *G*-values for hydrogen atoms, *G*(H), *i.e.*, $2G(H_2) + G(HD)$, and that for deuterium atoms, *G*(D), are listed in the third and fourth columns. With the exception of the poly-β-deuterostyrene, all the *G*(H) values appear to be comprised of additive terms, depending on the position in the basic monomer unit. Thus we may write

		Obsd.	Calcd.
$G(H)_0$	$= 4g_r + g_p + 2g_\beta + g_\alpha =$	0.0446	0.0444*
$G(H)_p$	$= 4g_r + 2g_\beta + g_\alpha =$	.0404	.0405
$G(H)_\beta$	$= 4g_r + g_p + fg_\beta + g_\alpha =$	.0470	.0470
$G(H)_\alpha$	$= 4g_r + g_p + 2g_\beta =$	.0346	.0345
$G(H)_{\beta\beta}$	$= 4g_r + g_p + g_\alpha =$	.0271	.0270
$G(H)_{\alpha\beta\beta}$	$= 4g_r + g_p =$	.0172	.0171

where the *g*'s refer to disruptions of particular C—H bonds. For example, the $4g_r$ refers to the disruption factor of the four ring-hydrogens, other than that of the *para*-hydrogen, which is represented by g_p. For the four ring-hydrogens other than the *para* hydrogen the disruption factor, g_r, has an average value slightly smaller than g_p. Using the last five equations above, the specific disruption values for the particular C—H bond can be calculated. They are listed in Table VI, together with the factor, *f*, which is required to account for the high yield of hydrogen from the poly-β-deuterostyrene. When a deuterium is attached to the same carbon as a hydrogen it appears that the C—H is broken 2.3 times as readily as a C—H bond in the structure, $-\overset{H}{\underset{H}{C}}-$, and the C—D appears to be broken 1.6 times as readily as a C—D bond in the structure $-\overset{D}{\underset{D}{C}}-$. Otherwise the data are comprised of additive terms dependent only on the position of the particular bond. The starred calculated value above is the only independent check. It is seen that it is in very good agreement with the observed quantity.

The *g*′-factors, where prime signifies that a C—D bond is involved, are also given in Table VI. These values are obtained very simply from the *G*(D) values for the deuterated polymers. For instance, $g_p' = G(D)_p$, and $g_\alpha' = G(D)_\alpha$, while $g_\beta' = G(D)_{\beta\beta}/2$. The g_r' is estimated by an extrapolation of the trends in the other values in Table VI. For an independent check the *G*(D) value for the α,β,β-trideuterostyrene polymer was computed from the expression

$$G(D)_{\alpha\beta\beta} = 2g_\beta' + g_\alpha' = 10.0$$

The observed value of 9.0 is only in fair agreement as compared with the agreement obtained above for the hydrogen bonds. The value in parentheses in Table VI for the isotope effect in the ring positions is, of course, speculative since g_r' is based on the trends in the table and therefore less certain. There is more spread between the various *g*-factors for the C—H bond than between those for C—D bonds.

(22) R. H. Schuler, THIS JOURNAL, **60**, 381 (1956).

TABLE VI

G-VALUES FOR SPECIFIC C—H AND C—D BONDS

Position	*G*-value g, C—H	g', C—D	Isotope effect[a]
α	9.9[b]	3.5	2.8
β	8.7	3.25	2.7
p	3.9	1.65	2.4
r	3.3	(1.5)	(2.2)
f	2.3	1.6	

[a] Ratio g(C—H)/g'(C—D). [b] *G*-values are multiplied by 10^3.

Discussion

Temperature Effect.—In general one visualizes a mechanism for the processes caused by high energy radiation[23] to be comprised of initial ionization which is quickly neutralized leaving relatively long-lived free radicals and atoms. These radicals recombine, disproportionate or react further with the surrounding material, depending on their relative rates of diffusion.[22] High local temperatures, presumably, cause the reactions to be unspecific and the small temperature effect observed. In this framework mutual termination of radicals and atoms may preponderate facilitated by the "cage effect." The correlation[24] of scission with low heats of polymerization, and cross-linking with high heats of polymerization, suggests that in the polymers which undergo scission disproportionation is more favored than in the polymers which cross-link. In the scissioning-type polymers diffusing radicals can cause further cleavages of chains and in each case regenerate a free radical. Hence, by going to subpyrolytic temperatures *G*-values for scission should become quite large. Depropagation into monomer would at very high temperatures overshadow random scission. On the other hand, cross-linking cannot become a chain process unless unsaturation exists in the polymer. Hence study at higher temperature would show for many of the cross-linking polymers lower *G*-values for cross-linking, or at least more concomitant scissions.

Oxygen Effect.—The effect of oxygen on scission reported here and on crosslinking[13,19,25] would fit the framework outlined above. Oxygen, it is readily seen, could decrease scissions by reacting with the small radicals and thereby prevent them from attacking polymer chains. It is also evident that peroxide structures are formed on the polymer chains which interfere with scission. Such structures will increase susceptibility to thermal degradation. In like manner, oxygen can prevent cross-linking. Only such polymers are more prone to oxidative scission. Hence these materials usually show decreases in molecular weight after irradiation in the presence of adequate oxygen.

Deuterostyrene Polymers.—Of the hydrogen evolved from ordinary styrene 22.3% appears to be derived from the α-position, 39.2% from the β-positions, and 38.5% from the ring. In other words, no simple mechanism can be pictured operating totally through a specific position in the monomer unit. However, the one α-hydrogen is equivalent to three atoms in the phenyl group. The isotope effect, 2.2–2.8, may indicate an average maximum local temperature of about 400°.[20] The lack of correlation between deuterium content and cross-linking suggests that this process involves the phenyl group and not the hydrogen atoms. This is fortified by the fact that the number of cross-links exceeds the number of hydrogen molecules produced. The cross-linking process does not apparently produce free hydrogen molecules, which is not surprising in view of the fact that more polymer is found in the radiolysis of benzene than gaseous products.[18]

The hydrogenation of the phenyl ring may account for the low hydrogen production, which is lower than the equivalent of cross-linking indicating the ring as a contributory, or even the predominant site, for cross-linking formation if we rule out hydrogenation of the ring by H_2 molecules. This is not, however, completely feasible due to the possibility of high local temperatures and the presence of radicals and atoms. However, in such an aromatic polymer cross-linking processes such as are quite possible as well as other variations.

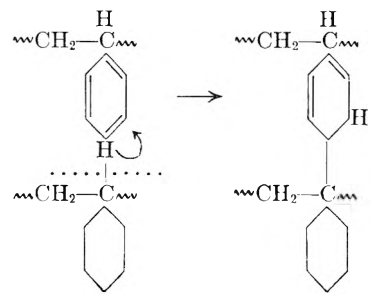

In this respect the observation of Dole[6] on the disappearance of the vinylidene group in polyethylene is suggestive of simultaneous hydrogenation and dehydrogenation processes in irradiation polymers. It is quite likely that in these systems the atoms react very rapidly, either to combine, add to unsaturation, or abstract, depending on the structure of the material being irradiated. Hence radical scavengers are not likely to have extremely large effects.

Polyethylene-d_4.—Some preliminary experiments have been carried out with polyethylene-d_4 and polyethylene-d_0. The results are tabulated in Table VII. The G(H) values obtained on several commercial polyethylenes ran from 6 to 8 depending on the sample. Therefore, the polyethylene compared in Table VII with deuterated polymer was made at the same time and under the same conditions as the polyethylene-d_4. At first sight the data appear to indicate a higher value for the deuterated polymer than for the hydrogenated substance. However, it was observed that the number of H atoms in the gas from the deuterated polymer was much higher than that which was likely to be in polymer. As in the earlier results with poly-β-deuterostyrene it appears that hydrogen in –CHD– structures is evolved during radiolysis with a greater probability than hydrogen from polyethylene-d_0. Assuming the polyethylene-d_4 contained 2.16 atom % of H, the initial *G*-values were corrected. For polyethylene-d_4 G(D) is estimated to be about 3.7. It may be slightly less if deu-

(23) A. H. Samuel and J. L. Magee, *J. Chem. Phys.*, **21**, 1080 (1953).

(24) L. A. Wall, *J. Polymer Sci.*, **17**, 141 (1955).

(25) A. Chapiro, *J. chim. phys.*, **52**, 247 (1955).

terium in –CHD– structures has an increased probability for rupture compared with $-CD_2-$ structure. The value of 3.7 for polyethylene-d_4, compared with a $G(H)$ of 3.8 for polyethylene-d_0, denotes an almost negligible isotope effect, a $G(H)/G(D)$ of 1.03. On the other hand, the hydrogen in the deuterated polymer, which is almost entirely contained in –CHD– type structures, appears to be evolved 8.3 times as easily as the hydrogen from the polyethylene-d_0. This is considerably larger than the 2.6 factor observed in connection with the poly-β-deuterostyrene. At the present time not too much can be said about this latter effect except that analogous but small effects have been obtained in the mass spectrometric dissociation patterns of partially deuterated paraffins.[26]

TABLE VII

γ-IRRADIATION OF POLYETHYLENE-d_0 AND POLYETHYLENE-d

Polyethylene-d_0 $G(H)$	Polyethylene-d_4 $G(H + D)$	Atom % H in gas[a]	Prior dose, e.v. $\times 10^{-20}$/g.
3.78	4.3	14.6	0
3.08			53.65
	3.1	12.1	57.25
	2.4	11.3	76.80

[a] Polyethylene-d_4 was prepared from monomer containing 2.16 atom % of H.

The fact that we find a relatively large ratio of $G(H)/G(D)$ for polystyrene and a negligible ratio for polyethylene, suggests a considerable difference in the mechanism of hydrogen formation in the two cases. Somewhat similar data are available for small molecules. The $G(H)/G(D)$ for benzene and benzene-d_6 is 0.070/0.0234 or 3,[18] while the ratio of the radiochemical yield of radicals from methanol-d_0 to that for methanol-d_4, $G(R)$ methanol-$d_0/G(R)$ methanol-d_4, is 24.0/23.0 or 1.04.[27] The latter measurement is based on the consumption of the radical "scavenger" diphenylpicrylhydrazyl.

The small molecule behavior, it is seen, has several similarities to that of the polymers. A high isotope effect is associated with the aromatic structure and the low G-values; and the low isotope effect is associated with the aliphatic structure and relatively large G-values. Comparison of the mass spectra of CH_4 and CD_4[26] and certain deuterated and undeuterated aromatic compounds[28] show little or no effects on the fragmentation patterns or on total ionization as a result of deuteration. There are effects in partially-deuterated methanes[26] due to the –CHD– type structure.

During γ-irradiation, it is evident that the mechanism in polystyrene differs fundamentally from that in polyethylene. If a negligible isotope effect is assumed in the initial production of hydrogen atoms, then the number of hydrogen molecules from polyethylene, whether formed by combination or abstraction processes, should not be more than 10–20% greater than the number of deuterium molecules from polyethylene-d_4. In polystyrene the isotope effect, −2.5–3, implies that the observed hydrogen molecules are formed by abstraction processes, in competition with atom addition to unsaturation. That is, assumption of no isotope effect in the production of primary atoms, requires for the appearance of the observed isotope effect, that some mode for the consumption of hydrogen atoms exists, which does not produce hydrogen molecules.

Alternative mechanisms for hydrogen production would be ionic reactions similar to those recently reported.[29] An example which could explain cross-linking is shown here

$$CH_3^+ + CH_4 \longrightarrow C_2H_5^+ + H_2$$

However, no scheme involving ionic processes alone can be devised readily to explain the results discussed above.

Another important point arises from the drop in the hydrogen yield from polyethylene with increasing dose, observed here and previously.[30] It has often been assumed that the cross-linking in this material is a linear function of dose. This non-linear hydrogen yield suggests that the cross-linking is really not linear with dose. If double bond formation were truly linear as some studies[6,21] appear to indicate, then stoichiometry would require non-linearity in cross-link production.

Acknowledgments.—The authors wish to express their appreciation to Dr. J. I. Schulman, Mr. William Price, J. Willis and Lee Johnson of the Naval Research Laboratory, and to Mr. T. Loftus of the Radiological Equipment Section of the National Bureau of Standards for assistance in performing the irradiations.

DISCUSSION

L. M. DORFMAN. (a) Dr. Wall has stated "In polyethylene it is clear that the number of hydrogen molecules formed is several times the number of cross links." This is in fact a matter of contention. The evolved hydrogen exceeds the number of cross links, but there is not general agreement as to whether this is a small excess (see A. A. Miller, *et al.*, THIS JOURNAL, 60, 599 (1956)) or a several-fold excess as Dr. Wall has stated.

(b) I believe that Dr. Wall and I have somewhat different results on the apparent isotope effect in the deuterated polyethylene. We find an over-all isotope effect of $k_H/k_D = 2.2$ for mixtures of normal and deuterated paraffins. I hasten to add, however, that this is not quite the same experiment, as we are irradiating mixtures. But in the radiolysis of the deuterated paraffin alone we do not find the disproportionately large effect reported by Dr. Wall. I would point out that if his deuteropolyethylene were 93% D (rather than the assumed 98% D), this would give an isotope effect in very close agreement with my observed value.

L. A. WALL.—(a) In regard to the ratio of hydrogen molecules to cross links produced in polyethylene, Miller's results indicate a value for DYNH polyethylene of ~1.7. Data of other earlier workers suggest considerably larger values. In view of the wide range of hydrogen yields found in our work with various polyethylenes it is unlikely that such ratios will not be subject to considerable variation.

(26) V. H. Dibeler and F. L. Mohler, *J. Research Natl. Bur. Standards*, **45**, 441 (1950).

(27) A. Prevost-Bernas, A. Chapiro, C. Cousin, Y. Landler and M. Magat, *Disc. Faraday Soc.*, **12**, 98 (1952).

(28) F. L. Mohler V. H. Dibeler, L. Williamson and H. Dean, *J. Research Natl. Bur. Standards*, **48**, 188 (1952).

(29) D. O. Schissler and D. P. Stevenson, *J. Chem. Phys.*, **24**, 926 (1956).

(30) E. J. Lawton, P. D. Zemany and J. S. Balwit, *J. Am. Chem. Soc.*, **76**, 3437 (1954).

MELTING BEHAVIOR OF IRRADIATED POLYETHYLENE

BY MALCOLM DOLE AND W. H. HOWARD

The Chemical Laboratory of Northwestern University, Evanston, Illinois

Received July 19, 1956

The specific heat of a sample of polyethylene exposed to 50 megarep of γ-radiation as well as one exposed to approximately 336 megarep of pile radiations has been measured from −20 to 140°. In the case of the 50 megarep sample a slight depression of the maximum melting temperature of about 1.5° was observed, although no flow of the polyethylene occurred above this temperature. In all other respects the specific heat of this sample was identical with that of unirradiated polyethylene. In the case of the pile irradiated sample, the crystallinity decreased 5.7%. No depression of the maximum melting point could be observed, probably because of a change in the character of the melting. The *G*-value for hydrogen evolution was estimated to be 3.75.

I. Introduction

It has been stated[1] that irradiation of polyethylene increases the melting point, that irradiated polyethylene[2] "no longer melts," even at temperatures of 300°, but "loses its crystalline character at 110°" that[3] the "transition temperature corresponding to melting in ordinary polyethylene is only very slightly decreased with increasing cross-linking, so that the temperature at which all crystalline structure vanishes is little affected," and that[4] irradiated polyethylene melted at about the same temperature as unirradiated polyethylene, "but instead of flowing, the material retains its form stability even at temperatures considerably above the melting point."

In order to clarify the question regarding the effect of high energy radiations on the melting point of polyethylene it was decided to study the specific heat and the heat of fusion of irradiated polyethylene. Previously, Charlesby[3] studied the melting of irradiated polyethylene by taking cooling curves from 220°. However, accurate determinations of the melting point and of the range of melting are not possible from cooling curve measurements because of super-cooling of the melt and because the rapid change of temperature prevents equilibrium from being established during the cooling. With precise colorimetric equipment much more accurate information can be obtained. Fortunately, the equipment[5] was at hand for making such studies as many specific heat measurements of synthetic high polymers had previously been carried out[6,7] in this Laboratory.

II. Theory of Melting

Part of the confusion regarding the exact melting point and melting range of polyethylene arises from the concept of melting as a process whereby a solid is converted to a liquid that will flow. Thermodynamically, the melting point is defined as the temperature at which the solid and liquid are in equilibrium with each other. For a partially crystalline, partially amorphous material such as polyethylene in which there are crystallites of varying sizes melting at various temperatures, the definition of the melting point has to be restricted to the temperature at which the last bit of crystallites to melt are in equilibrium with the melt. The maximum melting point is the temperature at which the last detectable crystallinity disappears. Because different methods have different sensitivities for crystallite detection, the different methods may yield different results.

We prefer to define the maximum melting point as the temperature of intersection of the enthalpy–temperature curve for the liquid polyethylene with the enthalpy–temperature curve as actually measured for the crystalline–amorphous solid. The latter enthalpy includes the heat required to melt the fraction of crystalline material that has melted at the temperature in question. Figure 2 illustrates such a curve.

The factors that influence the melting range and maximum melting point are the following: (a) the reduction in the melt of the activity of the crystallizing segments by increase of mole fraction of non-crystallizable units such as co-polymer units or units containing branch points, cross-links and double bonds, or irradiation degradation products, etc.; (b) change in nature of crystallizing units, such as higher molecular weight cross-linked units being the crystallizing substance instead of the CH_2 segments of the unirradiated polyethylene; (c) change in crystallite–melt interfacial area per gram of material by disruption of large crystallites into smaller ones[8]; (d) failure to attain equilibrium between "pockets" of impurities produced by the irradiation and the main bulk of amorphous material; (e) possibility of simultaneous presence of two kinds of crystallizing segments, either as discrete crystallites or in solid solution. Items (a) and (c) would cause a lowering of the melting point, while as a result of (b) the melting point would be increased. At low irradiation doses items (b), (d) and (e) probably would not produce detectable effects in the melting behavior. Item (c) might shift the melting curve in a direction to increase the proportion that melted at lower temperatures.

III. Experimental Details

The details of the apparatus for measuring the specific heat have been described elsewhere[5] and will not be repeated here. Each heating interval was about 10° at the lower temperature but only

(1) E. Collinson and A. J. Swallow, *Quart. Rev.*, **9**, 311 (1955).

(2) A. Charlesby, *Proc. Roy. Soc.* (*London*), **215A**, 187 (1952).

(3) A. Charlesby, *ibid.*, **217A**, 122 (1953).

(4) E. J. Lawton, J. S. Balwit and A. M. Bueche, *Ind. Eng. Chem.*, **46**, 1704 (1954).

(5) A. E. Worthington, P. C. Marx and M. Dole, *Rev. Sci. Instr.*, **26**, 298 (1955).

(6) M. Dole, W. P. Hettinger, Jr., N. R. Larson and J. A. Wethington, Jr., *J. Chem. Phys.*, **20**, 781 (1952).

(7) S. Alford and M. Dole, *J. Am. Chem. Soc.*, **77**, 4774 (1955) (polyvinyl chloride). This paper contains references to earlier work.

(8) M. Dole, *J. Polymer Sci.*, **19**, 347 (1956); see also P. J. Flory, *Trans. Faraday Soc.*, **51**, 848 (1955).

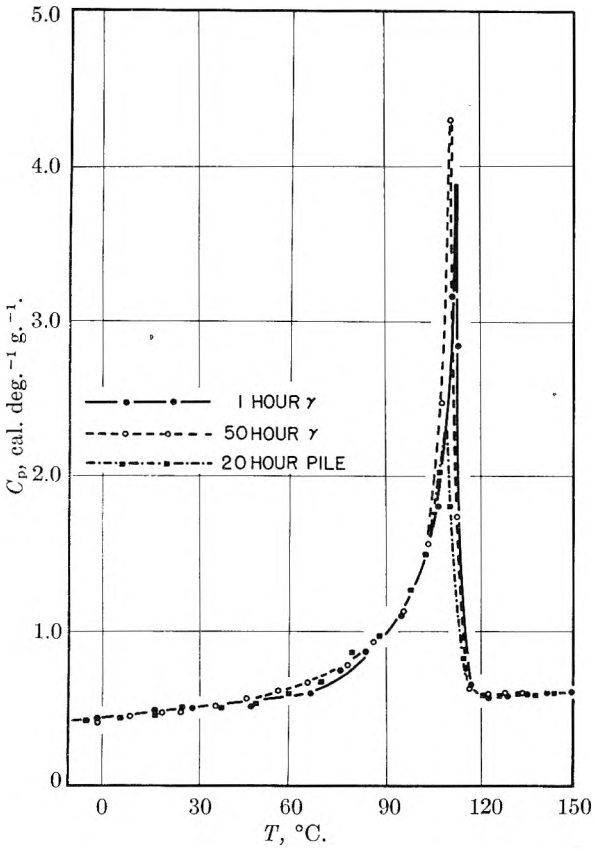

Fig. 1.—Specific heat of irradiated polyethylene in cal. g.$^{-1}$ deg.$^{-1}$.

about 2 to 5° in the significant melting range. As one hour approximately was required to regain a steady-state temperature drift of the calorimetric system and to determine this drift accurately, the rate of heating was slow enough to ensure nearly equilibrium conditions in the polyethylene. The highly irradiated pile sample required less time to come to thermal equilibrium after a heating interval than did the unirradiated sample.

The polyethylene samples studied were granular "alkathene," a polyethylene[9] produced commercially by I.C.I. Its maximum melting point was 113.8 ± 0.4°, see Fig. 2.

Three irradiations were carried out at the Argonne National Laboratory, two of them in the pure γ-radiation facility and one in CP-5, the heavy water pile. The first sample was exposed to 1×10^6 roentgens of γ-radiation, the second to 50×10^6 roentgens, while the third was in the pile for 20 hours at a thermal neutron flux of 1×10^{13} thermal neutrons/sq. cm./sec. The first two irradiations using γ-rays were performed with the polyethylene sealed in evacuated Pyrex tubes, while the third was carried out with the polyethylene in aluminum tubes, capped up, but open to the atmosphere. Oxidation occurred in this irradiation sufficient to produce a net weight increase of 0.82%.

In discussing quantitatively the irradiation dose it is convenient to take some significant unit. As our unit dose we have decided to take 10^6 rep or one megarep (one rep is defined as 93.1 ergs/g. energy absorbed in the ferrous sulfate dosimeter). One megarep liberated 0.722×10^{-5} g. of hydrogen per g. of polyethylene as determined from the experiment performed in which the polyethylene was exposed to 50 megarep. As Charlesby[2] quoted 7.7×10^{-4} g. of hydrogen per g. of sample for his unit dose in the Harwell B.E.P.O., his unit dose was 107 megareps. The irradiation dose of our third sample cannot be estimated accurately because of failure to collect the hydrogen evolved. A crude guess from a comparison of the slow neutron flux in the present Argonne CP-5 pile with that of the old heavy water pile yielded the value 340 megarep.[10]

From the value of 0.722×10^{-5} g. of hydrogen evolved per megarep the G-value was calculated to be 3.75 molecules of H_2 evolved per 100 e.v. assuming that the energy absorbed in polyethylene per g. was the same as in the ferrous sulfate dosimeter used to determine the γ-radiation intensity. This G-value is probably within the limits of uncertainty equal to 3.5 which Tolbert and Lemmon[11] report as to the limit to which the G-value of the saturated straight chain hydrocarbons approach as the molecular weight increases.

IV. Results and Discussion

The specific heat of the sample of polyethylene irradiated with 1 megarep of γ-radiation could not be distinguished in any way from that of the unirradiated material. It was used, therefore, as a standard to represent the unirradiated material.

The 50 megarep irradiated sample had a dosage sufficient to make the polyethylene almost completely insoluble. After taking this irradiated sample through the long heating cycle, up to 135°, over a heating period of 48 hours, from a visual standpoint it appeared not to have melted. Each granule had maintained its individuality and moved freely over the others when the material was shaken. Yet its specific heat–temperature curve, Fig. 1, showed definitely that it had melted to exactly the same extent as the unirradiated sample.

It was the cross-linking which had produced the insolubility which also prevented the material from flowing after melting. The molten irradiated polyethylene was a gel maintaining its physical form despite being practically completely liquid.

The crystallinity of the irradiated sample was calculated by the equation

$$\text{fraction of crystallinity} = f = \frac{H_L - H}{\Delta H_f} \qquad (1)$$

where H_L is the enthalpy of the liquid polyethylene, H the enthalpy of the sample and ΔH_f the heat of the fusion of the 100% crystalline material, all at the same temperature and per gram of polyethylene. For the 50 megarep irradiated sample no change in the crystallinity at room temperature could be detected. However, the hydrogen liberated, 3.61×10^{-4} g./g. sample, was only 0.25%

(9) Kindly supplied by Dr. R. B. Richards.

(10) The statement made in our previous publication, M. Dole, C. D. Keeling and D. G. Rose, *J. Am. Chem. Soc.*, **76**, 4304 (1954), that Charlesby's unit dose was equivalent to 974 hours of "goat hole" irradiation was probably incorrect. A better estimate based on a hydrogen evolution comparison yielded the value of 450 hours of goat hole irradiation.

(11) B. M. Tolbert and R. M. Lemmon, Univ. of Calif. Radiation Laboratory Report No. UCRL-2704 (unclassified), August, 1954.

of the whole. If the crystallinity had decreased by only 0.25%, this change could not have been detected.

The only detectable change in the thermal properties of the 50 megarep irradiated polyethylene was a decrease in the maximum melting point of about 1.5 ± 0.5°. From the enthalpy curves of Fig. 2, in which the enthalpy of the melting region is plotted, one can see that the maximum melting point has definitely decreased. The point of intersection of the curve of the liquid region with that of the solid is at a temperature 1.5 ± 0.5° lower for the irradiated sample than for the non-irradiated.

From the Flory[12] equation it is possible to calcu-

$$\frac{1}{T_m} - \frac{1}{T_0} = -\frac{R}{\Delta H_f} \ln X_A \qquad (2)$$

late the mole fraction of the crystallizing units, X_A, necessary to produce a decrease of the maximum temperature of melting of 1.5°. In equation 2 T_0 is the maximum melting temperature of the pure polymer, T_m is the maximum melting temperature of the polymer whose mole fraction of crystallizing units is X_A, R is the gas constant and ΔH_f is the heat of fusion per mole of crystallizing segments. Taking[6] ΔH_f to be 921 cal./mole of CH_2 units, T_0 to be 387 and T_m, 385.5°K., X_A turns out to be 0.995 or the change in composition of the amorphous region due to the presence of irradiation products is 0.5 ± 0.2%. In the 50 megarep irradiated sample, the hydrogen evolution was 2.53×10^{-3} mole of H_2 per mole of CH_2 units. This number must be multiplied by two as each molecule of hydrogen evolved involves removing a hydrogen atom from two CH_2 units. The expected change in X_A from hydrogen evolution is, therefore, $2 \times 2.53 \times 10^{-3}$ or 0.5%. Thus, the observed lowering of the maximum melting point is the correct order of magnitude expected from Flory's equation 2.

Turning now to the pile irradiated sample, the situation is less clear-cut because of the slight oxidation of the sample, and because the amount of hydrogen evolved could not be measured. However, from the estimates of the latter given above, it was calculated that the expected change in X_A was 2×0.017 or 3.4%. Such a decrease of X_A would have produced a maximum melting point depression of 10.8°. By inspection of Fig. 2 it will be seen that no such lowering of the melting point occurred, although if only the lowest points on the enthalpy curve are extrapolated to an extension of the enthalpy curve for the liquid, a freezing point lowering of 10.8° seems reasonable. The enthalpy curve for the pile irradiated sample suggests that there has been a redistribution of crystallite size and possibly molecular weight in a direction to produce a small amount of material melting at a somewhat higher temperature and to reduce the amount melting at the lower temperatures.

(12) P. J. Flory, *J. Chem. Phys.*, **17**, 223 (1949); *Trans. Faraday Soc.*, **51**, 848 (1955).

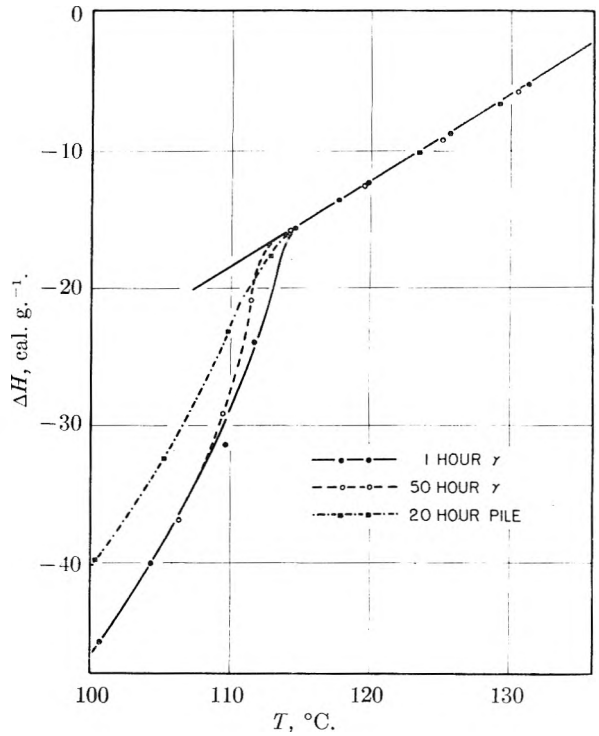

Fig. 2.—Enthalpy of irradiated polyethylene relative to the enthalpy at 140°.

The fraction of crystallinity of the pile irradiated sample was 49.9% as calculated by eq. 1, 5.7% less than the crystallinity of the unirradiated sample. This change is somewhat more than 3.4% estimated above for the decrease of X_A but, because of the uncertainty in the radiation dose, exact quantitative comparisons are meaningless.

Acknowledgments.—Grateful appreciation is expressed to the Office of Ordnance Research, U. S. Army, for support of this project, to Bernhard Wunderlich for assisting in the calculations and measurements, and to the members of the Technical Service Staff of the Argonne National Laboratory for their coöperation.

UREA DENATURATION OF IRRADIATED OVALBUMIN

BY ROBERT H. MAYBURY[1]

University of Redlands, Redlands, California

Received July 19, 1956

Irradiated ovalbumin, subjected to a light dosage of γ-radiation, is denatured by urea, the kinetics of the denaturation being obtained from the polarimetrically measured optical rotations. A comparison between the rate of denaturation of the irradiated protein and the rate of denaturation of unirradiated material reveals the former to be significantly larger. An explanation of the observations is given in terms of the radiation rupture of bonds in hydrogen-bonded groups.

Through coagulation studies Fricke has been able to demonstrate in X-rayed ovalbumin the presence of three fractions exhibiting a thermal lability greater than the native protein.[2] The fractions were characterized by marked lowering of both energy and entropy of activation of denaturation. The suggestion was made that certain structural injuries in the protein molecule arising from the irradiation give rise to the enhanced lability toward heat.

A comparison between the rate of urea denaturation of native and of irradiated ovalbumin provides information on the nature of the structural injuries sustained by the irradiated protein. The kinetics of urea denaturation of this particular protein have been studied in detail by Simpson and Kauzmann.[3] The denaturation proceeds by way of an unfolding of the polypeptide chain during which the solution becomes more negatively rotating. According to these authors the slower rate of denaturation found with ovalbumin compared to many other proteins is a consequence of the unique initial step in the denaturation. This initial step is pictured as the prying loose of the urea of an entire loop of the peptide chain, a process involving the rupture of about eight intramolecular hydrogen bonds. Recent work in which the same rate process has been studied with ovalbumin in D_2O provides additional evidence for such an initial step.[4] If the structural changes induced in the protein as a result of irradiation happen to involve any of the functional groups participating in the hydrogen bonding of this peptide loop, there is likely to be a significant alteration of the rate of denaturation when urea is added.

Experimental

Irradiations were carried out using radioactive cobalt (Co^{60}) as the source of γ-rays.[5] An aerated 10% aqueous solution of ovalbumin (no buffer) was irradiated in the capped 10-ml. Pyrex cells described by Hart.[5] The irradiation chamber was refrigerated at about 4°. Irradiation for about 120 minutes at a dose rate of 2×10^{17} e.v./g./min. produced 8×10^{17} ion pairs/g. (30 e.v. per ion pair) for a total of 11×10^{17} protein molecules/g. solution (ovalbumin mol. wt. = 45,000) or about 1 ion pair per protein molecule.

The denaturation was followed polarimetrically in a fashion identical to that described by Simpson and Kauzmann.[3] 2 cm. tubes jacketted at $30 \pm 0.5°$ were used with the Rudolph High Precision Model 80 Polarimeter and Monochromator (5893Å.). Protein concentrations were determined by dry weights or spectrophotometrically, $E^{1\%}_{1\text{ cm.}} = 7.5$.[6] Five times crystallized ovalbumin obtainable from Pentex Corporation, Illinois, was used without further purification. Reagent grade urea and buffer salts were used.

In each experiment a run was made with the native protein and one with the irradiated material. Only in this way is a valid comparison made possible since the protein seems to vary from lot to lot. The denaturation was carried out in 8 molar urea in 0.035 molar phosphate buffer of *p*H 7.7. Protein concentration was about 2%.

Results and Discussion

The marked increase in the rate of denaturation found with the irradiated ovalbumin over the rate found for the native protein is clearly indicated by the respective curves in Fig. 1. As was found to be the case by Simpson and Kauzmann, the kinetics are complex, departing somewhat from first order. The best course to take is to recognize that the denaturation proceeds in two stages, an initial fast stage followed by a slow stage which goes on for many days. α final, characterizing the termination of the initial stage, is considered to lie on the curve at about the place where the initially rapid rise appears to level off. The time for the change in rotation to reach the mid-point between the initial value and α final is termed the half-time, $t_{1/2}$ of the fast stage of the denaturation. From Fig. 1 it is seen that this half-time is 12 minutes for the irradiated protein, and is 24 minutes for the native protein. In other words, the irradiated protein denatures twice as fast as the native.

Clearly, the structurally injured ovalbumin shows greater sensitivity to both heat and urea as denaturants. Though it must be remembered that the courses of these two modes of denaturation are not necessarily related,[3] the result of the experiment indicated by the dotted line in Fig. 1 seems to argue for a close relationship. In this experiment, which is preliminary to more thorough work to be pursued,[7] the irradiated ovalbumin was first heated and coagulated to remove about 20% of the total protein. According to Fricke's work this heating should have removed about half of the extra labile protein, all of fraction A and most of B, the two most labile fractions. The protein remaining in solution was then subjected to urea denaturation to give the result shown. The fact that the curve now lies closer to that for native ovalbumin suggests that the radiation-damaged molecules which exhibited increased lability to urea are the same molecules in heat labile fractions A and B.

In this work the optical rotation for the undenatured but irradiated ovalbumin is identical with that observed for native ovalbumin. Apparently, therefore, the damage to the irradiated protein is of a latent nature which only expresses itself in the

(1) Work performed at Argonne National Laboratory during tenure of Resident Research Associateship.

(2) H. Fricke, THIS JOURNAL, **56**, 789 (1952).

(3) R. B. Simpson and W. Kauzmann, *J. Am. Chem. Soc.*, **75**, 5139 (1953).

(4) R. H. Maybury and J. J. Katz, *Nature*, **177**, 629 (1956).

(5) E. J. Hart, *J. Am. Chem. Soc.*, **73**, 68 (1951).

(6) J. F. Foster and J. T. Wang, *ibid.*, **76**, 1015 (1954).

(7) These heating precipitation experiments were done in collaboration with Dr. Wendell Landmann, Argonne National Laboratory.

TABLE I

OPTICAL ROTATIONS OF UNDENATURED OVALBUMIN SOLUTIONS

	$[\alpha]_D^{30}$
Native ovalbumin (measured in this work)	$-30.0 \pm 0.3°$
Irradiated ovalbumin	$-30.3 \pm .3°$
Native ovalbumin (ref. 3)	$-30.0 \pm .3°$

subsequent denaturation. This latent damage could be the rupture of a bond in a hydrogen-bonded group. Since such rupture does not necessarily cause movement of atoms relative to one another no change in optical rotation would be observed until the unfolding commences under the action of the urea. Such motion, even to a slight extent, is believed to produce changes in the optical rotation.[8-10] Since the urea is believed to attack some eight hydrogen bonds in the unirradiated protein in order to pry loose the first turn of the coiled peptide chain, in the irradiated protein the observed rate increase could very well be the result of fewer hydrogen bonds needing to be broken since some of these already have been ruptured. Further studies aimed at relating the thermal lability to the urea lability of irradiated ovalbumin are planned.

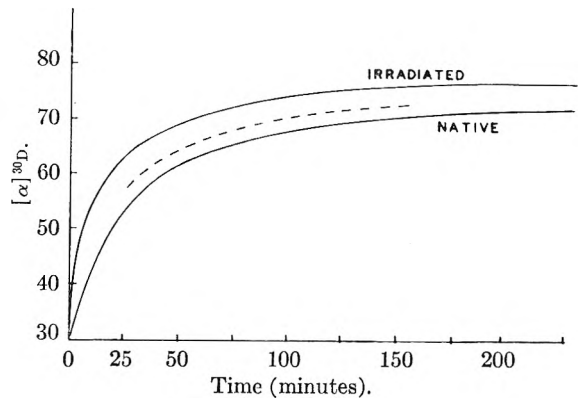

Fig. 1.—Time dependence of the optical rotation of ovalbumin preparation denatured by urea: urea concentration, 8 *M*; protein concentration, 2%; buffer, 0.035 *M* phosphate, *p*H 7.7. For dotted line see text.

Grateful acknowledgment is made of the encouragement and interest of Dr. Hugo Fricke and Dr. J. J. Katz.

(8) B. Jurgensons, *Arch. Biochem. Biophys.*, **57**, 376 (1955).

(9) J. A. Rupley, W. J. Dryer and H. Neurath, *Biochim. Biophys. Acta*, **18**, 162 (1955).

(10) J. F. Foster and J. T. Yang, *J. Am. Chem. Soc.*, **77**, 3895 (1955).

INTERPOLYMER ION-SELECTIVE MEMBRANES. I. PREPARATION AND CHARACTERIZATION OF POLYSTYRENESULFONIC ACID–DYNEL MEMBRANES

BY HARRY P. GREGOR, HAROLD JACOBSON, ROBERT C. SHAIR AND DAVID M. WETSTONE

Contribution from the Department of Chemistry of the Polytechnic Institute of Brooklyn, New York

Received July 19, 1956

Interpolymer ion-selective membranes were prepared by casting a film from a solution of linear polystyrenesulfonic acid and Dynel (a copolymer of acrylonitrile and vinyl chloride) in a suitable solvent, and allowing the solvent to evaporate. Films of varying thickness (5–50 μ) and polyelectrolyte–Dynel ratios (1/15 to 1/2) were cast from starting materials of different molecular weights and solvents. The ohmic resistances of these membranes varied upwards from about 5 ohm-cm.^{2} in 0.1 *M* potassium chloride; the concentration potentials (0.2 *M*|0.1 *M* potassium chloride) of some of the better membranes varied from 15.3 to 15.6 mv., as compared to a theoretical maximum of 16.1, showing a small anion leak. The interstitial molality of these membranes was calculated to be in the range 0.3 to 7. Osmotic flow rates using 1 *M* sugar were also measured. Bi-ionic potential measurements showed the membranes to be highly specific toward calcium. Some of the general properties of interpolymer membranes are discussed in detail.

Introduction

The duplication of physiological membranes possessing ion-selective properties (*i.e.*, the ability to restrict the transport of either cations or anions preferentially) by at least partly synthetic means dates prior to 1930. The early, classical work of Michaelis[1] on the dried collodion membrane represented the first major attempt to study these membranes and establish standard electrochemical criteria for membrane characterization. Ion-selective membranes have been formed from hydrated zeolitic materials by Marshall,[2] and from collodion and treated collodion by Sollner.[3,4] Membranes have been cast from sulfonated phenol–formaldehyde resins.[5,6] Polystyrenesulfonic acid–divinylbenzene ion-exchange resin particles were bonded with thermoplastic polymers to produce heterogeneous membranes by Wyllie,[7,8] and by Winger, Bodamer and Kunin.[9] Membranes were prepared by dissolving linear polystyrenesulfonic acid in collodion solutions and casting films therefrom, and also by adsorbing the acid into the pores of collodion films; this work was reported by Sollner and Neihof.[10,11] Homogeneous acid type membranes

(1) As described by K. Sollner, THIS JOURNAL, **49**, 47 (1945).

(2) C. E. Marshall and W. E. Bergman, *J. Am. Chem. Soc.*, **63**, 1911 (1941); C. E. Marshall and C. A. Krinbill, *ibid.*, **64**, 1814 (1942).

(3) C. W. Carr and K. Sollner, *J. Gen. Physiol.*, **28**, 119 (1944); C. W. Carr, H. P. Gregor and K. Sollner, *ibid.*, **28**, 179 (1945).

(4) K. Sollner, *J. Electrochem. Soc.*, **97**, 139C (1950); H. P. Gregor and K. Sollner, THIS JOURNAL, **58**, 409 (1954).

(5) T. R. E. Kressman and J. A. Kitchener, *J. Chem. Soc.*, 1190 (1949).

(6) W. Juda and W. A. McRae, *J. Am. Chem. Soc.*, **72**, 1044 (1950).

(7) M. R. J. Wyllie and H. W. Patnode, THIS JOURNAL, **54**, 204 (1950).

(8) M. R. J. Wyllie and S. L. Kanaan, *ibid.*, **58**, 73 (1954).

(9) A. G. Winger, G. W. Bodamer and R. Kunin, *J. Electrochem. Soc.*, **100**, 178 (1953).

(10) K. Sollner and R. Neihof, *Arch. Biochem. Biophys.*, **33**, 166 (1951).

were recently prepared by the copolymerization of *p*-styrenesulfonic acid and divinylbenzene,[12] and of methacrylic acid and divinylbenzene.[13]

This paper is the first in a series dealing with the preparation and characterization of interpolymer ion-selective membranes. These membranes are prepared by dissolving a polyelectrolyte or an ionogenic polymer together with an inert film-forming polymer in a suitable solvent or solvent mixture, casting a film therefrom, and wholly or partially evaporating the solvent before placing in water.

Two types of membrane phenomena can occur. A membrane may be ion-selective, *i.e.*, able to restrict the transport of either cations or anions preferentially; also a membrane may exhibit ion-specificity, *i.e.*, be ion-selective among cations or among anions. A membrane may be cation-selective (*i.e.*, permeable to cations rather than anions) and simultaneously be ion-specific toward a certain cation or cations. It obviously cannot be anion-selective and yet exhibit specificity toward any cation. However, it can be ion-specific without being appreciably ion-selective.

The considerations applied to the preparation of interpolymer membranes include: the desired electrochemical properties of the ionic or ionogenic material; the chemical and thermal stability of the film-forming matrix material as well as the polyelectrolyte; the mutual solubility relationships of these multi-component systems.

The membranes reported here were formed from solutions of polystyrenesulfonic acid (of varying molecular weights), a copolymer of vinyl chloride with acrylonitrile, and either N,N-dimethylformamide, dimethyl sulfoxide or a mixture of cyclohexanone with methanol.

Experimental

Most of the characterization procedures employed are similar to standard procedures in this field, developed largely by Sollner and his co-workers; the reader is referred to the original papers for details.[4]

Materials.—Dynel (DYN) is a copolymer of vinyl chloride and acrylonitrile (Bakelite Division, Union Carbide and Carbon, NYGL). The solvents used were N,N-dimethylformamide (DMF, du Pont), dimethyl sulfoxide (DSO, Stepan Chemical Co.), cyclohexanone and methanol (U.S.P. grade, Union Carbide and Carbon).

Polystyrenesulfonic acid (PSA) was prepared from polystyrene or, in some cases, a commercial product was used. The preparation and purification procedure for PSA followed that described previously.[14] Polystyrene powders (Monsanto) of three different average molecular weights, namely, 10,000, 30,000 and 70,000, were used. To ensure rapid and thorough sulfonation, only the −40 mesh fraction was used.

Sulfonations were carried out at 95° employing a 10 molar excess of concentrated sulfuric acid and silver sulfate as catalyst (1% of the weight of polystyrene). The 10,000 mol. wt. polystyrene was sulfonated for 2 hours, the 30,000 mol. wt. polymer for 3 hours, and the 70,000 mol. wt. product for 4 hours. Complete sulfonation was achieved as indicated by complete solubility of the polymer in water, with no evidences of cross-linking.

The large excess of sulfuric acid present could be removed by dialysis, by neutralization with sodium carbonate and subsequent salting-out of the sodium salt, or by an anion-exchange treatment. A convenient procedure for eliminating most of the sulfuric acid present was to add a limited amount of water to the sulfonation mixture, at which point most of the PSA precipitated. For example, when the 30,000 mol. wt. PSA–sulfuric acid mixture was diluted to a composition of one part of sulfuric acid to 2.7 parts of water, a gummy mass separated out. Less than 10% of the PSA remained in solution; the precipitate contained about 30% of the sulfuric acid originally used.

This concentrate was purified further by dialysis across cellophane diaphragms, at which point 95% of the acid present was PSA, as indicated by the solubility test with the barium salt. The last traces of sulfuric acid were removed by passage through a column of strong base (Type II) anion-exchange resin. These resins have lower capacities than do the weak base resins, but they can be rinsed free of sodium more readily. The resin columns were rinsed with water after passage of the PSA solutions to minimize loss of PSA.

The PSA solutions were evaporated to dryness at 105°. The dried polymers were completely re-soluble in water, indicating their stability at this temperature. The over-all yield by this procedure was 70%. The calculated acid value of pure PSA is 5.43 meq. per gram. The values for one group of PSA polymers prepared by these techniques were: 10,000 mol. wt., 5.22; 30,000, 5.24; 70,000, 5.15. It should be noted that these molecular weights are for unsulfonated polystyrene; the actual molecular weights would be 1.8 times the values stated, assuming no degradation of the polystyrene. This is difficult to ascertain by direct experiment. However, beads of loosely cross-linked polystyrene (0.1% divinylbenzene) are not degraded significantly by this sulfonation technique, as shown by visual observation.

The solubility of the different PSA materials in a number of solvents in which DYN was also soluble was measured. The solubility of the 10,000 mol. wt. fraction was somewhat greater than of the other fractions. At 25°, the solubility on a weight per cent. basis of this fraction was: acetone, 0.4; 2-ethoxyethanol (Cellosolve), 34; dipropylene glycol, 5.4; DMF, 35; methanol, 62. The solubility in DSO was comparable to that in DMF, being difficult to measure because of gel formation. The PSA was soluble in 3:1 mixtures of DMF and acetone, but only slightly soluble in 1:1 mixtures.

In an effort to increase the solubility of PSA in acetone and dipropylene glycol, the diethanolamine, isobutylamine and octylamine salts of PSA were prepared; the salts were less soluble than the free acids.

Solutions of PSA in DMF were found to become opalescent after a few days upon the absorption of even minute quantities of water. This is presumably the result of hydrolysis of DMF by the strong acid. The DSO solutions did not deteriorate in this fashion.

The viscosity of a 70,000 mol. wt. sample of PSA in different solvents was measured using a Brookfield Viscosimeter at 25°. The reduced specific viscosities $((\eta - \eta_0)/\eta_0 c$, with c expressed in weight per cent.) for 2% solutions were as follows: DMF, 57; water, 124; DSO, 137. Comparable values for the DYN were as follows: DMF, 93; acetone, 43; DSO, 99.

PSA is available commercially as the impure sodium salt of mol. wt. 10,000 (Lustrex 710) and mol. wt. 70,000 (Lustrex 770) (Monsanto Chemical Co., Springfield, Mass.). A fraction (10–15%) of these materials was insoluble because of cross-linking, presumably due to sulfone bridges. These materials were dissolved in water, the gel filtered off, and the solution passed through a column of sulfonic acid cation-exchange resin in the hydrogen form (Nalcite HCR, National Aluminate Corp.) for conversion into the acid. The sulfate present in the original products was converted to sulfuric acid which had to be removed since it charred the polymer during drying. Therefore, the PSA solution was passed through a hydroxide-regenerated anion-exchange resin as before, then evaporated to dryness. The acid values were: Lustrex 710, 5.02; Lustrex 770, 4.87, meq. per gram.

Membrane Preparation.—Casting solutions were prepared using DYN as the matrix material (M) and PSA as the polyelectrolyte (P), with either DMF, DSO, or a mixture of cyclohexanone and methanol as solvent. All polymer solutions were filtered before use through a glass wool mat. Varying P/M ratios were employed, the total solids content being chosen in each case so as to yield practical

(11) R. Neihof, THIS JOURNAL, **58**, 916 (1954).

(12) W. F. Graydon and R. J. Stewart, *ibid.*, **59**, 86 (1955).

(13) G. J. Hills, J. A. Kitchener and P. J. Ovenden, *Trans. Faraday Soc.*, **51**, 719 (1955).

(14) M. H. Waxman, B. R. Sundheim and H. P. Gregor, THIS JOURNAL, **57**, 969 (1953).

casting viscosities. For the casting of thicker membranes (>10 μ final thickness) viscosities in the range of 150 to 250 c.p. were found satisfactory. Below 150 c.p., the thicker films were found to spread uncontrollably over the casting plate before sufficient solvent could evaporate to make the film "set." The total solids content was kept in the range 10–15%.

The membranes were formed by casting films of the polymer solutions on glass plates, using a Boston–Bradley blade, and drying the plates at 70–75° for 48 to 96 hours. Membranes were stripped from the plates after soaking in water for 10 to 30 minutes. The membranes were conditioned for testing by about 24-hour equilibration with 1 *M* potassium chloride (plus a small amount of potassium acetate to buffer the solution at *p*H 5–6.5; this served to neutralize the acid present in the film). Prolonged equilibration in 0.1 *M* potassium chloride preceded all measurements.

Thickness.—Average thickness is reported in microns (μ) for a membrane equilibrated with 0.1 *M* potassium chloride. Average dried thickness is reported for the same membrane soaked briefly in water to remove diffusible electrolyte and dried as indicated below. The shrinkage is reported as per cent. of wet thickness.

Water Content.—The conditioned membranes were first soaked in water to elute diffusible salt, blotted quickly with filter paper to remove surface moisture and weighed quickly. They were then dried in a vacuum oven at 50° for about 24 hours and re-weighed. Water content is reported as per cent. of total wet weight. It was established that further drying under these conditions did not remove more than an additional 0.3% of water.

Exchange Capacity.—The active exchange capacity is defined experimentally as the number of exchange sites within the membrane structure which are titrable while leaving the membrane intact. Each sample was equilibrated with 1 *M* hydrochloric acid, rinsed free of diffusible acid, blotted quickly and eluted with an excess of 1 *M* potassium chloride. The eluent was titrated in conventional fashion with standard base. The theoretical equivalence of each membrane was calculated on the basis of the composition of the casting solution and dry weight as determined above; the available capacity is reported as per cent. of this theoretical maximum and as meq. of active groups per unit area of membrane. In addition, the molality of these groups was calculated on the basis of water content.

Osmotic Flow.—The movement of water across membranes resulting from osmotic pressure difference was determined with a conventional osmometer which supported the membrane horizontally on a wire screen. The osmometer was filled with water and immersed in a relatively large volume of 1 *M* sucrose; the latter solution was stirred vigorously. Interpolymer ion-selective membranes are almost completely impermeable to sucrose.[15] The entire assembly (less capillary and riser tubes) was thermostated at 25 ± 0.03°. Thirty minutes to one hour was required for attainment of thermal equilibrium and uniform osmotic flow, and the extent of capillary fall was then measured over a timed period of one to four hours, depending upon the rate. The effective area of the film was 6.4 cm.^{2}; the osmotic flow rates are reported as mm.^{3} per 100 cm.^{2} per hour. Rates were reproducible to ±10%.

Ohmic Resistance.—Resistance measurements were made in a simple methyl methacrylate cell employing fixed platinized platinum electrodes. The cells were rugged and simple to use. The membrane cross-section tested was 0.30 cm.^{2} to provide a measurably high resistance with highly conducting membranes. A Klett Conductivity Bridge at 1000 c.p.s. was used; additional capacitances up to 5,000 $\mu\mu$F. were required for some measurements. Readings were taken at the ambient temperature and corrected to 25° (2% per degree). Results are reported in ohm-cm.^{2}, equal to ρl, the product of the specific resistance and the thickness.

Concentration Potential.—Concentration potentials were measured using a methyl methacrylate cell; the exposed membrane area was about 3 cm.^{2}. The cell was so constructed that air could be bubbled across each membrane surface to reduce concentration overvoltage. Measurements were made during bubbling. The double compartment minimized diffusion from the salt bridge.

The cell circuit is represented by

$$\underset{\text{S.C.E.}}{(1)}\ |\text{sat. KCl}\ |\underset{c_1}{(2)}\ |\text{Memb.}\ |\underset{c_2}{(3)}\ |\text{sat. KCl}\ |\underset{\text{S.C.E.}}{(4)}$$

where S.C.E. is the saturated calomel electrode, and junctions 1–4 were effected by saturated potassium chloride–3% agar salt bridges; the bracket represents the plastic cell.

The measuring circuit employed a Leeds and Northrup Type K-2 potentiometer and Typo E galvanometer with a sensitivity of 3.5×10^{-10} amp./mm. when critically damped. The procedure was to clamp the membrane, previously equilibrated with the more dilute (c_2) solution, in position and take periodic readings until the potential remained constant to within 0.01 mv. Membranes of higher selectivity yielded potentials which rose quickly (in a minute or less) to a constant, maximum reading which did not decay measurably. With poorer membranes, the potential decayed in spite of the stirring action, and an approximate maximum reading was taken. For membranes yielding close to theoretical results, the cell solutions were changed several times before a final reading was recorded. The cessation of stirring resulted in no drop in potential with membranes of essentially maximum selectivity; as the selectivity of the film decreased, the potential drop increased correspondingly.

Three separate corrections were applied to each potential measurement: for the salt bridge liquid junctions, for the S.C.E. asymmetry, and for the temperature (except as noted below). The liquid junction potential error is the sum of the potentials of junctions (2) and (3), as written, in the concentration chain. This was obtained experimentally for different salts at varying concentrations by substituting for the polymer membrane a thin rubber membrane containing a pin-hole. The total potential of this chain was measured. The liquid junction potential at the pin-hole was calculated through use of the Nernst equation (for concentration potentials) and the Henderson equation (for bi-ionic potentials, neglecting activity coefficient corrections). The (calculated) potential at the pin-hole was subtracted from the total potential; the salt bridge liquid junction potential was the difference and was applied as a correction. This technique is similar to that described by Sollner and Gregor.[16]

Bi-ionic Potential.—Bi-ionic potentials were taken in substantially the same manner as the concentration potentials. Here 0.01 *M* potassium chloride was used as the reference salt (c_2). Corrections for liquid junction potential differences at the salt bridges were applied as described above. It is recognized that such corrections (which amounted to a few mv.) may be trivial, especially where applied to univalent–divalent cation systems.

Bi-ionic potentials were found to decay more rapidly than concentration potentials, even when the solutions were replaced within two minutes, and particularly when divalent ions were involved. In such cases, readings were approximated to the nearest 0.1 mv. In all cases, membranes were equilibrated with 0.01 *M* potassium chloride (c_2) before BIP measurements were made.

Results

In Table I are listed characterization data on a number of representative membranes. Thickness, resistance and concentration potential measurements were made on membranes equilibrated with 0.1 *M* potassium chloride. The table indicates the general effects noted with variation of polyelectrolyte to matrix material weight ratio (P/M), thickness and solvent. Concentration potentials are to be compared to the theoretical maximum of 16.11 mv., obtained from the relationship

$$E = (2t_+ - 1)\frac{RT}{\mathfrak{F}} \ln \frac{a_1}{a_2}$$

by setting $t_+ = 1$ (*i.e.*, the Nernst equation). The respective activities are obtained by converting concentrations to molality and utilizing mean activity coefficients in place of individual ion activity coefficients.[4] Data were obtained from Conway.[17]

(15) H. P. Gregor and H. Jacobson, to be published.

(16) K. Sollner and H. P. Gregor, THIS JOURNAL, **51**, 299 (1947).

(17) B. E. Conway, "Electrochemical Data," Elsevier Publishing Co., New York, N. Y., 1952.

TABLE I

GENERAL CHARACTERIZATION DATA FOR SOME PSA-DYN INTERPOLYMER MEMBRANES

(Theoretical Maximum Co. P. = 16.11 mv.)

No.	Mol. wt. × 10^3	P/M	Solvent	Thickness, μ	Ω Resistance, ohm-cm.²	Concn. potential 0.2/0.1 *M* KCl, mv.
39	70	1/.5	DMF	36	20,500	1.42
38	70	1/9	DMF	37	10,100	9.32
37	70	1/5	DMF	44	425	15.54
15	30	1/4	DMF	19	335	15.28
5	10	1/3	DMF	37	398	15.51
11	30	1/3	DMF	14	17.3	14.41
13	30	1/3	DMF	39	141	15.36
10	30	1/3	3 CHO[a] 1 MeOH	9	79.3	11.70
30	70	1/3	DMF	5	6.7	10.77
34	70	1/3	DMF	11	5.8	15.39
35	70	1/3	DMF	20	11.2	15.12
36	70	1/3	DMF	39	182	15.54
32	70	1/3	DSO	10	4.32	15.32
8	30	1/2	DMF	20	17.3	15.18
9	30	1/2	DMF	48	11.5	14.81
26	70	1/2	DMF	10	4.6	11.10
28	70	1/2	DMF	39	21.1	12.02

[a] Cyclohexanone.

Titrable exchange capacity, water content and shrinkage are listed in Table II for a number of membranes, differing primarily in the proportion of polyelectrolyte to matrix material employed. In addition, the interstitial molality of the active groups has been calculated on the basis of the titrated capacity and per cent. water.

TABLE II

CAPACITY AND WATER CONTENT OF SEVERAL PSA-DYN INTERPOLYMER MEMBRANES

No.	P/M	Thickness, μ	Capacity meq. cm.$^{-2}$ × 10^3	%	H_2O content, %	Interstitial molality	Shrinkage, %
34	1/3	11	1.0	79	10.5	7.1	9.1
36	1/3	39	3.4	88.2	21.2	3.7	2.6
32	1/3	10	0.9	77	20.5	3.4	0
9	1/2	48	1.2	27	37.6	0.68	34.8
26	1/2	10	0.1	8.3	15.1	0.73	0
28	1/2	39	0.4	13.7	35.0	0.29	0

In Table III are listed osmotic flow data for several selected membranes, together with their thicknesses. The results in the third column (osmotic flow) are generally inversely proportional to the membrane thickness while resistance is directly proportional; the product of these two quantities is shown in the last column.

As a matter of practical interest, the burst strength of several membranes was measured on a Mullen Burst Strength Tester. These films are quite strong and easy to use as regards laboratory procedure. They are somewhat plastic and stretch before they tear. The pressure in pounds per square inch to the point of stretching on the Mullen Tester was about 7, the pressure at the tear point about 15, for several of the stronger films. Dynel films are not particularly elastic; the elasticity of these films is probably a reflection of the plasticizing action of PSA.

TABLE III

OSMOTIC FLOW RATES FOR SELECTED PSA-DYN INTERPOLYMER MEMBRANES

No.	Thickness, μ	ω Osmotic flow rate, mm.³/100 cm.²-hr.	$\Omega\omega$
34	11	591	3440
35	20	328	3660
36	39	43	7800
32	10	1722	7400
9	48	267	3030
26	10	1722	7900
28	39	216	4580

Concentration potentials for the membranes being characterized were measured over a wide range of potassium chloride concentrations, maintaining a 2:1 concentration ratio between the ambient solutions. These results are listed in Table IV, and are to be compared to the calculated theoretical potential shown for each pair.

The cationic specificity of several selected membranes is indicated by the bi-ionic potential (BIP) data of Table V. These data should be compared to values of the potential for free diffusion and for free cation diffusion ($u_- = 0$) calculated from various forms of the Henderson equation. For the $Li^+ \mid K^+$ pair, free diffusion is given by

$$E = \frac{RT}{\mathfrak{F}} \ln \frac{\Lambda_1}{\Lambda_2}$$

and, when $u_{Cl^-} = 0$

$$E = \frac{RT}{\mathfrak{F}} \ln \frac{(t_+\Lambda)_1}{(t_+\Lambda)_2}$$

where Λ and t refer to the equivalent conductivity and transport number at that concentration. For the $Ca^{++} \mid K^+$ pair, the free diffusion potential is

$$E = -\frac{A(c_K)_2 - B(c_{Ca})_1 - (c_{Cl})_2 + (c_{Cl})_1}{A(c_K)_2 - 2B(c_{Ca})_1 + (c_{Cl})_2 - (c_{Cl})_1} \frac{RT}{\mathfrak{F}} \times \ln \frac{A(c_K)_2 + (c_{Cl})_2}{2B(c_{Ca})_1 + (c_{Cl})_1}$$

where

$$A = \frac{2(t_+\Lambda)_2}{(t_-\Lambda)_1 + (t_-\Lambda)_2}, \quad B = \frac{2(t_+\Lambda)_1}{(t_-\Lambda)_1 + (t_-\Lambda)_2}$$

and $(c_K)_2$ is the molar concentration of potassium ion in solution (2), etc. The free cation diffusion potential ($u_{Cl^-} = 0$) is given by

$$E = -\frac{(A/B)(c_K)_2 - (c_{Ca})_1}{(A/B)(c_K)_2 - 2(c_{Ca})_1} \frac{RT}{\mathfrak{F}} \ln \frac{(A/B)(c_K)_2}{2(c_{Ca})_1}$$

where A/B is obviously $(t_+\Lambda)_2/(t_+\Lambda)_1$, from above. The transport number and conductance data of Conway[17] were used for this purpose.

Discussion

This study is concerned with the development of improved techniques for the preparation of ion-selective membrane systems of superior properties. Those membranes previously described in the literature or available commercially are not completely desirable from many points of view. An ideal membrane system should be easy to prepare in a reproducible manner from readily available or prepared materials and it should possess a high level of chemical stability and reasonable mechanical stability. Further, the techniques employed should

TABLE IV

CONCENTRATION POTENTIALS IN MILLIVOLTS OF SELECTED PSA-DYN INTERPOLYMER MEMBRANES AS A FUNCTION OF CONCENTRATION OF POTASSIUM CHLORIDE

Concentration ratio—2:1

Membrane	Lower concn.—c_2 0.001 *M*	0.004 *M*	0.01 *M*	0.04 *M*	0.1 *M*	0.4 *M*	1 *M*
Theor. max.	17.43	17.14	16.87	16.39	16.11	15.89	17.18
34	17.10	16.91	16.59	15.89	15.39	13.56	11.23
35	17.11	17.01	16.75	15.85	15.12	12.52	9.67
36	16.95	16.90	16.74	16.04	15.54	14.09	12.31
32	17.79	16.95	16.57	15.80	15.32	12.59	9.93
9	17.46	16.90	16.42	15.45	14.81	10.00	6.87
26	16.89	16.59	15.90	13.62	11.10	7.26	4.58
28	17.28	16.58	16.21	14.14	12.02	7.60	4.83

TABLE V

BI-IONIC POTENTIALS AT 0.01 *M* IONIC STRENGTH FOR SELECTED PSA-DYN INTERPOLYMER MEMBRANES

No.	BIP 0.0033 *M* $CaCl_2$/0.01 *M* KCl, mv.	BIP 0.01 *M* LiCl/0.01 *M* KCl, mv.
34	19.31	−24.47
35	21.77	−24.51
36	41.03	−30.79
32	12.85	−21.54
9	24.53	−21.03
26	8.76	−19.32
28	15.52	−20.71
Theor. potentials for:		
Free diffusion	− 8.41	− 7.04
Free cation diffusion ($u_{Cl^-} = 0$)	−26.15	−19.09

permit utilization of a number of different polyelectrolytes or ionogenic materials, and should allow one to prepare any given membrane type with widely varying properties such as thickness, selectivity and permeability.

In principle, an ion-selective membrane need be no more than a film of a polyelectrolyte. Its selectivity would be proportional to the molal concentration of fixed ionic groups in the membrane. Consequently, it is important not only that a film be highly ionic, but also that it not sorb too much water, thereby reducing the concentration of active groups. Were it not for the fact that polyelectrolytes are water-soluble, the obvious and most direct procedure would be to cast films directly from them. Copolymers of an ionic or ionogenic monomer and a non-polar monomer can be prepared, but these are water-soluble when as little as 3% of the material is ionic. If the amount of ionic material is less than one per cent., the film is insoluble but also shows no electrochemical activity because the ionic groups are now isolated in an apolar matrix. While a polyelectrolyte could be insolubilized by cross-linking, which is not easily accomplished, the resulting film is rigid because a high level of cross-linking is required to counteract the swelling pressures. For example, the ion-exchange resin type membranes are 4–8% cross-linked.

The technique described in this paper involves combining the polyelectrolyte with a second, water-insoluble film-forming polymer, such that the polyelectrolyte is enmeshed with the inert polymer in the final film. One then obtains the mechanical advantages of an inert linear polymer, while retaining a high concentration of polyelectrolyte.

Phase Relationships.—A series of preliminary studies were carried out on a number of polyelectrolytes, film-forming polymers and solvent systems. Of the many possible combinations of polar polyelectrolytes and apolar film-forming polymers available, and solvents for either of these, only a few systems satisfy the requirement of compatibility at any but insignificant concentrations. In many cases a single solvent would dissolve either polymer, but not both together. In some cases an apparently homogeneous solution of the two polymers could be achieved using a single solvent, but the film cast from this solution showed little or no electrochemical activity. For example, polyacrylic acid and DYN are apparently soluble in DMF, but during the drying process there occurs the formation of agglomerates of PAA in the DYN matrix, such that almost none of the acid groups are available for exchange.

While in some cases it was found possible to employ mixed solvents, these were difficult to use because one of the polymers usually coagulated as the more volatile solvent evaporated. Two solvents, DMF and DSO, were found to be outstanding as regards their ability to dissolve two incompatible solutes. The casting solutions had to be stable as regards absence of any gelation, but these often showed an appreciable Tyndall beam. All cross-linked material had to be eliminated from the system, and it also appeared that highly branched polymers were not particularly desirable. If the polyelectrolyte were made more compatible with the inert polymer as by esterifying the former, it was often found that the film was not electrochemically active because the esters could not be hydrolyzed appreciably.

As a rule, the viscosity of the components in the system was studied in different solvents, because the reduced specific viscosity is indicative of the occluded volume of the polymer. Those solvents which gave polymer solutions of high viscosity were found to be desirable because here the polymer chain was relatively elongated, at least during the initial stages of drying. The films were consequently stronger mechanically, and the polyelectrolyte was held more firmly because both polymers were presumably better intertwined.

Intrinsic Properties of Membranes.—The intrinsic properties of a membrane system are those of the film itself such as molality of exchange groups, per cent. of available capacity, specific conductivity and mechanical properties. These are to be differentiated from its functional properties which are concerned with what the membrane does rather than what it is.

An examination of the data indicates that the molecular weight of the PSA used was not particularly critical. The 10,000 mol. wt. material was more soluble in the casting solution, but probably would more readily diffuse out of the final film. For this reason the 30,000 and 70,000 mol. wt. materials were preferred. As regards the choice of solvent, Table I shows that the cyclohexanone–methanol solvent gave apparently homogeneous solutions but rather inferior membranes of high resistance and poor selectivity.

Membranes cast from DSO rather than from DMF tended to swell somewhat more, and consequently were of lower resistivity.

An examination of Table II shows that not all of the PSA contained in the casting solution is titrable. When 25% of the film was PSA (P/M = $^1/_3$), the capacity varied from 75 to 90% of the PSA originally present. Part of this difference is presumably due to complete enclosure of the polar exchange group by the matrix. When 33% of the film was originally PSA, the capacity varied from 8 to 30%. Here, at these higher polyelectrolyte contents, enclosure is less of a factor; rather, part of the polyelectrolyte was found to diffuse out of the membrane. However, the part that remained was firmly bound.

It would be expected that the thicker membranes would have proportionately lower water contents and higher molalities than thinner membranes. However, often the atmospheric conditions during the casting and drying operations are important factors, as is the amount of moisture originally present in the casting solutions. PSA is extremely hygroscopic, as are DMF and DSO. Traces of moisture present in the casting solution resulted in membranes of somewhat lower resistances. All of these factors require control for reproducibility.

As a rule, the swelling of a membrane was found to vary directly with its PSA content. However, the extent of swelling is not independent of the film thickness. Usually, the thinner membranes (<30 μ) evidenced about the same specific resistances, while the thicker membranes often showed higher values. This effect was more prevalent with films cast from the lower P/M ratios; here, some phase separation may have occurred. The thicker films dried at relatively slow rates thereby permitting time for diffusion while the membrane is still fluid or gelatinous.

The specific conductance of films having a P/M ratio of $^1/_3$ was about 2×10^{-5} mho cm.$^{-1}$, while that of $^1/_2$ membranes was 2×10^{-4} mho cm.$^{-1}$. Since the latter films are about 20% water, the specific conductances of their interstitial solutions would be about 10^{-3} mho cm.$^{-1}$. The interstitial molality of these $^1/_2$ membranes being about 0.6, one may calculate their interstitial specific conductance also from the free solution conductance of the potassium ion at these concentrations, and obtain a value of 40×10^{-3} mho cm.$^{-1}$. The difference in these two values is obviously a reflection of steric factors. The interstitial conductivity of the $^1/_3$ membranes is one-fifth that of the $^1/_2$ films while the former possess an interstitial molality greater by an order of magnitude; a greater steric factor would be expected at the lower polyelectrolyte contents.

Functional Properties of Membranes.—The remaining data of Table I require little comment. They show that membranes prepared from mixed polymers low in PSA have high ohmic resistances and rather poor concentration potentials. Obviously, with these membranes, the conducting paths do not necessarily connect along the pores containing the polyelectrolyte. DYN membranes are characterized by an extremely fine pore structure even in the completely dried state, and may contribute to the conductance without, of course, making a parallel contribution to the potential of the system.

Membranes containing appreciable amounts of PSA, varying from 16 to 25%, all evidence specific conductances of about the same order of magnitude (10^{-3} mho cm.$^{-1}$), with concentration potentials which vary from good to excellent. A single example is given for a membrane prepared from a mixed solvent; as a rule, such membranes show inferior properties.

Membranes in the series 30, 34, 35 and 36 were cast from the same solution but had thicknesses ranging from 5 to 39 μ. Here the specific conductance is not the same for all membranes, being appreciably higher for the 39 μ membrane. Films with thicknesses of 10 μ or greater show excellent concentration potentials, but only a limited number of very thin membranes (*i.e.*, <5 μ) show good concentration potentials in these relatively concentrated solutions.

The effect of substituting DSO for DMF may be seen by comparing membranes 34 and 32. Other factors being the same, DSO membranes generally evidence lower ohmic resistances but equal concentration potentials.

Membranes cast from solutions containing the polymers in a P/M ratio of $^1/_2$ show lower resistances, as expected, but as a rule also somewhat lower concentration potentials in 0.1 *M* potassium chloride solutions. As has been described previously, these membranes swell more strongly and imbibe more water than do those membranes with less polystyrenesulfonic acid. Further work at restricting the swelling of membranes having high PSA contents is continuing.

The data of Table III indicate an excellent parallelism between the osmotic flow rate of a membrane and its ohmic resistance and thickness. The specific resistances of all the membranes listed are about the same ($2–5 \times 10^3$ ohm-cm.) except that of 32, which is 43×10^3 ohm-cm. Consequently, ω should vary inversely with thickness, which it does approximately except for some aberrant results which probably reflect individual variations between membranes. The relative constancy of the product $\Omega\omega$ (about a twofold variation) strongly suggests that the mechanical pathways for osmotic flow and conductance are the same here. This will not be found true for other membrane types, reported in later papers. Also, PSA membranes have generally evidenced much higher osmotic flow rates than have comparable membranes of other types.

The concentration potentials of Table IV are typical and require little comment. In dilute solutions the membranes approach (or in some cases exceed, although some of this may be due to experimental error) the theoretical maxima. Membranes which are of low ohmic resistance show relatively poor selectivity in concentrated solutions but approach the theoretical maximum as the concentration decreases toward 0.01 *M*.

Bi-ionic potentials, as are given in Table V, are a good measure of the relative transport numbers of competing diffusible ions within a membrane. This

current carrying ability is, of course, a function of both average mobility and effective concentration within the conducting pores of the membrane. If one assumes comparable effective concentrations for two competing cations, the Henderson equation may be employed to calculate a cation transport ratio from the measured bi-ionic potential. This may be done for the lithium–potassium system, revealing that, in comparison to the potassium ion, the lithium ion is only slightly less effective as a current carrying species in the membrane than it is in solution. Evidently in these systems there is little steric hindrance for the lithium ion as opposed to the potassium ion, as is shown in more dense membrane systems.

The results of bi-ionic potential measurements when calcium solutions are compared with potassium are quite interesting. The free cation diffusion potential is in this case −26 mv., while measured potentials as high as 40 mv. are encountered. Obviously, the membranes are considerably more permeable to calcium than to potassium, although the mechanism of preference is not evident from these data alone. Some of these phenomena are described in more detail in another paper,[18] which shows that while the membrane is highly specific toward calcium, the calcium is not bound by the exchange groups but rather is diffusible. In this case also one may calculate a cation mobility ratio from the Henderson equation, although the known calcium concentrating ability of the membrane tends to invalidate the result for any but indicative purposes. As an example, a bi-ionic potential of 23.4 mv. corresponds to a calcium to potassium ion transport ratio of 10. The transport data reported in the above-mentioned study indicate that this value is somewhat high, as would result from a calculation which assumed comparable membrane concentrations of the two cations.

Other trends in these potentials are as expected; increase of resistance and thickness tends to improve the results somewhat. However, higher PSA contents again appear to reduce the functionality of the film, presumably as a result of causing too great a matrix swelling. Data on other polyelectrolyte type membranes, to be reported, will show that the degree to which thickness and ohmic resistance can affect bi-ionic potentials is very much dependent upon the degree of hydrophilic character attributable to the polyelectrolyte component.

Acknowledgment.—The authors wish to thank the Bureau of Ships, Department of the Navy, for their support of this work.

(18) H. P. Gregor and D. M. Wetstone, *Trans. Faraday Soc.*, in press.

INTERPOLYMER ION-SELECTIVE MEMBRANES. II. PREPARATION AND CHARACTERIZATION OF POLYCARBOXYLIC ACID–DYNEL MEMBRANES

BY HARRY P. GREGOR AND DAVID M. WETSTONE[1]

Contribution from the Department of Chemistry of the Polytechnic Institute of Brooklyn, New York

Received July 19, 1956

Interpolymer ion-selective membranes were prepared by casting a film from a solution containing a linear copolymer of vinyl methyl ether and maleic anhydride, Dynel (a copolymer of acrylonitrile and vinyl chloride), and a suitable solvent. Films of varying thickness (1–113 μ) and polyelectrolyte–Dynel ratios (1/6 to 1/1) gave ohmic resistances upwards from 0.26 ohm-cm.^{2} in 0.1 *M* potassium chloride. The concentration potentials (0.2 *M*|0.1 *M* potassium chloride) of some of the better membranes varied from 14.9 to 15.8 mv., as compared to the theoretical maximum of 16.1, showing a small anion leak. The interstitial molality of these membranes was calculated to be in the range 0.4 to 4.4. Osmotic flow rates using 1 *M* sugar were also measured. Bi-ionic potential measurements showed the membranes to be highly specific toward calcium, with respect to potassium, but less specific toward lithium. The results are discussed and compared to those obtained with polystyrenesulfonic acid membranes.

Introduction

This paper is the second in a series[2] describing the synthesis and characterization of interpolymer ion-selective membranes. The membranes reported here were formed from a solution of a copolymer of maleic anhydride with vinylmethyl ether and a copolymer of vinyl chloride with acrylonitrile in N,N-dimethylformamide. On contact with water the maleic anhydride hydrolyzes to maleic acid. Some results are also reported on films made using polyacrylic acids and polymethacrylic acids.

(1) Taken in part from material which was submitted in partial fulfillment of the requirements for the degree of Doctor of Philosophy in Chemistry at the Polytechnic Institute of Brooklyn.

(2) H. P. Gregor, H. Jacobson, R. C. Shair and D. M. Wetstone, THIS JOURNAL, **61**, 141 (1957).

Experimental

The characterization procedures were exactly those employed in the previous study,[2] with such modifications as are noted here. The procedures included determination of thickness, water content, osmotic flow, ohmic resistance, concentration potential and bi-ionic potential. The materials used and the determination of exchange capacity differed, as noted below.

Materials.—PVM/MA is a 1–1 copolymer of vinyl methyl ether and maleic anhydride (General Aniline and Film). Polyacrylic and polymethacrylic acids were used, freeze dried from solutions supplied by the Rohm and Haas Company. Dynel (DYN), N,N-dimethylformamide (DMF) and dimethyl sulfoxide (DSO) are as previously described.

Exchange Capacity.—The buffer technique described by Gregor and Bregman[3] was used. The membranes were put

(3) H. P. Gregor and J. I. Bregman, *J. Am. Chem. Soc.*, **70**, 2370 (1948).

in the hydrogen form by treatment with 1 *M* hydrochloric acid, equilibrated with water, blotted and then treated with a measured amount of a solution which was 0.015 *M* in potassium acetate and 1 *M* in potassium chloride; the *p*H was read after 24 hours. These *p*H values were compared to the curve for the titration of the same concentration and amount of potassium acetate in potassium chloride with standard hydrochloric acid, and the equivalents of hydrogen ion contributed by the membrane was read. The theoretically expected equivalence of each membrane was calculated on the basis of its initial composition and its dry weight; the available capacity is reported as per cent. of this theoretical maximum and as meq. of active groups per unit area of membrane. In addition, the molality of the active groups is calculated and reported, based upon the determined interstitial water content.

The procedure just described is rapid and convenient, although it does not give as definitive results as a direct titration of the membrane itself. These were carried out by adding increments of standard base to a membrane sample in the hydrogen state in 1 *M* potassium chloride, reading the *p*H at 8–16 hours after each addition of base. The direct titration of the membrane gives an average first ionization constant of $pK_{a1} = 5$, and $pK_{a2} = 9$. Accordingly, since the buffer titrations were carried out at *p*H 5–7, only about 50% of the titrable hydrogen ions were detected; the capacities may in some cases be greater by a factor of 1.5–2.

Results

In Table I are listed characterization data on a number of representative membranes. Thickness, resistance and concentration potential measurements were made on membranes equilibrated with 0.1 *M* potassium chloride (except the dilute Co. P., which employed 0.01 *M* potassium chloride). The table indicates the general effects noted with variation of polyelectrolyte to matrix material weight ratio (P/M), thickness and solvent. Concentration potentials are to be compared to the respective theoretical maxima, as given, obtained from the Nernst relationships.

TABLE I

GENERAL CHARACTERIZATION DATA FOR SOME PVM/MA–DYN INTERPOLYMER MEMBRANES

(Theor. max. Co.P.: 0.2|0.1 *M* KCl, 16.11 mv., 0.02|0.01 *M* KCl, 16.87 mv.)

No.	P/M	Solvent	Thickness, μ	Ω Resistance, ohm-cm.^{2}	Concn. potential (Co.P.) 0.2|0.1 *M* KCl, mv.	0.02|0.01 *M* KCl, mv.
204	1/6	DSO	34	69	15.57	16.83
188	1/5	DMF	40	8500	10.70	15.96
189	1/4	DMF	40	728	15.77	16.75
206	1/4	DMF	37	2275	15.12	16.62
207	1/4	DMF	20	77	15.18	16.63
208	1/4	DMF	10	10.3	14.98	16.68
190	1/4	Acetone	29	8840	14.96	...
191	1/3	DMF	41	38	15.59	16.83
209	1/3	DMF	46	42	15.56	16.68
210	1/3	DMF	23	12.1	14.90	16.78
211	1/3	DMF	14	6.5	14.94	16.71
220	1/3	DMF	6	1.9	11.20	16.40
221	1/3	DMF	~1	0.32	~7.1	~12.7
205	1/3	DSO	49	18.4	15.11	16.78
192	1/2	DMF	57	12	15.43	16.83
212	1/2	DMF	65	10.9	15.09	16.74
213	1/2	DMF	41	4.7	14.67	16.68
214	1/2	DMF	22	2.7	13.62	16.17
222	1/2	DSO	61	0.26	~10.4	15.40
193	1/2	Acetone	105	7.1	13.29	...
194	1/1	DMF	113	5.1	14.19	16.63

Titrable exchange capacity, water content, shrinkage and interstitial molality are listed in Table II for five membranes, differing primarily in the proportion of polyelectrolyte to matrix material employed. In Table III are listed osmotic flow data for three additional, selected membranes, together with their thicknesses and resistances. The product of resistance and osmotic flow is shown in the last column.

TABLE II

CAPACITY AND WATER CONTENT OF SEVERAL PVM/MA–DYN INTERPOLYMER MEMBRANES

No.	P/M	Thickness, μ	Capacity (meq. cm.$^{-2}$) $\times 10^3$	Capacity %	H_2O content, %	Interstitial molality	Shrinkage, %
188	1/5	40	0.27	3.1	14	0.42	5
189	1/4	40	5.4	57	22	4.4	0
191	1/3	41	7.5	66	50	2.5	15
192	1/2	57	10.9	67	49	2.7	42
194	1/1	113	12.4	63	71	1.4	70

TABLE III

OSMOTIC FLOW RATES FOR SELECTED PVM/MA–DYN INTERPOLYMER MEMBRANES

No.	P/M	Thickness, μ	Ω Resistance, ohm-cm.^{2}	ω Osmotic flow rate, mm.^{3}/100 cm.^{2}-hr.	$\Omega\omega$
207	1/4	20	77	19.8	1530
210	1/3	23	12.1	340	4120
213	1/2	41	4.7	1166	5500

The burst strength of several membranes as measured on a Mullen Burst Strength Tester was about 2 pounds per square inch to the point of stretching, and the pressure at the tear point was about 5, for an average film. Pure Dynel films are not particularly elastic; the elasticity of these films is probably a reflection of the plasticizing action of PVM/MA.

Concentration potentials for two of the better membranes were measured over a wide range of potassium chloride concentrations, maintaining a 2:1 concentration ratio between the ambient solutions. These results are listed in Table IV together with the cationic transport numbers, calculated from the membrane potential, neglecting other effects. Table V lists similar data for hydrochloric acid at three concentrations in the same range.

TABLE IV

CONCENTRATION POTENTIALS OF SELECTED PVM/MA–DYN INTERPOLYMER MEMBRANES AS A FUNCTION OF CONCENTRATION OF POTASSIUM CHLORIDE

c_1/c_2 *M* KCl	Theor. max., mv.	No. 207 E, mv.	No. 207 t_+	No. 210 E, mv.	No. 210 t_+
0.002/0.001	17.43	17.10	0.991	(17.47)	(1.001)
0.008/0.004	17.14	16.48	.981	16.57	0.983
0.02/0.01	16.87	16.12	.978	16.18	.980
0.08/0.04	16.39	15.77	.981	15.72	.980
0.2/0.1	16.11	15.18	.971	14.90	.962
0.8/0.4	15.89	14.06	.942	12.14	.882
2/1	17.18	10.51	.806	8.15	.787
0.6/0.01	96.6	92.5	.958	90.7	.940

The cationic specificity of several selected membranes is indicated by the bi-ionic potential (BIP) data of Table VI. These data should be compared

TABLE V

CONCENTRATION POTENTIALS OF SELECTED PVM/MA–DYN INTERPOLYMER MEMBRANES AS A FUNCTION OF CONCENTRATION OF HYDROCHLORIC ACID

c_1/c_2 *M* HCl	Theor. max., mv.	No. 207 *E*, mv.	No. 207 t_+	No. 210 *E*, mv.	No. 210 t_+
0.002046/0.001023	17.44	(17.46)	(1.001)	(17.48)	(1.001)
.02046/0.01023	16.94	16.84	0.997	16.66	0.992
.2046/0.1023	16.85	15.07	0.947	15.02	0.946

to values of the potential for free diffusion and for free cation diffusion ($u_- = 0$), which are calculated from various forms of the Henderson equation.[2]

TABLE VI

BI-IONIC POTENTIALS AT 0.01 *M* IONIC STRENGTH FOR SELECTED PVM/MA–DYN INTERPOLYMER MEMBRANES

No.	BIP 0.0033 *M* $CaCl_2$/0.01 *M* KCl, mv.	BIP 0.01 *M* LiCl 0.01 *M* KCl, mv.
207	~+17.8	−40.79
210	~+11.9	−38.46
211	~+ 4.1	−35.41
220	~− 2.9	−33.48
213	~ 0.0	−34.14
Theor. potentials for:		
Free diffusion	− 8.41	− 7.04
Free cation diffusion ($u_{Cl^-} = 0$)	−26.15	−19.09

Discussion

Before discussing the properties of the PVM/MA–DYN membranes, a few remarks on the reasons for the choice of this particular system are in order. The first carboxylic acid systems investigated employed polyacrylic (PAA) and polymethacrylic (PMA) acids with DYN. Solutions prepared from these polymers were apparently homogeneous in several solvents, but did show evidences of settling-out after standing for some weeks, indicating some incompatibility between the three components. Membranes cast from these systems gave low concentration potentials in all cases. Microscopic examination of the films showed that they contained micro-globules of the acid, encapsulated by the matrix polymer.

Attempts also were made to prepare membranes by absorbing the acids in an already formed matrix. Films of DYN and polyvinylbutyral were cast, partially dried (various lengths of time), and coagulated with water. These films were then soaked in aqueous solutions of the polyacids, and dried in an attempt to "lock" molecules of the active material in the matrix pores.

The best membrane obtained by this technique was prepared by soaking a coagulated DYN film in a 10% aqueous solution of PAA for 18 hours, followed by drying. Its thickness was 51 μ, the resistance was 98 ohm-cm.^{2}, and the concentration potential (0.2 *M* | 0.1 *M* KCl) was 14.07 mv. All of the other membranes prepared by either of these techniques were inferior.

In an effort to obtain a polycarboxylic acid in such form as to be compatible with DYN, polymers of lower polarity were examined. It was found that the maleic anhydride copolymer formed homogeneous interpolymer membranes with DYN at different ratios, and that it readily hydrolyzed to the acid in contact with water. The initiation of this hydrolysis process was noted when the casting plates were first dipped in water to strip the membranes, and was further evidenced by the large swelling which occurred at high values of P/M.

In considering the characterization data of Table I, several general effects are to be noted. The resistance varied substantially in an inverse manner with P/M, since conductance in a membrane is by the gegenions. The magnitude of the resistance and thickness variations, however, merits additional comment. There is considerable swelling engendered by the hydrolysis of the anhydride which creates a considerably "opened" matrix structure, *i.e.*, a porous film. This is corroborated by a soft, gel-like appearance in the high P/M membranes.

The magnitude of the concentration potentials depends largely upon the extent to which fixed exchange groups of the polyelectrolyte screen the pores available for electrolyte transport. Among the relatively unswelled membranes (*e.g.*, 189, 191 and 192) the Co.P. decreases slightly, corresponding to a moderate increase in swelling. This is evidenced both by increase in thickness and decrease in resistance. That the Co.P. does not drop abruptly for this P/M range may be due to the increased amount of active sites present.

The two extremes (188 and 194) are also of interest. The considerable swelling of the 1/1 membrane probably has overcome any advantages gained by the large amount of polyelectrolyte present; thus both resistance and Co.P. drop sharply. Conversely, membrane 188 is probably composed of an essentially unporous, closed matrix, as evidenced by the resistance; what pores are present for transport contain few active sites. Thus the Co.P. is again quite low.

With respect to variation in thickness, 191, 211, 220 and 221 may be examined. As would be expected for macroscopically homogeneous systems, the specific resistances, particularly the last three, are about constant. An indication that a significant number of pores are unprotected by active sites may be gained from the significant drop in Co.P. with increasing thinness. It may be, however, that very thin membranes develop mechanical imperfections in the course of handling, which are not easily detectable visually.

Two additional solvent systems were used. Films cast from acetone showed high resistances, a high level of swelling and the same concentration potentials. It may be that much of the polyelectrolyte was hydrolyzed but was also encapsulated; acetone may be a better solvent for DYN than for PVM/MA. The results with DSO provided a more interesting case. While the Co.P. values obtained were slightly poorer than with DMF, resistances were remarkably low. Attention is particularly directed to 222, a 61 μ membrane of 0.26 ohm resistance, which still yielded an appreciable value for Co.P. in the more concentrated solution. These phenomena with DSO have not yet been fully explored and discussion here of the causative

factors would be premature. Many of these effects were found to occur also with polystyrenesulfonic acid–DYN systems.

The data of Table II on exchange capacity and water content are essentially self-explanatory. Increased water content and shrinkage upon drying are to be expected of the more swelled membranes of higher polyelectrolyte content. Capacities of 60–70% obtained at neutral *p*H levels indicate that almost all of the polyelectrolyte present in these membranes is available at pore sites.

The osmotic flow rates shown in Table III for three of the better membranes are to be compared to the parallel resistance data. While resistance and osmotic flow should be directly and inversely proportional, respectively, to thickness with uniform membranes, exactly the opposite is found here. Undoubtedly, this is largely the result of increasingly enhanced swelling of carboxyl membranes with larger polyelectrolyte contents. Ideally, the product of resistance and osmotic flow (last column) should be constant. However, this assumes that the mechanisms of conductance and of osmotic flow are always dependent upon the same factors, which is patently not reasonable. The gegenions of the fixed active sites in the pores contribute to conductance, as may be seen when membrane conductance is measured in dilute solutions.[4] Obviously, pure osmotic flow is not so affected. When the pores are relatively large and greater in number (213), the gegenions' contribution is small since the pores contain much diffusible salt, and conductance and osmotic flow should both depend directly upon variation in pore size. However, in smaller pores (207) the gegenions maintain a relatively high level of conductance (low resistance) while osmotic flow is sharply curtailed. Thus, the low value of $\Omega\omega$ for 207.

Two facts of significance are to be noted in the Co.P. data of Table IV, the decrease of potential with increasing concentration and the failure in one case to achieve theoretical maximum. The selectivity of a membrane is dependent upon a number of factors, many of which have been discussed elsewhere.[4–6] In the more concentrated solutions the "anion leak" is of consequence. Of greater interest is the lack of attainment of theoretical maximum potentials even at extreme dilution. At c_2 values of 0.004, 0.01 and 0.04 *M* potassium chloride, the cationic transport numbers in both membranes are remarkably the same, 0.980. This constancy in t_+ below 0.4 *M* potassium chloride suggests that here the Donnan concentration inside the membrane is not a factor.

Two other explanations are available for lack of selectivity in the high dilution range. Water movement is a dissipative process which may occur to an appreciable extent in membranes of moderate resistance, and acts to lower the concentration potential.[7] At high dilution this effect could be independent of concentration, as is the case here.

Hydrolysis (of the weak acid active sites) is a second factor to be considered, particularly in dilute solutions.[6,7] The replacement of the gegenion (*e.g.*, potassium) with a hydrogen ion derived from the solvent increases the concentration of diffusible anions and decreases the potential. This effect would also be relatively concentration independent at high dilution.

That hydrolysis plays an important role here is suggested by consideration of the hydrochloric acid data in Table V. Weak acid membranes should not be expected to evidence high selectivity in the presence of a strong acid, and at 0.1 *M* hydrochloric acid this is seen to be true. At higher dilutions these membranes are highly selective in acid, where hydrolysis may not occur, and evidence poorer selectivity in salts where it may. There is no comparable argument to show that water transport would be significantly different in salt than in acid.

In the case of the 0.6 | 0.01 *M* potassium chloride chain of Table IV, some comment should be made on an additional effect which obtains when the two concentrations are quite different. Here the two faces of the membrane have rather different degrees of selectivity, the concentrated side of the membrane dominating the selectivity of the over-all system. This effect is in part a function of the thickness of the membrane, since it is the gradient of non-exchange electrolyte in the membrane phase which determines its selectivity. The higher concentration can be so high that this flux of non-diffusible electrolyte moving across the membrane may make for poor selectivity even on the dilute side. Stirring would have a significant effect here.[8] Thicker membranes, in general, show concentration potentials corresponding to the selectivity of the more dilute solution; thin membranes, on the other hand, are more prone to show concentration potentials reflecting higher concentrations. For both membranes, the selectivity of the 0.6 *M* | 0.01 *M* chain lies between those of the 0.8 *M* and 0.2 *M* chains.

Turning from selectivity to specificity, the bionic potentials of Table VI are to be considered. The BIP of a particular membrane system is a measure of the relative transport of the two opposing cations. For the lithium–potassium chain, the BIP varies from −30 to −40 mv., compared to a theoretical BIP of −19 mv. at zero anion transport using the Henderson postulates. These BIP values indicate that the transport numbers of potassium ions in the membrane phase are four to five times as large as those for lithium. Since the mobility of lithium is about half that of potassium in free solution, it may be concluded that the effective concentration in the membrane phase of potassium is twice that of lithium. However, carboxyl membranes are known to concentrate lithium.[9] There may be a steric effect operative here but the phenomena are yet to be explained.

For the calcium–potassium chain, the free cationic diffusion potential is −26 mv., reflecting the greater mobility of potassium. Since the measured

(4) A. G. Winger, G. W. Bodamer and R. Kunin, *J. Electrochem. Soc.*, **100**, 178 (1953).

(5) R. Neihof, THIS JOURNAL, **58**, 916 (1954).

(6) K. Sollner, *J. Electrochem. Soc.*, **97**, 139C (1950).

(7) G. Scatchard, *J. Am. Chem. Soc.*, **75**, 2883 (1953).

(8) H. P. Gregor and D. M. Wetstone, *Trans. Faraday Soc.*, in press.

(9) H. P. Gregor, M. J. Hamilton, R. J. Oza and F. Bernstein, THIS JOURNAL, **60**, 263 (1956).

BIP values are positive and in some cases approach 20 mv., one may calculate that calcium has a transport number which is as much as 10 times that of potassium, again making use of the Henderson postulates, which cannot apply here in a strict sense.[2]

It is of particular interest to note that the BIP for lithium–potassium is affected but slightly by the ohmic resistance of the membrane, while the BIP for calcium–potassium is affected strongly. This may be seen by comparing the results for the membrane series 210, 211, 220. These membranes are in the sequence of decreasing ohmic resistance (and also decreasing thickness). Accordingly, one or both of these factors must play a significant role in these phenomena.

Acknowledgment.—The authors wish to thank the Office of Saline Water, United States Department of the Interior, for the support given this work.

INTERPOLYMER ION-SELECTIVE MEMBRANES. III. PREPARATION AND CHARACTERIZATION OF QUATERNARY AMMONIUM–DYNEL ANION-SELECTIVE MEMBRANES

BY DAVID M. WETSTONE[1] AND HARRY P. GREGOR

Contribution from the Department of Chemistry of the Polytechnic Institute of Brooklyn, New York

Received July 19, 1956

Interpolymer anion-selective membranes were prepared by casting a film from a solution containing polyvinylimidazole quaternarized with methyl iodide, Dynel (a copolymer of acrylonitrile and vinyl chloride), and a suitable solvent. Films of varying thickness (1–30 μ) and polyelectrolyte–Dynel ratios (1/5 to 1/1) gave ohmic resistances upwards from 5 ohm-cm.^{2} in 0.1 M potassium chloride. The concentration potentials (0.2 M|0.1 M potassium chloride) of some of the better membranes varied from −15.5 to −15.8 mv., as compared to the theoretical maximum of −16.1, showing a small cation leak. The interstitial molality of these membranes was calculated to be in the range 2.1 to 5.7. Osmotic flow rates using 1 M sugar also were measured. Bi-ionic potential measurements showed the membranes to transport chloride ion preferentially to iodate ion, but this may result from the operation of steric factors. The data are discussed and compared to those obtained with cation-selective membranes.

Introduction

This paper is the third in a series[2,3] describing the synthesis and characterization of interpolymer ion-selective membranes. The present contribution reports a membrane formed from a solution of polyvinylimidazole quaternarized with methyl iodide, Dynel and either N,N-dimethylformamide or dimethyl sulfoxide. The active exchange material (the quaternarized imidazole) functions as a strong base anion exchanger.

Experimental

The characterization procedures used were exactly those employed in the previous two studies, with such modifications as are noted here. These procedures included determination of thickness, water content, osmotic flow, ohmic resistance, concentration potential and bi-ionic potential. Materials, membrane preparation and determination of exchange capacity differed, as noted below.

Materials.—Polyvinylimidazole (Badische Anilin und Soda Fabrik) was quaternarized in these laboratories with methyl iodide to produce a polymer of 1-vinyl-3-methylimidazolium iodide (QPVI). Conventional techniques were employed, the reactants being refluxed in methanol and the product precipitated and washed with acetone. Details of the preparation and properties of this polybase are described elsewhere.[4] Dynel (DYN), N,N-dimethylformamide (DMF), and dimethyl sulfoxide (DSO) were as previously described.[2]

Membrane Preparation.—Preparative techniques were similar to those previously reported; since QPVI was quite slow to dissolve in DMF (somewhat faster in DSO), complete dissolution to form appropriate casting solutions usually required three to five days. Membranes were formed on glass plates with a Boston Bradley Blade as before, with the drying temperature reduced to 50° to preclude any decomposition of the imidazole group, thereby requiring about 96 hours for drying to occur. Stripping the membranes required prolonged soaking in water (30 minutes or more) to avoid tearing. Conditioning and storing in potassium chloride were employed as before.

Exchange Capacity.—The chloride form membranes were first washed with water to remove diffusible salt, then treated with a large excess of 1 M potassium nitrate for 24 hours. The decanted solution was titrated potentiometrically with standard silver nitrate using a silver–silver chloride electrode. Available capacity is reported as per cent. of the theoretical maximum, calculated from the composition of the casting solution and the dry weight, and also as milliequivalents per unit area of membrane. In addition, the molality of the active groups is calculated and reported, based upon the determined interstitial water content.

Results

In Table I are listed characterization data on a number of representative membranes. Thickness, resistance and concentration potential measurements were made on membranes equilibrated with 0.1 M potassium chloride (except the dilute Co.P., which employed 0.01 M potassium chloride). The table indicates the general effects noted with variation of polyelectrolyte to matrix weight ratio (P/M), thickness and solvent. Concentration potentials are to be compared to the theoretical maxima, as given.[2]

Titrable exchange capacity, water content, shrinkage and interstitial molality are listed in Table II for four membranes, differing primarily in the proportion of polyelectrolyte to matrix material employed.

In Table III are listed osmotic flow data for four additional, selected membranes, together with some

(1) Taken in part from material which was submitted in partial fulfillment of the requirements for the degree of Doctor of Philosophy in Chemistry at the Polytechnic Institute of Brooklyn.

(2) H. P. Gregor, H. Jacobson, R. C. Shair and D. M. Wetstone, THIS JOURNAL, **61**, 141 (1957).

(3) H. P. Gregor and D. M. Wetstone, *ibid.*, **61**, 147 (1957).

(4) H. P. Gregor and D. H. Gold, in preparation.

TABLE I

GENERAL CHARACTERIZATION DATA FOR SOME QPVI–DYN INTERPOLYMER MEMBRANES

(Theor. max. Co.P.: 0.2|0.1 *M* KCl, −16.11 mv., 0.02|0.01 *M* KCl, −16.87 mv.)

No.	P/M	Solvent	Thickness, μ	Ω Resistance, ohm-cm.²	Concn. potential (Co.P.) 0.2|0.1 *M* KCl, mv.	0.02|0.01 *M* KCl, mv.
176	1/5	DMF	30	930	−15.80	−16.66
179	1/4	DMF	29	366	−15.78	−16.67
182	1/3	DMF	29	52	−15.81	−16.72
184	1/3	DMF	8	22	−15.71	−16.72
225	1/3	DMF	3	139	−15.55	−16.01
229	1/3	DMF	~1	17.9	−14.99	.....
230	1/3	DSO	5	176	−15.25	.....
231	1/3	DSO	~1	5	~−11.3	.....
185	1/2	DMF	29	15.7	−15.70	−16.70
215	1/1	DMF	24	13.7	−15.29	−16.76

TABLE II

CAPACITY AND WATER CONTENT OF SEVERAL QPVI–DYN INTERPOLYMER MEMBRANES

No.	P/M	Thickness, μ	Capacity (meq. cm.⁻²) × 10³	%	H_2O content, %	Interstitial molality	Shrinkage, %
176	1/5	30	1.18	30	8	4.0	0
179	1/4	29	1.90	40	9	5.7	7
182	1/3	29	1.62	29	13	3.5	7
185	1/2	29	1.18	18	16	2.1	14

characterization data. The product of resistance and osmotic flow is shown in the last column.

TABLE III

GENERAL CHARACTERIZATION DATA AND OSMOTIC FLOW RATES FOR SELECTED QPVI–DYN INTERPOLYMER MEMBRANES[a]

No.	P/M	Thickness, μ	Ω Resistance, ohm-cm.²	ω Osmotic flow rate, mm.³/100 cm.²-hr.	$\Omega\omega$
177	1/5	20	1237	<5	<6200
180	1/4	16	149	30.9	4740
183	1/3	16	32	41.5	1330
186	1/2	16	10.5	106	1120

[a] These membranes cast from DMF solutions.

The burst strength of several membranes as measured on a Mullen Burst Strength Tester was about 4 pounds per square inch to the point of stretching, and the pressure at the tear point was about 8, for an average film. Dynel films are not particularly elastic; the elasticity of these films is probably a reflection of the plasticizing action of the QPVI.

Concentration potentials for three of the better membranes were measured over a wide range of potassium chloride concentrations, maintaining a 2:1 concentration ratio between the ambient pairs. These results are listed in Table IV together with the anionic transport numbers, calculated from the theoretical maximum potential which is listed for each pair.[2]

The anion specificity of several selected membranes, *i.e.*, their ability to distinguish between various diffusible anions, is indicated by the bi-ionic potential (BIP) of the chain: 0.01 *M* KIO_3 | Memb. | 0.01 *M* KCl. These BIP values were as follows: membrane 177, 50.77 mv.; 180, 36.28; 182, 28.58; 183, 30.86; 184, 27.75; 225, 43.56; 186, 22.64.

These data should be compared to values of the potential for free diffusion, 7.43 mv., and for free anion diffusion ($u_+ = 0$), 16.66 mv., calculated from various forms of the Henderson equation. For the IO_3^- | Cl^- pair, free diffusion is given by

$$E = -\frac{RT}{\mathfrak{F}} \ln \frac{\Lambda_1}{\Lambda_2}$$

and, when $u_{K^+} = 0$

$$E = -\frac{RT}{\mathfrak{F}} \frac{(t_-\Lambda)_1}{(t_-\Lambda)_2}$$

Transport and conductance data at 25° for potassium iodate (c_1) are difficult to find in the literature. A recent value[5] for the salt conductance at infinite dilution is $\Lambda_0 = 114.3$ and for the iodate ion,[6] $\lambda_0^- = 40.75$. A determination at about 0.01 *M* potassium iodate yielded[7] $\Lambda = 105.8$. Lacking a direct value for t_- in potassium iodate it was assumed that

$$(t_-\Lambda)_1 = \frac{\Lambda}{\Lambda_0}(\lambda_0^-) = \frac{105.8}{114.3}(40.75) = 37.7$$

Taken together with values already established[2] for potassium chloride, theoretical potentials for restricted and free diffusion may be readily calculated.

Discussion

As will be shown later, the iodide ion is strongly bound by the polybase, such as to make it difficult to displace from the membrane phase. Since the question of iodide contamination could be raised in connection with the data reported here, it was established that potassium chloride conditioning removed the last traces of iodide, as shown by the peroxide, carbon tetrachloride test.

In examining Table I, certain general patterns of data are again evidenced, as they were for the previous two membrane types.[2,3] The resistance decreased with increasing P/M ratios, being parallel to an increase in concentration and availability of active sites. The decrease in resistance from P/M = $^1/_5$ to $^1/_1$ is about 67-fold, whereas for the carboxyl membrane it was 1700-fold; this latter can be partly accounted for by swelling. If comparable values of P/M are considered, it is seen that the QPVI membranes range slightly higher in resistance but, concurrently, possess somewhat higher values for the concentration potential also. Whereas a sharp decrease in Co.P. was noted for extreme values of P/M (both high and low) in the carboxyl membranes, an apparently more homogeneous structure here permits the membranes described to manifest rather uniform values. A lower availability of through pores is clearly indicated, although those that are available appear to be well "protected" by active sites. Thus, the presence of a large amount of non-exchange electrolyte in the these membranes appears unlikely.

(5) E. G. Baker and C. A. Kraus, Natl. Bur. Standards Cir. No. 524, 27 (1953).

(6) C. B. Monk, *J. Am. Chem. Soc.*, **70**, 328 (1948).

(7) K. A. Krieger and M. Kilpatrick, *ibid.*, **64**, 7 (1942).

TABLE IV

CONCENTRATION POTENTIALS OF SELECTED QPVI-DYN INTERPOLYMER MEMBRANES AS A FUNCTION OF CONCENTRATION OF POTASSIUM CHLORIDE

	Theor.	No. 180		No. 183		No. 186	
c_1/c_2 *M* KCl	max., mv.	*E*, mv.	t_-	*E*, mv.	t_-	*E*, mv.	t_-
0.002/0.001	−17.43	−16.80	0.982	−16.71	0.979	−17.17	0.993
.008/0.004	−17.14	−16.86	.992	−16.96	.995	−16.86	.992
.02/0.01	−16.87	−16.66	.994	−16.66	994	−16.66	.994
.08/0.04	−16.39	−16.13	.992	−16.13	.992	−16.07	.990
.2/0.1	−16.11	−15.62	.985	−15.58	.984	−15.51	.981
.8/0.4	−15.89	−14.35	.952	−14.95	.970	−13.73	.932
2/1	−17.18	−12.40	.861	−12.05	.851	−12.36	.860
0.6/0.01	−96.6	−94.8	.982	−94.6	.979	−92.7	.960

Variation in membrane thickness (182, 184, 225, 229) and resistance appears initially to be directly proportional, as would be expected; unlike the sulfonic and carboxyl membranes, these amine membranes evidence anomalously high resistances when cast thinner than 8–10 μ. This phenomenon is not attributable solely to the solvent since the use of DSO yielded similar results (230 and 231). High Co.P. values for these unusually high resistance membranes is of course not unexpected. The reasons for these results with such thin membranes are not presently apparent; it may be associated with the ambient relative humidity at the time of casting and initial drying, and with the ease with which solvent evaporates.

Insofar as variation in solvent is concerned, it is seen that no significant alteration of properties is attendant upon substituting DSO for DMF.

The low availability of active sites is further corroborated by the titrable exchange capacities listed in Table II, and the shortage of through pores is demonstrated by extremely small water content and shrinkage. This behavior would appear to result from a blocking of exchange sites by the matrix material; the polyelectrolyte here is not as polar as the polyacids.[2,3]

The osmotic flow results of Table III for four of the better membranes may be compared to the parallel resistance data. First, it should be noted that although resistance and osmotic flow should be directly and inversely proportional, respectively, to thickness exactly the opposite is true here. Undoubtedly, this is largely the result of increasingly enhanced swelling of the membranes with larger polyelectrolyte contents. This effect was also strikingly demonstrated by the previously reported carboxyl membranes. Ideally, the product of resistance and osmotic flow should be roughly constant on the assumption that both phenomena originate with the same factors. Conductance, however, results not only from the gegenions but also from the presence of non-exchange ions within the membrane. High resistance and Co.P. values, even for high P/M membranes, and a relatively small variation of resistance with P/M, have both been postulated as resulting from the presence of fewer, well protected pores. That these pores are few and probably small is further demonstrated by the remarkable impenetrability of the membranes to water, even when P/M increases to $^1/_2$, where relatively low resistance has resulted in a sharp drop in the product $\Omega\omega$.

The Co.P. data of Table IV indicate that even in dilute solutions these membranes do not behave ideally. As previously reported,[3] the PVM/MA (carboxyl) membranes evidenced substantially the same behavior in potassium chloride. However, the possibilities for dissipation of free energy through water transport or increase of non-exchange ions through hydrolysis are not as likely in this case. However, the over-all performance here is somewhat better; the QPVI membranes maintain a fairly constant t_- value of 0.992 until $c_2 = 0.1$ *M* potassium chloride (indicating here the small effect of the Donnan concentration), and even then it does not drop below 0.980. Further, at no concentration does t_- drop below 0.850. The low values of 180 and 183 in 0.001 *M* potassium chloride probably are anomalous. It may be that a small amount of water transport is the causative factor in this case. It is seen that the 0.6|0.01 *M* potassium chloride chain produces substantially the same results here as it did with the carboxyl membranes; the Co.P. developed from a large concentration difference is still clearly a function of the selectivity on the concentrated side.

The anion specificity of these membranes may be examined from their bi-ionic potentials. The BIP here is a function of the relative transport of the opposing anions (iodate and chloride) in the membrane phase. In free anion diffusion ($u_+ = 0$) the current carrying ability of chloride is twice that of iodate. Accordingly, a perfectly selective but non-specific membrane would result in a BIP of 16.7 mv. However, a BIP of over 50 mv. (177) implies an absolute transport advantage of seven-fold for the chloride ion, indicating a definite ion specificity on the part of the membrane.

One could choose to interpret these results either as an advantage in mobility or in effective concentration since both lead to enhanced transport. Steric interference on the part of the membrane pores to the passage of iodate may be the factor, since iodate is considerably larger than chloride. The drop in BIP with decrease in resistance and P/M (*cf.* Tables I and III) is even more marked than is the variation with Co.P. Thus, the results are as would be expected were the movement of iodate enhanced by pore enlargement and increase in number attendant upon lower P/M ratios. The erratic variations in the series 182, 283, 184 are not significant since the resistance varied only between 52 and 22 ohm-cm.^{2}. It is pertinent to this argument that for the anomalous membrane 225 (139 ohm-cm.^{2}) the BIP rose abruptly. It seems therefore likely that any

ion specificity so far demonstrated by this membrane is one of mechanical origin.

Acknowledgment.—The authors wish to thank the Office of Saline Water, United States Department of the Interior, for the support given this work.

PREPARATION AND PROPERTIES OF STRONG BASE TYPE COLLODION MATRIX MEMBRANES

BY MELVIN H. GOTTLIEB,[1] REX NEIHOF[2] AND KARL SOLLNER[3]

Laboratory of Physical Biology, National Institute of Arthritis and Metabolic Diseases and Laboratory of Kidney and Electrolyte Metabolism, National Heart Institute, National Institutes of Health, Public Health Service, Bethesda 14, Maryland

Received December 27, 1955

Strong base type, electropositive collodion matrix membranes of extreme electrochemical activity were prepared by the adsorption of poly-2-vinyl-N-methylpyridinium bromide, called PVMP (quaternized to 65–85% of the theoretical bromine/nitrogen ratio) from aqueous solutions on preformed highly porous collodion membranes whose porosity can subsequently be reduced by drying. The PVMP collodion matrix membranes combine strong base character with the mechanical strength, flexibility and thinness characteristic of collodion membranes. Membranes of high porosity show high anomalous osmotic activity. The most useful permselective membranes give rise to concentration potentials which agree with the calculated thermodynamic maximum potential in potassium chloride cells up to 0.1 *N*/0.05 *N* within the meaningfulness of the method. At higher concentrations the measured potentials become gradually less than the theoretical value. The more highly selective membranes have anion permeabilities which in 0.1 *N* KCl are 500 to 1300 times greater than the cation permeabilities, and 5,000 to 32,000 times greater in 0.01 *N* solutions. With solutions of $CaCl_2$ these ratios are two to three orders of magnitude greater. The ohmic resistances of the permselective membranes of highest selectivity (as measured in 0.1 *N* KCl) may be adjusted from about 10 Ω cm.^{2} upward. The bi-ionic potentials across the permselective PVMP membranes with pairs of the common anions are substantially higher than with the previously described permselective protamine membranes.

Introduction

In a recent paper the preparation and properties of electro-negative strong acid type collodion matrix membranes were described.[4] The present paper outlines the preparation and properties of analogous strong base type collodion matrix membranes. For background references and general considerations concerning membranes of extreme ionic selectivity as well as for many experimental details the reader is referred to the previous paper.[4]

The heretofore most thoroughly studied and most useful anion selective, electropositive membranes were the protamine collodion membranes.[5–7] A minor shortcoming of these membranes is the only moderately strong basic character of their functional groups. More important, their anion permeability, even at the lowest concentrations, was only 30–50 times greater than their cation permeability, and declines sharply at higher concentrations.

Strong base membranes have been described repeatedly.[8,9] Some of these membranes[8] have either excessively low permeabilities for anions or ionic selectivities too low for our purposes. The permeability of some, of an undisclosed mode of preparation,[9] is high, but their selectivity, though good, is not adequate, especially at higher concentrations; their unit area exchange capacity is undesirably high for many physico-chemical applications. Contrary to the situation prevailing generally with collodion matrix membranes, the porosity of these membranes cannot be adjusted readily at will.

The Preparation of Strong Base Type Collodion Matrix Membranes

As in the case of the preparation of strong acid type membranes, most of our efforts to prepare strong base type membranes have been directed toward infixing basic polyelectrolytes in cellulose derivative membranes, particularly in collodion membranes.[4]

Attempts to prepare collodion solutions containing dissolved strong base polyelectrolytes were unsuccessful. Invariably, regardless of the solvents used, a precipitate formed when the polyelectrolyte was added to the collodion solutions. Therefore, one has to rely on the adsorption of the polyelectrolyte from aqueous solution on preformed membranes.

Of the several strong base polyelectrolytes considered, the most conveniently prepared material was poly-2-vinyl-N-methylpyridinium bromide (PVMP)

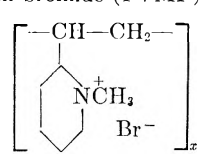

The synthesis should be directed to yield polyelectrolyte ions small enough to enter the pores of the membrane and large enough to be strongly adsorbed and permanently retained within the membrane.

For the preparation of PVMP, 2-vinylpyridine was polymerized by a procedure similar to that given by Harmon.[10] One hundred parts of 2-vinylpyridine (Reilly Tar and Chemical Co.) freshly distilled under nitrogen at 28 mm. pressure, were dissolved in 200 parts of 15% aqueous HCl of room temperature. One part ammonium persulfate catalyst, and

(1) Research Laboratories, Interchemical Corporation, New York 36, N. Y.

(2) Physiological Institute, University of Uppsala, Uppsala, Sweden.

(3) Laboratory of Physical Biology, National Institute of Arthritis and Metabolic Diseases.

(4) R. Neihof, THIS JOURNAL, **58**, 916 (1954).

(5) I. Abrams and K. Sollner, *J. Gen. Physiol.*, **26**, 369 (1943).

(6) C. W. Carr, H. P. Gregor and K. Sollner, *ibid.*, **28**, 179 (1945); H. P. Gregor and K. Sollner, THIS JOURNAL, **50**, 88 (1946); **54**, 325 (1950); *J. Colloid Sci.*, **7**, 37 (1952).

(7) H. P. Gregor and K. Sollner, THIS JOURNAL, **54**, 330 (1950).

(8) K. H. Meyer and J.-F. Sievers, *Helv. Chim. Acta*, **19**, 665 (1936); W. S. Albrink and R. M. Fuoss, *J. Gen. Physiol.*, **32**, 453 (1949); G. Manecke and K. F. Bonhoeffer, *Z. Elektrochem.*, **55**, 475 (1951).

(9) A. G. Winger, G. W. Bodamer and R. Kunin, *J. Electrochem. Soc.*, **100**, 178 (1953).

(10) T. Harmon, U. S. Patent 2,491,472 (Dec. 20, 1949).

one part ethyl mercaptan modifier, were added, the latter to obtain polymers of molecular weights sufficiently low for our purpose. The polymerization mixture was kept under nitrogen at 50° for 48 hours. The resulting somewhat viscous solution was diluted with an equal volume of water; 2 *N* NaOH was added with stirring until the mixture was alkaline. The white gummy mass which separated out was washed with water, redissolved in 1 *N* HCl, filtered and reprecipitated with *N* NaOH. The material obtained was washed with water and redissolved. A final precipitation with NaOH under vigorous stirring yielded a finely divided precipitate which was removed from the solution by decantation and filtration at intervals as it was formed. The purified polyvinylpyridine was dried *in vacuo* at room temperature. It was quaternized by a method similar to that given by Maclay and Fuoss.[11] Two parts of CH_3Br were added to one part of polyvinylpyridine dissolved in 30 parts of dimethylformamide. The mixture was kept in a stoppered flask for two days at room temperature. The solution, together with a small amount of white precipitate which formed, was poured into 100 parts of rapidly stirred dioxane. The resultant gummy product was redissolved in methyl alcohol, reprecipitated in dioxane, washed with ether, and dried *in vacuo*. Analyses for nitrogen and bromine in the various polymer samples so prepared indicate that 65–85% of the pyridine nitrogen was quaternized. No deterioration of the dry polymer in the bromide form was observed after storage for six months.

The membranes described below were prepared with 65–70% quaternized polymers which, as far as investigated, do not differ in their properties from membranes prepared with material with a higher degree (85%) of quaternization.

For the **preparation of membranes of high porosity**, PVMP is adsorbed from aqueous solution on collodion membranes of suitable porosity. The electrochemical activity of the membranes varies with the amount of PVMP taken up. With a given solution of polyelectrolyte this quantity increases with the porosity of the membranes, as discussed in an earlier report.[4] The amount of PVMP taken up by membranes of a given porosity is greater with preparations of lower molecular weight, and with higher concentrations of the PVMP solutions. Other factors which can be expected to influence the adsorption of PVMP to some extent are the *p*H of the PVMP solutions and the presence of inorganic electrolyte in the latter; these variables have not been fully investigated.[4]

The membranes of high porosity were prepared at room temperatures and at relative humidities between 20 and 40% from a 4.0% solution of Collodion Cotton, U.S.P. (Baker) in 50:50 ether–alcohol containing 2% water. The collodion solution was poured, usually in three successive layers, over 25 × 100 mm. test-tubes rotating in a horizontal position.[12] The first layer was dried 3 min., the second 4 min.; 4.5 min. after the third layer was poured the membranes were immersed in water. After being washed for an hour, the membranes were slipped off their casting tubes and reimmersed in water overnight. They were then placed for 2 to 3 days in a 1 to 2% solution of PVMP-bromide, adjusted to *p*H 6 to 7. After being kept in water for a day, the membranes were tied to glass rings and were ready for use. The electrochemical activity of these membranes decreases very gradually over a period of several months, so slowly, however, that even freshly prepared membranes can be considered as being unchanged over a period of several weeks.

The preparation of permselective membranes consists of casting collodion membranes of high porosity followed by adsorption of PVMP and controlled drying. Two layer membranes were routinely prepared. Three minutes after pouring the first layer, the second layer was added, and 4.5 minutes later the membranes were immersed in water which was repeatedly changed. On the following day, the membranes were removed from their casting tubes and immersed for two days in 0.5 to 2% solutions of PVMP at *p*H 6 to 7.[13] They were then washed for a few minutes in distilled water, replaced on their respective casting tubes and dried in air for at least 24 hours. Next, the membranes were placed in water for two hours, removed from their casting tubes, and tied with linen thread to glass rings slipped into their open ends. After being dried again in air for 24 hours, the membranes were placed in 0.1 *N* KCl solution. After an aging period of two days in this solution their properties are virtually constant. These membranes were about 30 μ thick, transparent, glass clear, smooth, and of test-tube shape. Some of these membranes, after two months' storage, were too brittle for use; others have maintained excellent mechanical strength for a year when stored in the dry state in the chloride form or in dilute potassium chloride solutions (to which a preservative such as thymol was added for protection against mold growth) and did not show any changes in their electrochemical properties aside from a very gradual decrease in ohmic resistance. The cause of the differences in the mechanical stability of different membranes is unknown.

The Properties of Strong Base Type Collodion Matrix Membranes of High Porosity

The electrochemical activity of the membranes was determined by the routine method used for this purpose in our laboratory, namely, by the measurement of the extent of anomalous osmosis across them.[14]

A membrane, tied to a glass ring, was filled with an electrolytic solution. A rubber stopper holding a capillary tube (1.25 mm. inside diameter) and a siphon tube provided with a stopcock was firmly inserted in the glass ring, and the membrane placed in a beaker filled with distilled water. The meniscus in the manometer tube was adjusted to a position corresponding to the capillary rise above the outside water level. The rise of the meniscus during the next 20 minutes was taken as the measure of the extent of anomalous osmosis. The experiment was repeated until successive 20 minute readings agreed within 5%.

As measures of the functional porosity of the membranes, the filtration rates and the "sucrose value" were employed. The sucrose value is the osmotic rise in mm. in the capillary manometer 20 minutes after the membrane, filled with 0.25 *M* sucrose solution, is placed in water.[14] Filtration rates are calculated from the rates of passage of a 1 *M* KCl solution through a membrane under a standard hydrostatic head.

Figure 1 shows the pressure rises obtained in a series of anomalous osmosis experiments with a typical PVMP membrane with three electrolytes having the same anion and uni-, bi- and trivalent cations, respectively. The membrane had an accessible area of about 50 cm.^{2}, a sucrose value of 175 mm. and a filtration rate of 2.9 ml./hr. 100 cm.^{2} for a pressure head of 10 cm. water.

The curves of Fig. 1 have the typical N-shape found ordinarily in anomalous osmosis studies.[14,15]

The Properties of Permselective Strong Base Type Collodion Matrix Membranes

A variety of permselective PVMP collodion matrix membranes were prepared and characterized by (a) anion-exchange capacity, (b) water content, (c) the rate of osmotic water movement, (d) the ohmic resistance in contact with 0.1 *N* KCl solution, and (e) the concentration potential in the cell 0.4 *N* KCl | membrane | 0.2 *N* KCl.[4] Following this survey, a few membranes of the types most useful for physico-chemical investigations were studied (1) for their electromotive properties in concentration cells over a wide range of KCl con-

(11) W. N. Maclay and R. M. Fuoss, *J. Am. Chem. Soc.*, **73**, 4065 (1951).

(12) H. P. Gregor and K. Sollner, THIS JOURNAL, **50**, 53 (1946).

(13) There is a typographical error in column 1 of Table II of the paper on "The Preparation of the Strong Acid Type Collodion Matrix Membranes."[4] The values given there for the concentration of sodium polystyrene sulfonate in the solution used for adsorption are too low by a factor of 10.

(14) K. Sollner and I. Abrams, *J. Gen. Physiol.*, **24**, 1 (1940); K. Sollner, I. Abrams and C. W. Carr, *ibid.*, **24**, 467 (1941); **25**, 7 (1941).

(15) K. Sollner, *Z. Elektrochem.*, **36**, 36 (1930) (with numerous references).

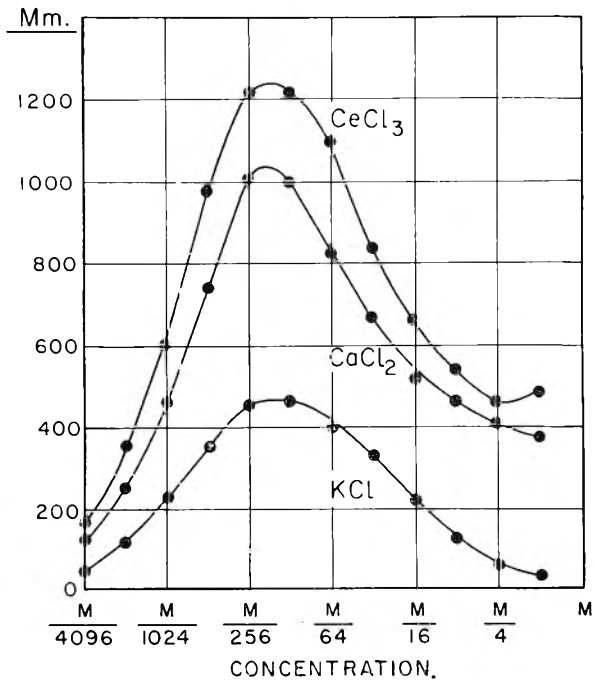

Fig. 1.—Anomalous osmosis across a poly-2-vinyl-N-methylpyridinium collodion matrix membrane.

centrations, (2) for the bi-ionic potentials which arise across them with various pairs of critical ions,[16] and (3) for the rates of exchange of critical ions (anions) and of non-critical ions (cations) across them, as a measure of their absolute permeability and ionic selectivity.

For the survey experiments, five sets of twelve membranes each were cast under as nearly the same conditions as possible. Each set was immersed for 48 hours in an aqueous solution of PVMP bromide varying in concentration from 0.6 to 1.6%. All membranes were washed and dried under the same conditions.

The **anion-exchange capacity** of the membranes was determined with three or four membranes selected at random from each of the five sets. The membranes were slit open lengthwise, and 5.0 × 7.0 cm. rectangles cut from the flat portion were placed in 0.1 *N* KCl solution. The KCl solution was changed several times during a week in order to assure that all accessible fixed charged groups were in the chloride form. Thereafter, the membranes were washed with distilled water for several days until chloride could not be detected in the wash water. The chloride ions in the membranes were then displaced by immersing the latter in 20 ml. of 0.5 *N* $NaNO_3$ solution. After standing three days with occasional stirring, the $NaNO_3$ solution was analyzed for chloride ion and the anion-exchange capacity of the membranes in μeq./cm.^{2} calculated. The dry weights of the membranes (see below) were used to calculate the anion-exchange capacities per gram of dry membrane.

To measure the **water content**, the flat membranes used in the anion-exchange measurements were reconverted to the chloride form, washed, blotted dry with filter paper, placed immediately in tared weighing bottles and weighed in the wet state. They were then dried over phosphorus pentoxide *in vacuo*. The loss in weight was taken as the water content. The reproducibility of the measurements was about ±0.5 g., when the results are expressed as g. water/100 g. wet membrane.

To measure the **rate of osmotic water movement** across a membrane, it was filled with 0.2 *M* solution of sucrose (for which the membranes are virtually impermeable), fitted with a rubber stopper carrying a graduated capillary manometer tube, and placed in a beaker of water at 25.00 ± 0.05°. After thermal equilibrium was reached, the rise of the liquid in the capillary gives the rate of water transport, the reproducibility of these measurements being about ±10%.

The **ohmic resistance** of the membranes in 0.1 *N* KCl solution, ρ^*, was measured at 25.00 ± 0.05° using the Kohlrausch method as previously described.[12] The reproducibility of the membrane resistance from day to day was about ±3%.

The **concentration potential** of the membranes in the series of survey experiments was measured with 0.4 *N* KCl inside and 0.2 *N* KCl outside after they had been kept overnight between solutions of these concentrations. All measurements were made at 25.00 ± 0.05° using saturated calomel half-cells with saturated potassium chloride–agar bridges. With membranes having a resistance of less than about 30 Ω cm.^{2} in 0.1 *N* KCl it was necessary to stir the solutions in order to obtain a steady, reproducible potential. The reproducibility of these measurements was about ±0.05 mv. Because of the asymmetry of the liquid junction potential at the tips of the potassium chloride bridges, the potentials obtained by the outlined procedure are too low by 0.33 mv. All concentration potentials reported in this paper are corrected accordingly.

The concentration potentials across some membranes selected for a more detailed study were determined in cells with potassium chloride solutions at ten concentration levels between 0.001 and 2.0 *N*, the concentration ratio being 2:1. An influence of stirring was not noticeable at any concentration with membranes of ρ^* of several hundred Ω cm.^{2} and more. With membranes having a ρ^* of about 100 Ω cm.^{2} stirring was necessary at concentrations below about 0.2 *N*/0.1 *N*; otherwise, particularly at the lowest concentrations, the potentials were up to 0.5 mv. too low.

The **bi-ionic potential** in cells of the type 0.1 *N* NaCl | membrane | 0.1 *N* NaX, where X may be any anion other than chloride, was measured (with all the precautions described recently elsewhere[17]), using saturated calomel half-cells with saturated potassium chloride–agar bridges. The measurements were reproducible in general within ±0.5 mv. No correction was made for the asymmetry of the liquid junction potentials at the tips of the two agar bridges.

For the measurement of the **rate of exchange of the anions** a membrane filled with a KCl solution containing radioactive Cl^{36} was placed in a large volume of solution of non-radioactive KCl of the same concentration. Both solutions were stirred. Aliquots of the outer solution were periodically withdrawn and their radioactivity determined. The initial rate of anion exchange was calculated from the fraction of the radioactive chloride exchanging for stable chloride per unit time.[18]

The strictly comparable initial **rate of exchange of the cations** can be obtained from analogous experiments only with membranes of very low resistance because of the short half life ($t_{1/2}$ = 12.4 hr.) of the available potassium isotope K^{42}. Instead, with the membranes of the extremely low cation leak of particular interest here, the rate of exchange of cations between an NH_4Cl and a KCl solution of equal concentration was determined by conventional microanalysis. This seems permissible in view of the great similarity in behavior of NH_4^+ and K^+ ions in solution as well as in cation selective membranes, and of the fact that the rates of exchange $K^{39+} \rightleftarrows K^{42+}$ and $NH_4^+ \rightleftarrows K^+$ agreed satisfactorily in the case of those PVMP membranes with which both rates could be determined.

In addition, a few analogous experiments were carried out with $CaCl_2$ solutions in which the rate of exchange of the bivalent non-critical Ca^{++} ions was obtained by the use of Ca^{45} ($t_{1/2}$ = 152 days).

Table I summarizes the properties of representative membranes (about 30 μ thick) prepared by the adsorption of PVMP from aqueous solutions of the various concentrations shown in column 1. Tables II and III are self-explanatory, the sign of the potentials referring to solution 2. Table IV is virtually so; its columns 4, 7 and 10 give the ratios

(16) K. Sollner, THIS JOURNAL, **53**, 1211, 1226 (1949).

(17) S. Dray and K. Sollner, *Biochem. et Biophys. Acta*, **18**, 341 (1955).

(18) A detailed account of the experimental technique is planned for a forthcoming paper on the exchange of ions across permselective membranes: M. H. Gottlieb and K. Sollner, in preparation.

TABLE I

PROPERTIES AND FUNCTIONAL BEHAVIOR OF VARIOUS PERMSELECTIVE POLY-2-VINYL-N-METHYLPYRIDINIUM COLLODION MATRIX MEMBRANES

1 Concn. of PVMP-Br in aq. soln., g./l.	2 Anion-exchange capacity, meq./g.	3 Anion-exchange capacity, μeq./cm.²	4 Water content, %	5 Rate of osmotic water movement (0.2 *M* sucrose), mm.³/hr. 100 cm.²	6 Av. unit area resistance[a] in 0.1 *N* KCl, ρ^* (*t* = 25.00°), Ω cm.²	7 Av. concn. potential[a] 0.4 *N* KCl/0.2 *N* KCl (*t* = 25.00°), mv.
6.0	0.045	0.16	5.8	6.0	440,000 (10,000)	−13.91 (0.92)
8.0	.084	0.30	6.9	11.1	8,000 (7,000)	−15.55 (0.07)
10.0	.104	0.37	7.6	18.7	825 (105)	−15.50 (0.16)
12.0	.200	0.74	7.9	93	165 (35)	−15.41 (0.05)
16.0	.405	1.43	14.4	475	10 (5)	−15.08 (0.18)

[a] Figures in parentheses indicate maximum deviations from the mean value.

of the permeabilities of the anions and cations across the various membranes.

TABLE II

THE CONCENTRATION DEPENDENCE OF THE CONCENTRATION POTENTIALS ($c_1:c_2$ = 2:1) WITH SOLUTIONS OF KCl ACROSS REPRESENTATIVE PERMSELECTIVE POLY-2-VINYL-N-METHYLPYRIDINIUM COLLODION MEMBRANES OF DIFFERENT RESISTANCE (*t* = 25.00 ± 0.05°)

Concn. of electrolyte soln. $c_1:c_2$, equiv./l.	Theor. max., mv.	Membrane resistance in 0.1 *N* KCl, mv. ρ^* = 70 Ω cm.²	ρ^* = 610 Ω cm.²	ρ^* = 7500 Ω cm.²
0.002/0.001	−17.45	−17.17	−17.22	−17.20
.004/0.002	−17.31	−17.15	−17.16	−17.12
.01/0.005	−17.10	−17.09	−17.10	−17.07
.02/0.01	−16.86	−16.73	−16.81	−16.82
.04/0.02	−16.63	−16.48	−16.54	−16.52
.1/0.05	−16.30	−16.09	−16.19	−16.14
.2/0.1	−16.11	−15.73	−15.86	−15.82
.4/0.2	−15.95	−15.37	−15.46	−15.52
1/0.5	−16.32	−14.48	−14.77	−14.61
2/1.0	−17.3	−13.31	−14.02	−13.81

The low **unit area ion-exchange capacity** of the permselective PVMP membranes (Table I, column 3) and their low **water permeability** (column 5) makes them well suited to many physico-chemical studies, as indicated in the introduction.

The **resistances** (Table I, column 6) of the membranes of a given type prepared under nominally identical conditions show substantial variations. Small increments in anion-exchange capacity are accompanied by great differences in resistance.[19]

The degree to which the **concentration potentials** (Table I, column 7) of the membranes deviate from the theoretical maximum at the 0.4/0.2 *N* KCl concentration level can be estimated by comparing them with the calculated theoretical maximum potential, 15.95 mv. Theoretical maximum potentials are computed assuming that the membrane acts electromotively like two ideal chloride electrodes connected by a metallic conductor and that the activity of the chloride ion is equal to the mean activity of potassium chloride. The activity coefficients were taken from the book of Harned and Owen,[20] and converted from the molality to a normality scale.

TABLE III

BI-IONIC POTENTIALS WITH VARIOUS PAIRS OF CRITICAL IONS ACROSS POLY-2-VINYL-N-METHYLPYRIDINIUM COLLODION MATRIX MEMBRANES OF DIFFERENT ELECTRICAL RESISTANCE

(*t* = 25.00 ± 0.05°)

Soln. 1 0.1 *N*	Soln. 2 0.1 *N*	Resistance in 0.1 *N* KCl: Ω cm.² 325	Ω cm.² 650	Ω cm.² 2300	Ω cm.² 4200	Ω cm.² 5900
		Bi-ionic potential, mv.				
NaCl	NaCNS	+58.0	+32.5	+49.6	+68.9	+67.8
NaCl	NaI	+25.8	+20.6	+29.1	+25.6	+29.5
NaCl	$NaNO_3$	+29.5	+15.9	+23.9	+23.4	+42.1
NaCl	NaBr	+13.9	+10.1	+13.5	+14.5	+16.3
NaCl	NaCl	± 0.00	± 0.00	± 0.00	± 0.00	± 0.00
NaCl	$NaBrO_3$	− 5.2	− 6.9	− 6.5	− 5.4	− 4.4
NaCl	Na Formate	−18.5	−18.0	−20.8	−19.4	−13.9
NaCl	Na Benzoate	−41.0	−30.2	−40.7	−40.4	−57.2
NaCl	$NaIO_3$	−53.7	−37.2	−47.4	−47.9	−81.2
NaCl	Na Acetate	−53.1	−40.2	−48.1	−50.1	−69.7
NaCl	Na Propionate	−61.0	−44.5	−58.9	−59.4	−87.8
NaCl	Na Butyrate	−66.6	−49.0	−62.6	−64.5	−94.5

Discussion

With the PVMP membranes of high porosity, the maximum pressure rises in the anomalous osmosis experiments occur in the same concentration range as with the sulfonated polystyrene collodion membranes[4] but with considerably more dilute solutions than with protamine collodion membranes of similar general characteristics which were studied earlier.[5] A satisfactory explanation of this observation is lacking.

(19) The standard resistances of 0.10 *N* KCl reported in the paper on the strong-acid membranes[4] were obtained with a faulty technique; the data given there are approximately 15–20 ohm cm.² too high. The inner electrode of the conductance cell had not been fitted with a glass ring for the blank measurement in absence of the membranes.

(20) H. S. Harned and B. Owen, "The Physical Chemistry of Electrolytic Solutions," 2nd Ed., Reinhold Publ. Corp., New York, N. Y., 1950.

TABLE IV

THE RATES OF MOVEMENT OF CRITICAL AND NON-CRITICAL IONS ACROSS SEVERAL PERMSELECTIVE POLY-2-VINYL-N-METHYL-PYRIDINIUM COLLODION MATRIX MEMBRANES AT VARIOUS CONCENTRATION LEVELS IN THE SYSTEM

KCl (c_1)||NH_4Cl (c_1)

	2	3	4	5	6	7	8	9	10
	Concentration								
	1.0 N			0.1 N			0.01 N		
Membrane ρ^*, Ω cm.²	Initial rate of movement of Cl^-, μeq./hr. cm.²	Initial rate of movement of NH_4^+, μeq./hr. cm.²	Ratio of initial rates of movement of Cl^- to NH_4^+	Initial rate of movement of Cl^-, μeq./hr. cm.²	Initial rate of movement of NH_4^+, μeq./hr. cm.²	Ratio of initial rates of movement of Cl^- to NH_4^+	Initial rate of movement of Cl^-, μeq./hr. cm.²	Initial rate of movement of NH_4^+, μeq./hr. cm.²	Ratio of initial rates of movement of Cl^- to NH_4^+
9500	0.146	5.8×10^{-3}	25	0.133	19×10^{-5}	700	0.114	8.1×10^{-6}	14,000
900	4.42	0.37	12	2.96	5.4×10^{-3}	550	1.88	3.4×10^{-4}	5,600
330	6.55	0.16	41	5.08	3.9×10^{-3}	1,300	3.15	9.8×10^{-5}	32,000
160	27.2	2.47	11	18.2	3.8×10^{-2}	480	8.7	1.05×10^{-3}	8,300
16	218	59	3.7	107	0.765×10^{-1}	140	43	1.43×10^{-2}	3,000

Table II on the concentration dependence of the concentration potential shows that the potentials at the lowest concentrations are 0.2 to 0.3 mv. below the calculated maximum; at 0.01/0.005 *N* and 0.02/0.01 *N* the agreement is perfect within the accuracy of the measurements[21]; with more concentrated solutions the deviation becomes greater. The electromotive behavior of the permselective PVMP membranes in this series of concentration cells is virtually the same (with negative sign) as that of the analogous strong-acid type membranes.[4] Electromotively, and therefore also with respect to ionic selectivity, the PVMP membranes are considerably superior to previously described anion selective membranes.

Table III shows that the **bi-ionic potentials** across the various permselective PVMP membranes differs widely with the nature of the critical ions. The bi-ionic potentials with the same pair of critical ions differ for different membranes. There is no clearcut correlation between membrane resistance and absolute magnitude of the bi-ionic potentials; generally, higher potentials tend to arise with membranes of higher resistance. If for each membrane the various anions are arranged (as in Table III) in the order of their relative electromotive efficacy, the resulting sequence is the Hofmeister series. With some of the membranes, as in many other situations where the anion series comes into play, the I^- and the NO_3^- ions, and IO_3^- and acetate ions appear in reversed order. In all these respects the PVMP membranes are similar to all other anion selective membranes of high selectivity which have been studied, particularly to the permselective protamine collodion membranes which were investigated in some detail.[17] The absolute magnitude of the bi-ionic potentials across the PVMP collodion membranes, however, is considerably greater than with the protamine collodion membranes, a point of some significance in certain model studies, in which large differences in the behavior of different ions are desirable.

Columns 2, 5 and 8 of Table IV show that the **initial rate of movement of the critical ions,** the anions, across the various membranes shows a rough inverse proportionality to their standard resistances shown in column 1.[22]

(21) The slightly higher discrepancy between calculated and experimental potential values at the lowest concentrations (found also with permselective protamine collodion membranes[7]) is not to be expected on the basis of existing theories. It deserves further investigation.

The **initial rate of movement of the non-critical ions,** the cations, (columns 3, 6 and 9) shows a considerably steeper inverse relationship with the standard membrane resistance.

The rates of exchange of the critical ions across a given membrane in 0.01 and 1 *N* solution differ by a factor of about 1.3 with the membrane of the highest standard resistance to a factor of about 5 with a membrane of extremely low resistance. The rate of exchange of the non-critical ions varies over the same concentration interval by a factor of about 700 for the membrane with the highest resistance, to a factor of about 4000 for the lowest resistance membrane.

The **ionic selectivities** of the various permselective membranes, that is, the ratio of the initial rates of exchange of critical over non-critical ions (columns 4, 7 and 10 of Table IV) are very much greater at the lower than at the higher concentrations, in agreement with all previous experience. The correlation between membrane resistance and selectivity is not straightforward; the best membrane with a selectivity of 32,000:1 in 0.01 *N* KCl solution is of medium resistance. The degree of ionic selectivity of the permselective PVMP membranes approaches, but does not quite reach, that of the analogous permselective sulfonated polystyrene collodion membranes.[4]

The selectivities of permselective PVMP membranes, in the presence of univalent anions and bivalent cations (not shown in the tables), as determined with 0.1 *N* $CaCl_2$ solutions containing radioactive Ca^{45}, were found to be of the order of several hundred thousand to one. With more dilute solutions this selectivity can be safely assumed to be even higher.

The small "leaks" of non-critical ions which correspond to these high ionic selectivities (numerically their reciprocals) circumscribe the conditions under which these membranes can be used without significant disturbances due to this imperfection.

Aside from their many other potential uses, some of which were referred to in the introduction, the development of anion selective permselective membranes of extreme ionic selectivity makes possible

(22) The numerical correlation between membrane resistance and rate of exchange of critical ions predicted by the Nernst–Einstein equation (and found with the permselective sulfonated polystyrene and with the protamine collodion membranes) is lacking with the PVMP membranes as well as with membranes prepared with several other strong-base polyelectrolytes. This topic will be treated in a separate paper.

the investigation, of particular interest in the electrochemistry of membranes, of concentration cells of the type c_1AX | ← ⊖ → | c_2AX | ← ⊕ → | c_1AX in which both the anion selective ← ⊖ →, and the cation selective membrane ← ⊕ → are of practically ideal ionic selectivity. The accurate quantitative study of such cells with membranes of insignificantly low leak (for which some data are contained in this and a preceding paper[4]) should be helpful in elucidating the basic differences between conventional and membrane concentration cells, namely, that in the membrane cells one is dealing with the transfer of hydrated ions, with osmotic and electroösmotic movement of solvent, and with a solvent whose ionic character gives rise to membrane hydrolysis.

THE TRANSITORY OVERSHOOTING OF FINAL EQUILIBRIUM CONCENTRATIONS IN MEMBRANE SYSTEMS WHICH DRIFT TOWARD THE GIBBS-DONNAN MEMBRANE EQUILIBRIUM

BY REX NEIHOF[1] AND KARL SOLLNER

Laboratory of Physical Biology, National Institute of Arthritis and Metabolic Diseases, National Institutes of Health, Public Health Service, Bethesda 14, Maryland

Received July 19, 1956

The existence of a transitory effect is postulated, which must arise in the course of the spontaneous drift toward the Gibbs-Donnan membrane equilibrium of systems in which two or more species of ions of the same charge coexisting in one solution exchange at greatly different rates across a membrane of high anionic or high cationic selectivity against some other species of ions in the other solution. On the basis of a consideration of the partial membrane equilibrium which would arise if the ratio of the intrinsic competitive permeabilities of any two species of ions coexisting in solution 1 were infinitely high, it can be predicted that a much faster exchanging species of ions in an experimental system which drifts toward the membrane equilibrium will reach, for a transitory period, a concentration in solution 2 which may be far in excess of that obtained in the state of the final, true membrane equilibrium. Similarly, the concentration of a species of ions existing in solution 2 may be lowered for a transitory period to a value well below that corresponding to the final true equilibrium state. The existence of these overshooting and depletion effects was verified experimentally in several systems with permselective collodion matrix membranes. In one instance the more readily exchanging ion reached in solution 2 a concentration about 250% above that corresponding to the final equilibrium state. In a depletion experiment the concentration of one species of ions in solution 2 was reduced to about one-half that corresponding to the final equilibrium. The possible biological significance of the overshooting and depletion effects is briefly discussed.

Introduction

In an earlier paper we have postulated and proved experimentally the occurrence of greatly different rates of permeation of ions of the same sign of charge across porous membranes of extreme ionic selectivity in systems such as System 1 which (for the case of exclusively cation-permeable anion-impermeable membranes of ionic character, | ← ⊕ → |) are represented by the scheme

Solution 1		Solution 2	
A^+X^-			
B^+X^-	← ⊕ →	L^+X^-	
C^+X^-		M^+X^-	(System 1)
etc.		etc.	

where A^+, B^+, C^+, etc. and L^+, M^+, etc., represent the exchangeable (permeable) ions, X^- the non-exchanging anions.[2] (Anionic systems with exclusively anion permeable membranes, | ← ⊖ → |, are analogous.)

The ratios of the rates of penetration, that is, the ratios of the net fluxes, of any two coexisting species of permeable (univalent) ions being present simultaneously in the one or in the other solution, ϕ_{A^+}/ϕ_{B^+}, ϕ_{B^+}/ϕ_{C^+}, ϕ_{L^+}/ϕ_{M^+}, etc., can be predicted on the basis of independent electrometric measurements in simple systems (with the same membrane) of the type of systems 2

Solution 1		Solution 2	
$a_1A^+X^-$	← ⊕ →	$a_1B^+X^-$	(System 2a)

Solution 1		Solution 2	
$a_1B^+X^-$	← ⊕ →	$a_1C^+X^-$	(System 2b)

etc. (and analogous systems with exclusively anion permeable membranes).[2]

For the potential arising in such systems, the so-called "bi-ionic" potential, one may write

$$E = \frac{+RT}{F} \ln \frac{\tau^\circ_{A^+}}{\tau^\circ_{B^+}} \qquad (1)$$

when $\tau^\circ_{A^+}$ and $\tau^\circ_{B^+}$ represent the transference numbers within the transition zone (membrane) of A^+ and B^+, any two permeable species of ions under consideration, the sign of the potential referring to solution 2.[3]

The ratios $\tau^\circ_{A^+}/\tau^\circ_{B^+}$, $\tau^\circ_{L^+}/\tau^\circ_{C^+}$, etc., obtained in this manner were shown to be numerically identical with the ratios of the initial flux rates of the same ions in systems of the type of system 1 in which the various coexisting species of ions in solution 1 (or in solution 2) are present at the same activity, $\phi^\circ_{A^+}/\phi^\circ_{B^+}$, $\phi^\circ_{B^+}/\phi^\circ_{C^+}$, etc.

$$\frac{\tau^\circ_{A^+}}{\tau^\circ_{B^+}} = \frac{\phi^\circ_{A^+}}{\phi^\circ_{B^+}}; \quad \frac{\tau^\circ_{B^+}}{\tau^\circ_{C^+}} = \frac{\phi^\circ_{B^+}}{\phi^\circ_{C^+}}; \quad \text{etc.} \qquad (2a,b)$$

These ratios may be considered as the ratios of the intrinsic competitive permeabilities (across a given membrane) of any two coexisting species of critical ions under consideration.[2-5] They can be as high as 1:100 and more.

(1) Physiological Institute, University of Uppsala, Uppsala, Sweden.

(2) R. Neihof and K. Sollner, *Disc. Faraday Soc.*, in press.

(3) K. Sollner, THIS JOURNAL, **53**, 1211, 1226 (1949).

(4) S. Dray and K. Sollner, *Biochim. Biophys. Acta*, **18**, 341 (1955).

(5) S. Dray and K. Sollner, *ibid.*, **21**, 126 (1956); **22**, 213, 220 (1956).

If in systems of the type of system 1, the ratio of the activities of any two species of exchangeable ions in solution 1 or in solution 2 is not 1:1, the ratio of their initial net fluxes across the membrane, ϕ_{A^+}/ϕ_{B^+}, ϕ_{B^+}/ϕ_{C^+}, etc., are equal to the corresponding ϕ° ratio times the ratio of the activities in solution 1, $a^{(1)}$, or in solution 2, $a^{(2)}$, as the case may be, of the two ions under consideration, according to equations of the type

$$\frac{\phi_{A^+}}{\phi_{B^+}} = \frac{\phi^\circ_{A^+}\, a_{A^+}{}^{(1)}}{\phi^\circ_{B^+}\, a_{B^+}{}^{(1)}}; \quad \frac{\phi_{B^+}}{\phi_{C^+}} = \frac{\phi^\circ_{B^+}\, a_{B^+}{}^{(1)}}{\phi^\circ_{C^+}\, a_{C^+}{}^{(1)}}; \quad \frac{\phi_{L^+}{}^{(2)}}{\phi_{M^+}{}^{(2)}} = \frac{\phi^\circ_{L^+}\, a_{L^+}{}^{(2)}}{\phi^\circ_{M^+}\, a_{M^+}{}^{(2)}}; \ \ldots \text{ etc.} \quad (3a\text{-}c)$$

In the course of time systems of the type of system 1 drift to the Gibbs–Donnan membrane equilibrium, provided that the movement of solvent is insignificantly slow, or that osmotic equilibrium is maintained by the addition of the proper concentration of non-diffusible non-electrolyte or by the application of hydrostatic pressure to the more dilute solution. In the final equilibrium state the ratios of the activities of all permeable ions in solution 1 are identical with the ratios of their activities in solution 2 according to equation 2 or its analog for anions

$$\frac{a_{A^+}{}^{(1)}}{a_{A^+}{}^{(2)}} = \frac{a_{B^+}{}^{(1)}}{a_{B^+}{}^{(2)}} = \frac{a_{C^+}{}^{(1)}}{a_{C^+}{}^{(2)}} = \frac{a_{L^+}{}^{(1)}}{a_{L^+}{}^{(2)}} = \ldots \text{ etc.} \quad (4)$$

where the $a^{(1)}$ and $a^{(2)}$ terms refer to the activities of various ions, A^+, B^+, etc., in the *equilibrium* solutions 1 and 2, respectively.

In the present paper we postulate and demonstrate experimentally the existence of an interesting and heretofore not explicitly described effect which must arise in the course of the spontaneous drift toward the Gibbs–Donnan membrane equilibrium of systems in which two or more species of ions of the same charge in solution 1 exchange at greatly different rates against some other species of ions in solution 2.

This effect, it might be added, is of a general nature. It is not restricted to any particular mechanism by which a system may drift toward a Gibbs–Donnan equilibrium; it can occur with "oil" membranes as well as with porous membranes. Aside from its purely physico-chemical interest it might be of significance in the preferential accumulation of ions against concentration gradients by living cells.

Theoretical

Consider a system, system 3, with an ideally cation selective membrane which in the initial non-equilibrium state, state I, corresponds to the following scheme (which for simplicity's sake is written in terms of concentration rather than in terms of activity)

Solution 1		Solution 2	
A^+X^- 0.005 N B^+X^- 0.005 N C^+X^- 0.005 N	←⊕→	C^+X^- 0.060 N	(System 3, State I)

Initial State: State I

The volume of solution 1 is so large compared with that of solution 2 that its composition can be considered as constant. The water permeability of the membrane is negligibly small (or the system may be equilibrated osmotically as stated before).

We assume now that the rate of exchange of A^+ against C^+ is exceedingly high compared with the rate of exchange of B^+ against C^+ or A^+. In this case, as pointed out by Donnan,[6] a partial membrane equilibrium fulfilling the requirements of equation 4 is established with respect to A^+ and C^+ ions before a significant quantity of B^+ ions have penetrated across the membrane (state II)

Solution 1		Solution 2	
A^+X^- 0.005 N B^+X^- 0.005 N C^+X^- 0.005 N	←⊕→	A^+X^- 0.030 N C^+X^- 0.030 N	(System 3, State II)

State of Partial Equilibrium: State II

If we wait long enough (remove from our system the restriction that the B^+ ion cannot exchange at a significant rate across the membrane), our system will degrade spontaneously until State III, the true Gibbs–Donnan equilibrium, is reached, in which equation 4 applies to all species of cations

Solution 1		Solution 2	
A^+X^- 0.005 N B^+X^- 0.005 N C^+X^- 0.005 N	←⊕→	A^+X^- 0.020 N B^+X^- 0.020 N C^+X^- 0.020 N	(System 3, State III)

Gibbs–Donnan Equilibrium: State III

A comparison of the concentrations in states II and III of the A^+ ions in solution 2 shows that the transitory overshooting effect in system 3 amounts to 50% of the final equilibrium concentration.

Finally we consider the experimentally readily realized case, that the A^+ and the B^+ ions exchange simultaneously across the membrane but at different rates. With the A^+ ion being the more readily exchanging ion, the system drifts through a sequence of states in which the concentration of A^+ in solution 2 will be between those described by the states II and III, (while the concentration of B^+ in solution 2 will be below that of the state III) until the final membrane equilibrium of state III is reached. This means that the concentration of the faster exchanging A^+ ion will transitorily exceed in solution 2 the concentration which corresponds to the true equilibrium of state III. If the ratio of the intrinsic permeabilities of the two competing species of ions, $\phi^\circ_{A^+}/\phi^\circ_{B^+}$, is high, this "overshooting effect" can be expected to amount to a considerable fraction of that calculated for the hypothetical condition of an infinitely high ϕ° ratio.

Systems in which the coexisting species of permeable ions are present in solution 1 not at the same concentration (as they are in System 2) but at different concentrations, are analogous. They drift through an intermediate state of partial equilibrium, fulfilling the conditions of equation 2 with respect to two species of permeable ions, until they reach the final equilibrium in which equation 4 holds true with respect to all ions of the same charge. A consideration of equation 4 leads for such systems to the conclusion that the overshooting effect in solution 2 will be, percentagewise, greater the lower the relative concentration of the overshooting ion in solution 1.

The converse of the transitory overshooting effect is the transitory depletion of an ionic species from a higher concentration level to a concentration

(6) F. G. Donnan, *Chem. Revs.*, **1**, 73 (1924).

below that corresponding to the final state of true equilibrium.

Consider the (anionic) system, system 4

Solution 1		Solution 2	
X^+A^- 0.015 N |	⟷	| X^+A^- 0.030 N	(System 4,
X^+B^- 0.030 N |		| X^+C^- 0.060 N	State I)

Initial State: State I

The volume of solution 1 is infinitely large. The rate of exchange of B^- for A^- is exceedingly fast compared to the rate of exchange of A^- against C^- as well as of B^- against C^-. The system, therefore, degrades first to the partial equilibrium of state II in which the ratio of the concentrations of A^- and B^- are the same (1:2) in both solutions.

Solution 1		Solution 2	
X^+A^- 0.015 N |	⟷	| X^+A^- 0.010 N	(System 4,
X^+B^- 0.030 N |		| X^+B^- 0.020 N	State II)
		| X^+C^- 0.060 N	

State of Partial Equilibrium: State II

State II in time degrades, at a much lower rate, to the true equilibrium state, state III in which the concentration of C^- in solution 2 (and also in the infinite volume of solution 1) is zero.

Solution 1		Solution 2	
X^+A^- 0.015 N |	⟷	| X^+A^- 0.030 N	(System 4,
X^+B^- 0.030 N |		| X^+B^- 0.060 N	State III)

Gibbs–Donnan Equilibrium: State III

The concentration of X^+A^- in solution 2, which in the initial system, state I, is the same as in the final stable Gibbs–Donnan equilibrium of state III, 0.03 N, drops in state II to a much lower level, 0.01 N, which in this instance is also lower than the concentration in solution 1.

Overshooting and depletion effects can, of course, occur with different ions in the same system. A given ionic species may go successively through phases of overshooting and of depletion as the system drifts toward final equilibrium. We add to solution 1 of the previous anionic system an ionic species D^-, the exchange of which against any other ions is very slow compared with all other exchange processes in system 5

Solution 1		Solution 2	
X^+A^- 0.015 N |	⟷	| X^+A^- 0.030 N	(System 5,
X^+B^- 0.030 N |		| X^+C^- 0.060 N	State I)
X^+D^- 0.045 N |			

Initial State: State I

With the volume of solution 1 infinitely large, system 4 drifts first through one state of partial equilibrium, state II, which is identical with state II of system 4, later through a second state of partial equilibrium, state III, identical with state III of the system 4, and finally reaches the true equilibrium state, state IV, in which (in this particular case) solution 2 has the same composition as solution 1.

Experimental

In proving experimentally the existence of the transitory overshooting and depletion effects it is necessary to construct systems which show within a reasonable period not only the overshooting or the depletion effect to a pronounced degree, but also the much slower disappearance of these effects as the systems drift toward the final equilibrium. In such experiments, all changes in the concentration in solution 2 of the ion or ions under consideration should occur essentially undisturbed by such effects as leakage of nominally impermeable ions, water movement, etc. Sizable effects can be expected only if the ratios of the intrinsic competitive permeabilities of the ions studied are fairly high.

By far the most suitable membranes for such experiments are the permselective collodion matrix membranes,[7] particularly the more recently described types, the strong acid, exclusively cation permeable sulfonated polystyrene collodion membranes,[8] and the analogous strong base, exclusively anion-permeable poly-2-vinyl-N-methylpyridinium collodion membranes.[9]

The practical problem is to select membranes with a suitable combination of properties in which the somewhat antagonistic requirements of the planned experiments are balanced. For instance, high ratios of the intrinsic competitive permeabilities of coexisting species of ions tend to occur with membranes of fairly high resistance which yield low rates of exchange of these ions across their thickness. Membranes of lower resistance which allow a fast exchange of ions, tend to show low ratios of intrinsic competitive permeabilities. The information available on the permselective membranes with respect to their ionic selectivity (absence of exchange of nominally impermeable ions), their water permeability, the rate of exchange of various permeable species across them, and the ratios of the intrinsic competitive permeabilities across them of various combinations of ions, etc., makes it possible to select systems suitable for the planned experiments.

The membranes were test tube shaped (25 × 100 mm.) and mounted on glass rings for easy handling.[8,9] They were tested by our standard methods (a) for their ohmic resistance, ρ^*, in 0.1 N KCl as an indication of the rates at which ions exchange across them, and (b) their electromotive properties in the concentration cell 0.4 N KCl/membrane/0.2 N KCl as a measure of their ionic selectivity. Membranes with resistances ρ^* of 30 to 300 ohm-cm.^{2} were considered potentially suitable. The concentration potentials, corrected for the asymmetry of the liquid junction potentials at the tips of the saturated KCl bridges used in the measurements, were in no instance more than 0.6 mv. below the theoretical maximum potential of ±15.95 mv., the plus sign referring to the selectively cation-permeable, the minus sign to the selectively anion-permeable membranes.

To determine the ratio of the intrinsic competitive permeabilities of any two species of ions across a given membrane the corresponding bi-ionic potential in a system like system 2a or 2b was measured by the Poggendorf compensation method (using saturated calomel half-cells with saturated KCl–agar bridges as reference electrodes) and evaluated according to equations 1 and 2.[3,4]

The experimental arrangement consisted essentially of a membrane containing a known volume of solution 2, which was inserted in a vessel through which solution 1 was flowed continuously at a rate rapid enough to keep its composition virtually unchanged, both solutions being stirred by streams of air bubbles.

During the rather prolonged experiments small but appreciable quantities of water entered the compartment of solution 2 from the outside due to the higher water activity of solution 1. In order to obviate any corrections for this effect, the volume of solution 2 was kept constant by regulating the stream of air (dried by passing it through a $CaCl_2$ column) which was used for stirring.

The speed at which an experimental system with a given membrane and solutions of given compositions drifts toward equilibrium is proportionate to the ratio of the effective membrane area to the volume of the inside solution 2. For practical reasons, therefore, the volume of this solution should be small. To achieve this, a test tube-shaped glass bulb was mounted coaxially inside the membrane by means of a rubber stopper inserted in the glass ring on which the membrane was mounted; this stopper was also provided with an inlet and an outlet tube for the air used in stirring.

For an experiment, the annular space between the membrane (of about 50 cm.^{2} effective area) and the glass bulb was filled with a known volume (11–17 ml.) of solution 2, so that the latter reached a level above the bottom of the glass ring. The membrane was mounted in solution 1 and both solutions were stirred. To establish a stationary or near-stationary state with respect to the distribution of ions

(7) K. Sollner, *J. Electrochem. Soc.*, **97**, 139C (1950); *Ann. N. Y. Acad. Sci.*, **57**, 177 (1953).

(8) R. Neihof, THIS JOURNAL, **58**, 916 (1954).

(9) M. Gottlieb, R. Neihof and K. Sollner, *ibid.*, **61**, 154 (1957).

within the membrane, a period of one to three hours (depending on the permeability of the membrane) was allowed to elapse before the solution inside the membrane was withdrawn and replaced by a measured amount of fresh solution 2. The moment of this replacement was taken as the zero time of the experiment proper. The experiments were carried out at room temperature, between 22 and 25°.

After measured intervals aliquots of the inside solution were removed with micropipets and analyzed for the ions entering from the outside solution.

Thiocyanate was determined colorimetrically at 460 mμ using $Fe(NO_3)_3$ acidified with HNO_3 to develop a color.[10] In order to avoid interferences due to other ions the standards used had approximately the same ionic composition as the unknowns.

The acetate analyses were made by a displacement titration in 90% or more of acetone with standard HCl (in 75% ethyl alcohol) using neutral red as an indicator.[11]

Lithium was determined by standard flame photometric techniques using a Beckman flame attachment with a Beckman Model DU spectrophotometer.

Hydrogen ion was titrated with standard NaOH solution. In the samples containing ammonium ion the end-point was determined (with a universal indicator) by comparison with the color of a solution containing approximately the same concentration of ammonium.

The accuracy of the analyses was in all cases better than ±5%.

All experimental data are presented below as obtained without correction for the small changes in the ratio of membrane area to volume of solution 2 which are due to the removal of liquid for analysis (never more than 10% in any experiment) and to small changes in total concentration which might have arisen because of lack of accuracy in the balancing of the osmotic inflow of water into solution 2 with the loss of water by the evaporation caused by the stirring with dry air.

In view of the low concentrations used, the similarity of the activity coefficients pertaining to the various ions in each system, and the limited accuracy of the analysis, all results are expressed on a concentration rather than on an activity basis, as are also all partial and final equilibria.

While these factors might impose some limitation in any attempt at a kinetic evaluation of the experimental data, their influence is of no consequence in the problem at hand—the demonstration of the postulated overshooting and depletion effects.

Figures 1a–1c show three examples of the overshooting effect. The system of Fig. 1a is the anionic analog of the cationic system 3, magnesium salts being used to minimize cation leakage. The system of Fig. 1d, showing an instance of the depletion effect, corresponds to system 4. The experimental points pertaining to the ions that show the overshooting or depletion effect are connected by a heavy solid line, the corresponding partial and final equilibrium concentrations are indicated by dotted lines. The experimental points pertaining to the simultaneously exchanging ions are connected by light solid lines; broken lines indicate the corresponding final equilibrium concentrations.

Discussion

Figures 1a–1d clearly demonstrate the existence of the postulated transitory overshooting and depletion effects. In the experiments of Figs. 1a–1c, the overshooting reaches about 75, 80 and 80%, respectively, of the maxima which are calculated for the partial equilibria in the hypothetical systems in which the intrinsic competitive permeability of the overshooting ion is assumed to be infinitely greater than that of the more slowly exchanging ions under consideration. The depletion effect shown in Fig. 1d reaches about 75% of the theoretically possible maximum.

The observed effects could, of course, have been larger or smaller than those shown in Fig. 1, if membranes with higher or lower ratios of the intrinsic competitive permeabilities of the permeable ions in solution 1 were used.

A comparison of the experiments of Figs. 1a and 1c which were carried out with similar membranes, having the same $\tau^\circ_{SCN^-}/\tau^\circ_{Ac^-}$-ratio, 84:1 (and standard resistances of 80 and 125 Ω cm.², respectively) is of some interest. In the system of Fig. 1c the overshooting ion, SCN^-, is present in solution 1 at a much lower relative concentration than in the comparable system of Fig. 1a. In agreement with the theoretical prediction the transitory overshooting is percentagewise (in terms of the final equilibrium) higher in the system of Fig. 1c, about 250% as compared to about 37% in the system of Fig. 1a.

A very substantial overshooting effect, about 120%, was also observed in the system of Fig. 1b with H^+ (of low concentration in solution 1) as the overshooting ion.

Overshooting effects of this order of magnitude thus far have not been obtained with pairs of the alkali ions, such as K^+ and Na^+ or K^+ and Li^+, corresponding to the low ϕ° ratios of these ions across permselective membranes that give conveniently fast reaction rates. Substantial effects, undoubtedly, could be obtained after prolonged periods with permselective membranes which give low reaction rates and rather high ϕ° ratios.[4]

The here-presented overshooting and depletion effects across membranes of extreme ionic selectivity show a considerable similarity to certain effects across membranes of high porosity, which were described by Straub under the term "harmony,"[12] and to the "diffusion effect" investigated by Teorell.[13] Concerning these effects and their theory the reader is referred to the recent review by Teorell.[14]

The discussion of the overshooting and depletion effects requires at least a brief reference to their potential biological significance.

Two of the most characteristic features of living cells are their ability (1) to accumulate electrolytes in their sap up to concentrations far in excess of the concentration of these electrolytes in the surrounding milieu and (2) to take up different species of ions of the same charge in ratios which are vastly different from the ratio in which these ions are present in the surrounding milieu.

It is generally felt that both these phenomena are closely related to the Gibbs–Donnan membrane equilibrium, the consideration of which has recently also led to the construction of a cell model which accumulates simultaneously anions and cations against concentration differences and thereby imitates *in vitro* the first of the named activities of living cells.[15]

With respect to the preferential uptake of certain ions (for instance K^+ over Na^+, or of I^- over Cl^-) it is now commonly realized that this effect must

(10) F. D. Snell and C. T. Snell, "Colorimetric Methods of Analysis," Vol. II, Van Nostrand Co., New York, N. Y., Third Edition, 1949.

(11) I. M. Kolthoff and V. A. Stenger, "Volumetric Analysis," Vol. II, Interscience Publishers, Inc., New York, N. Y., Second Edition, 1947.

(12) J. Straub, *Kolloid-Z.*, **62**, 13 (1933); *Chem. Weekblad*, **45**, 361 (1949).

(13) T. Teorell, *Skand. Arch. Physiol.*, **66**, 225 (1933); *Gastroenterology*, **9**, 425 (1947).

(14) T. Teorell, *Progr. Biophys. Biophys. Chem.*, **3**, 305 (1953).

(15) K. Sollner, *Arch. Biochem. and Biophys.*, **54**, 129 (1955).

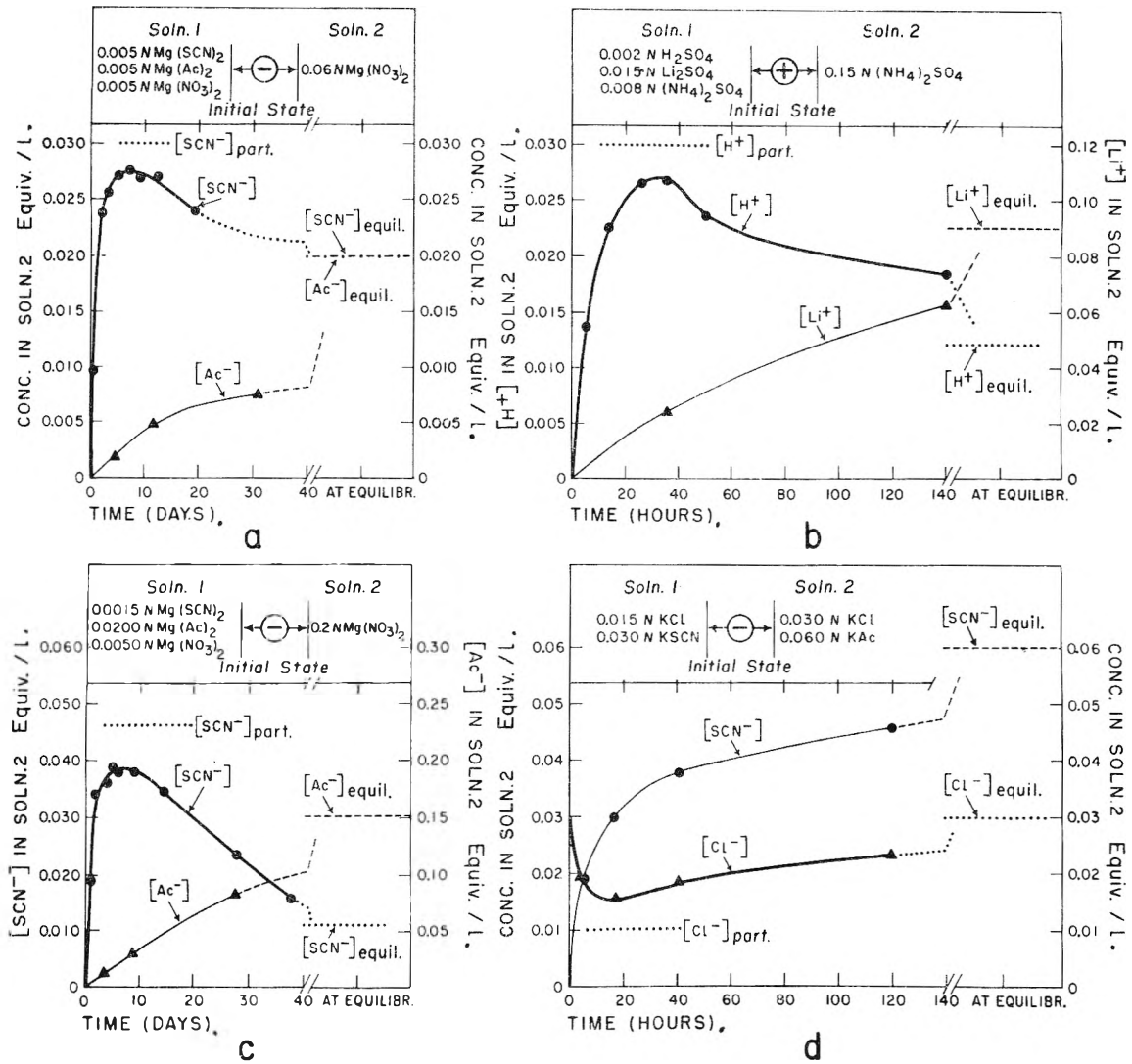

Fig. 1.—The time-concentration in solution 2 relationships in three representative systems with membranes of extreme ionic selectivity (Figs. 1a–1c) which show the overshooting effect, and one system (Fig. 1d) which shows the depletion effect.

be connected with a state of non-equilibrium. This state of non-equilibrium is maintained, generally at a fairly steady level, by the metabolic activity of the cell. The electrolyte content of the cell is commonly considered as the result of the exchange of the ions of some metabolic waste product, such as carbonic acid, for the ions of the surrounding milieu.

While the stationary state condition is maintained by the cell, the quantity of any ionic species which enters the cell per unit of time equals the quantity leaving it. The faster permeating ions must be present in the cell sap at relatively higher concentrations than the more slowly penetrating ones, provided no specific, ion-selective, counteracting mechanism is involved in the process by which the ions under consideration leave the cell. (An efflux of hypertonic cell sap in bulk caused by the turgor pressure of the cell, for instance, would fulfill this condition of a nonspecific process.)

This view of the cell as a non-equilibrium, stationary state system is commonly associated with the apparent common-sense assumption that the concentration (or activity) which a particular ion may reach within the sap of a cell must of necessity be between that in the outside milieu and that described by the Donnan equilibrium, if the latter ever were reached.

This latter assumption, however, as shown in this paper, is fallacious. The overshooting and depletion effects could cause a variety of selective accumulation and elimination effects well above or below the level of those which would be expected on the basis of the conventional approach to this problem. Cell models (involving both cation selective and anion selective membranes)[15] to demonstrate such selective accumulation and depletion effects against concentration differences are currently being studied. The possible role, however, which these effects may play in living cells and tissues remains at present an open question.

ION-EXCHANGE MEMBRANES. III. WATER TRANSFER[1]

BY R. J. STEWART AND W. F. GRAYDON

Department of Chemical Engineering, University of Toronto, Toronto, Canada

Received July 19, 1956

Direct measurements of electroösmotic water transfer across various polystyrene sulfonic acid ion-exchange membranes have been made. These data are correlated with the membrane properties of exchange capacity and water content. Membrane potentials for membranes of various capacity and divinylbenzene content have been measured. For several membranes exhibiting close to the ideal potential, the deviations from the ideal potential are in good agreement with the values calculated from the water transfer data. This conclusion has been substantiated by the measurements of membrane potentials under conditions of osmotic equilibrium. For membrane cell potentials less than 98% of the ideal potential the calculated deviations using the measured water transfer data and chloride-ion transfer data are less than the deviations measured. It is postulated that these cells degrade by chloride-ion diffusion so rapidly that the reversible potential has not been measured.

Introduction

Previously reported measurements of membrane potentials for a series of ion-exchangers permitted the estimation of water transfer.[2] Direct measurements of electroösmotic water transfer across the same and similar membranes are given in this report. The membranes used were prepared by the copolymerization of the propyl ester of *p*-styrenesulfonic acid with styrene and divinylbenzene and subsequent hydrolysis to produce polystyrenesulfonic acid. This method permitted the preparation of membranes of various capacities with the sulfonate groups distributed throughout the bulk of the membrane. These membranes contained no inert binder.

Experimental

Membranes.—The membranes used in this work were prepared as described previously.[2,3] In general the membranes previously prepared were used. The membrane characteristics, capacity, nominal cross-linking and moisture have been given.[2] The membranes are designated by two digits. The first digit represents the exchange capacity of the membrane to the nearest integer and the second digit represents the mole per cent. of divinylbenzene used in the preparation of the membrane. Two additional membranes have been prepared. The 2-2B membrane had a moisture content of 1.60 g. of water per g. of dry hydrogen resin and a capacity of 2.49 meq. per gram of dry hydrogen resin. For the 1-2B membrane these values were found to be 0.562 g. H_2O/g. and 1.08 meq./g.

Electroösmotic Water Transfer.—Measurements of electroösmotic water transfer were made using a lucite cell as shown in Fig. 1. The cell filled on both sides of the membrane with the same salt solution of known concentration was placed on a firm support in a water-bath controlled to 25 ± 0.1°. A measured current was passed through the cell for a time determined by stopwatch. The heights of the solutions in both the capillary tubes were measured using a cathetometer before and after the passage of current. All the data reported are average values of eight individual measurements. The solution was adjusted to about the same level in both capillaries at the time of filling. A constant current, usually 2 milliamperes, was passed for a measured time. The heights were then measured in both capillary tubes. The current was reversed and passed in the opposite direction for the same time. The two heights were again measured. This procedure was then repeated for a different current, usually 4 milliamperes. Various times (2 to 10 minutes) were chosen to give a change in height of 0.5–1 cm. in each capillary tube. The average deviation of a single measurement from the mean of eight was between 0.01 and 0.02 cm. for all measurements. Although the temperature for the whole series of measurements was controlled to ±0.1°, the temperature variation during a run was considerably less than 0.1°. It may be noted that a charge of about 5×10^{-5} faraday was passed in making a measurement. This corresponds to a maximum transfer of salt of 2.5×10^{-3} mole per liter. Hence concentration changes during a run are less than 5% for the most dilute solutions used. From time to time the cell was allowed to stand with the electrical circuit disconnected before the current was reversed to check for leaks, osmotic transfer and temperature variations. The greatest change observed was a steady decrease amounting to 0.03 cm. for a standing time of 100 minutes. It was attributed to cell leakage. It is evident that these variations were quite negligible for runs up to ten minutes duration. To extend the above indication that the volume changes were independent of current density a series of experiments were done with a constant charge passed of 0.600 coulomb. Four measurements were made at each of the currents 0.1, 0.5, 2, 4 and 10 milliamp. The average deviation of a single measurement from the mean of 20 was 1% of the volume change. These measurements were obtained for the 1–6 membrane and the 3–4 membrane in 0.1 *N* NaCl solution.

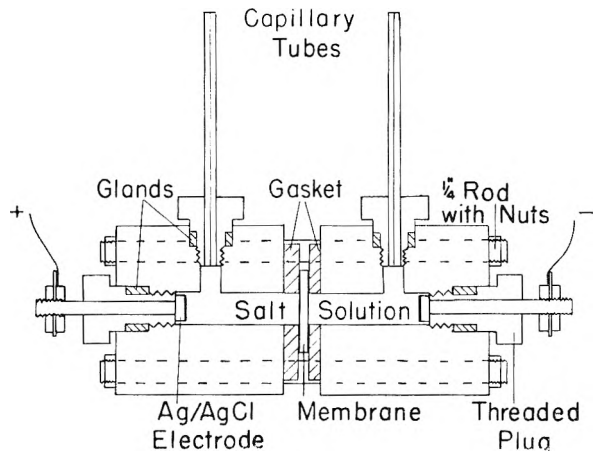

Fig. 1.—Water transfer cell. The membrane exposed was a circle of 1 cm. diameter. The volume of each half-cell was 2 cc. The diameters of the capillary tubes were each 0.0355 cm.

Membrane Cell Electromotive Force Measurements.—The apparatus used and the procedure followed were essentially the same as previously described[2] except that the solution in one side of the cell was subject, through an air cushion, to the pressure of a column of mercury. The pressure could be applied or released in 5 to 10 seconds. All measurements were taken at 25 ± 0.1° with the solutions at rest in the cell.

Membrane Moisture Content.—Samples of membrane in the leached sodium form were placed on a screen in the vapor space of a large glass desiccator fitted with a rotating fan blade. The bottom of the desiccator contained two liters of sodium chloride solution of known composition. The desiccator was immersed in a water-bath at 25.0°. After two weeks the membranes were rapidly transferred to weighing bottles and weighed. After weighing the mem-

(1) This report is abstracted from the thesis of R. J. Stewart submitted for the degree of Doctor of Philosophy, University of Toronto, October, 1955. It was presented at the Gordon Research Conference on Ion Exchange in New Hampshire, June, 1955.

(2) W. F. Graydon and R. J. Stewart, THIS JOURNAL, **59**, 86 (1955).

(3) I. H. Spinner, J. Ciric and W. F. Graydon, *Can. J. Chem.*, **32**, 143 (1954).

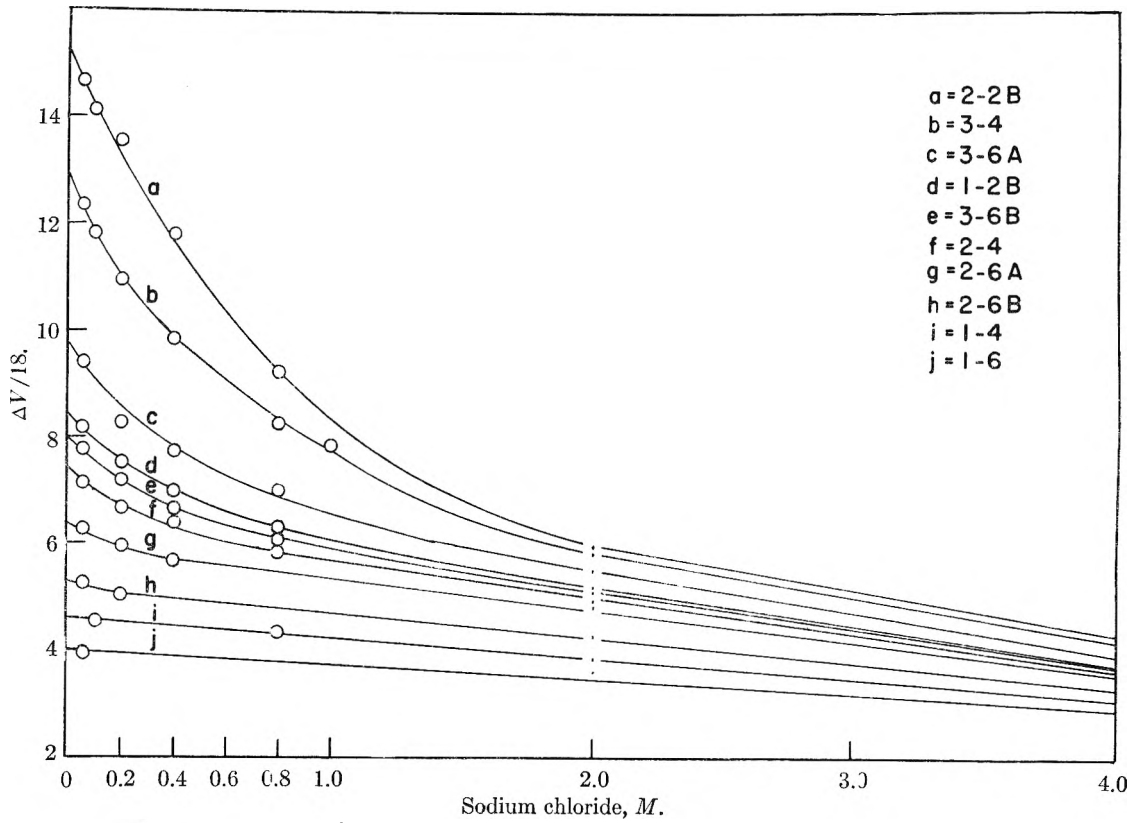

Fig. 2.—Electroösmotic water transfer for various membranes, 25°. $\Delta V/18$ is the volume change (cc.) per faraday in one half of the electroösmotic cell. This quantity is approximately the water transference number in moles/faraday. The experimental points obtained for 2 and 4 *M* sodium chloride solutions have not been encircled because of the closeness of the plots. All points are average values for eight measurements.

branes were returned to the desiccator for 24 hours and reweighed. This procedure was repeated on five successive days. Constant weights to about 1% of the total sample weight were obtained and the deviations showed no general trend. However, the values were not approached from both sides of the moisture adsorption equilibrium and therefore must be considered as indicative only. The dry weights of the samples were determined by drying for 16 hours at 110°.

Results and Discussion

The data obtained for the volume change in one half of the electroösmotic cell per faraday are given in Fig. 2. The quantity $\Delta V/18$ is a good approximation to the moles of water transported per faraday. The corrections for the volume change of the cell reaction estimated below reduces these values by about 0.1 mole of water per faraday in the dilute solution. This correction is probably no greater than ±0.2 mole of water per faraday at any of the concentrations used.

The variations in the water transfer data are very similar to the variations observed for membrane water content, as shown in Fig. 3. In Table I are given values for the ratio of water transfer $\Delta V/18F$ to water content (moles of water per equivalent of ion-exchange resin). The values for water transfer at zero sodium chloride concentration have been extrapolated from the data of Fig. 2 and are therefore in some doubt.

It may be noted that over a considerable range of membrane capacity, cross-linking and moisture content, about half the water per ion-exchange group in the resin is transferred per faraday. The ion concentration of the solution transferred across the membrane is to a first approximation the same as the internal ion concentration of the membrane pore solution. There is a tendency for the ratio to be less than 0.5 for membranes of low capacity and somewhat greater than 0.5 for membranes of high capacity.

TABLE I

RATIO OF WATER TRANSFER TO WATER CONTENT

Membrane no.	Sodium chlorine solution molarity 0	1	2	4
1–6	0.39	0.48	0.50	0.47
1–4	.38	.47	.47	.48
1–2B	.38	.41	.41	.38
2–6A	.48	.54	.57	.53
2–6B	.42	.47	.47	.48
2–4	.45	.48	.48	.47
2–2B	.54	.52	.48	.48
3–6A	.58	.55	.55	.51
3–6B	.54	.54	.55	.52
3–4	.60	.57	.54	.52

The numbers in the body of the table are $\Delta V \times (C/1000\ Wd_{Na})$ where

ΔV is the vol. change (cc.) per faraday in one-half of the electroösmotic cell

C is the membrane capacity in meq. per g. of dry sodium resin

Wd_{Na} is the membrane moisture content in grams of water per gram of dry sodium resin.

In order to calculate the water transfer term for the membrane potential equation it is necessary to consider the correction of the quantity $\Delta V/18$.

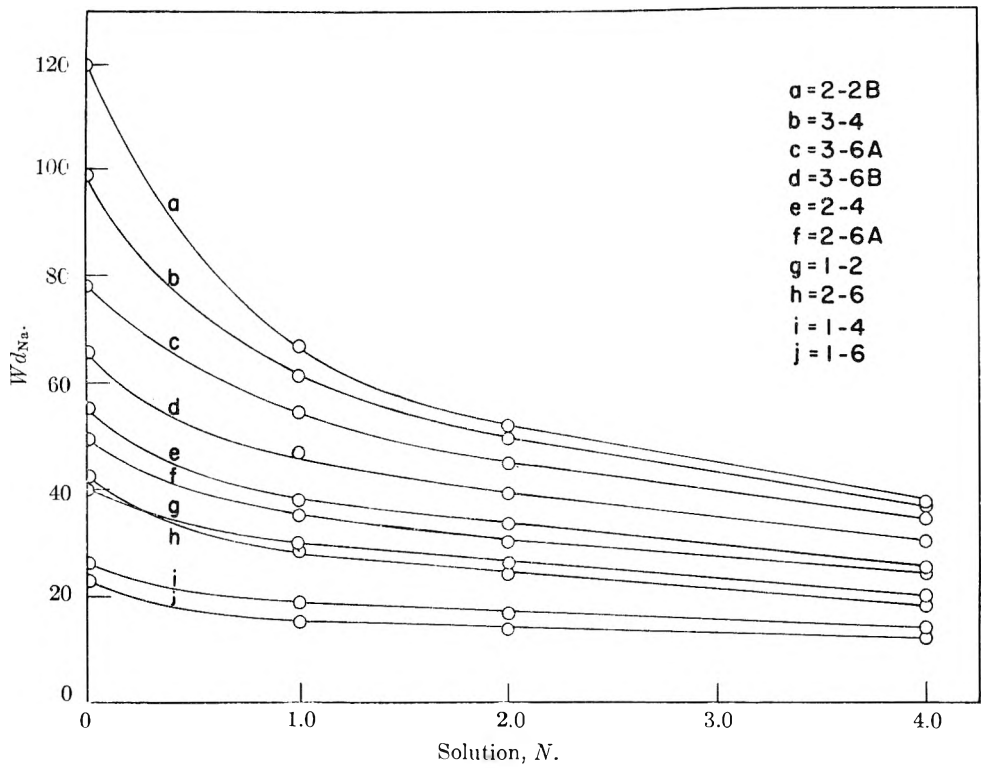

Fig. 3.—Membrane moisture content, 25°. Wd_{Na} is the weight of water in grams per 100 grams of dry resin in the sodium form. Solution normality refers to the solution with which the membrane was equilibrated. These values were not verified by approaching the equilibrium from both sides and must be regarded as indicative only.

$$\Delta V = t_w \bar{V}_w + t_{Na} \bar{V}_{NaCl} - V_{AgCl} + V_{Ag} \quad (1)$$

where

ΔV is the vol. change per faraday in the cell
t_w and t_{Na} are moles of water and sodium ion transferred per faraday
$\bar{V}$ signifies partial molal volume
V_{AgCl} taken as 25.8 cc.
V_{Ag} taken as 10.3 cc.

Using the equations given by Harned and Owen[4] the partial molal volume of water $\bar{V}_w$ is calculated to be 18.0 ± 0.1 cc. for the solutions used here.

For the 0.1 M solutions the value, $t_{Na} \geqq 0.98$, for these membranes has been estimated previously[2] and confirmed by direct ion-transfer measurements.[5] In 0.1 M solutions $\bar{V}_{NaCl}$ = 17.42 cc.[4] and equation 1 becomes

$$\frac{\Delta V}{18} - 0.1 \pm 0.01 = t_w$$

For the more concentrated solutions the correction term cannot be so readily evaluated because t_{Na} is not known. One may assume as a reasonable range of values for the 1 M solution, t_{Na} = 0.90 to 0.98. Since $\bar{V}_{NaCl}$ = 19.60 ml. a correction of 0.12 to 0.20 is calculated. For the 4 M solution $\bar{V}_{NaCl}$ = 22.73. The correction of $\Delta V/18$ to give t_w will be within ±0.2 mole per faraday if t_{Na} is in the range 0.52–0.84.

Since the membrane potentials were measured between 0.05 and 0.1 M solutions the values $\Delta V/18$ may be used for t_w without serious error. In Table II are listed the electromotive force measurements for various membrane cells and the water transfer term calculated.

Table II

Electromotive Force Measurements for Membrane Cells

E.m.f. for sodium transfer only = 32.55; solutions 0.05 M NaCl, 0.1 M NaCl.

Membrane no.	Measured e.m.f., mv.	Water transport term, mv.	Chloride transport term, mv.	Total	Dev. from ideal
1–4	32.35	0.19	0.01	32.55	0
2–6B	32.30	.22	.01	32.53	0.02
2–6A	32.24	.26	.01	32.51	.04
3–6B	32.14	.33	.01	32.48	.07
3–6A	32.06	.40	.01	32.47	.08
2–4	31.90	.30	.01	32.21	.34
3–4	31.64	.52	.02	32.18	.37
1–2B	31.70	.34	.03	32.07	.48
2–2B	30.40	.62	.04	31.06	1.49

It may be noted that the chloride transfer terms, calculated as previously reported,[2] are in all cases small with respect to the water transport terms. Direct ion transfer measurements[5] indicate that the values given for the chloride transfer terms may be low. However, for the first five membranes listed in Table II the water transport term accounts for the deviation from ideality within the experimental error. For the remaining four membranes the sum of the water and chloride transference terms is too small to account for the deviation of the measured from the ideal values.

In order to verify the above, measurements were made of electromotive force for various membrane

(4) H. S. Harned and B. B. Owen, "The Physical Chemistry of Electrolytic Solutions," Reinhold Publ. Corp., New York, N. Y., 1950.
(5) R. J. Stewart and W. F. Graydon, This Journal, 60, 750 (1956).

cells under conditions of constant pressure of one atmosphere on the dilute solution and varying pressure differences up to 3 atmospheres between the dilute and the concentrated solution (0.05 and 0.1 M). If the water transfer is the only significant cause of membrane potential deviations from ideal values then at conditions of equal chemical potential for water (ΔP = 2.3 atmospheres) the electromotive force measured should be the ideal. As shown in Fig. 4 the values for cell e.m.f. measured at 3 atmospheres were above the theoretical values for the first five membranes in Table II. Since the ideal e.m.f. is the same for all membranes the pressure e.m.f. plots should intersect at ΔP = 2.3 atmospheres if the only cause for deviation is water transfer. The two most nearly ideal membranes approach this behavior closely as shown in Fig. 4. It may be noted that the quantity $\Delta P \times (\bar{V}_{NaCl} - \bar{V}_{AgCl} - V_{Ag})$ is negligible in these measurements. The slopes of all the plots in Fig. 4 are qualitatively consistent with t_w values calculated from the measured volume changes above. These data verify the conclusion that for four of the membranes, the water transport is insufficient cause for the deviation from ideality. Some degradation of the cell by a non-reversible diffusive process is indicated.

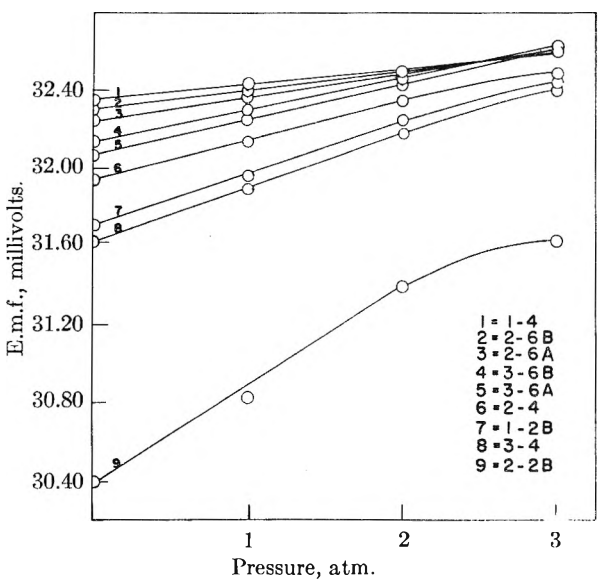

Fig. 4.—Variation of membrane cell electromotive force with pressure differences at 25°. The values given for pressure are pressure differences across the membrane, which is the applied pressure on the concentrated solution above one atmosphere. The solutions used were 0.05 and 0.10 M NaCl. The calculated ideal e.m.f. for sodium ion transfer only was 32.55 millivolts.

As noted previously[2] it is possible that the measured e.m.f. values for cells showing large deviations were not reversible values for the cell reaction stated. To investigate the question of cell reversibility somewhat further the data given in Fig. 5 have been obtained. Considering the curves with zero subscripts which were obtained without a pressure difference across the membrane a marked difference may be seen between the plots for the membranes of low deviation from ideality ($1\text{–}4_0$ and $2\text{–}6A_0$) and those for membranes with a much

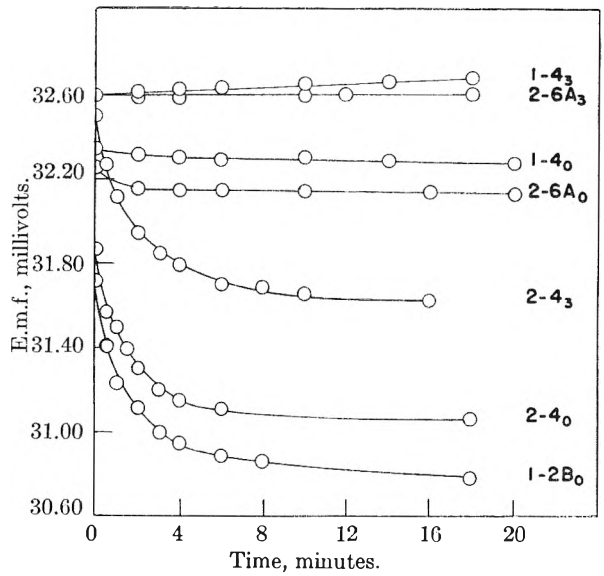

Fig. 5.—Variation of membrane cell electromotive force with time. The subscripts 3 and 0 on the membrane designation for each plot refer to the hydrostatic pressure difference in atmospheres across the membrane. The solutions used were 0.05 and 0.1 M NaCl. The calculated ideal e.m.f. was 32.55 millivolts.

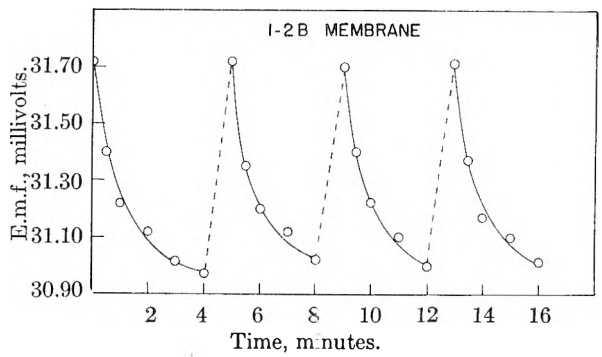

Fig. 6.—Membrane cell electromotive force measurements with intermittent stirring. The cell solutions were stirred vigorously at 4-minute intervals. The ideal e.m.f. was 32.55 millivolts. The solutions were 0.05 and 0.10 M NaCl solutions.

greater deviation ($2\text{–}4_0$, $1\text{–}2B_0$). For the poorer membranes there is certainly some doubt that the reversible e.m.f. values have been measured for the cell without liquid junctions. Since both chloride ion diffusion and water diffusion reduce the e.m.f. measured no indication of the relative magnitude of these processes can be obtained from these data. However with a pressure differential of three atmospheres applied to the more concentrated sodium chloride solution the two diffusive processes may be distinguished. Under these conditions degradation by water flow increases the e.m.f. of the cell while degradation by chloride ion diffusion reduces the e.m.f. of the cell. Considering the curves labeled with subscripts 3 in Fig. 5, one membrane shows an increasing e.m.f. with time ($1\text{–}4_3$). For this membrane it is concluded that the major degradation is caused by flow of water across the membrane. The two degradation processes mutually cancel for the ($2\text{–}6_3$) plot. For the ($2\text{–}4_3$) the degradation resulting from chloride ion diffusion is much the greater effect.

The changes with time noted in Fig. 5 are greater than would be expected if the entire solution in each half-cell remained at uniform concentration. Chloride ion transfer rates of the order of 10^{-6} gram ions per hour are to be expected. Hence it is supposed that the major concentration changes resulting from diffusion must be limited to small volumes adjacent to the membrane surfaces. This view is confirmed by the measurements illustrated in Fig. 6. In this experiment the solution in the cell was stirred rapidly at four minute intervals. The cell solutions were not changed and the potentials were measured with the solutions at rest in the cell. As may be seen the original e.m.f. could be restored at will by mixing. However, it should be noted that on the basis of the above discussion the highest e.m.f. obtained is by no means the reversible e.m.f. for the cell reaction considered.

In the dilute solutions used for these measurements we concluded that reversible e.m.f. values within 0.1 mv. have been measured only for membrane cells exhibiting a potential >98% of the ideal value. For these membranes the deviation is almost entirely because of reversible water transfer. The chloride transference number is almost negligible. For membrane cells showing a potential <98% of the ideal value it is doubtful that the reversible e.m.f. for the assumed cell reaction has been measured. The degradation of cells of this sort may be considered as the establishment of significant concentration gradients in the liquid layers at the membrane interfaces as a result of chloride ion diffusion.

Acknowledgment.—The authors are indebted to the National Research Council, Ottawa, Ontario, and to the Advisory Committee on Scientific Research, University of Toronto, for financial support.

ELECTROGRAVITATIONAL TRANSPORT AT SYNTHETIC ION EXCHANGE MEMBRANE SURFACES

BY VINCENT J. FRILETTE*

Permutit Co., New York, N. Y.

Received July 19, 1956

Electrogravitational effects associated with vertical ion-exchange membranes are investigated and found to be of large magnitude. The development of a vertical concentration gradient is explained by regarding the membrane as a type of electrode; the flow of current, just as with an ordinary electrode, leads to concentration polarization and the convective transport of matter. The limiting current behavior of an ion-exchange membrane, however, is complex, and a new concept is required to explain how membranes conduct current above the limiting current density. A qualitative discussion of the possible mechanisms is offered. Electrogravitational fractionation of cations or anions was found to take place when electrolytes were concentrated in a small cell. Simple considerations indicate that fractionation is a consequence of the relative mobility of the fractionated ions in the solution phase. Confirmation of this hypothesis would lead to a simple method for the estimation of relative mobilities. Although much remains to be done, the electrogravitational membrane process suggests a new approach to a commercial method for water demineralization and ion fractionation.

Introduction

The relatively recent development of highly efficient, synthetic ion-exchange membranes has extended the interest in membrane processes from the biochemistry laboratory to industry. Important projected uses for membranes now include the large-scale demineralization of brackish waters and seawater, recovery of waste pickle liquor and the production of chlorine. An excellent review of recent work in this field is given by Spiegler.[1]

Most of the studies concerned with ion-exchange membranes have centered around their ability to hinder gross diffusion of salts while at the same time permitting either anions or cations to move freely through the barrier. Some attention has been given to changes of *p*H accompanying electrodialysis,[2] and the fact that membranes polarize has been recognized and discussed.[3] None of the prior investigators appears to have studied or has attempted to utilize the concentration polarization which occurs whenever a current is passed through an immersed ion-exchange membrane.

In our laboratories we have found that any vertical ion exchange membrane on the passage of current gives rise to a vertical concentration gradient, the latter being formed presumably by gravitational convection of the polarized layers of depleted or enriched electrolyte. The magnitude of this effect is quite large and may have commercial significance. The means by which a flow of current in the horizontal plane generates a vertical concentration gradient, and the role of the membrane in the process, are not simple. Quantitative treatment has been applied with success to the behavior of vertical electrodes with natural convection,[4,5] and one is tempted to assume that the treatment is valid for ion-exchange membranes, regarding the latter as another form of reversible electrode. However, as we shall see, ion-exchange membranes do not appear to behave as simple electrodes. In this paper we shall attempt to present our findings with particular emphasis on the phenomenological aspects of the problem.

Basic Cell

Construction.—The basic element with which

* Socony-Mobil Research Laboratories, Paulsboro, New Jersey.

(1) K. S. Spiegler, *J. Electrochem. Soc.*, **100**, No. 11, 303C (1953).

(2) E. Manegold and K. Kalauch, *Kolloid Z.*, **84**, 313 (1938).

(3) K. H. Meyer and W. Strauss, *Helv. Chim. Acta*, **23**, 795 (1940).

(4) B. Levich, *Acta Physicochim. U.R.S.S.*, **19**, 117 (1944).

(5) B. Levich, *Disc. Faraday Soc.*, 37 (1947).

this study concerns itself is the single, vertical ion-exchange membrane together with the polarized surface layers of electrolyte. For convenience, we shall refer to the membrane surface nearest the cathode as the anode surface, and the corresponding electrolyte film as the anode diffusion film; the membrane surface nearest the anode will be referred to as the cathode surface.

To provide a basic element for laboratory study, and at the same time to avoid the chemical and physical disturbances caused by electrodes, it was found desirable to use two membranes in the three-chamber cell shown in Fig. 1. The central chamber of this cell is physically isolated from the electrodes and yet contains an anode and cathode membrane surface, *i.e.*, the components of a single membrane. When the cell is in use, the electrode chambers are rinsed by a continuous, moderate flow of the same solution as used to fill the central chamber; by this means, the accumulation of alkali and acid is avoided without unduly disturbing the system. Two additional buffer chambers are sometimes desirable to separate the central chamber from the electrodes; when used, these chambers are filled with the solution under study and serve to further isolate the important central chamber from the chemical products formed at the electrodes.

The cell shown in Fig. 1 was constructed with molded circular polyethylene spacers having an inner diameter of 5.6 cm. and a thickness of 1.4 cm. When assembled with membranes, each of the chambers had a capacity of approx. 35 ml. Two flat graphite electrodes were used to form the ends of the cell, and the whole assembly was held together in a frame composed of two Lucite blocks bolted at the four corners. As shown in Fig. 1, each of the spacers is provided with an inlet and overflow tube inserted through the body of the spacer.

The membranes used in this study are similar to Permutit Cation Membrane 1373 and Permutit Anion Membrane 1374 which were described in a prior publication; the present membranes, however, have better selectivity.[6] The characteristics of these membranes are summarized below, the values shown having been obtained by methods already described.[6]

MEMBRANE CHARACTERISTICS

	Permutit Cation 3141	Permutit Anion 3145
Thickness, mm.	0.22	0.18
60 cycle effective areal resistance, 0.1 *N* NaCl, ohms-cm.^{2}	13.8	11.3
Transport No., 0.01 *N* NaCl	0.995	0.975
0.15 *N* NaCl	.995	.962
0.60 *N* NaCl	.995	.897
1.50 *N* NaCl	.960	.793
3.00 *N* NaCl	.868	...

Behavior of Basic Cell.—In the experiments about to be described, the basic cell was assembled with two Permutit Cation Membranes 3141. The cell was rinsed and equilibrated with the electrolyte solution, in these instances 0.0996 *N* NaCl, before each experiment. Finally, the central chamber was filled, several minutes were allowed for the convection eddies within the chamber to damp, and the current was turned on. The current, kept constant by a suitable rheostat, was turned off after the predetermined time had elapsed. After the completion of the experiment, several minutes again were allowed to pass before the contents of the central chamber were drained off slowly and collected in two equal portions; the portion first collected corresponded to the solution in the lower half of the central chamber. The two portions were analyzed for chloride ion by Mohr titrations. In all experiments it was found that a net movement of sodium chloride into the lower half of the chamber had occurred, with no significant change in total electrolyte content of the chamber.

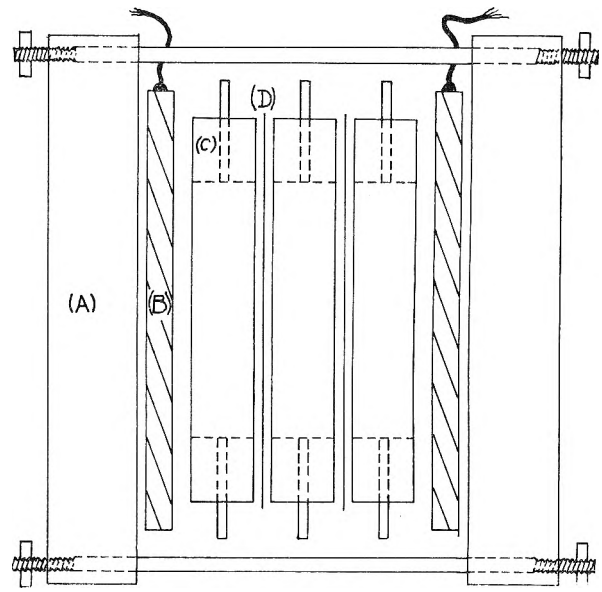

Fig. 1.—Cross-section of basic cell: (A) = lucite end block; (B) = graphite plate; (C) = spacer; (D) = membrane.

The results of this series of experiments are given in Tables I and II. Table I summarizes the results obtained for a series in which the time and current density were varied, but the total coulombs passed was constant for all runs. Table II summarizes the effects of varying the time of treatment at a fixed current density. All of the results are characterized by a relatively large vertical transfer of salt from the upper half into the lower half of the chamber.

Coulomb Efficiency.—Concentration polarization at ordinary electrodes and convective movement of vertical polarized films are concepts which are well known to electrochemists.[7] Most prior studies, however, are of systems characterized by forced convection and they are designed to evaluate the role of the Nernst layer on potential rather than to investigate concentration changes in the bulk of the solution. A noteworthy exception is found in the work of Murphy, who designed an electrogravitational cell with two silver–silver chloride electrodes.[8] Although this investigator was limited by the nature of his electrodes to low current densities and to chloride solutions, he did obtain

(6) V. J. Frilette, THIS JOURNAL, **60**, 435 (1956).

(7) C. W. Tobias, M. Eisenberg and C. R. Wilke, *J. Electrochem. Soc.*, **99**, No. 12, 359 C (1952).

(8) G. W. Murphy, *ibid.*, **97**, No. 11, 405 (1950).

considerable vertical transport of salt and commented that "the magnitude of convection effects has not been fully appreciated." In the paragraphs which follow we shall attempt to explain the high efficiencies observed in the present study.

Ion-exchange membranes may be considered electrodes in the sense that a particular ion, *e.g.*, sodium, is in reversible equilibrium between a solution phase and the membrane surface. The membranes are not electrodes in the ordinary sense because they do not serve as oxidation–reduction sites, and also because they are to some extent permeable to water. Water transport, in particular, is a factor which must be considered before any quantitatively satisfactory theory of the behavior of membranes in an electric field can be obtained.

The transport number of Cation Membrane 3141 in dilute solution, as determined from Nernst potentials, indicates that the membrane behaves almost as an ideal sodium electrode. Based solely on these potentials, one might predict that the passage of one faraday of current leads to the deposition on the surface of the membrane (or release from the surface) of one equivalent of sodium ion. However, it has been noted in our laboratory and also elsewhere that the kinetic transport number is less than the Nernst value; this discrepancy has been attributed to the transfer of water in the hydration shell of the ion.[9,10] In our laboratory, based on the behavior of the pair of membranes in an electrodialysis cell, the discrepancy between the kinetic and Nernst transport numbers was estimated at *ca.* 0.05 for both membranes; assigning the deviation equally, the kinetic transport number of Cation Membrane 3141 in 0.1 *N* NaCl may be estimated as $t_m^+ = 0.97$; thus the membrane may be regarded as a slightly leaky electrode.

The first mechanism that may be proposed to explain the vertical transport of electrolyte is identical with that suggested by Murphy for a pair of Ag–AgCl electrodes. Consider the anode diffusion layer; at the solution interface the Na^+ transport number t_s^+ is 0.395,[11] while at the membrane interface, $t_m^+ = 0.97$. The coulomb efficiency for the concentration of electrolyte in the anode layer is thus the difference between these two values, or 0.585. If no extraneous electrode reaction occurs, and no movement of water other than that already taken into account, one faraday of current would cause the concentration of 0.585 equivalent of NaCl in the anode film, and the depletion of an identical amount from the cathode film. As the concentration gradient develops between the membranes in the horizontal directions, two processes are initiated; the first is ordinary diffusion which tends to modulate the gradient in the vicinity of the membrane surface, and the second gravitational convection of the films in the vertical plane. At first one might suspect that diffusional transport would nullify extensively the effects of electromigration; however, provided the membranes are sufficiently far apart and highly selective, diffusion will serve only to thicken the anode and cathode films, resulting perhaps in a slower linear convection velocity but a higher total volume movement. In other words, for diffusion to cause a loss of coulomb efficiency, there must be a transference of salt across a hypothetical vertical plane situated equidistant between the membranes; but, it is in just this region that there is the smallest concentration gradient and the lowest diffusional flux. In the absence of eddy diffusion, one would expect that the horizontal gradient generated by electromigration would be transformed into a vertical gradient with very high efficiency, at least during the early stages of a separation. Eventually, the vertical gradient must develop less efficiently because of the superposition of the horizontal generating gradient on the resultant vertical gradient.

A graph of the vertical transfer of electrolyte per faraday is shown in Fig. 2, the data being derived from Tables I–II. The two curves are superimposable within the limits of the techniques used. One infers from the graph that vertical gradient development efficiency is independent of current density, but depends essentially on the duration of the experiment. The deterioration of efficiency with longer times of operation probably is the result of eddy diffusion. Experimental evidence for eddy diffusion exists and will be described in the latter part of this paper. Loss of coulomb efficiency because of eddy diffusion should be at a minimum at zero time; extrapolation of the curve of Fig. 1 indicates a maximum efficiency of 0.54 equivalent per faraday, in reasonable agreement with 0.585 equivalent per faraday calculated.

Voltage–Current Relations.—The potential *vs.* current behavior of ion-exchange membranes as electrogravitational elements is perhaps even more interesting than the observed high coulomb efficiency. Constant-current operations with the basic cell were found to give essentially constant-voltage operation; there was very little drift in the voltage required to maintain the current except

TABLE I

VERTICAL TRANSFER OF ELECTROLYTE IN BASIC CELL; CONSTANT CURRENT × TIME[a]

Current, mamp.	Current density, mamp./cm.²	Time, min.	Meq. NaCl Lost, upper layer	Meq. NaCl Gained, lower layer	Equiv. transferred per faraday Upper layer	Equiv. transferred per faraday Lower layer
46	1.87	40	0.303	0.310	−0.264	+0.270
61.3	2.49	30	.345	.310	.301	.270
92	3.74	20	.367	.365	.320	.318
138	5.61	13⅓	.465	.457	.406	.400
184	7.48	10	.483	.488	.422	.426
230	9.35	8	.506	.493	.442	.430
368	14.96	5	.504	.511	.440	.446

[a] Total of 1.840 ampere minutes for all runs, or 1.147×10^{-3} faraday.

what could be explained by the heat generated in the operation. The stability of the system permitted one to increase the voltage in steps and note the corresponding currents after brief intervals, much in the same manner as one develops a polarographic curve. A large number of points could be determined in very little time so that no substantial vertical gradient was produced in the operation.

The basic cell, assembled as in previous studies

(9) Rosenberg, Gordon Research Conference, July (1953).

(10) G. Scatchard, *J. Am. Chem. Soc.*, **75**, 2883 (1953).

(11) Kortum-Bockris, "Electrochemistry" Vol. II, Elsevier Press, New York, N. Y., p. 719.

TABLE II

VERTICAL TRANSFER OF ELECTROLYTE IN BASIC CELL FOR 3.74 MAMP./CM.^{2}

Time, min.	Meq. NaCl Lost, upper layer	Meq. NaCl Gained, lower layer	Equiv. transferred per faraday Upper layer	Equiv. transferred per faraday Lower layer
60	0.6406	0.6390	−0.187	+0.186
45	.5804	.5652	.226	.220
30	.4745	.4690	.276	.273
20	.3902	.3762	.340	.328
10	.2520	.2313	.440	.404
5	.1634	.1188	.570	.414

but without membranes, was filled with 0.1 *N* NaCl and was run at different voltages to determine the stable current. Voltages were determined with a high impedance voltmeter connected across the terminals of the cell. An essentially straight line function resulted, with no indication of an inflection. The same procedure was repeated after the cell was reassembled with two cation membranes. The curve obtained in the latter instance was distinctly non-linear. Both curves are shown in Fig. 3; the curve for the cell without membranes is adjusted in slope to simulate the presence of hypothetical membranes which behave simply as an additional one ohm resistor. The curve shown for membranes was found to be highly reproducible and characteristic of this general type of membrane.

An examination of Fig. 3 reveals three distinct regions in which the overvoltage–current relations are different. The interpretation of this curve is associated intimately with the theory of membrane behavior; therefore, an attempt to interpret the overvoltage in terms of possible mechanisms appears to be justified.

Theory of Membrane Behavior.—The first region of the curve, which extends approximately up to 7 mamp. per cm.^{2}, is characterized by a low overvoltage which diminishes with decreasing current density. In this region the membrane appears to behave very much like an ordinary electrode; the overvoltage observed may be accounted for by the concentration cell potential and the added resistance of the cathode diffusion film. The mechanism for the generation of a vertical concentration gradient is the one we have tacitly assumed, *i.e.*, concentration polarization with free convection.

The second region of the curve, extending in a diffuse manner from 7 to 9 mamp. per cm.^{2}, evidently is a transition zone. This zone was found to occur in other cells of quite different size and shape, but usually at current densities of *ca.* 3 mamp. per cm.^{2}. There seems to be little question that the rapid rise is caused by an approach to the limiting current density which results, as with an ordinary electrode, when the solution at the cathode surface of the membrane is almost free of ions. That the rise does not continue can only mean that a consecutive process is initiated in this region.

The third region, beginning at 9 mamp. per cm.^{2}, is characterized by a high overvoltage. In this region the membrane no longer appears to behave as an ordinary electrode for no obvious consecutive process is available to explain conduction. Three mechanisms not found with ordinary electrodes, however, could well have significant roles and will

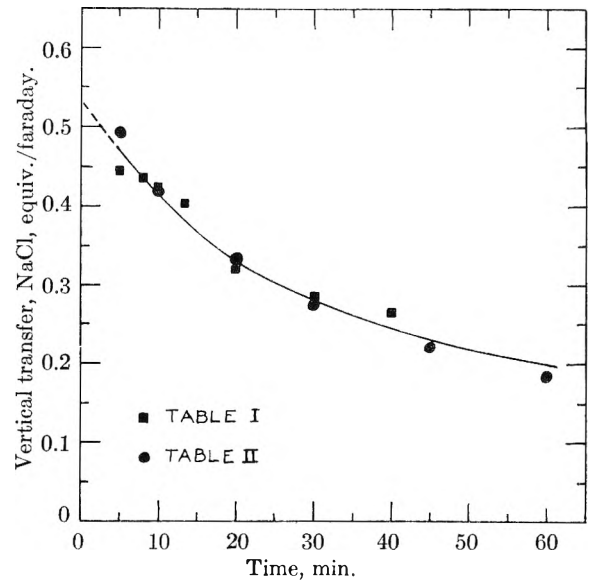

Fig. 2.—Efficiency of basic cell.

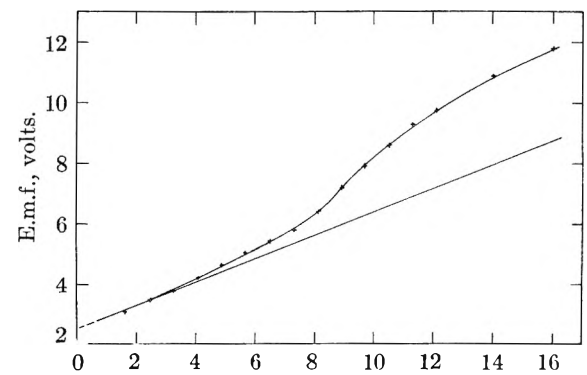

Fig. 3.—Current–voltage behavior.

be discussed. These are proton conduction, electroösmosis and interfacial microstreaming.

Proton transfer was found to be very high with bipolar ion-exchange membranes.[6] These membranes consist of two faces, of which one is highly cation selective and the other anion selective. Passage of current leads to depletion of electrolyte at the interface between the lamina at very low current densities, and very efficient proton transfer is observed as the current density is increased. It was thought originally that beyond the limiting current density a simple membrane, such as we are concerned with, would behave in the same manner, the Nernst layer serving as a preferentially selective anion membrane. A necessary consequence of proton transfer, however, is the formation of acid and alkali. Analysis of the upper and lower layers, contrary to what was expected, indicated that less than 5% of the total current in the basic cell is carried by this mechanism, even at the highest current densities. Evidently there is another mechanism present, which interferes in some manner with proton transfer.

Electroösmosis, which would require water to be transported toward the cathode, would support conduction by transporting ions toward the cathode surface of the membrane. A necessary consequence

of this process is the deterioration of coulomb efficiency with increasing current density. With the present membranes, however, the coulomb efficiency is not diminished, indicating minimal electroösmosis. Experiments in which glycerol was added to the electrolyte confirm this view. It might be mentioned that in our laboratories, however, membranes of a somewhat different type have been found to show a very pronounced loss of coulomb efficiency at high current densities, and the same phenomenon has been reported from another laboratory.[12] It appears, then, that although with the membrane under study the role of electroösmosis is a minor one, other membranes could behave differently.

The third mechanism, interfacial microstreaming, is suggested by simple considerations. From Fick's first law

$$J = -D\frac{\partial c}{\partial x}$$

and the only way in which J may be increased is to decrease the diffusion film thickness. If we conceive of a membrane surface as consisting of a series of quasi-blind pores, electroösmotic streaming could occur at the surface of the membrane, and the Nernst layer, due to short-range turbulence, would be effectively thinner. This type of streaming is well-known to colloid chemists who use it to demonstrate the presence of a double layer.[13] A phenomenon similar to the above streaming is also known in polarography, and is associated with appearance of polarographic maxima. Antweiler was successful in observing the streaming, and noted a turbulent disturbance of the diffusion layer.[14] Thus, it seems reasonable tentatively to assume that a similar type of streaming occurs in membrane systems at the cathode surface of the membrane, the resulting disturbance in the diffusion layer providing a mechanical eddy-like transport of cations to the surface of the membrane to enhance the total flux of ions. This mechanism actually would be expected to overlap electroösmosis, the dominance of one or the other being determined by the extent of hydraulic constriction of the pores. The streaming phenomenon also accounts for the absence of any large amount of proton transfer in the high current density region.

Ion Fractionation

Murphy, in his work with silver–silver chloride electrodes, recognized that electrogravitational separation of ions which had different mobilities could take place along with the concentration effect, and demonstrated the partial separation of HCl from NaCl.[8] It is easy to see why fractionation occurs; in the case of sodium and hydrogen, for example, the faster-moving hydrogen ion tends to become more concentrated than the sodium ion in the cathode diffusion layer, and in turn the electrolyte in the lower half of the cell will be richer in acid than the upper half. The use of ion-exchange membranes instead of silver–silver chloride electrodes provides a general system with which either cations or anions may be fractionated, depending on the choice of membranes.

The behavior of the basic cell in the fractionation of ions indicates that the loss of coulomb efficiency with time (Fig. 2) is due mainly to eddy convection. Consider, for example, a mixture of two cations of different mobilities, denoted by cation$_1$ and cation$_2$. The rate of transport of cations$_1$ across a hypothetical median plane parallel to the membranes may be written

$$\frac{dn_1}{dt} = k_1c_1u_1 - k_en_1 \qquad (1)$$

in which n_1 is the number of cations$_1$ transported, c_1 and u_1 the concentration and absolute ionic velocity in the bulk solution, and k_1 is a constant which depends on applied voltage, cell dimensions, faraday's constant and activity coefficient. In this equation we have made the tacit assumption that the reverse transport, or coulomb loss, is due entirely to a fixed rate of eddy loss, the rate being associated with the constant, k_e. A similar equation may be written for cation$_2$, noting that k_e is the same for both cations, but k_2 differs from k_1, their ratio reducing to the ratios of the activity coefficients of the two cations. If a cell is operated so that the total transport across the median plane is small, then it seems justified to regard c_1 as constant and we may integrate to obtain

$$\int_0^{n_1}\frac{dn_1}{k_1c_1u_1 - k_en_1} = \int_0^t dt \qquad (2)$$

$$\frac{1}{k_e}[\ln(k_1c_1u_1 - k_en_1)]_{n_1}^{\circ} = t \text{ or} \qquad (3)$$

$$\ln\frac{k_1c_1u_1}{k_1c_1u_1 - k_en_1} = k_et \qquad (4)$$

Since the transport of the second cation gives rise to an identical equation, we may equate the logarithmic terms

$$\frac{k_1c_1u_1}{k_1c_1u_1 - k_en_1} = \frac{k_2c_2u_2}{k_2c_2u_2 - k_en_2} \qquad (5)$$

Taking cross products and eliminating leads to

$$\frac{n_1}{n_2} = \frac{k_1c_1u_1}{k_2c_2u_2} \qquad (6)$$

For the special case in which the activities of the two ions in the bulk of the mixture are equal, the ratio of the amounts transported becomes simply the ratio of their mobilities. Without restricting ourselves to this case, however, equation 6 indicates that if eddy convection alone is responsible for coulomb efficiency loss, the ion-transport ratio is independent of time or coulomb efficiency, provided the total transport is small. A parallel analysis for coulomb efficiency loss due to ordinary diffusion could not be completed, but qualitatively it is evident that the faster moving ion also must be lost faster, so that n_1/n_2 is always closer to one than the corresponding mobility × activity ratio.

A series of partial separations were run to compare ion transport with mobility ratios. The basic cell was assembled with anion membranes; two buffer chambers were inserted to guard against incidental errors. Results for five experiments with hydrogen–sodium mixtures are shown in Table III.

(12) Report T.A. 270, of General Technical Dept., T.N.O., p. 93, The Hague (1952).

(13) Ref. 11, p. 339.

(14) I. M. Kolthoff and J. J. Lingane, "Polarography," Vol. 1, Interscience Publishers, New York, N. Y., 1952, p. 173.

Analyses for hydrogen and chloride ions were made volumetrically, sodium being determined by difference. Table III also includes results from the separation of sodium–potassium and lithium–potassium mixtures. In these cases sodium, lithium and potassium were determined with a Perkin–Elmer flame spectrophotometer, chloride being determined by Mohr titration.

An examination of Table III shows that the sodium–hydrogen behavior is variable. Experiments 1–2, run for a short time, give evidence for ordinary diffusion losses, the bulk of the coulomb-efficiency loss being attributable to eddy diffusion. The separations for the other alkali ions appear to confirm this reasoning. A short-term experiment with a lithium–potassium mixture (expt. no. 8) showed no anomaly comparable with that found for the hydrogen–sodium mixture.

An interesting case arises when one considers what might happen in an attempt to separate two cations by use of cation-exchange membranes. In this case separation should occur only if the ratio of

TABLE III

FRACTIONATION OF CATIONS IN CELL WITH ANION MEMBRANES

Expt.	Total current, mamp.	Time, min.	Cation$_1$ Identity	Cation$_1$ Initial concn., N	Cation$_2$ Identity	Cation$_2$ Initial concn., N	Net vertical transfer Cation$_1$ meq. transpt.	Net vertical transfer Cation$_2$ meq. transpt.	Cl^- meq. transpt.	Over-all coulomb efficiency,[a] %	n_1/n_2	Calcd. mobility ratio cation$_1$/cation$_2$ From eq. 6[b]	Calcd. mobility ratio cation$_1$/cation$_2$ Lit.[b]
1	92	5	H^+	0.0504	Na^+	0.0500	0.105	0.025	0.130	45.7	4.1	4.1	7.0
2	368	5	H^+	.0504	Na^+	.0500	.314	.072	.386	33.7	4.4	4.4	7.0
3	92	20	H^+	.0504	Na^+	.0500	.276	.036	.312	27.3	7.7	7.7	7.0
4	92	35	H^+	.0500	Na^+	.0501	.387	.063	.450	22.4	6.2	6.2	7.0
5	92	45	H^+	.0504	Na^+	.0500	.424	.060	.485	18.8	7.0	7.0	7.0
6	92	20	Li^+	.0504	K^+	.0492	.077	.161	.238	20.8	0.48	0.47	0.53
7	92	20	Na^+	.0504	K^+	.0492	.112	.158	.270	23.5	.71	.69	.68
8	368	5	Li^+	.0504	K^+	.0484	110	.221	.331	28.9	50	.48	.53

[a] Calculated as equivalents total salt transferred per faraday × 100. [b] Activity coefficient ratio taken as = 1.0; ionic mobilities at 25° taken from Appendix 6.2, Robinson and Stokes, "Electrolyte Solutions," Academic Press, New York, N. Y., 1955.

diffusional loss even with fairly high coulomb efficiency. On the other hand, experiments 3–5 give transport ratios which closely approximate those expected from the mobility of the ions, even though the over-all coulomb efficiency is relatively poor. It is the writer's belief that this peculiar relationship arises from an unfortunate property of the anion-exchange membranes, *viz.*, that they tend to leak hydrogen ion at fairly low concentrations.[6] In the first two experiments, the vertical transport of the polarized films has not proceeded to any great extent before the applied potential is removed; with the loss of the polarizing force, the ion-depleted cathode diffusion layer, in which environment the anion membrane is highly selective, begins to acquire more electrolyte; the latter in turn permits the concentrated hydrogen ion from the anode diffusion layer to leak through the thin membrane and causes further loss of efficiency of the membrane as a hydrogen ion barrier. Thus, although experiments 1–2 indicate loss by ordinary diffusion, the diffusion takes place not through the bulk solution but rather through the membrane. With long-term experiments the polarizing force is maintained sufficiently long so that convection removes the films from immediate contact with the membranes; as shown by experiments 3–5, these conditions are not associated with large ordinary-

the products of mobility × activity for the two cations is different in the solution and membrane phases, *i.e.*, if the membrane is "kinetically selective." The results of attempts to separate several pairs of cations are summarized in Table IV. The complete lack of any selectivity, even for the sodium–calcium pair, is somewhat surprising and indicates that kinetic selectivity is not a natural consequence of mass-action selectivity, *i.e.*, the selective concentration of one species in the membrane phase. Also, because these membranes are characterized by high biionic potentials for the ion-pairs studied, this property, too, is apparently unrelated. Whether or not the lack of selectivity found is a result of the current density used in the experiments is a question which remains to be explored; it may well be that at extremely low current densities, when concentration polarization is at a minimum, the results will be quite different from these found in the present study.

Continuous Process

The use of ion-exchange membranes in electrogravitational systems appears to offer an interesting tool for the study of both membrane behavior and solutions. The preliminary study presented in this paper is of a highly qualitative nature, and much remains to be done to elaborate the quantita-

TABLE IV

RESULTS OF CATION FRACTIONATION UTILIZING CATION EXCHANGE MEMBRANES

Expt.	Total current, mamp.	Time, min.	Over-all coulomb efficiency, %	Cation$_1$ Identity	Cation$_1$ Initial concn., N	Cation$_2$ Identity	Cation$_2$ Initial concn., N	Final ratio cation$_1$/cation$_2$ Upper layer	Final ratio cation$_1$/cation$_2$ Lower layer
9	184	20	32	Na^+	0.099	Ca^{++}	0.074	1.33	1.35
10	184	20	13	H^+	.097	Na^+	.101	0.94	0.96
11	92	40	9.5	H^+	.097	Na^+	.101	.95	.96
12	276	6	9.4	H^+	.097	Na^+	.101	.95	.97

tive aspects of the problem, especially since the latter may vary with the fine detail of membrane structure. Although this report is restricted to the behavior of a single membrane, it is possible to multiply the single membrane effect simply by inserting additional membranes loosely between the two active surfaces in the basic cell. The multimembrane electrogravitational cell so formed may be operated continuously by feeding an influent solution at an intermediate height in the cell and withdrawing two product streams, one from the uppermost level and the other from the bottom of the cell. Such cells have been constructed and operated successfully in our laboratories. The results of these studies will be reported elsewhere.

Acknowledgment.—The author expresses his appreciation to Dr. C. Calmon and Mr. M. E. Gilwood of the Permutit Company for encouraging the above investigation, and to Dr. Dwight D. Prater of Socony Mobil Laboratories for comments on the manuscript.

SALT FILTERING BY ION-EXCHANGE GRAINS AND MEMBRANES[1]

By J. G. McKelvey, Jr., K. S. Spiegler and M. R. J. Wyllie

Gulf Research & Development Co., Pittsburgh, Pennsylvania

Received July 30, 1956

A 0.1 solution of sodium chloride was forced through a "Permaplex C-10" cation-exchange resin membrane in the sodium form. It was found that the exuding solution was depleted in salt. This salt filtering action probably is due to ion exclusion and not to ion exchange. Various types of ion-exchange resin granules were equilibrated with sodium chloride solution and synthetic sea water. The resin granules were then separated from the solution and subjected to pressure. It was found that the concentration of salt in the solution expressed from the resin decreased gradually. The ratio of the concentrations of the various dissolved salts also changes as the compression proceeds.

It is well known that an ion-exchange resin when in equilibrium with an aqueous electrolyte solution, contains less of the soluble electrolyte per unit weight of water than the solution.[2] This electrolyte exclusion phenomenon, which is essentially a "Donnan" effect, may be utilized in various ways to separate an electrolyte solution into a more concentrated and a more dilute portion. This note deals with two methods by which this may be achieved: namely, (a) equilibration of resin grains with a salt solution; separation of the grains; application of pressure to the grains and collection of the dilute solution squeezed from them, and (b) compression of a salt solution through an ion-exchange membrane and collection of the dilute filtrate.

It is important that these separation processes are probably caused primarily by the electrical properties of the ion-exchange resins; the filtering action is probably not due to the relative size of the ions and resin "pores". These processes are quite different from regular ion-exchange demineralization since chemical regeneration of the resins is not required. They are related to the new process of "Ion Exclusion"[3] in which separation between electrolytes and non-electrolytes is effected by a column technique but without application of pressure.

1. Squeezing of Solutions from Ion-exchange Resins.—The resins used in these experiments were "Dowex 50," a sulfonated polystyrene cation exchanger (Dow Chemical Co., Midland, Mich.) and "Amberlite IRA 411" a quaternary amine anion exchanger (Rohm & Haas Co., Philadelphia, Pa.). The resin grain size was 20–50 mesh (wet U. S. Standard Screen). The solutions used were sea water from the Gulf of Mexico (chlorinity 17.9‰) and magnesium chloride (0.204 normal).

The ion-exchange resin granules were equilibrated with the respective salt solution, filtered on a "Buechner" filter and the moist resin granules were then loaded into a steel cylinder. They were subjected to pressure by means of a steel piston with "O" ring seals and a hand operated hydraulic press. A "341-20" press (Loomis Engineering & Mfg. Co., Newark, N. J.) was used for the cation-exchange resin while a "1315" press (Buehler Co., Chicago, Ill.) was used for the experiments with the anion-exchange resin. The resin bed was supported by a micro-metallic porous disc (Micro Metallic Corp., Glen Cove, N. Y.) which allowed the exuded solution to pass through and be collected. The apparatus is shown schematically in Fig. 1. The volume of the resin bed was decreased stepwise and the liquid exuding after each step collected as a separate sample. At first, the application of pressure did not cause any liquid to emerge at the top, since the solution squeezed from the resin merely filled the interstitial space of the bed. Later, solution emerged and the volume exuding after each pressure increase was collected as a separate sample.

The position of the piston and hence the depth of the resin bed were measured before the initial application of pressure, when the particles were loosely packed, and after each subsequent pressure increase. After application of pressure in each step the pressure gage rose sharply and then dropped rapidly, leveling off to a time-independent value. This latter pressure was recorded and served as reference to the particular stage of the experiment. Chloride concentration in the effluent was determined by titration with standard mercuric nitrate solution,[4a] magnesium and calcium concentration

(1) The results of these experiments have been reported in part at the AAAS Gordon Conference on "Ion Exchange," 1954.

(2) J. Schubert, *Ann. Rev. Phys. Chem.*, **5**, 413 (1954).

(3) R. M. Wheaton and W. C. Bauman, *Ind. Eng. Chem.*, **45**, 228 (1953.)

(4) (a) F. E. Clarke, *Anal. Chem.*, **22**, 553 (1950); (b) M. Calvin and A. E. Martell, "Chemistry of the Metal Chelate Compounds," Prentice-Hall, Inc., New York, N. Y., 1952.

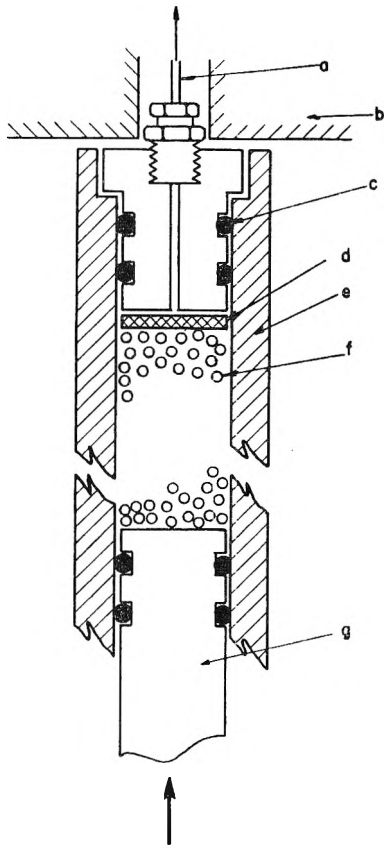

Fig. 1.—Steel apparatus for squeezing of solutions from ion-exchange resin grains through a steel assembly, effluent is collected at top: a, Saran tube; b, top section of hydraulic press; c, "O" ring; d, microporous disc; e, steel body; f, resin grains; g, piston.

either by titration with ethylenediaminetetraacetic acid,[4b] or with the flame photometer. Sodium and potassium concentrations were determined only with the flame photometer.

Figure 2 shows typical results for a squeezing experiment with "Dowex 50" initially equilibrated with sea water. The figure shows the amount of solution exuding from the resin bed as a function of the applied pressure, and also the Cl^-, Ca^{++} and Mg^{++} concentrations in this solution. The points of curve 1 relate to the pressure necessary to remove a certain volume of solution from the resin bed; the points on curve 2 refer to the average effluent concentration in the sample collected between two necessary pressures; they are, therefore, plotted midway between these pressures. The results of a similar experiment with an anion-exchange resin originally in equilibrium with a magnesium chloride solution (0.204 *N*) are shown in Fig. 3.

It is seen that on application of pressure, the solution is first squeezed out rather easily, but a stage is reached at which large additional pressure causes only a minor increase in the volume of solution collected. At this stage, about 45 and 62% of the total water content of the cation- and anion-exchange resin, respectively (as determined by drying at 110°) has been squeezed out. It is well to remember that not all the water determined by this drying procedure is free to migrate, since some

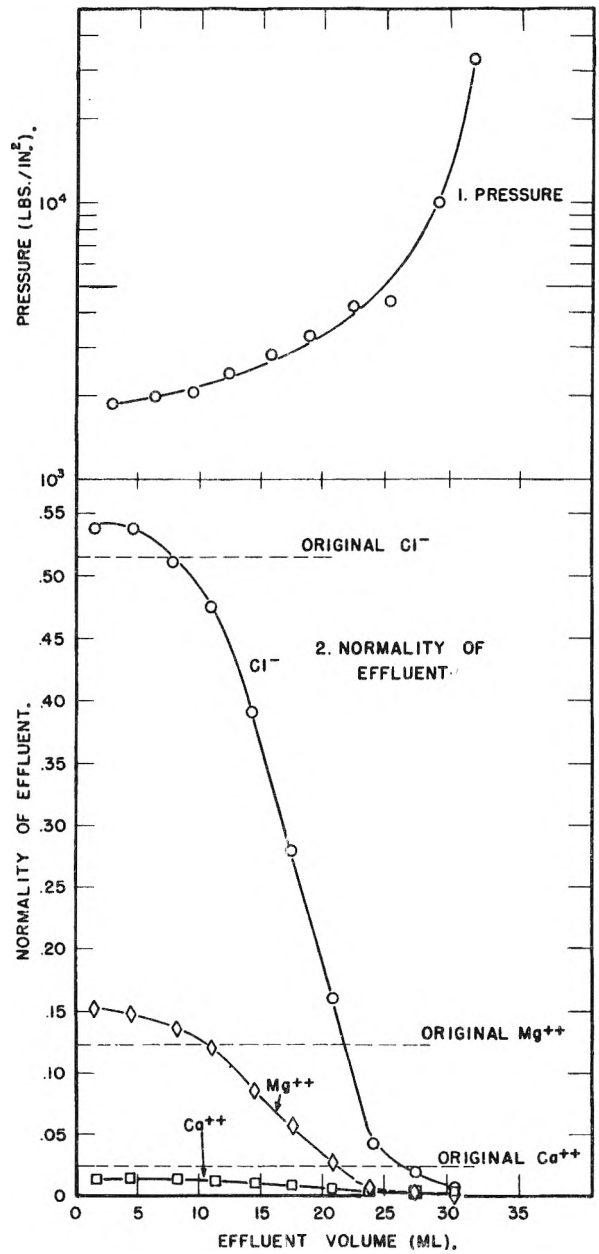

Fig. 2.—Squeezing of solution from cation-exchange resin grains: 150 g. (moist weight) "Dowex 50" (20–50 mesh) previously equilibrated with sea water. Initial and final volumes of resin bed—160 and 74 ml., respectively. Total volume of solution exuded—32.2 ml. (1) applied pressure *vs.* effluent volume; (2) normality of Cl^-, Mg^{++} and Ca^{++} in effluent *vs.* effluent volume.

must be considered tightly bound.[5,6] It is seen that the total chloride concentration in the first few samples was about the same as in the original equilibrium solution while the concentration in the later samples was much lower. The first samples represent surface adsorbed fluid not removed by filtration. The slight initial increase in chloride concentration, as compared to the equilibrium solution was also observed in several other experiments. It may be due to some evaporation. Later samples are more representative of the solution held in

(5) H. P. Gregor, *J. Am. Chem. Soc.*, **73**, 642 (1951).

(6) K. W. Pepper, D. Reichenberg and D. K. Hale, *J. Chem. Soc.*, 3129 (1952).

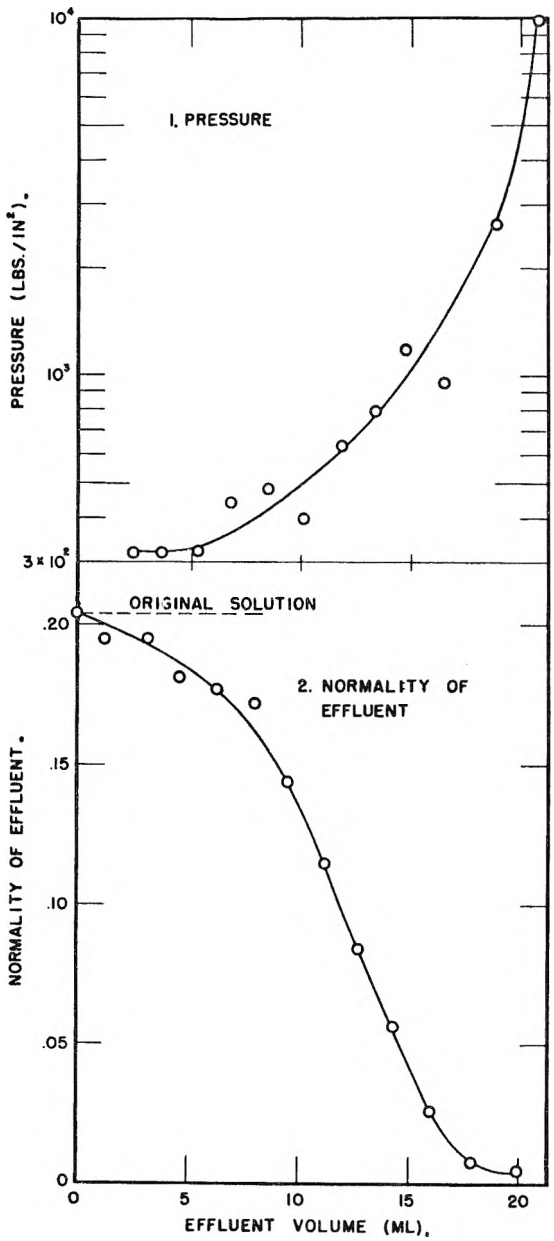

Fig. 3.—Squeezing of solutions from anion-exchange resin grains: 58 g. (moist weight) Amberlite IRA-411 (20–50 mesh) previously equilibrated with 0.204 *N* $MgCl_2$. Initial and final volumes of resin bed—80 and 41 ml., respectively. Total volume of solution exuded—20.8 ml.: (1) applied pressure *vs.* effluent volume; (2) normality of Mg^{++} in effluent *vs.* effluent volume.

the resin phase but, because of mixing along the column, the solution emerging at any pressure does not exactly represent the equilibrium solution for that pressure.

In the experiment involving squeezing of a cation-exchange resin originally in equilibrium with sea water, the ratio of sodium to potassium in the exuded solutions stayed relatively constant throughout the experiment while the ratio of magnesium to calcium in the first samples was higher than in sea water, then decreased to a much lower value than in the sea water.

These observations may be of geological significance. When sedimentation occurs in a marine or non-marine basin, the uppermost sediment layers are of high porosity and thus contain large amounts of interstitial solutions. Many sediments contain considerable amounts of hydrated clays of high base exchange capacity such as montmorillonite. As these sediments become buried and compaction proceeds under high pressure, these solutions are gradually squeezed out and the porosity of the sediment is thus reduced. In addition, some of the water originally contained in the solid particles and not strongly bound may also be squeezed from the solid. At this stage, the situation is somewhat similar to that prevailing in our experiments with cation exchange resins and rather complex concentration changes in the liquid phase are liable to occur as in these experiments.

2. **"Filtration" of Salt by a Cation-exchange Membrane.**—It is often believed that a solute cannot be separated by filtration from a solvent unless the sizes of the solvent and solute molecules are appreciably different. In particular, it has been believed until recently that separation of sodium chloride from water by filtration is impossible, since the molecular sizes of these two compounds are not sufficiently different. Recently, however, Reid and Breton[7] have shown that such a filtration process may be effected by forcing the solution through certain cellulosic membranes. The exact mechanism of this action is not yet known. It has been claimed on the strength of electric transference measurements, that the salt filtering action is not due to selective permeability to cations or anions.

Schmid[8] measured the streaming potential across collodion membranes and from the shape of the potential *vs.* time curve he concluded that the membrane acted as a salt filter. The filtration of salt solutions through charged-net (ion exchange) membranes has been suggested[9,10] as a theoretical possibility to produce fresh water from sea water. A similar filtration through compacting shale membranes has been suggested as a possible mechanism for the high salt concentrations of connate waters in porous sedimentary rocks.[11] Here it is assumed that salt held back by clay-containing shales accumulates in the water not squeezed from the geologic column as compaction proceeds. The process of salt removal or concentration depends upon the large excess charge permanently attached to the membrane which prevents the passage of like charged ions. In this case the separation is effected because of the electrical properties rather than the size of the solute. Consider, for instance, the case of a cation-exchange membrane through which a dilute solution of sodium chloride is being compressed. (The hydraulic permeability of commercial ion exchange membranes is generally very low, but if sufficient pressure is applied, it is possible

(7) C. E. Reid and E. J. Breton, 30th National Colloid Symposium, Madison, Wisconsin, June, 1956.

(8) G. Schmid and H. Schwarz, *Z. Elektrochem.*, **53**, 35 (1952).

(9) United States Department of the Interior "Saline Water Conversion," Annual Report of the Secretary of the Interior for 1952.

(10) C. B. Ellis, "Fresh Water from the Ocean," Ronald Press, New York, N. Y., 1954.

(11) M. R. J. Wyllie, Proc. First National Conference on Clays and Clay Technology, p. 282, *Bulletin 169*, Division of Mines, State of California (1955).

to compress liquids through them.) Since the salt is largely excluded from the resin phase, the concentration of chloride ions in the membrane is quite low. Because of the electroneutrality condition, sodium ions cannot leave the membrane without being accompanied by chloride ions except for a minor amount of Na^+ which enters the solution on the low pressure side and thus creates a streaming potential which prevents further unequal flow of Na^+ and Cl^-. Since the flux of the chloride ions is low, because of their low concentration in the membrane, the total flux of salt across the membrane is low. This is true only in the absence of an electrical short circuit between the liquids separated by the membrane. On the other hand, if silver–silver chloride electrodes are inserted in the two solutions and connected, chloride is withdrawn from the high-pressure side and supplied to the low-pressure side by electrode reactions and thus the flux of sodium ions in the membrane is no longer dependent on the flux of chloride ions through the membrane and can, therefore, proceed at a much faster rate.[12] Similarly other electrodes can modify the concentration changes by their characteristic electrode reactions. At any rate, if no such short circuit exists, sodium chloride can travel through the membrane only at a slow rate. On the other hand, no such electrical restrictions are placed on the water molecules. The water molecules therefore "overtake" the salt and the result is a lower salt concentration in the filtrate than in the original solution. Thus the salt is filtered by virtue of its electrolytic dissociation and the ionic nature of the ion-exchange membrane. These considerations hold mainly for dense membranes containing no large pores. If such pores are present, their central portions act as internal short circuits and thus decrease both the streaming potential[13] and the desalting effect.

We have now directly demonstrated the salt filtering action of synthetic ion-exchange membranes, using a cation-exchange membrane "Permaplex C-10"[14] (United Water Softeners, Ltd., London, England), a solution of NaCl about 0.1 *N*, and a pressure differential of about 1500 p.s.i.

The membrane used was conditioned by cycling between the sodium and hydrogen forms prior to the experiment. At the start of the experiment, it was in the sodium form and in equilibrium with a 0.099 *N* sodium chloride solution. The effective membrane area was 9.0 cm.^{2} and the thickness 0.06 cm. The membrane was held at one end of a "Lucite" tube and supported against high pressures by a micro-metallic porous disc. The Lucite tube was surrounded by a close-fitting steel cylinder. The Lucite cylinder was partially filled with 45 ml. of a 0.099 *N* sodium chloride solution and pressure was applied to the solution *via* a close-fitting weighted piston with "O" ring seal and a hand operated "Buehler 1315" hydraulic press. After initially raising the piston pressure, a slow drop occurred, as the liquid moved through the membrane. This was corrected by raising the piston again, causing the pressure to rise to the higher level. This was continued in about half-hour intervals during daytime, but was not done during the night. Accordingly, the pressure dropped to a very low value during the night periods. Because of these pressure fluctuations the hydraulic permeability of the membrane cannot be calculated from the data with any degree of accuracy. However, the salt filtering effect was clearly demonstrated by collecting and analyzing the solution filtered through the membrane. This fluid was collected in a loosely stoppered test-tube about every second day. Under these conditions, the size of each sample was about 1.5 ml. The experiment lasted 45 days. The chloride concentration in each sample was determined volumetrically by Clark's method.[14a]

After about four-fifths of the original solution had been "filtered," the pressure cell was disassembled and the remaining solution was analyzed.

The results of this experiment are shown in Fig. 4. Curve 1 shows the salt concentration in the filtrate as determined by titration. The salt concentration in the concentrate (curve 2) was calculated from the amount of filtrate collected and its concentration. This mass balance calculation was confirmed at the end of the experiment by titration of the concentrate which had remained in the cell. It is seen that the salt concentration in the filtrate was about 30% less than in the remaining solution in the pressure cell.

Several additional experiments were conducted at pressures below 100 p.s.i. At these pressures, no desalting was observed and the hydraulic permeability was much higher than in the experiment conducted at a maximum pressure of 1500 p.s.i. A possible explanation is that the membrane contains pores which pass salt and water at low pressures but which are reduced in size by the high pressure and then reduce the passage of salt more efficiently.

Experiments with membranes of similar chemical composition, but different hydraulic permeability, confirmed that the desalting effect is critically dependent on the hydraulic permeability of the membrane. Other things equal, membranes of lower hydraulic permeability produced higher desalting effects.

It is possible that the true desalting efficiency of the membrane at high pressure is higher than reported here since the frequent drops in pressure which occurred in our experiment might have allowed a considerable volume of relatively concentrated solution to pass through the membrane at periods of low pressure.

(12) The presence of this effect might prove to be a criterion for the electrical nature of the salt filtering action of the membrane.

(13) A. S. Michaels and C. S. Lin, *Ind. Eng. Chem.*, **47**, 1249 (1955).

(14) The "Permaplex C-10" membrane used in this experiment was a sample of an early experimental membrane supplied by Dr. T. R. E. Kressman of United Water Softeners Ltd., London. "Permaplex C-10" membranes of later manufacture did not show the desalting effect and appeared to be quite different in physical properties as well. Dr. Kressman informed the authors that these membranes were prepared in a different manner. The early membranes had higher electrical resistance and much lower hydraulic permeability than the present commercial membranes. Dr. Kressman kindly supplied the authors with additional membranes of early manufacture. With these membranes the desalting effect was again confirmed.

Samples of the older "Permaplex C-10" membranes are now no longer available. However, it was found that certain other membranes also show a desalting effect, *e.g.* "Nalfilm-1" (National Aluminate Corp., Chicago, Ill.).

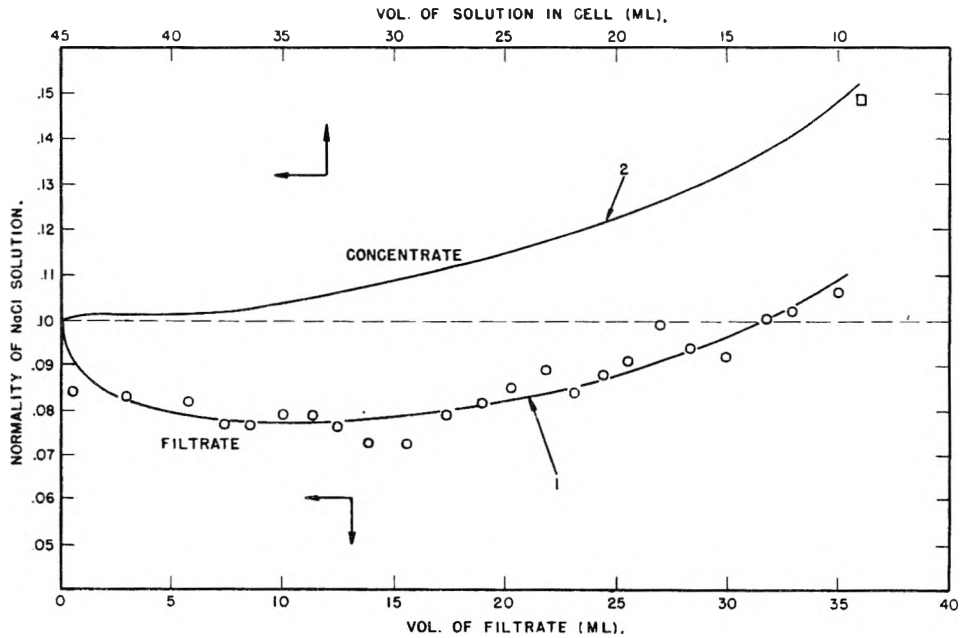

Fig. 4.—Filtration of a salt solution through an ion-exchange membrane. "Permaplex C-10" membrane—0.099 *N* NaCl maximum pressure about 1500 p.s.i.: (1) normality of filtrate *vs.* volume filtered; (2) normality of NaCl solution in cell *vs.* volume in cell (calculated except initial and final points). Dotted line shows normality of original solution.

The observed salt filtering effect of the ion-exchange membranes is believed to be due to the electrical properties of the membrane, but we have no proof yet that it is not a size or shape effect. If it is indeed an electrical effect, then it is related to other ion transport phenomena across the membrane such as electric conductance, electric ion transfer, electro-osmosis and diffusion. These relationships are expressed by the general flux equations of the thermodynamics of the steady state.[15,16] Additional studies on the relationship between these processes as well as further experiments are in progress.

(15) A. J. Staverman, *Trans. Faraday Soc.*, **48**, 176 (1952).

(16) S. W. Lorimer, E. I. Boterenbrood and J. J. Hermans, Discussion of the Faraday Society on "Membrane Phenomena," Nottingham, 1956 (in press).

SOME PROPERTIES OF DIFFUSION COEFFICIENTS IN POLYMERS

BY R. M. BARRER

Contribution from the Chemistry Department, Imperial College of Science and Technology, London, S. W. 7, England

Received July 30, 1956

An account has been given of several recent developments in sorption and diffusion in some polymers. The five diffusion coefficients characteristic of any binary mixture can all be obtained in penetrant–polymer mixtures, but past measurements in a variety of systems have probably given erroneous diffusion coefficients D because it has only recently been realized that in them the diffusion coefficients are a function of time as well as of concentration. Present methods of interpretation cannot allow for simultaneous time and concentration dependence of D. The most reliable results for this reason refer to elastomer–penetrant systems, where time effects are at a minimum owing to short relaxation times of polymer molecules. For the same reason in polymers exhibiting less chain mobility and stronger inter-chain bonds the steady-state methods of measuring diffusion coefficients are preferable to transient state procedures. A classification of penetrant–polymer systems has been given, with examples of each category. Factors influencing the concentration dependence of diffusion coefficients D are discussed, and also the experimental observations leading to the zone theory of the diffusion mechanism and the quantitative formulation of this theory. Relations between viscous resistance and diffusion are indicated, and generalized functional relationships between D_0 and E_a/T in the Arrhenius equation $D = D_0 \exp(-E_a/RT)$ are considered. Selectivity in the transmission of molecules through organic membranes also has been considered.

Investigation of transport processes of simple molecules within polymers usually involves measurements of sorption, permeability and diffusion of penetrant in and through the polymer. Interpretation of these basic phenomena brings contact with a considerable region of the physical chemistry of high polymers. Sorption and solubility are equilibrium properties characteristic of polymer and penetrant amenable to thermodynamic and statistical thermodynamic analysis[1-6]; diffusion coefficients are rate constants, amenable to "irre-

(1) *E.g.*, G. Gee, *Quart. Rev.*, **1**, 265 (1947).

(2) M. Huggins, *J. Chem. Phys.*, **9**, 440 (1941); *Ann. N. Y. Acad. Sci.*, **43**, 1 (1942).

(3) W. Orr, *Trans. Faraday Soc.*, **40**, 320 (1944).

(4) P. J. Flory, *Proc. Roy. Soc. (London)*, **A234**, 60, 73 (1956).

(5) R. M. Barrer, *Trans. Faraday Soc.*, **43**, 3 (1947).

(6) H. L. Frisch and C. V. Stannett, *J. Polymer Sci.*, **13**, 131 (1954).

versible thermodynamic" and kinetic treatment.[7,8] Diffusion may be connected with other rate processes such as dielectric relaxation or viscous flow for which a spectrum of relaxation times is expected.[7,9,10] In this paper some recent progress is considered.

1. The Five Diffusion Coefficients in a Binary Mixture.—Meyer,[11] Darken,[12] Hartley and Crank,[13a] and Carman and Stein[13b] have discussed the physical significance of diffusion coefficients measured under different conditions. Five diffusion coefficients characterize any binary mixture of species A and B (whether gaseous, liquid or solid). First we may think of pure diffusion streams of A and B along the x-coördinate uncomplicated by any kind of mass flow. That is, the origin of the x-coördinate is in a plane normal to it and moving so that there is no mass flow across it. Per unit cross-section normal to the x-direction, in which diffusion occurs, the streams are

$$J_A = -D_A \frac{\partial C_A}{\partial x}; \quad J_B = -D_B \frac{\partial C_B}{\partial x} \qquad (1.1)$$

where D_A, D_B, C_A and C_B are, respectively, intrinsic diffusion coefficients and concentrations of A and B.

However, in a binary mixture which undergoes no volume change on mixing at constant pressure and which fills a constant volume vessel, a complication arises when we consider transport through a unit cross-section fixed with respect to the walls of the vessel and normal to x. Since in general, $J_A \neq J_B$, a compensating mass flow must occur to maintain uniform pressure throughout the diffusion volume. If V_A and V_B are the specific volumes of A and B, and C_A and C_B are their concentrations in g. per unit volume, then for unit volume of solution

$$V_A C_A + V_B C_B = 1 \qquad (1.2)$$

and so

$$V_A \frac{\partial C_A}{\partial x} + V_B \frac{\partial C_B}{\partial x} = 0 \qquad (1.3)$$

Moreover the total volume flow of A through the fixed unit cross-section (due to mass flow and pure diffusion) must equal the corresponding total volume flow of B through unit cross-section, since uniform pressure is maintained. These two equal and opposite flows, J'_A, J'_B are

$$J'_A = -D_{AB} V_A \frac{\partial C_A}{\partial x}; \quad J'_B = -D_{BA} V_B \frac{\partial C_B}{\partial x} \qquad (1.4)$$

where D_{AB} and D_{BA} are two interdiffusion coefficients, and where

$$J'_A = J'_B \qquad (1.5)$$

Since V_A and V_B are not in general equal to zero the only way in which 1.3, 1.4 and 1.5 can simultaneously be satisfied requires that $D_{AB} = D_{BA}$. Thus only one *mutual* interdiffusion coefficient describes the combination of mass flow and pure diffusion. It can now be shown easily that[14]

$$D_{AB} = V_A C_A D_B + V_B C_B D_A \qquad (1.6)$$

and that when $V_A = V_B$

$$D_{AB} = N_A D_B + N_B D_A \qquad (1.7)$$

where N_A and N_B are mole fractions of A and B, respectively.

Two other diffusion coefficients, D_A^* and D_B^* can be measured directly. These are the self-diffusion coefficients. Suppose a mixture consists of $n_A + n_A^*$ molecules of A (where the * denotes isotopically labeled molecules) and n_B molecules of B. In the solution we have $dn_B/dx = 0$ and $d(n_A + n_A^*)/dx = 0$. However if dn_A^*/dx, and so dn_A/dx, are not zero the pure diffusion flux $J_A^* = -D_A^*(\partial C_A^*/\partial x)$ can be measured and D_A^* evaluated. One may obtain D_B^* in a similar way.

A relation between D_A and D_A^* exists, and is derived as follows. If μ_A is the chemical potential of A, the driving force causing diffusion of A is usually assumed proportional to $-\partial\mu_A/\partial x$. The total force on all molecules of A at a point x is then proportional to $-C_A(\partial\mu_A/\partial x)$ and so the flux J_A through unit area is

$$J_A = -B_A C_A \frac{\partial \mu_A}{\partial x} \qquad (1.8)$$

Since $d\mu_A = RT\, d \ln a_A$, substitution in 1.8 gives

$$J_A = -RTB_A \frac{d \ln a_A}{d \ln C_A} \times \frac{\partial C_A}{\partial x} \qquad (1.9)$$

where B_A is the intrinsic mobility of A, and a_A denotes its activity. A comparison of 1.1 and 1.9 shows that

$$D_A = RTB_A \frac{d \ln a_A}{d \ln C_A} \qquad (1.10)$$

Next we may apply the same argument to the diffusion of labeled molecules of A and obtain

$$D_A^* = RTB_A \frac{d \ln a_A^*}{d \ln C_A^*} \qquad (1.11)$$

the intrinsic mobility B_A being the same for labeled and unlabeled molecules of A. However since

$$\frac{d(n_A + n_A^*)}{dx} = 0 = \frac{dn_B}{dx}$$

we must have

$$\frac{d \ln a_A^*}{d \ln C_A^*} = 1 \text{ and so}$$

$$D_A^* = RTB_A \qquad (1.12)$$

Comparison of 1.12 and 1.10 then shows that

(7) R. M. Barrer, *Trans. Faraday Soc.*, **35**, 644 (1939); **38**, 322 (1942); **39**, 237 (1943).

(8) H. Eyring, *J. Chem. Phys.*, **4**, 283 (1936). See S. Glasstone, K. J. Laidler and H. Eyring, "Theory of Rate Processes," McGraw-Hill Book Co., Inc., New York, N. Y., 1941.

(9) W. Kauzmann, *Rev. Mod. Phys.*, **14**, 12 (1942).

(10) W. Kuhn, *Rubber Chemistry and Technology*, **27**, 36 (1954).

(11) O. E. Meyer, "Kinetische Theory von Gase," 1st ed., Breslau, 1877.

(12) L. S. Darken, *Trans. Am. Inst. Mech. Eng.*, **175**, 184 (1948).

(13) (a) G. S. Hartley and J. Crank, *Trans. Faraday Soc.*, **45**, 801 (1949); (b) P. C. Carman and L. Stein, *ibid.*, **52**, 619 (1956).

(14) Consider a cross-section moving at such a rate that no mass flow occurs across it. There is now only pure diffusional transport through this cross-section and, according to 1.1, because $J_A \neq J_B$, a rate of accumulation of volume dV/dt on one side of it which is

$$\frac{dV}{dt} = D_A V_A \frac{\partial C_A}{\partial x} + D_B V_B \frac{\partial C_B}{\partial x} \qquad (1.8a)$$

Then dV/dt must equal the rate of transfer of total volume by mass flow through a fixed cross-section. Accordingly the rate of transfer of A by mass flow is $(dV/dt)C_A$, and the total rate of transfer of A is thus

$$-D_{AB} \frac{\partial C_A}{\partial x} = -D_A \frac{\partial C_A}{\partial x} + \frac{dV}{dt} C_A \qquad (1.9a)$$

by equating two expressions for the total transport of A. Using 1.2 and 1.3, substitution of 1.8a in 1.9a then gives 1.6.

$$D_A = D_A^* \frac{\mathrm{d} \ln a_A}{\mathrm{d} \ln C_A} \qquad (1.13)$$

as the desired relation between D_A and D_A^*. Similar relations follow for D_B and D_B^*.

We may further relate D_A^* and D_B^* with D_{AB}. The Duhem–Margules relationship gives

$$\frac{\partial \ln a_A}{\partial \ln N_A} = \frac{\partial \ln a_B}{\partial \ln N_B} \qquad (1.14)$$

Also, $C_A = N_A/(V_A N_A + V_B N_B)$; $C_B = N_B/(V_A N_A + V_B N_B)$
and so

$$\frac{\mathrm{d} \ln a_A}{\mathrm{d} \ln C_A} = \frac{\mathrm{d} \ln a_A}{\mathrm{d} \ln N_A} \frac{N_A V_A + N_B V_B}{V_B} \qquad (1.15)$$

with an analogous expression for species B. Equations 1.13, 1.14 and 1.15 may be substituted in 1.6 to give

$$D_{AB} = \frac{\mathrm{d} \ln a_A}{\mathrm{d} \ln N_A} \{N_B D_A^* + N_A D_B^*\} \qquad (1.16)$$

The above relations assume no volume change on mixing A and B.

2. Measurement of the Five Diffusion Coefficients.—For two interdiffusing liquids one may determine directly D_{AB} and D_A^* and D_B^*, but not D_A and D_B. This is the case because in liquids no way of separating mass flow and intrinsic diffusion rates has been devised. However, from a knowledge of d ln a_A/d ln C_A and d ln a_B/d ln C_B, one may obtain D_A and D_B from D_A^* and D_B^*.

For two solids, *e.g.*, Ag and Au, mass flow accompanying diffusion may be measured by placing markers at the Ag–Au interface, and observing the rate at which the markers move (the Kirkendall effect).[15] Indeed for one composition of the Ag–Au alloy (~50:50 atomic %) all five diffusion coefficients have been separately determined.[16] When a liquid or vapor diffuses in a polymer, B, it may be assumed that D_B is extremely small, so that it will be difficult to measure. Also over nearly all the composition range eq. 1.6 reduces to

$$D_A = \frac{D_{AB}}{V_B C_B} \qquad (2.1)$$

Finally, if we refer to permeation rates in the steady state through a membrane of *unswollen* thickness, l, it can be shown that[13]

$$J_A = \frac{1}{l} \int_0^{C_A} D_A (V_B C_B)^3 \, \mathrm{d}C_A; \quad \text{or}$$

$$\frac{1}{l} \frac{\mathrm{d}J_A}{\mathrm{d}C_A} = D_A (V_B C_B)^3 = D_{AB} (V_B C_B)^2 \qquad (2.2)$$

Thus, the slope of a curve of J_A against C_A serves to measure D_A. Finally the self-diffusion coefficient D_A^* may be measured in the polymer just as in the case of liquids.

3. Classification of Penetrant–Polymer Systems in Diffusion and Solution.—Many penetrant–polymer systems may from the standpoint of diffusion and solution be placed into four categories

(1) $\dfrac{\partial C_A}{\partial t} = D_{AB} \dfrac{\partial^2 C_A}{\partial x^2}$; $C_A = k p_A$

(2) $\dfrac{\partial C_A}{\partial t} = \dfrac{\partial}{\partial x}\left(D_{AB} \dfrac{\partial C_A}{\partial x}\right)$; $D_{AB} = \mathrm{f}(C_A)$; $C_A = k p_A$

(3) $\dfrac{\partial C_A}{\partial t} = \dfrac{\partial}{\partial x}\left(D_{AB} \dfrac{\partial C_A}{\partial x}\right)$; $D_{AB} = \mathrm{f}(C_A)$; $C_A = \mathrm{F}(p_A)$

(4) $\dfrac{\partial C_A}{\partial t} = \dfrac{\partial}{\partial x}\left(D_{AB} \dfrac{\partial C_A}{\partial x}\right)$; $D_{AB} = \mathrm{f}(t, C_A)$; $C_A = \mathrm{F}(p_A)$

Into the first category fall diffusion and solution of permanent and inert gases in rubber, synthetic elastomers and probably in many harder polymers. Solubility and diffusion have been rather extensively investigated in the author's laboratory in elastomer systems.[5,17–19] Since $V_B C_B \sim 1$, $D_B << D_A$, all measurements of D_{AB} are in fact measurements of the intrinsic diffusion coefficient D_A. Moreover, at equilibrium d ln a_A/d ln C_A = d ln p_A/d ln C_A = 1, and so $D_A = D_A^*$. Further comment on these systems is made later.

The second category of penetrant–polymer systems is well represented by C_4 and C_5 paraffins diffusing and dissolving in rubber.[19] D_{AB} is no longer independent of C_A, but Henry's law is still valid, so that

$$D_{AB} = \frac{D_A}{V_B C_B} \text{ and } D_A = D_A^*$$

Since $D_A^* = RTB_A$ one may easily obtain the intrinsic mobility, B_A, from measurements made on the first two categories of penetrant–polymer systems. The intrinsic mobility is inversely proportional to the viscous resistance, η, brought into play by the relative motion of molecule and polymer. The constant of proportionality has been derived theoretically by Kuhn,[10] and for self-diffusion of polymers by Barrer.[7] Aitken and Barrer[19] for C_4 and C_5 paraffins found in the concentration range studied that

$$B_A = B_{C=0}(1 + bC_A) \qquad (3.1)$$

When values of b were measured at a series of temperatures this coefficient was found to decrease rapidly with rising temperature (Fig. 1). It was suggested that the internal mobility of polyisoprene chains increased so much at the higher temperatures that small increments of concentration of paraffin no longer led to much additional plasticizing of polymer. At lower temperatures the natural mobility of polymer chains was much less and so plasticizing by penetrant molecules produced a greater effect.

For penetrant–polymer systems in the third category, typified by the sorption and diffusion of heavier hydrocarbon vapors[20–22] or chloroform[23] in rubber, we no longer have a linear isotherm. Often the isotherm contours can be represented over a

(15) (a) A. D. Smigelskas and E. O. Kirkendall, *Trans. Am. Inst. Mech. Eng.*, **171**, 130 (1947); (b) For discussion see W. Seith, "Diffusion in Metallen," Springer Verlag, Berlin, 1955, p. 129, *et seq.*

(16) (a) W. A. Johnson, *Trans. Am. Inst. Mech. Eng.*, **143**, 107 (1941); **147**, 331 (1942); (b) W. Seith, "Diffusion in Metallen," Springer Verlag, Berlin, 1955, p. 148, *et seq.*

(17) R. M. Barrer, *Trans. Faraday Soc.*, **35**, 628 (1939); **36**, 645 (1940); *Koll. Z.*, **120**, 177 (1950).

(18) R. M. Barrer and G. Skirrow, *J. Polymer Sci.*, **3**, 549, 564 (1948).

(19) A. Aitken and R. M. Barrer, *Trans. Faraday Soc.*, **51**, 116 (1955).

(20) G. Gee and L. R. Treloar, *ibid.*, **38**, 147 (1942).

(21) J. Ferry, G. Gee and L. R. Treloar, *ibid.*, **41**, 340 (1945).

(22) K. H. Meyer, E. Wolff and C. Boissonas, *Helv. Chim. Acta*, **23**, 430 (1940).

(23) (a) P. Stamberger, *J. Chem. Soc.*, 2318 (1929); (b) J. Lens *Rec. trav. chim.*, **51**, 971 (1932).

substantial range of concentrations by expressions based on the lattice theory of penetrant–polymer mixtures (Fig. 2). In the isotherm for a vapor with zero heat of mixing there is only one adjustable parameter,[5] as against two for B.E.T. or Langmuir isotherms, yet the equation can be very successful indeed, as the figure shows. Normally we would still expect $D_B << D_A$, and so

$$D_{AB} \simeq D_A(V_B C_B) \qquad (3.2)$$

The polymers in this category are rubbers with high chain mobility and short relaxation times.

The fourth category of penetrant–polymer systems includes many more rigid and internally viscous polymers, with long relaxation times. This category includes the group of "anomalous" diffusions[24,25] in which it seems likely that time-components enter the diffusion coefficient in the transient state of flow. The process of sorption on occasions takes place in two distinct stages (Fig. 3, curve a). Both stages involve swelling of the polymer. The first stage involves a spectrum of smaller relaxation times, and in part may be elastic. However, there are also semi-permanent bonds the relaxation times for which are very great and so which resist swelling until the content of penetrant reaches a high enough value in the region of polymer concerned and the stress builds up sufficiently. Then these bonds begin to break, and the ambient stress system is relieved by further swelling. The more of such bonds which break the greater the stress on the remainder and so the process can be and often is an "autocatalytic" one (Fig. 3). Taken as a whole this two-stage process could be represented as a diffusion with a complex time and concentration dependence of D_{AB} ($D_{AB} = f(c, t)$). It is also possible that slow relaxation is occurring as a result of past treatments of polymer and that these are largely independent of the penetrant. In this case $D_{AB} = f_1(t) \times f_2(C)$.

We have recently examined ethylcellulose as a diffusion medium using vapors[26] of different polarity (C_6H_6, $(CH_3)_2CO$ and CH_3OH) and also C_4 and C_5 paraffins.[27] These systems exhibit history-dependent sorption and diffusion, but by working in regions of lower penetrant concentration (volume fractions <0.1) it was found possible to control history-dependence and to obtain "settled" sorption and permeation data. As penetrant concentrations increased time-dependent processes were increasingly evident. It therefore seems likely that such processes occur even before completion of the first stage of sorption (curve a in Fig. 3). Indeed many "anomalous" diffusions do not show the two stages, but follow the course shown in curve b, and are "autocatalytic" in shape from the beginning.

The four categories of penetrant–polymer mixture already referred to are not the only possible cases. Where there is a steady thermal gradient across a membrane (as in thermoösmosis[28]) or where a mem-

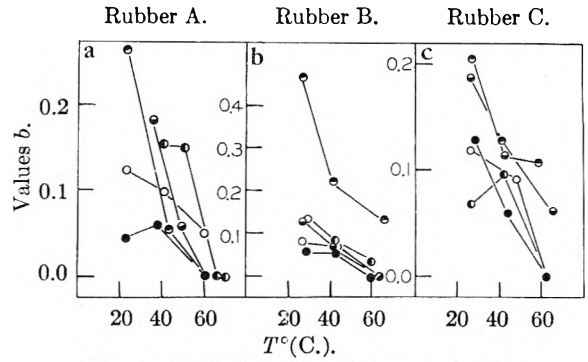

Fig. 1.—Variation of b with temperature.[19]

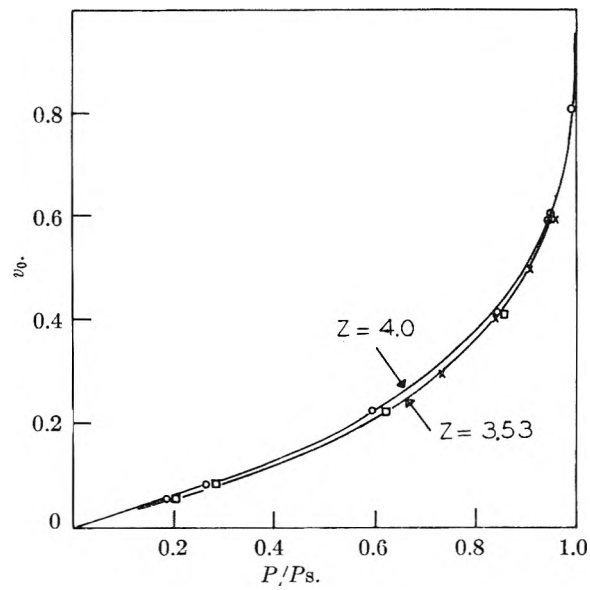

Fig. 2.—Calculated isotherms[5] using lattice theory with zero heat of mixing, and observed isotherm points, for benzene–rubber mixtures.

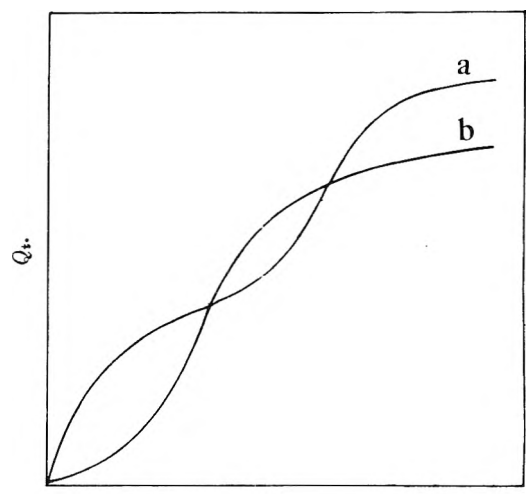

Fig. 3.—Some characteristic rates of sorption in polymers of the fourth category.

(24) (a) J. Crank and G. S. Park, *Trans. Faraday Soc.*, **47**, 1072 (1951); (b) G. Park, *J. Polymer Sci.*, **11**, 97 (1953); (c) J. Crank, **11**, 151 (1953).

(25) (a) F. A. Long, E. Bagley and J. Wilkens, *J. Chem. Phys.*, **21**, 1412 (1953); (b) L. Mandelkern and F. A. Long, *J. Polymer Sci.*, **4**, 457 (1951); (c) R. J. Kokes, F. A. Long and J. L. Hoard, *J. Chem. Phys.*, **20**, 1711 (1952); (d) P. Drechsel, J. L. Hoard and F. A. Long, *J. Polymer Sci.*, **10**, 241 (1953).

(26) (a) R. M. Barrer, J. A. Barrie and J. Slater, *J. Polymer Sci.*, in press; (b) R. M. Barrer and J. A. Barrie, *J. Polymer Sci.*, in press.

(27) R. M. Barrer, J. A. Barrie and J. Slater in preparation.

(28) K. Denbigh and G. Raumann, *Proc. Roy. Soc. (London)*, **A210**, 377, 518 (1951).

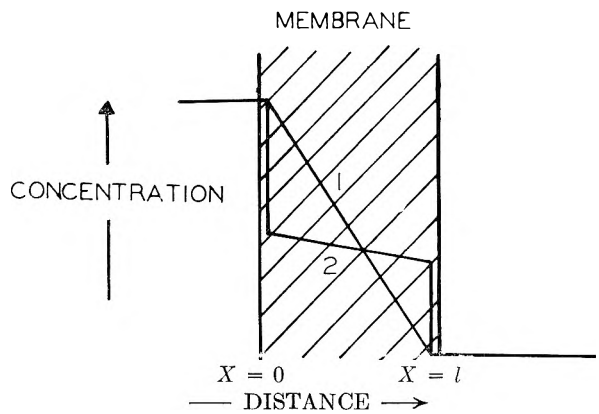

Fig. 4.—Gradients across a polymer membrane with (curve 2) and without (curve 1) surface barrier layers.

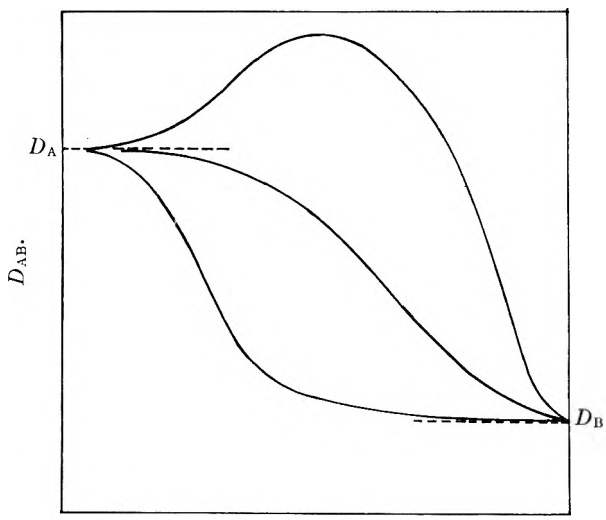

Fig. 5.—Possible changes in D_{AB} over a complete composition range from 100% B to 100% A.

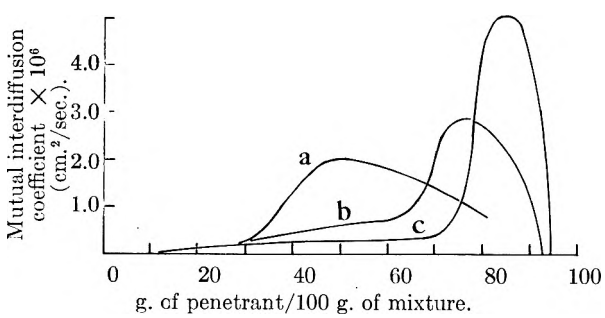

Fig. 6.—Mutual diffusion coefficients for three penetrants and cellulose acetate at 25°[31]: a, acetone; b, chloroform; c, methylene chloride.

brane consists of laminae of different polymers we may have

$$\frac{\partial C}{\partial t} = \frac{\partial}{\partial x}\left(D_{AB}\frac{\partial C}{\partial x}\right);\quad D_{AB} = f(x);\quad C = kp$$

$$\frac{\partial C}{\partial t} = \frac{\partial}{\partial x}\left(D_{AB}\frac{\partial C}{\partial x}\right);\quad D_{AB} = f(x, C);\quad C = F(p)$$

Moreover when thermal transients are combined with material diffusion we could have (5) with $D_{AB} = f(x, t)$ and (6) with $D_{AB} = f(x, t, C)$. Such systems could have considerable importance. Those where $D = f(x)$ only can often be solved explicitly.

A final possibility arises when the polymers are covered by impermeable boundary layers of molecular thicknesses which form surface resistances to entry or to exit from the polymer. Such behavior can arise with metallic membranes and has been investigated both theoretically and experimentally.[29,30] It converts concentration gradients such as (1) in Fig. 4 to (2) in the same figure.

4. Concentration Dependence of Diffusion Coefficients.—The way in which diffusion coefficients change with penetrant concentration has now been investigated for a number of penetrant–polymer systems. It would be expected that, as the concentration of A approaches 100%, D_{AB} would approach the coefficient D_B. In nearly pure polymers D_{AB} should approach $D_A \sim D_A^*$ (since d ln a/d ln $C_A \sim 1$), as indicated in section 3. Between these extremes D_{AB} may follow various paths as shown in Fig. 5. Figure 6 shows examples of a complex dependence of D_{AB} upon the composition of the mixtures of cellulose acetate with acetone, chloroform and methylene dichloride.[31] Several factors contribute to the form of the curves.

(1) In some parts of the concentration range time-dependent components will enter into the diffusion.

(2) In D_{AB} appears a contribution due to mass flow, to which the maxima in Fig. 6[31] have been attributed. This mass flow component is absent in the intrinsic diffusion coefficient, D_A, which does not in fact exhibit a maximum (Fig. 7).[31]

(3) In D_{AB} and in D_A appears also the quantity d ln a_A/d ln C_A (eq. 1.16 and 1.10). To a first approximation d ln a_A/d ln C_A may be derived from the appropriate lattice theory equation. For example, for zero heat of mixing[5]

$$\frac{v_A}{\left\{1 - \frac{2}{Z}(1 - v_A)\right\}^{\frac{Z}{2}}} = \frac{p}{p_s} = a_A \qquad (4.1)$$

where v_A is the volume fraction of A ($= V_A C_A$), Z is the coördination number of a lattice point, and p/p_s is the relative pressure of vapor. However such expressions may not give d ln a_A/d ln C_A at all concentrations, and in particular must not be relied on as $C_A \rightarrow 100\%$ (pure liquid A).

The concentration dependence of D_A^* (and so of mobility B_A) then remains after allowance for all three of the above effects. As yet no satisfactory theory of concentration dependence of D_A^* exists. A number of investigations have shown that D_{AB}, D_A, or

$$\bar{D} = \frac{1}{C_A}\int_0^{C_A} D_{AB}\,dC_A$$

can be represented as exponential functions of penetrant concentration.[32] Many of these investigations refer to polyvinyl acetate, cellulose acetate, cellulose nitrate and polystyrene as diffusion media and therefore time components may enter D_{AB}, etc., and the concentration dependence may

(29) R. M. Barrer, *Trans. Faraday Soc.*, **36**, 1235 (1940).

(30) R. M. Barrer, *Phil. Mag.*, **28**, 148 (1939); see also R. M. Barrer, "Diffusion in and through Solids," Chap. 4, (C.U.P.), 1951.

(31) J. Crank and C. Robinson, *Proc. Roy. Soc.* (*London*), **A204**, 549 (1951).

(32) (a) G. Park, *Trans. Faraday Soc.*, **46**, 684 (1950); **47**, 1007 (1951); (b) J. Crank and G. Park, *ibid.*, **45**, 240 (1949); (c) R. J. Kokes and F. A. Long, *J. Am. Chem. Soc.*, **76**, 6142 (1953).

be wrongly assessed. However, data of Prager and Long[33] for polyisobutylene–hydrocarbon systems (which should give the correct concentration dependence of the diffusion coefficient, since the diffusion medium is an elastomer) still follow the exponential expression ($\bar{D} = \bar{D}_{C=0} \exp \alpha C_A$). As a corrective to any tendency to read undue significance into an exponential relation one notes that Fujita[34] was just as successful in representing the relation between C_A and D_{AB} for $CHCl_3$ diffusing in polystyrene by means of the relation $D_{AB} = D^0_{AB}(1 - bC_A)^{-2}$ as Crank and Park[32] had previously been with the exponential relation. Barrer, Barrie and Slater[27] in studies of diffusion in ethylcellulose, in which time-dependent effects were eliminated, have come to a similar conclusion.

5. Temperature and Diffusion.—It was pointed out by Barrer[17,35] that diffusion coefficients in elastomers depend exponentially upon temperature T

$$D_{AB} = D_0 \exp(-E_a/RT) \qquad (5.1)$$

and thus that diffusion is an activated process. Values of the constants D_0 and E_a were obtained and considerable light thrown upon the nature of the diffusion process.[7,17,18,36] In Table I are summarised values of E_a and D_0 for various natural and synthetic polymers, in which elastomers predominate. Barrer[18] drew attention to two features of special significance: (1) the size of the diffusing molecule has in elastomers a much smaller influence than would be inferred from analogous experiments on diffusion through a rigid membrane such as silica glass.[17,37] E_a is given for the latter in Table II. (2) the magnitudes of D_0 in elastomers are far above those usually observed in diffusion processes. This is shown in Fig. 8 for various types of interdiffusion process.

TABLE I

E AND D_0 IN THE EQUATION $D = D_0 e^{-E/RT}$ FOR DIFFUSION IN ELASTOMERS[17,18,36]

Gas	Polymer	E (cal./mole)	D_0 (cm.^{2} sec.$^{-1}$)
Helium	Perbunan 18	4200	0.019
	Natural rubber	4300	.031
	Isoprene–acrylonitrile copolymer	4900	.031
	Perbunan (German)	5200	.077
	Hycar OR 25	5200	.074
	Hycar OR 15	5500	.087
	Butyl rubber	5800	.015
Hydrogen	Polybutadiene	5100	0.053
	Natural rubber	6000	.26
	Perbunan 18	6200	.23
	Perbunan (German)	6900	.52
	Isoprene–methacrylonitrile copolymer	6900	.41
	Hycar OR 25	7000	.52
	Isoprene–acrylonitrile copolymer	7400	.67
	Methyl rubber	7500	1.3
	Vulcaprene A	7600	0.98
	Hycar OR 15	7600	0.92
	Butyl rubber	8100	1.36
	Neoprene (vulcanized)	9250	9.0
	Chloroprene	9900	39.4
Oxygen	Polybutadiene	6800	0.15
	Perbunan 18	8100	0.69
	Natural rubber	8300	1.94
	Perbunan (German)	9200	2.4
	Isoprene–methacrylonitrile copolymer	9600	2.6
	Polymethylpentadiene	9800	8.5
	Vulcaprene A	10200	7.0
	Hycar OR 25	10300	9.9
	Hycar OR 15	10900	13.6
	Methyl rubber	11100	20
	Butyl rubber	11900	43
	Isoprene–acrylonitrile copolymer	12700	70
Argon	Butadiene–styrene copolymer	9000	1.84
	Butadiene–methylmethacrylate copolymer	10300	15.1
	Neoprene (vulcanized)	11700	54.6
Nitrogen	Polybutadiene	7200	0.22
	Perbunan 18	8500	0.88
	Natural rubber	8700	2.6
	Butadiene–styrene copolymer	8900	0.93
	Perbunan (German)	10400	10.7
	Polymethylpentadiene	11100	42
	Butadiene–methylmethacrylate copolymer	11500	38
	Butadiene–acrylonitrile copolymer	11500	28.1
	Isoprene–methacrylonitrile copolymer	11600	39
	Hycar OR 25	11700	56
	Vulcaprene A	11700	55
	Neoprene (vulcanized)	11900	79
	Butyl rubber	12100	34
	Methyl rubber	12400	105
	Hycar OR 15	12700	131
	Isoprene–acrylonitrile copolymer	14500	1880
Carbon dioxide	Polybutadiene	7300	0.24
	Natural rubber	8900	3.7
	Perbunan 18	9200	2.4
	Perbunan (German)	10700	13.5
	Vulcaprene A	11800	42
	Butyl rubber	12000	36
	Hycar OR 25	12000	67
	Isoprene–methacrylonitrile copolymer	12200	81
	Methyl rubber	12800	160
	Hycar OR 15	13400	260
	Isoprene–acrylonitrile copolymer	14400	1150

D_0 in Fig. 8[7] has the dimensions cm.^{2} sec.$^{-1}$ and is equal to d^2k_0 where d is the average distance jumped per unit diffusion process and k_0 is entirely analogous with the pre-exponential factor in first-order velocity constants, k ($k = k_0 \exp(-E_a/RT)$). Taking $d = 2.1 \times 10^{-8}$ cm. one obtains values for k_0 for the

(33) S. Prager and F. A. Long, *J. Am. Chem. Soc.*, **73**, 4072 (1951).
(34) H. Fujita and A. Kishimoto, *Textile Res. Jr.*, **23**, 59 (1953).
(35) R. M. Barrer, *Nature*, **140**, 106 (1937).
(36) (a) R. M. Barrer, *Trans. Faraday Soc.*, **39**, 48, 59 (1943); (b) G. J. van Amerongen, *J. Polymer Sci.*, **5**, 307 (1950); *J. Appl. Phys.*, **17**, 972 (1946).
(37) R. M. Barrer, *J. Chem. Soc.*, 378 (1934).

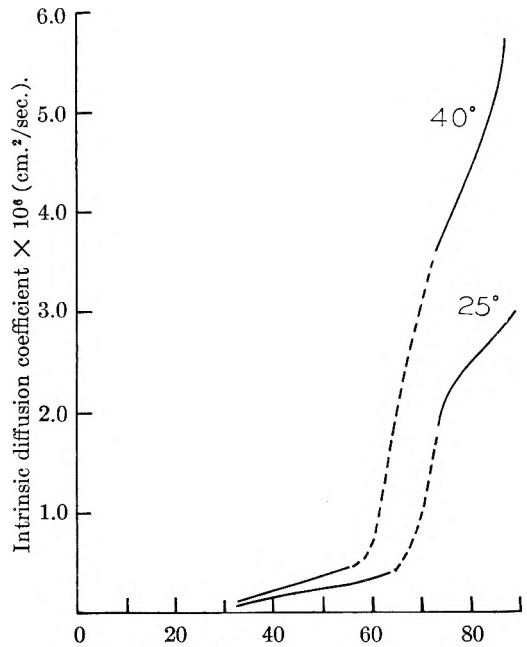

Fig. 7.—Intrinsic diffusion coefficients for chloroform and cellulose acetate[31] at 25 and 40°.

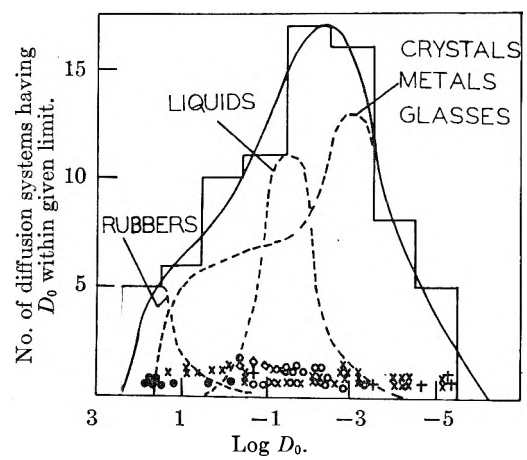

Fig. 8.—Periodicity curve for D_0 in $D = D_0 e^{-E/RT}$ for activated diffusions.[17]

TABLE II

DIFFUSION IN SILICA GLASS

Gas	Diameter,[a] Å.	Arrhenius energy of activation
He	~2.2	5,600
H_2	3.14, 2.4	10,100
Ne	3.20	9,500
N_2	4.1, 3.0	26,000
A	3.84	~32,000

[a] For the dumbbell shaped molecules H_2 and N_2 length and cross-sectional diameters both are given.

several maxima in the curves of Fig. 8, as shown in Table III. k_0 is much the highest for diffusion in elastomers and so an analogy may be drawn between such diffusions and fast unimolecular reactions. In the latter, where chain mechanisms are absent, the energy of activation has been considered to be first stored in a considerable number, f, of degrees of freedom. In this event the constant k_0 should contain a term

$$\left(\frac{E}{RT}\right)^{f-1} \frac{1}{(f-1)!} \exp -(f-1)$$

where $E_a = E - (f-1)RT$. This term is $>>1$ for suitable values of f and E. Such an analogy for diffusion requires a "zone" of activation in

TABLE III

Type of rate process	Value of k_0 (sec.$^{-1}$) at max. in periodicity curve of Fig. 7	Spread in values of k_0
Some first-order reactions	10^{13} to 10^{14}	10^{13}-fold
Diffusion in some rubbers	3×10^{16}	10^3-fold
Diffusion in some liquids	3×10^{13}	10^4-fold
Diffusion in some crystals	10^{12}	10^8-fold

which polymer segments adjacent to the diffusing molecule (A, H_2, CH_4, etc.) share in E. The essential act of diffusion then involves a loosening of polymer segments by absorption of energy and their rearrangement while in this loosened state by various synchronized movements so that the penetrant molecule within the activated zone is thrust to a new position. The penetrant molecule need not of course play an entirely inert role in the process but may share in it.

This viewpoint also provides an explanation of Barrer's first point, that the size of the penetrant molecule while not without influence is yet less important than might be expected if it alone determined E_a in elastomers.

6. Evaluation of Diffusion and Viscosity Coefficients According to the Zone Theory.—The energy of activation appears in any region of the polymer as a result of thermal fluctuations in it. The chance that there is a total energy $\geqslant E$ in a small region surrounding the solute molecule and which, including the solute molecule contains n degrees of freedom[38] is

$$P = \sum_{f=1}^{f=n} \left(\frac{E}{RT}\right)^{f-1} \cdot \frac{1}{(f-1)!} \exp(-E/RT) = \sum_{f=1}^{f=n} P_f \exp(-E/RT) \quad (6.1)$$

where $P_f = (E/RT)^{f-1}\, 1/(f-1)!$ If for any value of E/RT P_f is plotted against f the family of curves, with maxima, as shown in Fig. 9 is obtained. The locus of the maxima corresponds to $E = \bar{U} = fRT$, where therefore $\bar{U}$ is the average energy in the chosen f degrees of freedom. This most probable distribution is not the one of importance in diffusion because the rate process would then occur with zero value of E_a, contrary to experience. Certainly then the value of n in the region need not exceed f_{max} to include all energy distributions likely to contribute to a successful unit process, for we may exclude all "colder" than average distributions.

We then consider "hot" distributions ($E > \bar{U}$; $E_a > 0$). The important "hot" distributions are decided by two balancing factors: (1) $E_a = E - \bar{U}$ must be as concentrated as possible to give the

(38) In general internal vibrational degrees of freedom need not be considered because energies of activation are too small to excite them.

most energized zone compatible with (2); (2) there must be an *a priori* probability $P_f = (E/RT)^{f-1}\,1/(f-1)!$ which is as large as possible, bearing (1) in mind.

This means the optimum zone of activation will have values of f somewhere between 1 and f_{max} ($f_{max} = E/RT$). In addition there will normally be need for coöperation or synchronization between segmental rotations and intermolecular vibrations within the zone of activation if a successful unit diffusion is to occur within the life-time of the important energy fluctuations defined by conditions (1) and (2). For example, if each of p groups must simultaneously move in one of m directions the chance of this is $(1/m)^p$, and since various coöperations may be successful the total chance of all individual possible chances of coöperation is the sum of all individual chances, ρ_f. ρ_f will be expected to depend on f, and is <1.

In general a spectrum of terms $\rho_f P_f$ for different values of f may contribute to the probability of each act of diffusion, viscous flow or dielectric relaxation. Then[7,36]

$$D = {}^1/_2 d^2 \sum_{f=1}^{f=f_{max}} \rho_f \nu \left(\frac{E}{RT}\right)^{f-1} \frac{1}{(f-1)!} \exp(-E/RT) \tag{6.2}$$

where ν is a vibration frequency $\sim 10^{12}$ sec.$^{-1}$ characteristic of the diffusing units. With $d = 3.5 \times 10^{-8}$ cm.

$$D = 6 \times 10^{-4} \sum_{f=1}^{f=f_{max}} \rho_f \left(\frac{E}{RT}\right)^{f-1} \frac{1}{(f-1)!} \exp(-E/RT) \tag{6.3}$$

The coefficient η of the viscous resistance called into play by any shearing force F may be defined as

$$\eta = \frac{F\lambda}{\Delta\mu} \tag{6.4}$$

where $\Delta\mu$ is the relative velocity parallel to the direction of shear of two adjacent hydrocarbon chains λ apart. In this case[7]

$$\eta = \frac{F\lambda}{d}\,\frac{2kT}{b}\,\frac{1}{\sum_{f=1}^{f=f_{max}} \rho_f \nu \left(\frac{E}{RT}\right)^{f-1} \frac{1}{(f-1)!} \exp(-E/RT)} \tag{6.5}$$

where $b \sim 10^{-22}$ cm.^{3} is the volume of a flow unit. With $d \simeq \lambda$ and $\nu \simeq 10^{12}$ sec.$^{-1}$

$$\eta = 1.8 \times 10^{11}\, kT \times \frac{1}{\sum_{f=1}^{f=f_{max}} \rho_f \left(\frac{E}{RT}\right)^{f-1} \frac{1}{(f-1)!} \exp(-E/RT)} \tag{6.6}$$

For self-diffusion and viscous flow of polymer under gentle shearing forces, ρ_f and f_{max} should be identical and so $D^*_B \eta_B = kT(1.2 \times 10^7)$, for the values assigned above to d, b and λ. Stokes law gives for a sphere diffusing in a continuum $D_A \eta = kT/6\pi r = kT(1.8 \times 10^6)$ if $r = 3 \times 10^{-8}$ cm. Another quite different approach to the relation between D and η for self-diffusion has been developed by Bueche[39] who found for a particular polymer $D^*_B \eta_B = \rho kT\,(0.8 \times 10^6)$ where ρ is the density of the polymer.

(39) F. Bueche, *J. Chem. Phys.*, **20**, 1959 (1952).

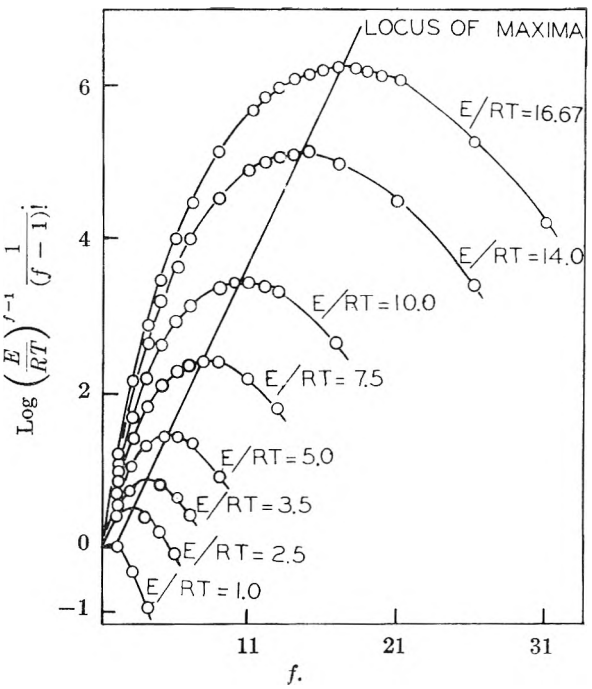

Fig. 9.—Curves showing log $[(E/RT)^{f-1}\,1/(f-1)!]$ *vs.* f for different values of E/RT.[7]

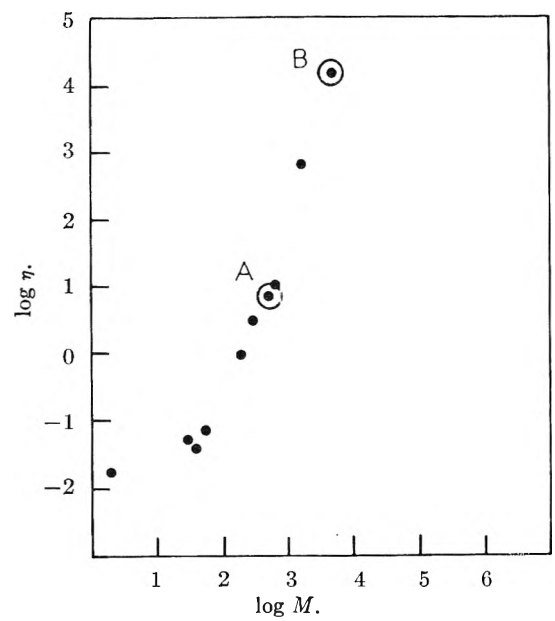

Fig. 10.—Viscous resistances calculated (points A and B) and obtained from diffusion data with Stokes law, for diffusion in rubber.[10]

For diffusion of a dissolved molecule in a polymer D_A and the viscous resistance η_A its movement calls into play have been investigated by Kuhn.[10] He concluded on theoretical grounds that η_A for a linear chain molecule diffusing in a flexible linear polymer will rise exponentially with its chain length. The calculated values of η_A for two chains of isoprene segments, one of mol. wt. 500 and the other of mol. wt. 5000 are points A and B of Fig. 10. He also computed a viscous resistance from Stokes law using D_{AB} obtained by Grun[40] for colored molecules of systematically increasing

(40) F. Grun, *Experientia*, **3**, 490 (1947).

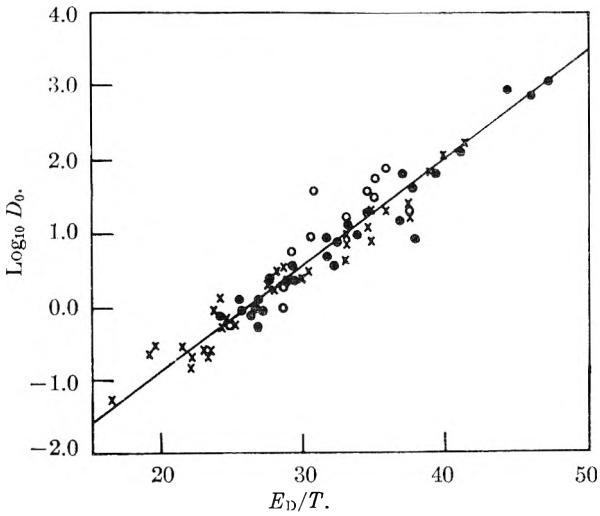

Fig. 11.—Functional relation between $\log_{10} D_0$ and E_D/T for diffusion in numerous elastomers.[18]

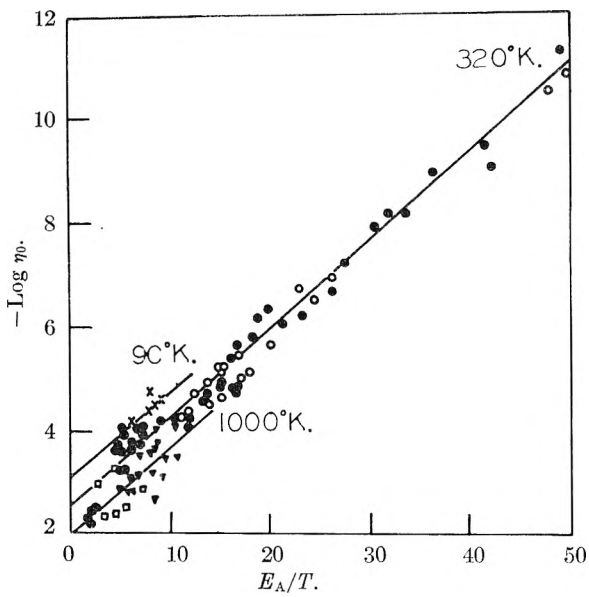

Fig. 12.—η log η_0 *vs.* E_A/T[36]: ×, A-polar liquids; ●, polar liquids; ○, hydrogen or hydroxyl bonded liquids; □, liquid metals; ▽, ionic melts.

molecular weights, getting the points in Fig. 11. There is an interesting continuity in the whole curve. It is not however possible to say at what point on the curve η for self-diffusion of rubber would appear, for movement of chains occurs segmentally.

7. Curvature in Plots of Log D or Log η *vs.* $1/T$.—When log D or log η is plotted against $1/T$ the plot is usually linear or nearly linear. This suggests that the summations in eq. 6.2 or 6.5 may often be replaced by their largest term. Even in this case a small curvature may arise, for then $E_a = E - (f-1)RT$ and so $dE_a/dT = -(f-1)R$. In addition however the dominant zone size may change with temperature, corresponding to a temperature coefficient in f, and curvature become enhanced. Thus measurements of f from dE_a/dT would be an upper limit only.

8. Functional Relationships.—Whether for diffusion, or for fluidity $\phi(\phi = 1/\eta)$, log D_0 and log $\phi_0(\phi = \phi_0 \exp(-E_a/RT))$ have been found[17,18,36] to be functionally related to E_a/T

$$\log D_0 \text{ (or } \log \phi_0) = A + \frac{BE_a}{T} \qquad (8.1)$$

where A and B are constants. This is seen in Figs. 11 and 12. The significance of this relationship is as follows. From the Arrhenius equation

$$\log D = \log D_0 - \frac{E_a}{4.60T} \qquad (8.2)$$

and if the range in values of log D is small compared with that in $E_a/4.60\ T$, then to a first approximation log D is a constant, A. Accordingly $\log D_0 = A - 0.22E_a/T$, which has the form of 8.1. In fact it is always found that the range in log D or log η is less than that in $E_a/4.60\ T$, either due to experimental limitations of measurements, or because of a fundamental property of rate processes in condensed phases.

For a substantial group of diffusion coefficients in rubber Barrer and Skirrow[18] found

$$\log D_0 = -3.6 + 0.14E_a/T \qquad (8.3)$$

while Barrer[36] found for viscous flow in many different kinds of molecular and atomic fluids (including liquid metals)

$$\log \phi_0 = 2.43 + 0.17E_a/T \qquad (8.4)$$

The constants 0.14 and 0.17 fall below the slope of 0.22, which is the maximum value to be expected only if the range in log D or log ϕ is wholly negligible compared with that in $E_a/4.60\ T$. This situation was approached in some measurements of Aitken and Barrer.[19] For the extended viscosity data embodied in Fig. 12 and eq. 8.4 there is some justification for setting up a universal fluidity function

$$\log \phi = 2.43 - \frac{0.05E_a}{T} \qquad (8.5)$$

As a result of research upon the pressure coefficient of viscosity of hydrocarbons[41] it has recently emerged that there is a clear functional relationship between

$$\left(\frac{\partial \ln \eta}{\partial P}\right)_T = \frac{\Delta V^*}{RT}$$

and

$$\left(\frac{\partial \ln \eta}{\partial T}\right)_P = \frac{\Delta H^*}{RT^2}$$

where ΔV^* and ΔH^* are the volume increment and heat of activation, respectively, on passing from the normal to the transition state in an Avogadro number of unit flow processes. It follows that there must be a correlation between ΔV^* and $\Delta H^*/T$. Since the work of Barrer, *et al.*, has already established correlations between ΔS^* and E_a/T (and so $\Delta H^*/T$) for diffusion in elastomers and for viscous flow in liquids, it follows that there should be a correlation between ΔS^* and ΔV^*, certainly for viscous flow and for self-diffusion, and probably for diffusion in general.

Such a correlation is readily understood from the viewpoint of the zone theory. The heat of activation, ΔH^*, is accumulated as a result of thermal energy fluctuations in a number of degrees of freedom significant from the viewpoint of diffusion or

(41) ASME Research Publication, 1953.

TABLE IV

INTERPOLATED P_0 AND $D_{c=0}$ FOR VARIOUS RUBBERS

Gases	$P_0 \times 10^7$ 30°	40°	50°	60°	$D_{c=0} \times 10^6$ (cm.² sec.⁻¹) 30°	40°	50°	60°
				Rubber A				
n-Butane	5.38	7.61	9.88	12.20	2.32	4.28	7.15	11.20
Isobutane	2.34	3.39	4.60	5.89	1.50	2.75	4.65	7.33
n-Pentane	16.27	21.73	25.33	27.75	2.28	4.24	6.80	10.02
Isopentane	4.87	8.94	12.95	16.70	0.91	2.27	4.40	7.46
Neopentane	1.86	2.80	3.92	5.14	0.72	1.41	2.55	4.24
				Rubber B				
n-Butane	4.76	6.79	8.86	11.00	2.00	3.72	6.21	9.73
Isobutane	1.79	2.81	3.94	5.15	1.18	2.34	4.09	6.50
n-Pentane	8.40	14.22	19.34	23.46	1.22	2.94	5.52	9.13
Isopentane	5.96	8.30	10.80	13.61	1.16	2.22	3.94	6.63
Neopentane	1.37	2.26	3.28	4.39	0.55	1.17	2.17	3.66
				Rubber C				
n-Butane	3.61	5.23	7.01	9.11	1.69	3.23	5.66	9.45
Isobutane	1.47	2.30	3.24	4.36	1.08	2.21	3.99	6.80
n-Pentane	8.96	12.97	16.60	19.50	1.38	2.79	4.91	7.76
Isopentane	4.39	6.40	8.46	10.78	0.87	1.75	3.13	5.29
Neopentane	1.26	1.88	2.75	3.81	0.54	1.08	2.04	3.72

flow (*e. g.*, intermolecular vibrations). This causes a local loosening of the fluid or polymer structure, and so its expansion. The more degrees of freedom involved, and so the larger ΔH^*, the greater will ΔS^* and ΔV^* both tend to be.

9. Selective Transmission through Membranes.—Barrer and Skirrow[18] have demonstrated the marked influence which cross-linking of rubber (up to 11.3% of combined sulfur) can have upon permeability and diffusion coefficients of nitrogen and of paraffins (Fig. 13). In contrast the solubility constants were not greatly influenced by this degree of vulcanization. Similar relations were observed in rubbers cross-linked by *t*-butyl peroxide.[19]

The influence of the molecular weight of the penetrant upon permeability, diffusion and solubility coefficients is also very striking (*e.g.*, Fig. 14). Moreover molecular shape, in isomeric C_4 and C_5 paraffins, has its own strong influence, as seen in Table IV for diffusion and permeability and in Table V for solubility constants in three increasingly cross-linked rubbers A, B and C. These data lend themselves to interesting analyses in terms of molecular dimensions[32,19] (for diffusion) and cohesive energy density (for solubility[42]). A statistical mechanical analysis of solubility constants has been given for zero and non-zero heats of mixing,[5] and extended to include effects of cross-linking.[6] However, here we shall consider possible fractionations of mixtures. Fractionation factors, S, in the steady state can be estimated to a first approximation from the ratios of individual permeabilities, since, at least in the regions where Henry's law is valid and solubility rather small, interference effects are not likely to be very large. S may also be defined as Q_1C_2/Q_2C_1 where Q_1 and Q_2 are the amounts of species 1 and 2 diffusing through a membrane in time t and C_1, C_2 are the concentrations of gaseous species 1 and 2 at the ingoing surface of the membrane. Values of permeability ratios are shown in Table VI for various paraffin pairs in rubber, the permeated mixture being enriched in the first mentioned component.

TABLE V

INTERPOLATED SOLUBILITIES, σ (cm.³ at S.T.P./cm.³)

	30°	40°	50°	60°
		Rubber A		
N_2[a]	0.071	0.065	0.061	0.057
n-C_4H_{10}	17.66	13.52	10.50	8.28
iso-C_4H_{10}	11.88	9.39	7.51	6.11
n-C_5H_{12}	54.26	38.89	28.31	21.04
iso-C_5H_{12}	40.93	29.99	22.39	17.02
neo-C_5H_{12}	19.81	15.10	11.68	9.20
		Rubber B		
N_2[a]	0.060	0.061	0.058	0.053
n-C_4H_{10}	18.09	13.91	10.86	8.60
iso-C_4H_{10}	11.56	9.14	7.37	6.02
n-C_5H_{12}	52.12	36.81	26.61	19.54
iso-C_5H_{12}	39.22	28.47	20.89	15.63
neo-C_5H_{12}	19.05	14.71	11.48	9.10
		Rubber C		
n-C_4H_{10}	16.26	12.30	9.42	7.33
iso-C_4H_{10}	10.33	7.93	6.17	4.88
n-C_5H_{12}	49.43	35.32	25.70	19.10
iso-C_5H_{10}	38.37	27.83	20.56	15.51
neo-C_5H_{12}	17.62	13.30	10.26	7.80

[a] Solubilities of N_2 were determined by the time-lag method.

In the transient state of flow separation factors may be very great indeed. The faster moving component may reach the outgoing surface of the membrane long before the slower moving component. If $\rho = S(\sigma_B/\sigma_A)$ where σ_A and σ_B are the solubilities of two components which dissolve according to Henry's law, and neglecting concentration dependence of D_A and D_B (a procedure valid only for smaller concentrations of A and B in the membrane), one obtains[19]

(42) G. Gee, *I.R.I. Trans.*, **18**, 266 (1943).

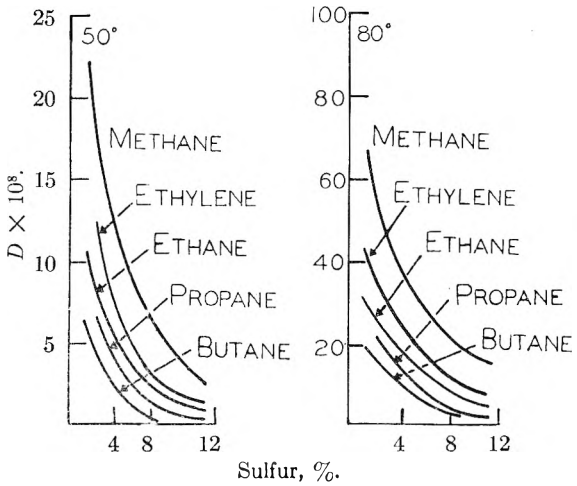

Fig. 13.—Diffusion constants as a function of the per cent combined sulfur in natural vulcanizates.[18]

TABLE VI

FRACTIONATION FACTORS FOR PARAFFIN DIFFUSION IN STEADY STATE

Rubber	T, °C.	Molecular pair A–B	Permeability ratio of A to B
Natural rubber,[18]	40	CH_4–N_2	3.0₅
2.9% combined		C_2H_6–CH_4	2.6
S		C_3H_8–CH_4	4.1
		n-C_4H_{10}–CH_4	10.0
Natural rubber[19]	30	n-C_4H_{10}–*iso*-C_4H_{10}	2.3
cross-linked by		n-C_5H_{12}–n-C_4H_{10}	3.0
t-butyl chloride		n-C_5H_{12}–*iso*-C_5H_{12}	3.3
		n-C_5H_{12}–*neo*-C_5H_{12}	8.7

$$\rho = \frac{(k-1) + \frac{12}{\pi^2}\sum_{n=1}^{\infty}\frac{(-1)^{n+1}}{n^2}\exp\left(-\frac{n^2\pi^2 k}{6}\right)}{\left(k\frac{L_A}{L_B}-1\right) + \frac{12}{\pi^2}\sum_{n=1}^{\infty}\frac{(-1)^{n+1}}{n^2}\exp\left(-\frac{n^2\pi^2 k L_A}{6L_B}\right)}$$

where $t/L_A = k$ defines the constant k and L_A and L_B are the time lags[17] for A and B. The amount of A which has diffused through the membrane in time $t = kL_A$ is

$$Q_A = \frac{\sigma_B p_A l}{76 \times 6}\left\{(k-1) + \frac{12}{\pi^2}\sum_{n=1}^{\infty}\frac{(-1)^{n+1}}{n^2}\exp\left(-\frac{n^2\pi^2 k}{6}\right)\right\}$$

In Table VII are summarized ratios of amounts diffused after a series of times for a rubber[19] and for an ethylcellulose membrane.[27] The very high separations arise in the early stages of emission of the faster moving component before much has actually passed through the membrane. The transient state method of fractionation has therefore this limitation. If the membrane is doubled in thickness the theory shows that twice as much of A diffuses before the separation factor drops to a given value. On the other hand the total time involved is correspondingly increased. For the diffusions given in Table VII involving n- and *iso*-C_4H_{10}, and rubber, the calculated separations assume that each gas diffuses in presence of the other just as fast as when it alone is present. This assumption has not yet been tested experimentally. In the rubber system

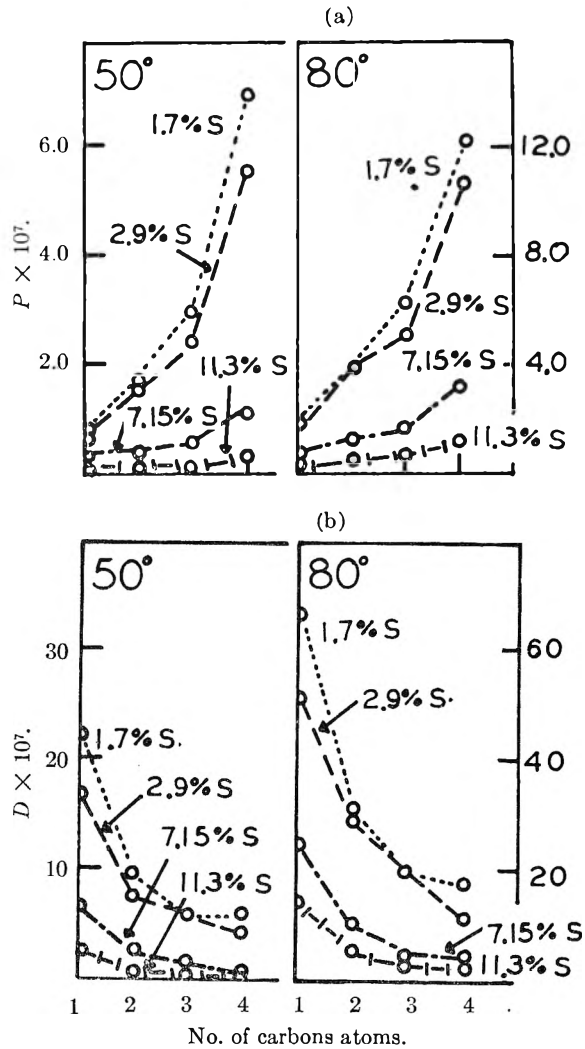

Fig. 14.—(a) Dependence of permeability constant upon the number of carbon atoms in simple n-paraffins[18]; (b) dependence of diffusion coefficient upon the number of carbon atoms in simple n-paraffins.[18]

the diffusion is moreover somewhat concentration dependent; and in the transient state for ethylcellulose it is both time and concentration dependent.[27]

TABLE VII

CALCULATED SEPARATIONS OF n-C_4H_{10} AND *iso*-C_4H_{10} IN TRANSIENT STATE

Partial pressure of each vapor (cm.)	k	Time (min.)	Separation factor S	Amounts diffused cm.³ at S.T.P. per meter² at p = 7.6 cm. n-C_4H_{10}	Amounts diffused cm.³ at S.T.P. per meter² at p = 7.6 cm. *iso*-C_4H_{10}
Rubber A,[19] cross-linked by *t*-butyl peroxide, at 50°, 0.5 mm. thick					
	0.5	4.9	14.8	1.98	0.134
	1.0	9.7	10.2	20.5	2.01
7.6	2	19.4	3.3	90.1	27.3
	5	48.5	2.5	350	141
	∞	∞	2.3	...	...
Cellulose ether[27] at 50°, 0.1 mm. thick					
	2	162	333	56.7	0.17
7.6	5	405	32.7	217	6.63
	∞	∞	7.6	...	...

These dependences are not allowed for in the simple theory, and so the results in Table VII are necessarily approximate.

Acknowledgment.—I am indebted to Mr. J. Slater of this Department for some of the calculations in Table VII.

ALUMINIZED EXPLOSIVES[1]

By Melvin A. Cook, Aaron S. Filler, Robert T. Keyes, William S. Partridge and Wayne O. Ursenbach

Explosives Research Group, University of Utah, Salt Lake City, Utah

Received March 23, 1956

Experimental velocity–diameter $D(d)$ and velocity–density $D(\rho_1)$ curves are presented for 80/20 TNT–Aluminum (Al), 45/30/25 RDX–TNT–Aluminum (Al), 75/25 Composition B–Al (HBX), and various mixtures of ammonium nitrate and aluminum ranging from pure ammonium nitrate to 60% AN. Also presented are some results with AN–DNT mixtures. Results show that aluminum reacts too rapidly for the energy release as a function of time to be a limiting factor in TNT–Al and RDX–TNT–Al mixtures at diameters above 5 cm., but it reacts relatively slowly in the AN–Al mixtures and the rate of reaction of aluminum (and AN), or the rate of energy release is a limiting factor in this case. The familiar properties of the high temperature Al-explosives are here attributed to the thermodynamics of Al-reactions in which the $Al_2O(g)/Al_2O_3(c)$ ratio is appreciable in the detonation wave but becomes negligible later on during adiabatic expansion. The change of this ratio from a high value in the detonation wave to an ultimate low value gives aluminized explosives low "brisance" but high blast potential. The AN–Al mixtures were shown to be "non-ideal" ($D < D^*$) over the entire range of conditions studied. Reaction rates in these mixtures are shown to depend on the particle size of both the AN and the Al. They seem to be controlled by mass transfer which leads to anomalous $D(\rho_1)$ curves each showing a maximum at a relatively low density (1.0 to 1.2 g./cc.).

Introduction

Aluminized explosives are characterized in general by relatively low "brisance" but high (underwater, open air and underground) blast potential. The low relative "brisance" of aluminized explosives has been attributed in the past to incomplete reaction of Al at the "Chapment-Jouguet plane," and the high blast-potential to after-burning of aluminum. Thus early unpublished shaped charge studies with aluminized explosives, interpreted in light of the observed linear variation with detonation pressure of hole depth and volume from jets in uniform targets indicated that aluminum acts effectively as a diluent as far as the end effect, *e.g.*, shaped charge action, is concerned. More careful study showed, however, that aluminum lowers the "detonation" pressure and velocity even more, sometimes quite considerably more, than an ideal diluent. The effectively endothermic reaction of Al in the detonation wave may be seen, for example, in the results of detonation pressure measurements,[2] summarized in Table I, by the shaped charge method (using calibration curves established with known ideal explosives). These data show that the detonation pressures of tritonal and HBX were less than in TNT and composition B, respectively, even though the densities of the former explosives were 6 to 8% higher. This is significant particularly in view of the known pronounced effect of density on pressure. This same situation may also be seen by comparing detonation velocity (Table II), realizing that pressure is given hydrodynamically by the equation $p_2 = \rho_1 DW \doteq \rho_1 D^2/4$. These results show that aluminum lowers the velocity of TNT, 60/40 RDX–TNT and composition B *even more than salt*, sand and similar ingredients which act, if not as pure diluents, at least as (slightly) heat absorbing or endothermic materials.[3] Clearly, therefore, aluminum must have a strongly endothermic effect at the C–J plane. This would be the result, if, for example, $Al_2O(g)$ were to form in appreciable amount in the detonation wave. But if $Al_2O_3(c)$ were the sole aluminum product, the (large diameter) velocity of the TNT–Al and RDX–TNT–Al mixtures would be appreciably higher (even at the same density) than the velocity in the corresponding explosives without aluminum owing to the large heat of formation of $Al_2O_3(c)$.

Table I

Detonation Pressures Determined from Shaped Charge Method

Explosive	ρ_1	Measured detonation pressure p_2(atm. $\times 10^{-3}$)[a]
TNT	1.59	150
80/20 TNT–Al	1.68	140
TNT	0.81	46
80/20 TNT–Al	0.94	45
Composition B	1.71	230
80/20 Composition B–Al (HBX)	1.81	170
73.2/26.8 Composition B–Al (HBX)	1.83	155

[a] Average deviation from mean less than 10%.

This article presents experimental studies designed to provide data for the determination of the behavior of aluminum in explosives. Since some theoretical treatments of non-ideal detonation make use of wave shape, measurements of the shapes of the wave fronts of these explosives are also presented.

Experimental

$D(d)$ Curves for Tritonal and HBX.—Velocity–diameter studies of cast and loose-packed 80/20 TNT–Al, cast 75/25 HBX and loose-packed 45/30/25 RDX–TNT–Al are presented in Fig. 1. Velocities were measured by a "pin-

(1) This investigation was supported by Office of Naval Research, Contract No. N7-onr-45107, Project No. 357,239.

(2) M. A. Cook and A. M. Spencer, "The Determination of Reaction Rates of Non-Ideal Explosives from Shaped Charge Penetration Data," Technical Report XLVII, ERG, University of Utah, August 19, 1955.

(3) M. A. Cook, Paper #25, Discussion of Faraday Society, Physics of High Pressures, Sept. 20, 21, 1956.

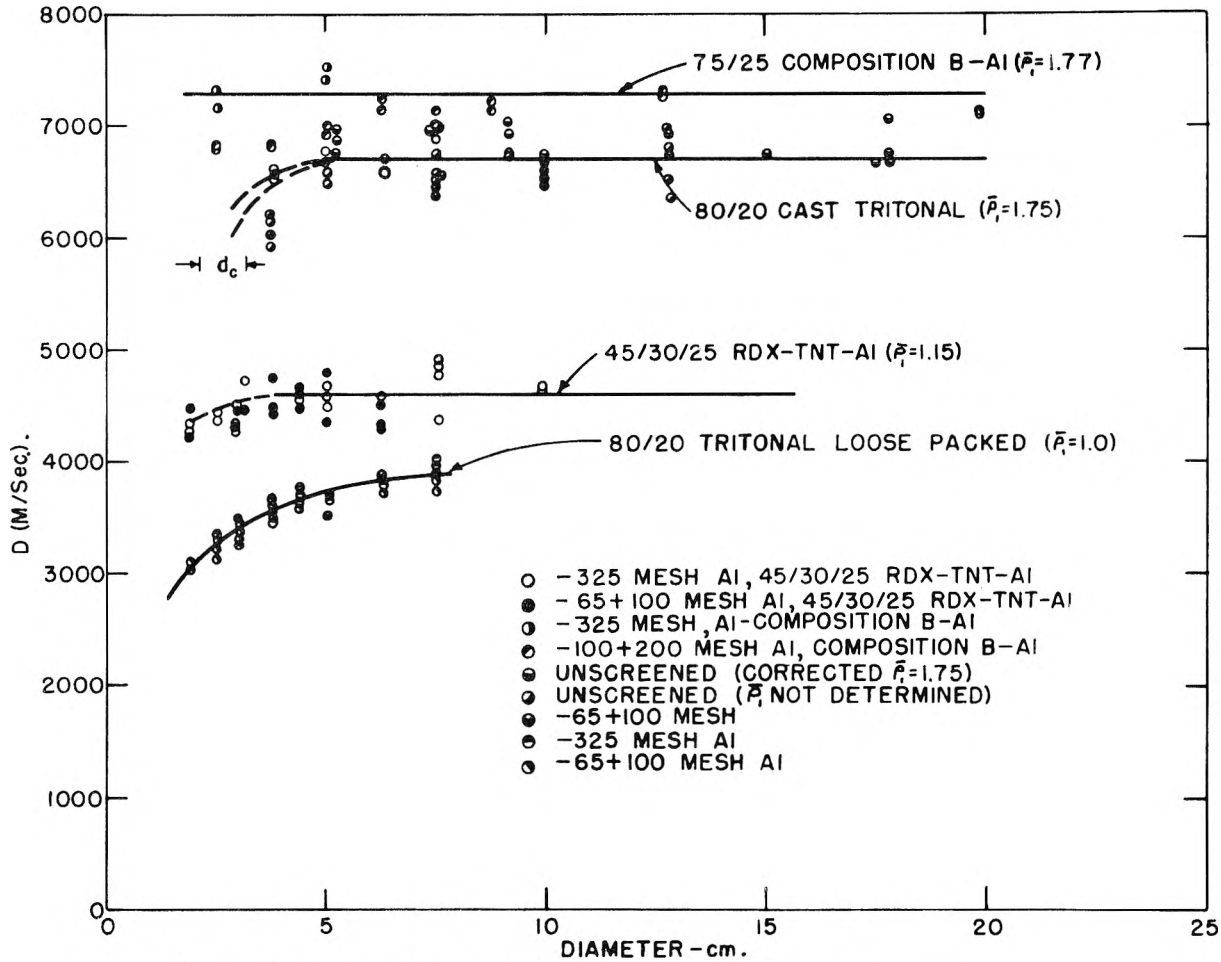

Fig. 1.—Experimental detonation velocity–diameter curves for explosive–metal mixtures.

Table II

Velocity Comparison

Explosive	ρ_1	D(m./sec.)
TNT	1.59	6910
80/20 TNT–Salt	1.75	6900
80/20 TNT–Al	1.75	6800
TNT	0.85	4525
80/20 TNT–Salt	1.00	4400
80/20 TNT–Al	1.00	3840
60/40 RDX–TNT	1.70	7800
45/30/25 RDX–TNT–Salt	1.77	(7430)[a]
45/30/25 RDX–TNT–Al	1.77	7200
60/40 RDX–TNT	1.00	(5650)[a]
45/30/25 RDX–TNT–Salt	1.15	(5400)[a]
45/30/25 RDX–TNT–Al	1.15	4600

[a] By linear interpolation of results for TNT–salt and RDX–salt mixtures.

oscillograph" and by a rotating mirror or "streak" camera as desired. The charges all had a length/diameter (L/d) ratio of six or more. The large diameter charges were contained in thin-walled cardboard tubes and the small diameter ones in thin rolled plastic tubes. Densities were measured in samples of the cast charges by sectioning them. While they were found to show some axial and radial density fluctuations, these variations were limited in all cases to 2% or less. The loose-packed charges were vibrated for density uniformity, care being taken to avoid segregation by excessive vibration. Densities were determined in all cases by total weight/total volume measurements. Velocities were corrected to an average density in each case by appropriate $D(\rho_1)$ relations, only small density corrections being required in any case.

No systematic aluminum particle size or diameter effects were found in either the 80/20 TNT–Al or 45/30/25 RDX–TNT–Al except for the former at diameters less than 5 cm. In fact, in the HBX series no definite influence of diameter on velocity was found in the diameters studied. These results show clearly that the reaction rate of aluminum is not a limiting factor in the behavior of Tritonal and HBX. One must, therefore, look elsewhere for an explanation of low "brisance" in the Al-explosives.

Since theoretical velocity calculations indicated that the $D(\rho_1)$ curve for Tritonal and HBX should not be linear, measurements also were made to determine the velocity–density curves for pressed 80/20 TNT–Al in 8.5 cm. (L/d = 6) charges and for 45/30/25 RDX–TNT–Al at d = 5.2 cm. and L/d = 6. These diameters were chosen to ensure "ideal" detonation. The results are shown in Fig. 2. In accord with predictions, it may be seen that these curves are indeed non-linear; they are quite different from the normal (generally linear) ones. They are evidently characteristic of an $Al_2O(g)/Al_2O_3(c)$ ratio which decreases rapidly with density as discussed below.

$D(a)$ Curves for AN–Al Mixtures.—Experimental $D(d)$ and D *vs.* per cent. Al (constant ρ_1) data for AN–Al mixtures varying in composition from 100/0 to 70/30 are shown in Figs. 3 and 4. The influence of Al particle size is indicated by some of the results shown in Fig. 3 for 8 to 20% Al. Additional data showing Al particle size effects are given in Tables III and IV. The AN–Al mixtures were all "non-ideal" ($D < D^*$ where D^* is the ideal velocity) at velocities far below the ideal velocities in all cases irrespective of the particle size of either the AN or Al. No attempt was made to correct velocities for small density fluctuations owing to the anomalous $D(\rho_1)$ relations as noted from the data in Fig. 3. For example, the velocity was in general considerably lower on the high density side than on the low density side. Previous unpublished studies have shown that this is

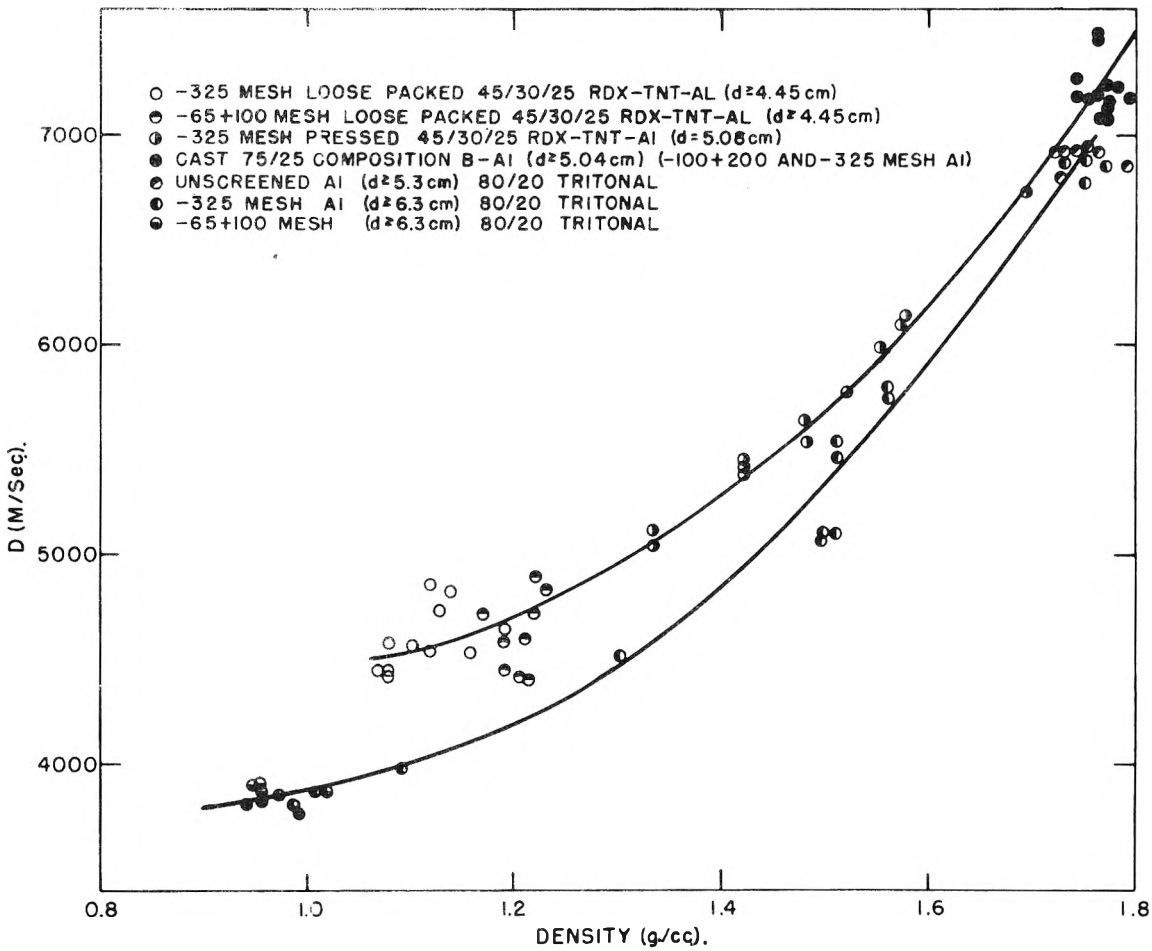

Fig. 2.—Experimental ideal detonation velocity-density curves for 45/30/25 RDX-TNT-AL and 80/20 Tritonal.

a characteristic of fuel or combustible-sensitized AN explosives at D/D^* considerably less than unity.

In order to bring out the anomalous density effect unambiguously, $D(\rho_1)$ measurements were carried out with the 90/10 AN-Al mixture using a single, uniform, unscreened Al sample throughout. These results are shown in Table V. In the first series using a fine AN product (sample 1, Table V) the $D(\rho_1)$ curve was found to go through a maximum between a density of from 1.09 to 1.28. These measurements were repeated about three weeks later using the same lot of AN. However, clearly the sample had changed during the three week interval as a result of partial recrystallization, as observed, for example, by the fact that it then packed to a lower density. In this series the maximum velocity (3485 m./sec.) was observed at about $\rho_1 = 1.12$ and the velocity was 950 m./sec. lower at $\rho_1 = 1.25$ than at $\rho_1 = 1.12$. Pressing crushes the AN somewhat; but to investigate the anomalous $D(\rho_1)$ effect one should use constant particle size. To accomplish this, several shots were made in which the pressed charges were compared with loose-packed ones made by first pressing the AN to the density of the corresponding pressed charge, crumbling the mixture and loose packing it in charges of the same diameter and length. Three comparisons of this sort are shown in Table V (AN samples 3, 4 and 5). Note that the low density product showed a higher velocity than the higher density one, and the difference increased with the density difference. These results show that the $D(\rho_1)$ curve for 90/10 AN-Al with fine AN and fine Al exhibited a maximum at some value of density below $\rho_1 = 1.25$.

A more easily reproducible example of the anomalous $D(\rho_1)$ effect in AN explosive is shown in Table V for a 90/10 AN-DNT mixture using solid DNT and fine AN. Again the $D(\rho_1)$ curve was shown to go through a maximum in this case near $\rho_1 = 1.08$ g./cc.

The AN-Al mixtures are complicated non-ideal explosives; besides the anomalous $D(\rho_1)$ relations, particle size effects may be observed not only in Al but also in AN. The AN particle size was not allowed to vary more than the amount caused by crystal growth in the AN and the inability to reproduce particle size in AN from one lot to another. As a result, no definite particle size effects of AN were noted. To show that the AN particle size also influences velocity in these mixtures, two shots were made in 10 cm. diameter charges using a much coarser AN product and the same grade of aluminum as in the comparative examples. The results (AN sample 6 in Table V) showed an average velocity about 1000 m./sec. lower than for the finer grade AN charges of the same density and Al particle size.

TABLE III

INFLUENCE OF Al PARTICLE SIZE IN AN-Al MIXTURES IN 9.94 (d) × 61 (L) CM. CHARGES

Al particle size[a]	ρ_1 (g./cc.)	$\bar{D}$ (obsd.) (m./sec.)	Al particle size	ρ_1 (g./cc.)	$\bar{D}$ (obsd.) (m./sec.)
6% Al			10% Al		
−100 + 150	1.13	Failed	− 65 + 100	1.15	Failed
−150 + 200	1.13	Low	−100 + 200	1.12	3085
−200 + 325	1.14	2495	−200 + 325	1.15	3090
−325	1.20	3050	−325	1.20	3225
15% Al			AN particle size		
− 65 + 100	1.15	Failed	+ 48	13.3%	
−100 + 150	1.14	3170	− 48 + 65	60.2%	
−150 + 200	1.16	2865	− 65 + 100	22.5%	
−200 + 325	1.18	2880	−100 + 150	4.0%	
−325	1.20	2900			

[a] Standard Tyler Mesh.

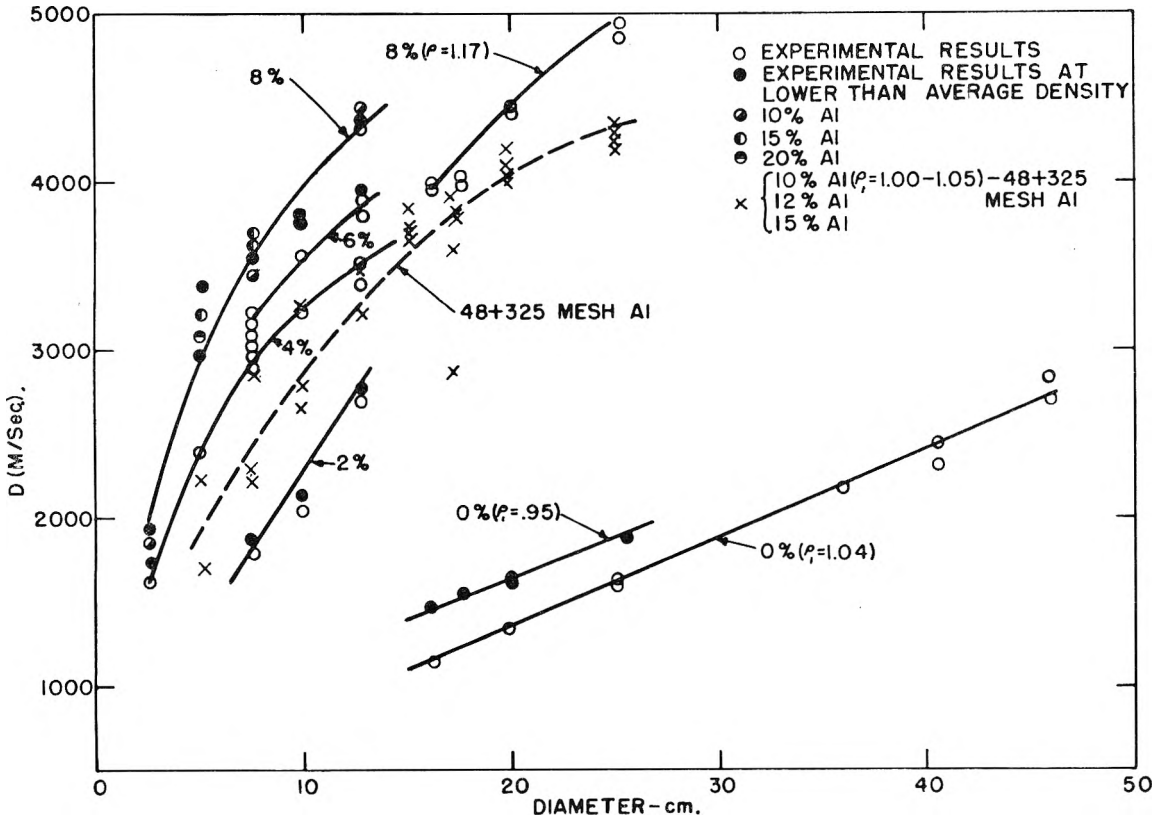

Fig. 3.—Experimental detonation velocity–diameter curves for various AN–Al mixtures.

Table IV

Critical Diameter Data for AN–Al Mixtures

Al, %	Particle size[a]	Critical diameter
0	−325	$12.7 < d_c < 16.0$
2	−325	5.0
4	−325	2.5
6	−325	2.5
8	−325	<2.5
10	−325	2.5
15	−325	2.5
20	−325	$2.5 < d < 5.0$
30	−325	5.0
40	−325	>7.5
10	− 48 + 325	5.0
12	− 48 + 325	$5 < d_c < 75$
15	− 48 + 325	5.0
6	−150 + 200	10.0
10	−100 + 200	10.0
15	− 65 + 100	10.0

[a] AN approximately the same throughout—see Table III.

Table V

Variations of Velocity with Density in AN–Al and AN–DNT Mixtures

90/10 AN–Al (10 × 60 cm.)				90/10 AN–DNT (1) (10 × 60 cm.)			
AN sample	$\bar{\rho}_1$ (g./cc.)	Charge[b]	D (m./sec.)	AN sample	$\bar{\rho}_1$ (g./cc.)	Charge[b]	D (m./sec.)
1[a]	1.07	LP	3280	1	0.88	LP	3310
1	1.09	p	3460	1	.99	LP	3480
1	1.19	p	3410	1	1.08	p	3560
1	1.28	p	3350	1	1.18	p	3330
2	0.96	LP	3365	1	1.27	p	3120
2	1.12	p	3380	7	1.08	p	3315
2	1.17	p	3290	7	1.04	pc	3440
2	1.25	p	2530	7	1.17	p	3210
3	1.07	p	3570	7	1.03	pc	3680
3	0.96	pc	3490	7	1.27	p	2890
4	1.18	p	3405	7	1.07	pc	3700
4	1.00	pc	3715				
5	1.28	p	Failed				
5	0.95	pc	3650				
6	1.12	LP	2595				
6	1.11	LP	2525				

[a] Screen Analysis of samples 1, 6, 7, were

AN Particle Size Data

Mesh	(1)	(6)	(7)
− 10 + 20	..	5.1	..
− 20 + 35	..	70.9	..
− 35 + 48	..	20.2	6.0
− 48 + 65	48.5	2.9	48.4
− 65 + 100	28.5	0.9	36.9
−100 + 150	10.1	..	4.3
−150 + 200	4.8	..	2.0
−200	8.1	..	2.4

Samples 2, 3, 4 and 5 were the same as sample 1 but had aged to 27 days. Aging of AN causes definite changes, the most significant of which is the packing quality. [b] LP = loose packed, p = pressed, pc = pressed and crushed to a loose powder which was then loose-packed. This gave a loose-packed product of the same particle size as in the corresponding pressed charges.

Wave Shape Measurements in Aluminized Explosives.—After considerable effort to obtain quantitative wave shape results in cast Tritonal and HBX, studies were discontinued owing to the very erratic results obtained. The cause of these irreproducible results is associated with the difficulties inherent in casting such mixtures without incurring some density and composition fluctuations; tendency toward segregation of the aluminum causes it to concentrate along the charge axis enough to attenuate the wave at this position more than toward the sides. Only relatively slight segregation of this sort is sufficient to flatten and even in-

TABLE VI

OBSERVED VARIATIONS OF THE STEADY-STATE RADIUS OF CURVATURE/DIAMETER (R_m/d) WITH COMPOSITION AND d IN AN–Al EXPLOSIVES

Al %	d = 2.5 (cm.)	5.0	7.5	10.0	12.5	15.0	17.5	20.0	25.0	40.0	46.0
				A. −325 Mesh Al, Fine AN[a]							
0					Failed		1.16	1.09	0.96	0.78	1.03
2		Failed		1.26							
4	Failed	1.33	1.31	1.27	1.31						
6	0.92	1.25	1.55	1.35	1.38						
8	1 35	1 37	1.39	1.39	1.43	1.21	1.31	1.21	1.35		
10		1.68	1.56	1.49	1.39						
15	1.07	1.54									
20	Failed	1.39	1.53								
30		Failed	1.59								
				B. Fine AN, +325 Mesh Al (by removing −325 mesh material from standard[b])							
10		Failed	1.61	1.48	1.50		1.50	1.37	1.67		
12		Failed			1.36	1.29	1.36	(1.26)	1.55		
15		Failed	1.30		1.33	1.63	1.52	1.42	1.45		
				C. 150 to 200 Mesh Al							
6				0.99							
10				1.31							
15				1.30							

[a] AN particle size: + 48 mesh, 0–31%; −48 + 65 mesh, 24–40%; −65 + 100 mesh, 8–40%; −100 + 100 mesh, 4–25%; −150 mesh, negligible. [b] Standard Al particle size: + 65 mesh, 14.9%; −65 + 100 mesh, 13.1%; −100 + 200 mesh, 20.9%; −200 + 325 mesh 12.7%; −325 mesh, 38.4%.

vert the wave from its normal value for an homogeneous charge. The effect of Al segregation on wave shape is more pronounced than density fluctuations along the charge axis which also tends to flatten or distort the wave.

In loose-packed and pressed charges of 80/20 TNT–Al and 45/30/25 RDX–TNT–Al, the observed wave shapes were obtained with normal reproducibility and showed normal curvature.[4] The waves were spherical in shape and exhibited a normal (constant or steady state) value R_m at large L/d. Values of R_m/d obtained for the loose-packed mixtures of TNT–Al and RDX–TNT–Al with two grades of Al (−325 mesh and −65 + 100 mesh) are plotted against diameter in Fig. 5. R_m/d *vs.* ρ_1 curves for pressed 80/20 TNT–Al and 45/30/25 RDX–TNT–Al obtained at d = 8.3 cm. and d = 5.2 cm., respectively, are also shown in Fig. 5. R_m/d increased for TNT–Al from 1.45 at ρ_1 = 1.0 to 2.5 at ρ_1 = 1.56 at which density the R_m/d *vs.* ρ_1 curve still had a fairly steep slope. In the RDX–TNT–Al mixture, however, R_m/d increased from 1.95 at ρ_1 = 1.18 to an apparent limiting value of about 3.85 at ρ_1 = 1.48. This mixture showed no further increase in R_m/d with density as the wave increase from ρ_1 = 1.48 to 1.57.

Wave shape data obtained for the AN–Al mixtures are given in Table VI. They show R_m/d to be confined to the relatively narrow range between 0.9 and 1.7 in the diameters studied.

Discussion of Results

At low temperatures and pressures aluminum oxide exists as crystalline Al_2O_3 (corundum), the stable form of which has a heat of formation of 399.1 kcal./mole (using the convention that heat given off is positive). At a pressure of one atmosphere it melts at 2313°K., with a heat of fusion of 26 kcal./mole. The normal boiling point has not been observed directly, but on the basis of experiments made around 2500°K.[5] it has been calculated to be 3770 ± 200°K. Al_2O_3 apparently does not exist in the vapor state; decomposition occurs on vaporization, and apparently the oxide of aluminum in the gas phase consists of AlO.[4] If other materials are present AlO may react with them, and in the presence of reducing mixtures the sub-oxide replaces AlO as the dominant aluminum containing gas. Indirect methods indicate that this sub-oxide is Al_2O.[4] AlO has been studied spectroscopically giving a value for the heat of formation of +45 kcal./mole. However it is pointed out in reference 5 that the lower electronic state found in the spectroscopic studies may not be the ground state of the molecule. Chemical evidence is presented there which indicates a heat of formation of about −8 kcal./mole for AlO. Reference 5 gives results which indicate a heat of formation for Al_2O of about 39 kcal./mole.

The only compounds of aluminum which might conceivably form in detonation besides the oxides are AlN and AlH. Al_4C_3 exists only in the solid state, decomposing on vaporization. However, careful considerations show that none of these can be important as detonation products and the significant products are considered therefore to be only Al_2O_3(c), Al_2O(g) and AlO(g).

The heat capacities at constant volume for Al_2O and AlO were calculated on the basis of rigid-rotor and harmonic-oscillator approximations. The spectroscopically observed frequency of 977 cm.$^{-1}$ was used for AlO. For Al_2O no data were available. Comparing with other triatomic molecules, and assuming that Al_2O is non-linear, it was assumed that Al_2O has vibration frequencies of 500, 977 and 1580 cm.$^{-1}$. The harmonic oscillator heat capacities were taken from a table given by Aston.[6] Heat capacity data for Al_2O_3 are given by Ginnings and Corruccini up to 900°.[7] The reactions yielding Al_2O(g) and AlO(g) may be reduced to

(4) M. A. Cook, G. S. Horsley, R. T. Keyes, W. S. Partridge and W. O. Ursenbach, *J. App. Phys.*, **27**, 269 (1956).

(5) L. Brewer and A. W. Searcy, *J. Am. Chem. Soc.*, **73**, 5308 (1951).

(6) H. S. Taylor–S. Glasstone "Treatise on Physical Chemistry," Vol. I, D. Van Nostrand Co., Inc., New York, N. Y., 1942, Appendix I.

(7) D. C. Ginnings and R. J. Corruccini, Paper 1797, *J. Research Natl. Bur. Standards*, **30**, 593 (1947).

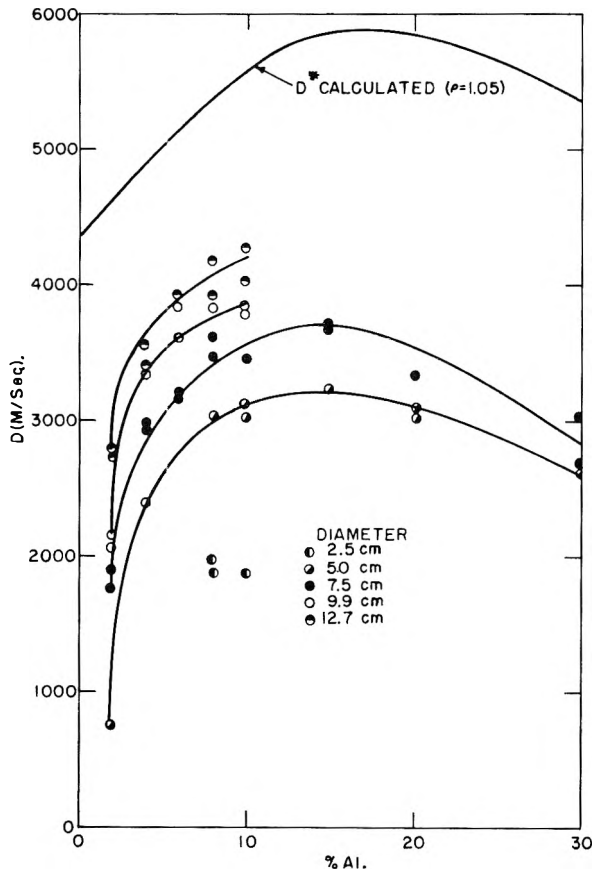

Fig. 4.—Detonation velocity *vs.* per cent. aluminum curves for AN–Al mixtures.

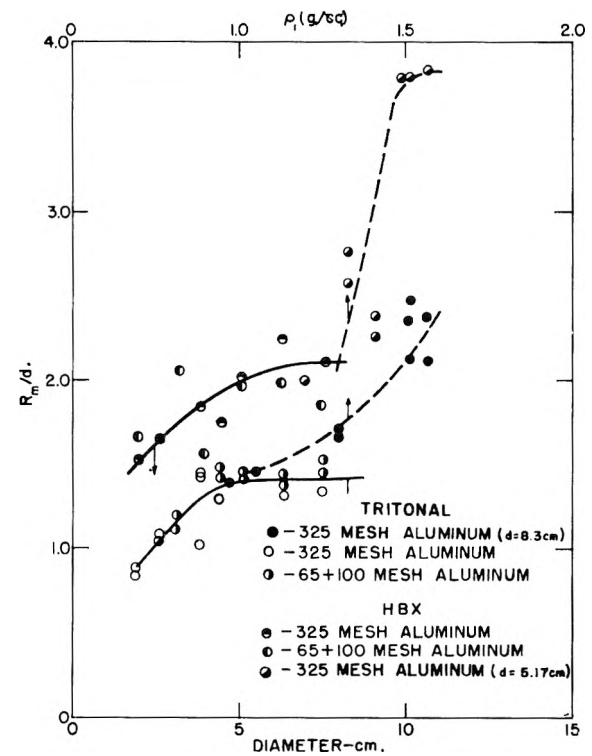

Fig. 5.—R_m/a (steady-state radius of curvature/charge diameter) *vs.* charge diameter and density for 80/20 TNT–Al and 45/30/25 RDX–TNT–Al.

$$Al_2O + 2CO_2 \rightleftarrows Al_2O_3 + 2CO$$
$$AlO + {}^1/_2CO_2 \rightleftarrows {}^1/_2Al_2O_3 + {}^1/_2CO$$

Their equilibrium constants (using definitions published elsewhere) are[8]

$$K_{p28} = \frac{f_{Al_2O} f^2_{CO_2}}{f^2_{CO_2}}; \quad K_{28} = K_{p28}\left(\frac{1.2181}{T}\right) = \frac{(Al_2O)(CO_2)^2}{(CO)^2} F$$

$$K_{p29} = \frac{f_{AlO} f_{CO_2}{}^{1/2}}{f_{CO}{}^{1/2}}; \quad K_{29} = \left(\frac{1.2181}{T}\right) K_{p29} = \frac{(AlO)(CO_2)^{1/2}}{(CO)^{1/2}} F$$

(Definition of F given by equation 12, reference 8.) Solving these expressions for (Al_2O) and (AlO)

$$y_{22} = (Al_2O) = K_{28}\frac{(CO)^2}{(CO_2)^2}\frac{1}{F}$$

$$y_{23} = (AlO) = K_{29}\frac{(CO)^{1/2}}{(CO_2)^{1/2}}\frac{1}{F}$$

Putting the remaining aluminum into Al_2O_3 one finds

$$y_{21} = (Al_2O_3) = {}^1/_2Al_0 - y_{22} - {}^1/_2y_{23}$$

where Al_0 is the number of gram-atoms of Al in 100 grams of explosive. (Designations here adopted conform to extensive tabulations and conventions using derivations previously published.[8])

There is sufficient uncertainty in the available thermochemical data for Al_2O and AlO that a considerable variation is possible in the values of the equilibrium constants calculated by statistical mechanics. While it does not, therefore, seem possible at the present time to give precise values for the K_p, the following are considered to be the best data available at present

$$K_{p28} = 10^{21.4}10^{-63,200/T}$$
$$K_{p29} = 10^{13.3}10^{-49,000/T}$$

Heat capacity data computed by the approximate methods outlined above are given in Table VII. With these data one may carry out at least qualitative thermo-hydrodynamic calculations for aluminized explosives.

Temperatures and pressures at the C–J plane for low density TNT–Al and RDX–TNT–Al mixtures are according to calculations based on the above data such that the chief product of aluminum should be Al_2O(g). This forms endothermically with respect to the products of detonation of these explosives, (*i.e.*, by removing oxygen from more exothermic reactions) and as a result the intensity of the detonation wave is reduced by aluminum. Owing to the much more rapid increase of pressure than temperature with density, however, the ratio $Al_2O(g)/Al_2O_3(c)$ should decrease with density, but evidently remains appreciable even at the maximum density possible. As a result the influence of the highly exothermic product Al_2O_3(s) apparently never is sufficient in Tritonal and HBX to overcome the endothermic effect at Al_2O(g) at the C–J plane. The detonation velocities and detonation pressures (or "brisance") of these high temperature aluminized explosives are thus always lower than those of the corresponding explosives without aluminum even at the maximum densities, despite a 6 to 8%

(8) M. A. Cook, R. T. Keyes, G. S. Horsley and A. S. Filler, This Journal, **58**, 1114 (1954). See also M. A. Cook, *J. Chem. Phys.*, **16**, 1081 (1948).

TABLE VII

IDEAL MOLAL HEAT CAPACITIES FOR ALUMINUM OXIDES

	$\overline{Cv}$			Cv	
T, °K.	Al_2O_3(c)	AlO(g)	Al_2O(g)	Al_2O_3(c)	AlO(g)	Al_2O(g)
1000	26.67	6.22	9.69	27.89	6.658	10.868
1100	27.10	6.28	9.84	30.32	6.705	11.024
1200	27.48	6.33	9.98	30.70	6.743	11.150
1300	27.82	6.37	10.10	31.02	6.772	11.252
1400	28.13	6.41	10.21	31.34	6.800	11.339
1500	28.40	6.44	10.31	31.60	6.816	11.405
1600	28.66	6.47	10.40	31.83	6.832	11.463
1700	28.89	6.50	10.47	32.06	6.845	11.512
1800	29.11	6.52	10.54	32.28	6.857	11.553
1900	29.32	6.54	10.61	32.48	6.867	11.589
2000	29.51	6.56	10.67	32.66	6.875	11.620
2100	29.69	6.58	10.72	32.80	6.885	11.649
2200	29.86	6.60	10.77	32.92	6.889	11.670
2300	30.01	6.61	10.82	33.05	6.894	11.690
2400	30.16	6.63	10.86	33.15	6.899	11.709
2500	30.30	6.64	10.90	33.23	6.903	11.724
2750	30.59	6.67	10.98	33.41	6.912	11.757
3000	30.85	6.69	11.06	33.55	6.919	11.783
3250	31.09	6.71	11.12	33.67	6.924	11.804
3500	31.29	6.73	11.17	33.74	6.928	11.820
3750	31.47	6.74	11.22	33.79	6.932	11.833
4000	31.63	6.75	11.26	33.83	6.934	11.843
4250	31.77	6.76	11.30	33.85	6.937	11.852
4500	31.89	6.77	11.33	33.87	6.939	11.860
4750	32.01	6.78	11.36	33.89	6.940	11.866
5000	32.11	6.79	11.39	33.90	6.942	11.873
5250	32.20	6.80	11.41	33.91	6.943	11.878
5500	32.28	6.81	11.44	33.92	6.944	11.882
5750	32.36	6.81	11.46	33.93	6.945	11.886
6000	32.43	6.82	11.48	33.94	6.946	11.889

higher density for the aluminized explosive. Compare, for example, Fig. 2 with the experimental $D(\rho_1)$ curves for TNT and RDX, namely

$$D = 5900 + 3650(\rho_1 - 1.0) \quad \text{(RDX)}$$
$$D = 5010 + 3225(\rho_1 - 1.0) \quad \text{(TNT)}$$

See also Tables I and II.

The ratio $Al_2O(g)/Al_2O_3(c)$ falls to zero at temperatures below about 3500°K. at the "explosion pressures" p_3 of the high density aluminized explosives, or below about 3000°K. at very low densities. (The "explosion" state here follows the usage of Schmidt.[9] The subscript 3 refers to the initial conditions of the real work process corresponding to the gaseous products at the same density as the original explosive, and subscript 4 to the final state of the work integral. This quite correctly ignores the influence of the detonation wave since this wave has only a transient influence compensated by the rarefaction wave as far as the work integral A is concerned). This apparently causes the temperature to be buffered at a value between 3000 and 3500°K. during adiabatic expansion. The maximum available energy or total blast potential is determined by the work integral

$$A = \int_{v_3}^{v_4} p\,dv = Q - q$$

where A is the maximum available work in adiabatic expansion of the products of detonation from specific volume v_3 to v_4, Q is the heat of explosion and q is the heat retained by the products of detonation at v_4. In general, explosives are very efficient in utilizing Q in work processes as long as the confinement of the burden is adequate. In open air blasts the compressibility of air is such that A/Q is only about 0.15 to 0.2, but in underground and underwater blasting A/Q −0.8 to 1.0 depending primarily on ρ_1. In either case, however, the buffering action of the ratio $Al_2O(g)/Al_2O_3(c)$ on temperature will tend to increase Q and A in aluminized explosive approaching as far as the maximum available energy is concerned, the high value corresponding to zero in this ratio. Only where v_4 is effectively only slightly greater than v_3, as in applications requiring high brisance (*e.g.*, end effect phenomena including impulsive loading of targets, cavity effect, etc.) will the high $Al_2O(g)/Al_2O_3(c)$ ratios applicable in the wave front of detonation be important in lowering intensity. In cases where v_4 is much greater than v_3, this ratio should be effectively zero. The thermodynamics of the $Al_2O(g)/Al_2O_3(c)$ ratio thus appears to give a satisfactory explanation of the behavior of the important high temperature, aluminized explosives. Quantitative computations accurate within the accuracy of the thermodynamic data presented above are possible for any particular set of conditions.

The situation is somewhat different in AN–Al mixtures. In the first place these mixtures have low enough detonation temperature and sufficient oxygen at Al < 15% that $Al_2O(g)/Al_2O_3(c)$ ratio is practically zero in this range. At 20% Al, where the explosive is approximately oxygen balanced, this ratio is still quite low and Q for detonation conditions is a maximum (at 1355 kcal./kg.) since the ratio $Al_2O(g)/Al_2O_3(c)$ increases rapidly as Al is further increased owing to the rapidly increasing temperature. However, in work processes where v_4 is effectively much greater than v_3, A should continue to increase with per cent. aluminum in the AN–Al mixtures, perhaps to as high as 35 to 40% Al. The AN–Al explosives in this composition range should thus be very powerful ones for underwater, air-blast and underground use. However, while they should develop sustained pressures, their peak pressures under all circumstances will be very low, particularly in small sizes where $D/D^* << 1$.

Finally, let us consider some aspects of the kinetics of the reactions of AN–Al and AN–DNT mixtures in detonation. In previous studies of non-ideal explosives, including both pure explosives and mixtures, the surface burning (two-thirds order) rate law described by Eyring, *et al.*,[10] was found to apply. The explosive mixtures studied, however, were of a type in which the temperature generated by the reaction of at least one of the ingredients alone without mixing with those of any of the other components would raise the temperature in the products to or above the final equilibrium T_2. In AN–Al mixtures, on the other hand, the temperature attained by reaction of AN alone cannot exceed about 1700°K., whereas that for the complete mixtures goes much higher. Hence mass transfer

(9) A. Schmidt, *Z. ges. Schiess und Sprengstoffw.*, numerous articles from 1929 to 1939.

(10) H. Eyring, R. E. Powell, H. H. Duffey and R. B. Parlin, *Chem. Revs.*, **45**, 1 (1949).

and possibly heat transfer are much more important factors in these mixtures than in TNT–Al and TNT–RDX–Al mixtures. The temperature of the latter will always be in the neighborhood of the final temperature, irrespective of the fraction of explosive reacted, but this is by no means true in fuel sensitized AN mixtures. Two other possible limiting factors besides heat transfer in the condensed phases thus arise. The limiting factor determining rate in the AN–Al mixtures thus might be either (1) mass transfer (or mixing) in the gas phase, or/and (2) heat transfer in the gas phase. In the previous examples studied these processes were apparently unimportant and the rate of reaction was limited by the upper limit of temperature and reaction rate in the solid (the Eyring process). However, in AN–Al mixtures the gaseous phase is apparently not in equilibrium, and factor (1), (2) or both thus limit the rate of reaction. The fact that the rate decreases rapidly with density indicates that the limiting factor is mass transfer. (Diffusion falls rapidly with increasing density or pressure in the vapor phase, but thermal conductivity does not.) This situation corresponds approximately to that occurring in granular "low" explosives such as black powder in which the burning rate decreases with increasing density.

Single and double-base propellants in which the solid phase is homogeneous apparently have thermal conductivity as the rate-determining factor. That is, the rate in these explosives is probably determined by the temperature at the solid-vapor interface, but the initial process of decomposition is endothermic or much less exothermic than the over–all reaction. Most of the heat is thus generated a short distance away from solid–vapor interface and must be transferred back by thermal conduction to support the reaction. The temperature gradient away from the surface (temperature being smallest at the solid surface), therefore, increases with pressure, and the effective surface temperature also increases with pressure. The result is that the burning rate increases with pressure.

The anomalous $D(\rho_1)$ curves observed at $d = 10$ cm. in 90/10 AN–DNT are characteristic of nearly all AN-combustible mixtures in small diameter. Quantitative studies of the D/D^* *vs.* ρ_1 curves of such mixtures should thus lead to valuable information on mass transfer in gases at higher densities and pressures in addition to important practical and theoretical information regarding the reaction kinetics of AN-combustible mixtures.

THERMODYNAMIC FUNCTIONS FOR THE SOLUTION OF SILICA IN WATER

BY S. A. GREENBERG[1]

Laboratory for Inorganic and Physical Chemistry, University of Leiden, Holland

Received July 4, 1956

The thermodynamic functions connected with the equilibria between both high surface area, amorphous silica and quartz and aqueous solutions saturated with monosilicic acid (H_4SiO_4) were calculated from data reported in the literature.

Introduction

Although accurate measurements have been made of the solubility of high surface area amorphous silicas[2–5] and quartz[2,4] in water at various temperatures, the thermodynamic functions connected with these equilibria have not yet been reported.

The equilibrium between solid silica and saturated aqueous solutions may be written

$$SiO_2(s) + mH_2O(l) \rightleftharpoons H_4SiO_4\cdot aq \qquad (1)$$

Since the silicic acid is very weak[6] no appreciable dissociation in neutral water would be expected. It has been established fairly conclusively that the soluble species of silica in neutral solutions of low ionic strength is monosilicic acid.[2,4] Therefore, the equilibrium constant for the reaction K_c is equal to the activity of the monosilicic acid. Because the concentration of silicic acid in saturated solutions is small, it is possible to equate activity with concentration (moles/l.) without introducing a large error.

Results

Calculation of ΔH, ΔF°_{2000} and ΔS_{2000}.[7]—Data for the evaluation of these quantities were taken from Iler[2] and Kennedy.[4]

In order to calculate the heat of reaction ΔH for the equilibrium (eq. 1) the van't Hoff equation was used. In Fig. 1 the negative logarithm of the concentration of silicic acid is plotted as a function of the reciprocal of the absolute temperature. ΔH values were determined from the average slopes (Table I).

TABLE I

THERMODYNAMIC FUNCTIONS FOR SOLUTION OF SILICA

	Amorphous silica	Quartz
ΔH, kcal./mole	$+2.65 \pm 0.28$	$+7.34 \pm 0.37$
ΔF°_{2000}, kcal./mole	$+3.98 \pm 0.04$	$+5.20 \pm 0.04$
ΔS_{2000}, cal./deg. mole	-2.82 ± 0.50	$+4.53 \pm 0.71$

It is obvious from the deviations from the average

(1) Chemistry Department, Seton Hall University, South Orange, New Jersey.

(2) For review see R. K. Iler, "The Colloid Chemistry of Silica and the Silicates," Cornell University Press, Ithaca, N. Y., 1955.

(3) G. B. Alexander, W. M. Heston and R. K. Iler, THIS JOURNAL, **58**, 453 (1954).

(4) G. C. Kennedy, *Econ. Geol.*, **45**, 629 (1950).

(5) C. S. Hitchen, *ibid.*, **40**, 361 (1945).

(6) S. A. Greenberg and J. J. Hermans, *J. Phys. Chem.*, in press.

(7) For discussion see F. H. MacDougall, "Physical Chemistry," The Macmillan Co., New York, N. Y., 1936.

slopes and the differences between the measured and average values of the concentrations that the ΔH quantities for both the amorphous and the crystalline silica are essentially constant over the temperature range investigated.

From the usual relationships between $\Delta F°$ and K_c, and between ΔS and ΔH, $\Delta F°$ and T, the values at 200° for $\Delta F°$ and ΔS were obtained. In Table I these quantities are listed for amorphous silica and quartz.

The free energy change for the crystallization of amorphous silica into quartz may be found at 200° from the difference in the free energy relationships for each substance

$$\Delta F°_{Q} - \Delta F°_{AS} = RT \ln K_{AS}/K_{Q} \qquad (2)$$

where the subscripts refer to amorphous silica and quartz. It readily may be observed that because of the lower free energy state of quartz the solubility of the amorphous silica is greater than that of quartz by the above equation. The free energy change at 200° on going from amorphous silica to quartz is −1.22 kcal./mole which compares fairly well with the −1.5 kcal./mole of the 25° transition of silica glass to quartz.[8] Moreover, the ΔH on going from hydrated amorphous silica to quartz as found in the present study is −4.69 and from reported data,[8] −4.4 kcal./mole was calculated for this change.

Ramsberg[9] has evaluated the heat of formation of silicic acid from quartz and reports it to be +2.8 kcal./mole. If the heat of solution ΔH of quartz (Table I) is +7.34 kcal./mole then the heat of solution of solid silicic acid must be approximately +4.5 kcal./mole.

Discussion

The silicas, as has been pointed out previously,[2,10] are condensation polymers of silicic acid, H_4SiO_4, and, therefore, to form a silicic acid solution a depolymerization reaction must proceed by hydrolysis. Tourky[11] estimates the heat of polymerization at −8.0 kcal./mole. Therefore, the heat of depolymerization would be approximately of this order of magnitude. The heats of solution for quartz and amorphous silica found in the present study are +7.34 and +2.65 kcal./mole, respectively. Since the product obtained by Tourky on the polymerization of silicic acid most closely resembles amorphous silica, the value of 8.0 kcal. reported by him is probably much too high.

An amorphous silica with a surface area of 250 sq. m./g. contains approximately 3 g. of water per 100 g. SiO_2 in $Si\langle^{OH}_{OH}$ groups.[10] Therefore, such an amorphous silica is about 5% hydrolyzed, whereas quartz because of its small surface area has a negligible amount of SiOH water.

The negative value of $\Delta S_{200°}$ of −2.82 found for amorphous silica is not surprising. First, because the silica is already in an amorphous state, and, secondly, because of the reduction in entropy of the water bound to silicic acid SiOH groups by hydrogen bonds.[12] The estimated heat of solution of solid silicic acid of +4.5 kcal./mole is to be expected. Although silicic acid possesses four OH groups to interact with water, which would lead to a more stable state and a negative change in the heat content, there is probably a large amount of energy necessary to separate the silicic acid molecules in the formation of a solution.

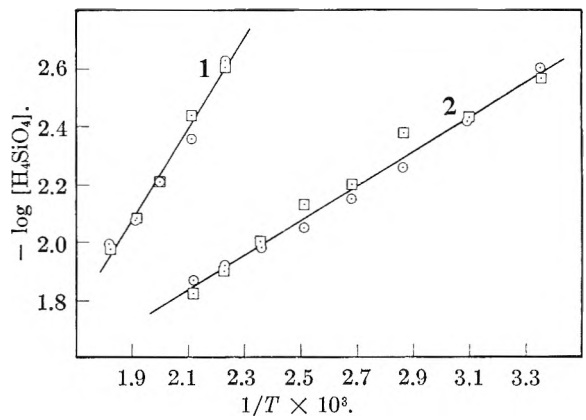

Fig. 1.—Solubility of amorphous silica (1) and quartz (2) expressed in log $[H_4SiO_4]$ *vs.* $1/T$ plots (○, ref. 2; □, ref. 4).

The higher ΔH, $\Delta F°_{200°}$ and $\Delta S_{200°}$ values found for quartz are reasonable. Certainly, quartz is at a lower free energy state than amorphous silica. A greater amount of energy would also be necessary to hydrolyze the Si–OSi bond in quartz than in amorphous silica which would lead to a higher ΔH change. However, the difference in entropy of 7.35 cal./deg. mole between amorphous silica and quartz for this process appears to be quite high.

From the results of this discussion it appears that the treatment of the solubility data as an equilibrium is reasonable. Although theoretically the solubility of crystals is a function of particle size and surface area, according to Alexander and Johnson[13] experimentally this has not been found to be the case. Apparently, small amounts of impurities can change the character of the surface to such a degree that the theoretical relationships do not hold. Since particle size seems to have no influence on solubility,[3] it can perhaps be assumed that at equilibrium the amorphous silicas exhibit the same surface energies.

Acknowledgements.—The author wishes to thank Professor J. J. Hermans for helpful suggestions on the manuscript and the Foundation for Fundamental Research of Matter (FOM) supported by the Netherlands Organization for Pure Research (ZWO) under whose auspices this research was performed.

(8) E. L. Brady, THIS JOURNAL, **57**, 706 (1953); National Bureau of Standards, Circular 500, "Selected Values of Thermodynamic Properties," U. S. Govt. Printing Office, 1952, p. 148.

(9) H. Ramsberg, *J. Geol.*, **62**, 388 (1954).

(10) S. A. Greenberg, THIS JOURNAL, **60**, 325 (1956).

(11) A. R. Tourky, *Chemistry and Industry*, 254 (1942).

(12) G. H. Haggis, J. B. Hasted and T. B. Buchanen, *J. Chem. Phys.*, **20**, 1452 (1952).

(13) For review see A. E. Alexander and P. Johnson, "Colloid Science," Oxford Univ. Press, London, 1949.

WIEN EFFECT IN SIMPLE STRONG ELECTROLYTES*

BY LARS ONSAGER AND SHOON KYUNG KIM†

Contribution No. 1377 from the Sterling Chemistry Laboratory, Yale University, New Haven, Connecticut

Received July 9, 1956

Wilson's computation of the Wien effect in strong binary electrolytes is simplified and extended to simple electrolytes of all valence types. The results appear as double integrals, which are reduced to closed form by elliptic substitutions. Alternative forms for evaluation by descending power series (for high field intensities) or by numerical quadrature (best for low field intensities) are described in detail.

Introduction

Deviations from Ohm's law in electrolytic conductors were discovered by Poole[1] for solid dielectrics and by Wien[2] for liquid electrolytes. In both cases the conductance increases with the intensity of the field. This increase has been shown in general to arise from two different effects: *i.e.*, a destruction of the "ionic atmosphere" and a modification of the dissociation kinetics. In weak electrolytes the latter effect is rather more important; a theory has been developed by Onsager.[3] The former effect was first computed by Joos and Blumentritt[4] using a method of successive approximations. Their convergence difficulties and one incorrect assumption severely limit the value of their results. Formulas applicable to simple binary electrolytes over an unrestricted range of field intensities were derived by Wilson[5] from the basic equations formulated by Onsager and Fuoss.[6] We shall presently extend Wilson's computation to simple strong electrolytes of arbitrary valence type. Wilson solved the fundamental equation by means of the one-dimensional Fourier transformation. We shall prefer the three-dimensional Fourier transformation, which substantially simplifies the analysis.

We start from Onsager's linearized equation of continuity and Poisson's equation, which are valid for field strengths from zero to infinity in the case of very low concentrations. We shall first simplify the system of differential equations by introducing the symmetric part and the asymmetric part of the potential and the distribution function. Then by applying the three-dimensional Fourier transformation to the differential system, we obtain the transformed potential and the distribution function specialized for simple electrolytes. From the asymmetric part of the potential we get the relaxation force. Upon substituting the charge density into the Stokes' hydrodynamic equation we obtain the electrophoretic velocity of an ion; the symmetrical part of the atmosphere determines this effect. The two results together give us the conductivity as a function of the field.

The result appears directly as a double integral, which is readily reduced to a single integral and may be expressed in closed form in terms of elliptic integrals of the first and second kind. Unfortunately, the limits of these integrals are determined implicitly by a cubic equation, so that the numerical quadrature seems simpler for weak fields. For strong fields we provide a convenient series in descending powers of the field intensity (with occasional logarithmic terms).

2. The Fundamental Equation

We shall consider a solution containing $n_1, n_2, \ldots n_s$ ions (per cm.^{3}) of species 1, 2, . . ., s. The solvent is assumed to be a viscous dielectric continuum with dielectric constant D, so that a j-ion is characterized by its electric charge e_j and absolute mobility ω_j (the reciprocal of the friction constant). We shall assume that a homogeneous electric field acts upon the ions in the solution at rest; then the distribution function f_{ji} for an ion pair (j, i) depends upon only the relative location $\mathbf{r}$ of the j- and i-ion. We denote by $\psi_j(\mathbf{r})$ the (average) electrostatic potential at a directed distance $\mathbf{r}$ from the j-ion. This potential is related to the distribution function $f_{ji}(\mathbf{r})$ by Poisson's equation

$$\nabla^2\psi_j(\mathbf{r}) = -\frac{4\pi}{D}\sum_{i=1}^{s} f_{ji}(\mathbf{r})e_i/n_j; \quad (\mathbf{r} \neq 0) \qquad (2.1)$$

The symmetry condition for $f_{ji}(\mathbf{r})$

$$f_{ji}(\mathbf{r}) = f_{ij}(-\mathbf{r}) \qquad (2.2)$$

is obvious. The motion of an ion pair (j, i) is governed by the equation of continuity in the six-dimensional space of the coördinates of the ion pair. With the aid of well-known approximations which are permissible for low concentrations of ions[6] we may obtain the linearized equation of continuity

$$kT(\omega_j + \omega_i)\nabla^2 f_{ji}(\mathbf{r}) + \omega_i e_i n_i n_j \nabla^2\psi_j(\mathbf{r}) + \omega_j e_j n_j n_i \nabla^2\psi_i(-\mathbf{r}) + (\omega_j e_j - \omega_i e_i)X\frac{\partial}{\partial x} f_{ji}(\mathbf{r}) = 0 \qquad (2.3)$$

where we have assumed that the applied homogeneous field X is parallel to the x-direction. This equation is valid with homogeneous boundary conditions; there are no sources or sinks where ions are created or destroyed. On the other hand, the boundary condition for the Poisson equation is inhomogeneous at $\mathbf{r} = 0$ because of the point charge e_j of the central ion. Thanks to the principle of linear superposition, the equation

* This paper is based on the dissertation submitted by Shoon K. Kim to the Faculty of the Graduate School of Yale University in partial fulfillment of the requirements for the Degree of Doctor of Philosophy.

† Institute for Fluid Dynamics and Applied Mathematics, University of Maryland, College Park, Maryland.

(1) H. H. Poole, *Phil. Mag.*, **32**, 112 (1916); **34**, 204 (1917).

(2) M. Wien, *Ann Physik*, [4] **83**, 327 (1927); [4] **85**, 759 (1928).

(3) L. Onsager, *J. Chem. Phys.*, **2**, 599 (1934).

(4) G. Joos and M. Blumentritt, *Physik. Z.*, **28**, 836 (1927); M. Blumentritt, *Ann. Physik*, **85**, 812 (1928).

(5) W. S. Wilson, Dissertation, Yale University, 1936; also H. C. Eckstrom and C. Schmelzer, *Chem. Revs.*, **24**, 367 (1939); H. S. Harned and B. B. Owen, "The Physical Chemistry of Electrolytic Solutions," second edition, Reinhold Publ. Corp., New York, N. Y., 1950, p. 95.

(6) L. Onsager and R. Fuoss, THIS JOURNAL, **36**, 2689 (1932); also, H. S. Harned and B. B. Owen, ref. 5, p. 24.

$$\nabla^2\left[\psi_j(\mathbf{r}) - \frac{e_j}{Dr}\right] = -\frac{4\pi}{D}\sum_{i=1}^{s} f_{ji}(\mathbf{r})\, e_i/n_j \quad (2.4)$$

is valid everywhere with homogeneous boundary conditions. The functions $\psi_j(\mathbf{r})$ and $f_{ji}(\mathbf{r})$ satisfy the following boundary conditions for large r

$$\begin{aligned} \psi_j(\infty) &= 0 \ (\text{and } \nabla\psi_j(\infty) = 0) \\ f_{ji}(\infty) &= n_j n_i \ (\text{and } \nabla f_{ji}(\infty) = 0) \end{aligned} \quad (2.5)$$

Equations 2.3 and 2.4 together with the boundary condition give us the complete system of differential equations for the present problem.

The ψ_i term in the equation of continuity has a negative sign. Before we deal with this complication, we first introduce a dimensionless variable, $\mathbf{r}_0$ (x_0, y_0, z_0) by

$$\kappa\mathbf{r} = \mathbf{r}_0; \quad \nabla = \kappa\nabla_0 \quad (2.6)$$

where

$$\kappa = \sqrt{\frac{4\pi\Gamma_0}{DkT}}; \quad \Gamma_0 = \sum_{i=1}^{s} n_i e_i^2$$

We next define the even and odd-parts of the functions by

$$\left.\begin{aligned} \tfrac{1}{2}[\psi_j(\mathbf{r}) + \psi_j(-\mathbf{r})] - \frac{e_j}{Dr} &\equiv \frac{\kappa e_j}{D}\psi^+{}_j(\mathbf{r}_0) \\ \tfrac{1}{2}[\psi_j(\mathbf{r}) - \psi_j(-\mathbf{r})] &\equiv \frac{\kappa e_j}{D}\psi^-{}_j(\mathbf{r}_0) \\ \tfrac{1}{2}[f_{ji}(\mathbf{r}) + f_{ji}(-\mathbf{r})] - n_j n_i &\equiv \frac{\kappa n_j n_i e_j e_i}{DkT} f^+{}_{ji}(\mathbf{r}_0) \\ \tfrac{1}{2}[f_{ji}(\mathbf{r}) - f_{ji}(-\mathbf{r})] &\equiv \frac{\kappa n_j n_i e_j e_i}{DkT} f^-{}_{ji}(\mathbf{r}_0) \end{aligned}\right\} \quad (2.7)$$

By definition, these functions satisfy the following symmetry relations

$$\left.\begin{aligned} &\psi^+{}_j(-\mathbf{r}_0) = \psi^+{}_j(\mathbf{r}_0), \ \psi^-{}_j(-\mathbf{r}_0) = -\psi^-{}_j(\mathbf{r}_0) \\ &f^+{}_{ji}(-\mathbf{r}_0) = f^+{}_{ji}(\mathbf{r}_0) = f^+{}_{ij}(-\mathbf{r}_0), \\ &\qquad f^-{}_{ji}(-\mathbf{r}_0) = -f^-{}_{ji}(\mathbf{r}_0) = -f^-{}_{ij}(-\mathbf{r}_0) \end{aligned}\right\} \quad (2.8)$$

In terms of these functions, the boundary conditions become

$$\psi^\pm{}_j(\infty) = \nabla_0\psi^\pm{}_j(\infty) = 0, f^\pm{}_{ji}(\infty) = \nabla_0 f^\pm{}_{ji}(\infty) = 0 \quad (2.9)$$

and the Poisson eq. 2.4 is separated into two equations

$$\left.\begin{aligned} \nabla_0^2\psi^+{}_j(\mathbf{r}_0) &= -\sum_{i=1}^{s} f^+{}_{ji}(\mathbf{r}_0)\,\mu_i \\ \nabla_0^2\psi^-{}_j(\mathbf{r}_0) &= -\sum_{i=1}^{s} f^-{}_{ji}(\mathbf{r}_0)\,\mu_i \end{aligned}\right\} \quad (2.10)$$

where μ_i is the relative ionic strength of an i-ion

$$\mu_i = n_i e_i^2/\Gamma_0$$

Finally, if we define the quantities

$$\omega_{ji} = \frac{\omega_j}{\omega_j + \omega_i} \quad (2.11)$$

$$a_{ji} = \frac{X}{\kappa kT}\frac{\omega_j e_j - \omega_i e_i}{\omega_j + \omega_i} \quad (2.12)$$

then the equation of continuity may be written in the forms

$$\left.\begin{aligned} \nabla_0^2 f^+{}_{ji}(\mathbf{r}_0) + \omega_{ij}\nabla_0^2\psi^+{}_j(\mathbf{r}_0) + \omega_{ji}\nabla_0^2\psi^+{}_i(\mathbf{r}_0) + \\ a_{ji}\frac{\partial}{\partial x_0} f^-{}_{ji}(\mathbf{r}_0) = 4\pi\delta(\mathbf{r}_0) \\ \nabla_0^2 f^-{}_{ji}(\mathbf{r}_0) + \omega_{ij}\nabla_0^2\psi^-{}_j(\mathbf{r}_0) - \omega_{ji}\nabla_0^2\psi^-{}_i(\mathbf{r}_0) + \\ a_{ji}\frac{\partial}{\partial x_0} f^+{}_{ji}(\mathbf{r}_0) = 0 \end{aligned}\right\} \quad (2.13)$$

Here $\delta(\mathbf{r}_0)$ is Dirac's delta-function defined by

$$\delta(\mathbf{r}_0) = 0 \ (\mathbf{r}_0 \neq 0), \ \int\delta(\mathbf{r}_0)d^3\mathbf{r}_0 = 1$$

In obtaining eq. 2.13, we have used the following property of the delta-function

$$\nabla_0^2\left(\frac{1}{r_0}\right) = -4\pi\delta(\mathbf{r}_0)$$

Since we are going to integrate eq. 2.13, the use of the delta-function is appropriate and particularly convenient in solving the system of equations by the Fourier transformation.

It may be profitable to discuss the physical significance of the antisymmetric matrix $\| a_{ji} \|$. The order of magnitude of its elements for $j \neq i$ is determined by a parameter a_0

$$a_0 = X\epsilon/\kappa kT \quad (2.14)$$

where ϵ is the absolute electronic charge. It is apparent that for a system whose relative concentrations of various valences and mobilities of ions are fixed, our fundamental eq. 2.10 and 2.13 are completely determined by the single parameter a_0. According to Falkenhagen,[7] the time of relaxation Θ_{ji} of the ionic atmosphere with regard to j-th and i-th ions is given by

$$\Theta_{ji} = \frac{1}{\kappa^2 kT(\omega_j + \omega_i)}$$

In the zero'th approximation, the relative speed v_{ji} between two ions of species j and i equals $|\omega_j e_j - \omega_i e_i| X$. The mean diameter of the ionic atmosphere (in equilibrium) equals $1/\kappa$. Therefore, the parameter a_0 has the following physical meaning

$$a_0 \cong |a_{ji}| = \Theta_{ji}\kappa v_{ji}$$

where Θ_{ji} is the time of relaxation and $1/(\kappa v_{ji})$ is the time required for two ions to drift apart to a distance $1/\kappa$. Accordingly, if $a_0 >> 1$ the ionic atmosphere of any ion is reduced to a deficiency of similar ions in its neighborhood; the conductivity increases because the relaxation effect becomes relatively negligible, and the electrophoretic effect is reduced although a certain fraction of it always remains. The perturbations are small and Ohm's law holds whenever[3]

$$a_0 \equiv \frac{X\epsilon}{\kappa kT} = \frac{1}{2\mathbf{c}\times 10^{-10}\sqrt{10\pi R}}\sqrt{\frac{D}{T}}\,\Gamma^{-1/2}\,V \ll 1 \quad (2.15)$$

where V is the applied field strength expressed in volt/cm., R the molar gas constant, $\mathbf{c}$ the velocity of light in cm./sec., Γ the ionic strength of the solution defined in terms of the molar concentration, m_i (moles/1000 cm.^{3}) and the valence z_i of an i-ion as

$$\Gamma = \sum_{i=1}^{s} m_i z_i^2$$

3. The Fourier Transform

Let us assume that the Fourier transforms[8] of the functions $f^+{}_{ji}(\mathbf{r}_0)$ and $\psi^+{}_j(\mathbf{r}_0)$ exist, *i.e.*, we can define functions

$$\left.\begin{aligned} F^\pm{}_{ji}(\lambda) &= (2\pi)^{-3/2}\int f^\pm{}_{ji}(\mathbf{r}_0)e^{-i(\lambda\cdot\mathbf{r}_0)}\,d^3\mathbf{r}_0 \\ \bar{\Psi}^\pm{}_j(\lambda) &= (2\pi)^{-3/2}\int \psi^\pm{}_j(\mathbf{r}_0)e^{-i(\lambda\cdot\mathbf{r}_0)}\,d^3\mathbf{r}_0 \end{aligned}\right\} \quad (3.1)$$

(7) H. Falkenhagen, "Electrolytes" (English edition), Clarendon Press, Oxford, 1934, p. 176.

(8) R. Courant and D. Hilbert, "Methods of Mathematical Physics," English Edition, Interscience Publishers, New York, N. Y., 1953, p. 79.

which satisfy Fourier's inversion formulas

$$\left.\begin{aligned} f^{\pm}{}_{ji}(\mathbf{r}_0) &= (2\pi)^{-3/2}\int F^{\pm}{}_{ji}(\boldsymbol{\lambda})e^{i(\boldsymbol{\lambda}\cdot\mathbf{r}_0)}\,d^3\boldsymbol{\lambda} \\ \psi^{\pm}{}_{j}(\mathbf{r}_0) &= (2\pi)^{-3/2}\int \bar{\Psi}^{\pm}{}_{j}(\boldsymbol{\lambda})e^{-i(\boldsymbol{\lambda}\cdot\mathbf{r}_0)}\,d^3\boldsymbol{\lambda} \end{aligned}\right\} \quad (3.2)$$

where $\boldsymbol{\lambda}$ is a vector whose components are ξ, η and ζ. If we apply the transformation (3.1) to the differential eq. 2.10 and 2.13, and use Gauss' theorem and the boundary condition (2.9) we obtain

$$\lambda^2\bar{\Psi}^{+}{}_{j}(\boldsymbol{\lambda}) = \sum_{i=1}^{s} F^{+}{}_{ji}(\boldsymbol{\lambda})\mu_i \quad (3.3)$$

$$\lambda^2\bar{\Psi}^{-}{}_{j}(\boldsymbol{\lambda}) = \sum_{i=1}^{s} F^{-}{}_{ji}(\boldsymbol{\lambda})\mu_i \quad (3.4)$$

$$\lambda^2(F^{+}{}_{ji}(\boldsymbol{\lambda}) + \omega_{ij}\bar{\Psi}^{+}{}_{j}(\boldsymbol{\lambda}) + \omega_{ji}\bar{\Psi}^{+}{}_{i}(\boldsymbol{\lambda})) = i\xi a_{ji}F^{-}{}_{ji}(\boldsymbol{\lambda}) - \sqrt{\frac{2}{\pi}} \quad (3.5)$$

$$\lambda^2(F^{-}{}_{ji}(\boldsymbol{\lambda}) + \omega_{ij}\bar{\nu}^{-}{}_{j}(\boldsymbol{\lambda}) - \omega_{ji}\bar{\Psi}^{-}{}_{i}(\boldsymbol{\lambda})) = i\xi a_{ji}F^{+}{}_{ji}(\boldsymbol{\lambda}) \quad (3.6)$$

We have used here

$$\int \delta(\mathbf{r}_0)e^{-i(\boldsymbol{\lambda}\cdot\mathbf{r}_0)}d^3\mathbf{r}_0 = 1$$

Before trying to solve these algebraic equations for the case of simple electrolytes where $s = 2$, we shall obtain some simple relations. First of all, we note that the symmetry property, (2.8), of the functions does not change by the transformation. Accordingly, we have

$$F^{+}{}_{ji}(\boldsymbol{\lambda}) = F^{+}{}_{ij}(\boldsymbol{\lambda}) \quad (3.7)$$

$$F^{-}{}_{ji}(\boldsymbol{\lambda}) = -F^{-}{}_{ij}(\boldsymbol{\lambda}) \quad (3.8)$$

If we apply eq. 3.8 to eq. 3.4, we immediately obtain

$$\sum_{j=1}^{s}\mu_j\bar{\Psi}^{-}{}_{j} = 0 \quad (3.9)$$

Since the diagonal elements of the matrix $\| a_{ji} \|$ are zero, equation 3.5 yields

$$F^{+}{}_{jj} + \bar{\Psi}^{+}{}_{j} = -\frac{1}{\lambda^2}\sqrt{\frac{2}{\pi}} \quad (3.10)$$

Equations 3.7–3.10 give us $(s^2 + s + 1)$ equations for the $2(s^2 + s)$ unknown functions. The remaining $(s^2 + s - 1)$ equations independent from these would be obtained from eq. 3.3–3.4 and the off-diagonal part $(j < i)$ of eq. 3.5–3.6.

Now, it is a simple matter to solve the algebraic equations for $s = 2$. Routine elimination yields the results

$$\bar{\Psi}^{-}{}_{j}(\boldsymbol{\lambda}) = -i\sqrt{\frac{2}{\pi}}\,a_{ji}\mu_i\xi(\lambda^2 + q)/W(\boldsymbol{\lambda});\ (i \neq j) \quad (3.11)$$

$$\bar{\Psi}^{+}{}_{j}(\boldsymbol{\lambda}) = -\sqrt{\frac{2}{\pi}}\{\lambda^2(\lambda^2 + q)^2 + a^2\xi^2(\lambda^2 + 1 - \mu_j)\mu_j\}/\lambda^2W(\boldsymbol{\lambda}) \quad (3.12)$$

$$F^{-}{}_{ji}(\boldsymbol{\lambda}) = -i\sqrt{\frac{2}{\pi}}\,a_{ji}\xi\lambda^2(\lambda^2 + q)/W(\boldsymbol{\lambda}) \quad (3.13)$$

$$F^{+}{}_{ji}(\boldsymbol{\lambda}) = -\sqrt{\frac{2}{\pi}}\{\lambda^2(\lambda^2 + q)^2 + (a^2 - a_{ji}{}^2)(\lambda^2 + 1 - \mu_j)\}/W(\boldsymbol{\lambda}) \quad (3.14)$$

where $j, i = 1, 2$

$$q = \mu_1\omega_{12} + \mu_2\omega_{21},\ a \equiv |a_{12}| = a_0q(|z_1| + |z_2|) \quad (3.15)$$

and

$$W(\boldsymbol{\lambda}) \equiv \lambda^2(\lambda^2 + 1)(\lambda^2 + q)^2 + a^2\xi^2(\lambda^2 + \mu_1)(\lambda^2 + \mu_2)$$

4. The Ionic Field

Since the symmetric part of the ionic atmosphere, $\psi^{+}{}_{j}$, does not produce any field at the central ion, we have for the x-component of the ionic field ΔX_j at the central ion

$$\Delta X_j = -\frac{\partial}{\partial x}\left(\psi_j(\mathbf{r}) - \frac{e_j}{Dr}\right)\Big|_{r=0} = -\frac{\kappa^2e_j}{D}\frac{\partial}{\partial x_0}\psi^{-}{}_{j}(\mathbf{r}_0)\Big|_{\mathbf{r}_0=0}$$

The y- and z-components naturally vanish.

The Fourier inversion formula 3.2 applied to the above equation yields

$$\Delta X_j = -\frac{\kappa^2e_j}{D(2\pi)^{3/2}}\int i\xi\bar{\psi}^{-}{}_{j}(\boldsymbol{\lambda})\,d^3\boldsymbol{\lambda} = -\frac{\kappa^2e_ja_{ji}\mu_i}{2\pi^2D} \times \int \frac{\xi^2(\lambda^2 + q)}{\lambda^2(\lambda^2 + 1)(\lambda^2 + q)^2 + a^2\xi^2(\lambda^2 + \mu_1)(\lambda^2 + \mu_2)}\,d^3\boldsymbol{\lambda}$$

where $i \neq j$. Since we are dealing with a simple electrolyte, the electro-neutrality condition gives

$$\mu_i = e_i/(e_i - e_j),\ a_{ji}\mu_i = -Xqe_i/\kappa kT;\ (i \neq j)$$

The integrand is invariant to rotation around the ξ-axis. We perform the trivial integration over the azimuthal angle and denote by $t = \xi/\lambda$ the cosine of the polar angle; then our expression for the ionic field takes the form

$$\Delta X_1 = \Delta X_2 \equiv \Delta X = X\frac{\kappa qe_1e_2}{DkT}A(a) \quad (4.1)$$

where

$$A(a) \equiv \frac{2}{\pi}\int_{t=0}^{1}dt\int_{\lambda=0}^{\infty}d\lambda \times \frac{t^2\lambda^2(\lambda^2 + q)}{(\lambda^2 + 1)(\lambda^2 + q)^2 + a^2t^2(\lambda^2 + \mu_1)(\lambda^2 + \mu_2)} \quad (4.2)$$

When $a << 1$, the integral $A(a)$ becomes

$$A(a) = \frac{1}{3(1 + \sqrt{q})} + O(a^2) \quad (4.3)$$

and accordingly, the field ΔX becomes

$$\Delta X/X = \frac{\kappa e_1e_2}{3DkT}\frac{q}{1 + \sqrt{q}} + O(a^2) \quad (4.4)$$

This is the result first obtained by Onsager[9] for low field strengths where the Ohm law holds.

When $a \simeq \infty$

$$A(a) = \frac{1}{2a} + O(a^{-2});\ A(\infty) = 0$$

which will be shown later in Sec. 9.

Now the integral A as a function of a^2 is a monotonic decreasing function which does not have any inflection points, because by differentiating eq. 4.2 with respect to a^2 we can show

$$\frac{\partial A}{\partial(a^2)} < 0,\ \frac{\partial^2A}{\partial(a^2)^2} > 0 \quad (4.5)$$

5. Electrophoresis

We shall now compute the additional velocity of an ion, say j-ion, caused by the electrophoretic flow of the medium surrounding the ion. This effect may be calculated by the Stokes' hydrodynamic equations for an incompressible liquid

$$\left.\begin{aligned} \eta_0\nabla^2\mathbf{v}_j &= \nabla p_j - \mathbf{f}_j \\ \nabla\cdot\mathbf{v}_j &= 0 \end{aligned}\right\} \quad (5.1)$$

where $\mathbf{v}_j(\mathbf{r})$ is the velocity, $p_j(\mathbf{r})$ the pressure, η_0 the

(9) L. Onsager, *Physik. Z.*, **27**, 388 (1926); **28**, 277 (1927).

viscosity of the medium and $\mathbf{f}_j(\mathbf{r})$ is the force density which arises from the action of the external field $\mathbf{X}$ upon the charge density in the ionic atmosphere. (For the justification of the procedure see references 7 and 9.)

The charge density ρ_j in the atmosphere is most easily obtained from the Poisson equation

$$\rho_j = -\frac{D}{4\pi}\nabla^2\left(\psi_j - \frac{e_j}{Dr}\right) = -\frac{\kappa^3 e_j}{4\pi}\nabla_0^2(\psi^+{}_j(\mathbf{r}_0) + \psi^-{}_j(\mathbf{r}_0))$$

Accordingly, the force density is given by

$$\mathbf{f}_j = -\mathbf{X}\frac{\kappa^3 e_j}{4\pi}\nabla_0^2(\psi^+{}_j(\mathbf{r}_0) + \psi^-{}_j(\mathbf{r}_0)) \qquad (5.2)$$

The action of the external field upon the asymmetric part of the charge density contributes a total of zero to the hydrodynamic velocity at the origin because the contributions from corresponding volume elements located at $\mathbf{r}$ and $-\mathbf{r}$ cancel each other.

In terms of the dimensionless variable $\mathbf{r}_0$ eq. 5.1 becomes

$$\left.\begin{aligned}\nabla_0^2\mathbf{v}_j &= \frac{1}{\kappa\eta_0}\nabla_0 p_j + \mathbf{X}\frac{\kappa e_j}{4\pi\eta_0}\nabla_0^2(\psi^+{}_j(\mathbf{r}_0) + \psi^-{}_j(\mathbf{r}_0))\\ \nabla_0\cdot\mathbf{v}_j &= 0\end{aligned}\right\} \qquad (5.3)$$

If we assume that the Fourier transforms, like eq. 3.1, of the functions in eq. 5.3 exist, we have

$$\left.\begin{aligned}\lambda^2\mathbf{V}_j &= -\frac{1}{\kappa\eta_0}i\lambda P_j + \mathbf{X}\frac{\kappa e_j}{4\pi\eta_0}\lambda^2(\bar{\Psi}^+{}_j(\lambda) + \bar{\Psi}^-{}_j(\lambda))\\ \lambda\cdot\mathbf{V}_j &= 0\end{aligned}\right\} \qquad (5.4)$$

where the capital letter functions indicate the Fourier transforms of their respective small letter functions. Eliminating P_j from eq. 5.4, we easily obtain

$$\mathbf{V}_j(\lambda) = \frac{\kappa e_j}{4\pi\eta_0}\frac{\lambda^2\mathbf{X} - \lambda(\lambda\cdot\mathbf{X})}{\lambda^2}(\bar{\Psi}^+{}_j(\lambda) + \bar{\Psi}^-{}_j(\lambda))$$

Since we have assumed that the external field $\mathbf{X}$ has a component X only in the x-direction, we obtain by means of the Fourier inversion formula

$$v_{jx}(0) = X\frac{\kappa e_j}{4\pi\eta_0}(2\pi)^{-3/2}\int\frac{\lambda^2 - \xi^2}{\lambda^2}\bar{\Psi}^+{}_j(\lambda)\,d^3\lambda \qquad (5.5)$$

$$v_{jy}(0) = v_{jz}(0) = 0$$

So far, our results are entirely general. For the case of simple electrolytes, we substitute eq. 3.12 into eq. 5.5 and we obtain for the electrophoretic effect, $\Delta v_j \equiv v_{jx}(0)$

$$\nabla v_j = -X\frac{\kappa e_j}{8\pi^3\eta_0}\int d^3\lambda \times \frac{(\lambda^2 - \xi^2)\{\lambda^2(\lambda^2 + q)^2 + a^2\xi^2(\lambda^2 + 1 - \mu_j)\mu_j\}}{\lambda^4\{\lambda^2(\lambda^2 + 1)(\lambda^2 + q)^2 + a^2\xi^2(\lambda^2 + \mu_1)(\lambda^2 + \mu_2)\}} \qquad (5.6)$$

If we define an integral $B_j(a)$ by

$$B_j(a) = \frac{2}{(1 - \mu_j)\pi}\int_{t=0}^{1}dt\int_{\lambda=0}^{\infty}d\lambda \times \frac{(1 - t^2)\{(\lambda^2 + q)^2 + a^2t^2(\lambda^2 + 1 - \mu_j)\mu_j\}}{(\lambda^2 + 1)(\lambda^2 + q)^2 + a^2t^2(\lambda^2 + \mu_1)(\lambda^2 + \mu_2)} \qquad (5.7)$$

the electrophoretic effect Δv_j takes the following final form

$$\Delta v_j = X\frac{\kappa e_1 e_2}{4\pi\eta_0(e_j - e_i)}B_j(a),\ (i \neq j) \qquad (5.8)$$

When $a << 1$, we easily obtain

$$B_j(a) = \frac{2}{3(1 - \mu_j)} + O(a_2) \qquad (5.9)$$

and accordingly

$$\Delta v_j/X = -\frac{\kappa e_j}{6\pi\eta_0} + O(a^2)$$

which is the result first obtained by Onsager[9] for low field strengths. When $a \sim \infty$

$$B_j(a) = \frac{2}{3}\frac{\sqrt{\mu_j}}{(1 - \mu_j)} + a^{-1}\log a + O(a^{-1});$$

$$B_j(\infty) = \frac{2}{3}\frac{\sqrt{\mu_j}}{(1 - \mu_j)}$$

which will be shown later in Sec. 9.

Now the integral $B_j(a)$, as a function of a^2, has the same property as the integral A, *i.e.*, B_j is a monotonic decreasing function of a^2 which does not have any inflection points, because by differentiating eq. 5.7 we can easily show

$$\frac{\partial B_j}{\partial(a^2)} < 0,\ \frac{\partial^2 B_j}{\partial(a^2)^2} > 0$$

6. Evaluation of the Integrals $A(a)$ and $B(b)$ for Binary Electrolytes

For the case of binary electrolytes, we have

$$|z_1| = |z_2| \equiv |z|,\ n_1 = n_2 \equiv n,\ \mu_1 = \mu_2 = q = \frac{1}{2} \qquad (6.1)$$

and accordingly from (3.15)

$$a = |a_{12}| = a_0 z = \left(\frac{DX^2}{8\pi nkT}\right)^{1/2} \qquad (6.2)$$

which depends neither on the mobilities nor on the valences of ions. Substituting (6.1) into the integrals (4.2) and (5.7), we obtain

$$A(a) = \frac{2}{\pi}\int_{t=0}^{1}dt\int_{\lambda=0}^{\infty}\frac{t^2\lambda^2}{(\lambda^2 + 1/2)(\lambda^2 + 1 + a^2t^2)}\,d\lambda \qquad (6.3)$$

$$B_1(a) = B_2(a) = B(a) = \frac{4}{\pi}\int_{t=0}^{1}dt \int_{\lambda=0}^{\infty}\frac{(1 - t^2)\left(\lambda^2 + \frac{1}{2} + \frac{1}{2}a^2t^2\right)}{\left(\lambda^2 + \frac{1}{2}\right)(\lambda^2 + 1 + a^2t^2)}\,d\lambda \qquad (6.4)$$

If we expand the integrands into partial fractions and integrate over λ, we obtain

$$A(a) = \int_{t=0}^{1}\left(-\frac{1}{\sqrt{2}}\frac{t^2}{\left(\frac{1}{2} + a^2t^2\right)} + \frac{t^2\sqrt{1 + a^2t^2}}{\left(\frac{1}{2} + a^2t^2\right)}\right)dt \qquad (6.5)$$

$$B(a) = \int_{t=0}^{1}\left(\sqrt{2}\,a^2\frac{(1 - t^2)t^2}{\left(\frac{1}{2} + a^2t^2\right)} + \frac{(1 - t^2)\sqrt{1 + a^2t^2}}{\left(\frac{1}{2} + a^2t^2\right)}\right)dt \qquad (6.6)$$

It is a simple matter to evaluate these integrals. The results are

$$A(a) = \frac{1}{2a^3}\left\{a(\sqrt{1 + a^2} - \sqrt{2}) + \left(\tan^{-1}(\sqrt{2}a) - \tan^{-1}\frac{a}{\sqrt{1 + a^2}}\right)\right\} \qquad (6.7)$$

$$B(a) = \frac{\sqrt{8}}{3} + \frac{1}{2a^2}\left\{2a^3 \sinh^{-1} a - a(\sqrt{1+a^2} - \sqrt{2}) - (1+a^2)\left(\tan^{-1}(\sqrt{2}a) - \tan^{-1}\frac{a}{\sqrt{1+a^2}}\right)\right\} \quad (6.8)$$

Now, from eq. 4.1 and 5.8 the ionic field ΔX and the electrophoretic velocity $\Delta v_\pm$ for binary electrolytes become

$$\Delta X = -X\frac{\kappa\epsilon^2 z^2}{2DkT}A(a) \quad (6.9)$$

$$\Delta v_\pm = \pm X\frac{\kappa\epsilon|z|}{8\pi\eta_0}B(a) \quad (6.10)$$

where the sign is to be taken depending on the sign of the charge of the ion at the origin. Wilson, who first obtained these results,[5] expressed them by using the functions $g(x)$ and $f(x)$ defined as

$$g(x) = A(a);\ x = a \quad (6.11)$$

$$f(x) \equiv \frac{3}{\sqrt{8}}B(a) \quad (6.12)$$

For numerical computation, convenient forms of $g(x)$ and $f(x)$ valid for x from 0 to ∞, can be found in the monograph of Harned and Owen.[5] Using these forms Wilson tabulated the numerical values of the functions from $x = 0$ to $x = 65$, to four significant figures. Although we could not find such convenient forms for the case of general simple electrolytes, for strong fields we shall provide a convenient series in descending powers of field strengths.

7. Evaluation of the Integrals for General Simple Electrolytes

In order to carry out the integrals (4.2) and (5.7) we put $\sigma = at$ to obtain

$$A(a) = \frac{2}{\pi a^3}\int_{\sigma=0}^{a}\sigma^2 d\sigma\int_{\lambda=0}^{\infty}\frac{\lambda^2(\lambda^2+q)}{Q(\lambda^2,\sigma)}d\lambda \quad (7.1)$$

$$B_j(a) = \frac{2}{(1-\mu_j)\pi a}\int_{\sigma=0}^{a}\left(1-\frac{\sigma^2}{a^2}\right)d\sigma \times\int_{\lambda=0}^{\infty}\frac{(\lambda^2+q)^2+\sigma^2(\lambda^2+1-\mu_j)\mu_j}{Q(\lambda^2,\sigma)}d\lambda \quad (7.2)$$

where

$$Q(\lambda^2,\sigma) \equiv (\lambda^2+1)(\lambda^2+q)^2+\sigma^2(\lambda^2+\mu_1)(\lambda^2+\mu_2) \quad (7.3)$$

$$= (\lambda^2+\rho_1)(\lambda^2+\rho_2)(\lambda^2+\rho_3) \quad (7.4)$$

and $-\rho_1, -\rho_2, -\rho_3$ are the roots of the cubic equation, $Q(\lambda^2, \sigma) = 0$, with respect to λ^2. We take the three roots in turn as independent variables, then σ can be expressed as

$$\sigma^2 = \frac{(\rho_\nu-q)^2(\rho_\nu-1)}{(\rho_\nu-\mu_1)(\rho_\nu-\mu_2)};$$

$$\sigma = |\rho_\nu - q|\sqrt{\frac{\rho_\nu-1}{(\rho_\nu-\mu_1)(\rho_\nu-\mu_2)}} \geqslant 0 \quad (7.5)$$

Since $\sigma(\geqslant 0)$ is a one-valued function of each ρ_ν, each ρ_ν must be a monotonic function of $\sigma(\geqslant 0)$, and their ranges of variation can be found from the set of inequalities (see Fig. 1)

$$0 < \mu_1 \leqslant \rho_1 \leqslant q \leqslant \rho_2 \leqslant \mu_2 < 1 \leqslant \rho_3 \leqslant \infty \quad (7.6)$$

Here we have adopted the convention $\mu_2 > \mu_1$; *i.e.*, the absolute value of the valence of type-1 ions is less than that of type-2 ions. After substituting (7.4) into (7.1) and (7.2), we expand the integrands into partial fractions, thus

$$A(a) = \frac{2}{\pi a^3}\int_{\sigma=0}^{a}\sigma^2 d\sigma\int_{\lambda=0}^{\infty}d\lambda \times\sum_{\nu=1}^{3}\frac{\rho_\nu(\rho_\nu-q)}{Q'(-\rho_\nu)(\lambda^2+\rho_\nu)} \quad (7.7)$$

$$B_j(a) = \frac{2}{(1-\mu_j)\pi a}\int_{\sigma=0}^{a}\left(1-\frac{\sigma^2}{a^2}\right)d\sigma\int_{\lambda=0}^{\infty}d\lambda \times\sum_{\nu=1}^{3}\frac{(\rho_\nu-q)^2-\sigma^2(\rho_\nu-1+\mu_j)\mu_j}{Q'(-\rho_\nu)(\lambda^2+\rho_\nu)} \quad (7.8)$$

where

$$Q'(-\rho_\nu) = \left(\frac{\partial Q}{\partial(\lambda^2)}\right)_\sigma\Big|_{\lambda^2=-\rho_\nu}$$

We integrate (7.7) and (7.8) over λ to obtain

$$A(a) = \frac{1}{a^3}\sum_{\nu=1}^{3}\int_{\sigma=0}^{a}\sigma^2\frac{(\rho_\nu-q)\sqrt{\rho_\nu}}{Q'(-\rho_\nu)}d\sigma \quad (7.9)$$

$$B_j(a) = \frac{1}{a}\sum_{\nu=1}^{3}\int_{\sigma=0}^{a}\left(1-\frac{\sigma^2}{a^2}\right)\frac{(\rho_\nu-q)^2\sqrt{\rho_\nu}}{(\rho_\nu-\mu_j)Q'(-\rho_\nu)}d\sigma \quad (7.10)$$

where we have substituted the value (7.5) for σ^2 in the second factor of the integrand (7.10). Since in eq. 7.5 σ is an explicit function of each ρ_ν, we shall transform the integration variable σ to ρ_ν. Differentiating $Q(-\rho_\nu, \sigma) = 0$, we obtain

$$\frac{d\sigma}{Q'(-\rho_\nu)} = \frac{d\rho_\nu}{(\partial Q/\partial\sigma)} = \frac{d\rho_\nu}{2\sigma(\rho_\nu-\mu_1)(\rho_\nu-\mu_2)}$$

Substituting this and (7.5) into the integral (7.9), we get

$$A(a) = \frac{1}{2a^3}\sum_{n=1}^{2}\int_{\rho'_n}^{\rho''_n}\frac{(\rho-q)^2}{(\rho-\mu_1)(\rho-\mu_2)}\times\sqrt{\frac{\rho(\rho-1)}{(\rho-\mu_1)(\rho-\mu_2)}}d\rho \quad (7.11)$$

where $\rho'_1 = \tau_1$, $\rho''_1 = \tau_2$, $\rho'_2 = 1$, $\rho''_2 = \tau_3$, and τ_1, τ_2, τ_3 are the roots of the cubic equation

$$(\tau-1)(\tau-q)^2 - a^2(\tau-\mu_1)(\tau-\mu_2) = 0 \quad (7.12)$$

and satisfy the set of inequalities (see Fig. 1)

$$0 < \mu_1 \leqslant \tau_1 \leqslant q \leqslant \tau_2 \leqslant \mu_2 < 1 \leqslant \tau_3 \leqslant \infty \quad (7.13)$$

In the same way, we obtain for the integral, $B_j(a)$, of the hydrodynamic effect

$$B_j(a) = H_j(a) - D_j(a) \quad (7.14)$$

where

$$H_j(a) = \frac{1}{2a}\sum_{n=1}^{1}\int_{\rho'_n}^{\rho''_n}\frac{\rho(\rho-q)}{(\rho-\mu_j)(\rho-\mu_1)(\rho-\mu_2)}\times\sqrt{\frac{(\rho-\mu_1)(\rho-\mu_2)}{\rho(\rho-1)}}d\rho \quad (7.15)$$

$$D_j(a) = \frac{1}{2a^3}\sum_{n=1}^{2}\int_{\rho'_n}^{\rho''_n}\frac{(\rho-q)^3}{(\rho-\mu_j)(\rho-\mu_1)(\rho-\mu_2)}\times\sqrt{\frac{\rho(\rho-1)}{(\rho-\mu_1)(\rho-\mu_2)}}d\rho \quad (7.16)$$

These integrals (7.11), (7.15) and (7.16) belong to the class of elliptic integrals[10]; in fact, they can be reduced to elliptic integrals of the first and second kinds. We introduce the substitution

$$\rho = \frac{1}{2}(1+ks);\ k = \mu_2-\mu_1 = \frac{|z_2|-|z_1|}{|z_2|+|z_1|} > 0 \quad (7.17)$$

(10) E. T. Whittaker and G. N. Watson, "A Course of Modern Analysis," 4th Ed., Cambridge Univ. Press, 1953, pp. 491–521.

then we obtain

$$\left.\begin{aligned}(\rho - 1) &= -\frac{1}{2}(1 - ks),\\ (\rho - q) &= \frac{1}{2}k(s - m)\\ (\rho - \mu_1) &= \frac{1}{2}k(1 + s),\\ (\rho - \mu_2) &= -\frac{1}{2}k(1 - s)\end{aligned}\right\} \quad (7.18)$$

where

$$m = \frac{\omega_2 - \omega_1}{\omega_2 + \omega_1} = \omega_{21} - \omega_{12} \quad (7.19)$$

Accordingly, the integral (7.11) takes the form

$$A(k, m, a) = -\frac{1}{4a^3}\sum_{n=1}^{2}\int_{s'_n}^{s''_n}\frac{(s - m)^2}{(1 - s^2)} \times \sqrt{\frac{1 - k^2s^2}{1 - s^2}}\,ds \quad (7.20)$$

where we have designated the dependence of the integral on k and m as well as a. The limits of the integration are $s'_1 = s_1$, $s''_1 = s_2$, $s'_2 = 1/k$, $s''_2 = s_3$ where s_1, s_2, s_3 are the roots of the cubic equation

$$(1 - ks)(s - m)^2 - 2a^2(1 - s^2) = 0 \quad (7.21)$$

and satisfy the set of inequalities (see Fig. 2)

$$-1 \leq s_1 \leq m \leq s_2 \leq 1 < 1/k < s_3 \leq \infty \quad (7.22)$$

The same transformation (7.17) applied to the integrals (7.15) and (7.16) yields for $j = 1$

$$H_1(k, m, a) = -\frac{1}{2a}\sum_{n=1}^{2}\int_{s'_n}^{s''_n}\frac{(1 + ks)(s - m)}{(1 + s)(1 - s^2)} \times \sqrt{\frac{1 - s^2}{1 - k^2s^2}}\,ds \quad (7.23)$$

$$D_1(k, m, a) = -\frac{1}{2a^3}\sum_{n=1}^{2}\int_{s'_n}^{s''_n}\frac{(s - m)^3}{(1 + s)(1 - s^2)} \times \sqrt{\frac{1 - k^2s^2}{1 - s^2}}\,ds \quad (7.24)$$

In view of the original expression (7.2) of $B_j(a)$ $(= H_j(a) - D_j(a))$, $B_1(a)$ and $B_2(a)$ must satisfy the relation

$$B_2(k, m, a) = B_1(-k, -m, a) \quad (7.25)$$

Therefore, once we evaluate B_1 as a function of k, m and a we can evaluate B_2 too.

We shall give here only the results of computations for $A(k, m, a)$ and $B_j(k, m, a)$ $(= H_j(k, m, a) - D_j(k, m, a))$ (the derivation will be seen in the Appendix 1)

$$4a^3A(k, m, a) = -(1 + m^2)I + (2 + m^2)J - 2mkL + \sum_{\nu=1}^{3}(2m - (1 + m^2)s_\nu)r_\nu \quad (7.26)$$

$$\left.\begin{aligned}2aH_1(k, m, a) &= mI - \frac{1 + m}{1 + k}J + L - \frac{1 + m}{1 + k}\sum_{\nu=1}^{3}(1 - s_\nu)r_\nu\\ 4a^3D_1(k, m, a) &= -M_3I + (1 + M_3 - M_1)J - M_2kL + \sum_{\nu=1}^{3}\left\{(M_2 - M_1) - (M_3 - M_1)s_\nu - M_1(k'/k)^2\frac{1}{1 + s_\nu}\right\}r_\nu\end{aligned}\right\} \quad (7.27)$$

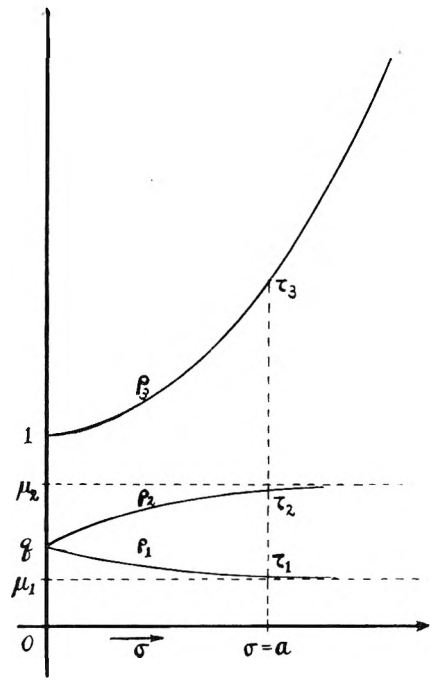

Fig. 1.—The roots ρ_1, ρ_2, ρ_3 *versus* σ.

$$\left.\begin{aligned}2aH_2(k, m, a) &= -mI - \frac{1 - m}{1 - k}J + L + \frac{1 - m}{1 - k}\sum_{\nu=1}^{3}(1 + s_\nu)r_\nu\\ 4a^3D_2(k, m, a) &= -\bar{M}_3I + (1 + \bar{M}_3 - \bar{M}_1)J + \bar{M}_2kL - \sum_{\nu=1}^{3}\left\{(\bar{M}_2 - \bar{M}_1) + (\bar{M}_3 - \bar{M}_1)s_\nu - \bar{M}_1(k'/k)^2\frac{1}{1 - s_\nu}\right\}r_\nu\end{aligned}\right\} \quad (7.28)$$

where

$$k' = \sqrt{1 - k^2},\ r_\nu = a\sqrt{2(1 + ks_\nu)}/(s_\nu - m) \quad (7.29)$$

$$\left.\begin{aligned}M_1 &= \tfrac{1}{3}(k/k')^2(1 + m)^3,\ M_2 = 1 + 3m\\ M_3 &= 2 + 3m + 3m^2 - \tfrac{2}{3}(1 + m)^3\end{aligned}\right\} \quad (7.30)$$

$$\left.\begin{aligned}\bar{M}_1 &= \tfrac{1}{3}(k/k')^2(1 - m)^3,\ \bar{M}_2 = 1 - 3m\\ \bar{M}_3 &= 2 - 3m + 3m^2 - \tfrac{2}{3}(1 - m)^3\end{aligned}\right\} \quad (7.31)$$

$$I = F(k, \phi_2) - F(k, \phi_1) + F(k, \phi_0) - K(k) \quad (7.32)$$

$$J = E(k, \phi_2) - E(k, \phi_1) + E(k, \phi_0) - E(k) + (s_3 - s_3^{-1})r_3 \quad (7.33)$$

$$L = \frac{1}{2}\log\prod_{\nu=1}^{3}\frac{(k + r_\nu)}{(k - r_\nu)} \quad (7.34)$$

and

$$\sin\phi_1 = s_1,\ \sin\phi_2 = \phi_2,\ \sin\phi_0 = 1/(ks_3) \quad (7.35)$$

The functions $F(k, \phi_\nu)$ and $E(k, \phi_\nu)$ are incomplete elliptic integrals of the first and second kind, respectively. Tables of these integrals by intervals of 5° in the "modular angle," $\alpha = \sin^{-1}k$, and of 1° in the "amplitude" ϕ are available.[11] The notation

(11) E. Jahnke and F. Emde, "Tables of Functions," 4th Ed., Dover Publications, New York, N. Y., 1945, pp. 53–97.

$$F(k,\phi)=\int_0^{\phi}\frac{d\psi}{\sqrt{1-k^2\sin^2\psi}},\quad K(k)=F\left(k,\frac{\pi}{2}\right)$$

$$E(k,\phi)=\int_0^{\varphi}\sqrt{1-k^2\sin^2\psi}\,d\psi,\quad E(k)=E\left(k,\frac{\pi}{2}\right)$$

is standard, although $F(\sin\alpha,\phi)$ is often written simply $F(\alpha,\phi)$, etc. When ϕ is negative, we have

$$F(k,-\phi)=-F(k,\phi),\ E(k,-\phi)=-E(k,\phi)$$

The ordinary types of simple electrolytes are NaCl-type ($k=0$), $BaCl_2$-type ($k=1/3$), $LaCl_3$-type ($k=1/2$), $K_4[FeCN_6]$-type ($k=3/5$) and $Al_2(SO_4)_3$-type ($k=1/5$). For the case of $k=0$, the results are elementary. When $k=1/2$, the modular angle $\alpha=\sin^{-1}1/2$ equals 30°, so that the elliptic integrals can be evaluated easily by the table of Jahnke and Emde[11] with interpolations for the amplitude ϕ. For the case of $k=1/3$, we can attain similar advantage with the aid of a Landen's transformation,[10,11] which generally relates elliptic functions of modulus k to those of modulus

$$k_1=\frac{2\sqrt{k}}{1+k} \tag{7.36}$$

because when $k=1/3$, $k_1=\sin 60°$. The elliptic integrals transform as follows (see Appendix 2)

$$\left.\begin{aligned} I&=\frac{1}{1+k}\{F(k,\phi^1_2)-F(k_1,\phi^1_1)+F(k_1,\phi^1_3)-K(k_1)\}\\ J&=\frac{1+k}{2}\{E(k,\phi^1_2)-E(k_1,\phi^1_1)+E(k_1,\phi^1_3)-E(k_1)\}+\frac{k'^2}{2}I-\sum_{\nu=1}^{3}(\sin\phi^1_\nu-s_\nu)r_\nu \end{aligned}\right\} \tag{7.37}$$

where the amplitudes ϕ^1_ν are given by

$$\sin\phi^1_\nu=\frac{(1+k)s_\nu}{1+ks_\nu^2},\quad -\frac{\pi}{2}\leqslant\phi^1_\nu\leqslant\frac{\pi}{2};(\nu=1,2,3) \tag{7.38}$$

It may not be difficult to solve the cubic equation 7.21 over the entire range of the value of a^2; but it is easier to use one of the roots, s_i, as the independent variable instead of a^2. We write the cubic equation in the form

$$ks^3-(1+2km+2a^2)s^2+(2m+km^2)s+(2a^2-m^2)=0 \tag{7.39}$$

The relation between the roots and the coefficients of the equation gives the equations

$$\left.\begin{aligned} \sum_{\nu\neq i}s_\nu&=k^{-1}(1+2km+2a^2)-s_i\\ \prod_{\nu\neq i}s_\nu&=-(2a^2-m^2)/ks_i \end{aligned}\right\} \tag{7.40}$$

If we eliminate a^2 in these equations by the cubic equation 7.21, we obtain

$$\left.\begin{aligned} \sum_{\nu\neq i}s_\nu&=\frac{(k^{-1}+1)(1+m)^2}{2(s_i+1)}-\frac{(k^{-1}-1)(1-m)^2}{2(s_i-1)}\equiv 2B_i\\ \prod_{\nu\neq i}s_\nu&=\frac{(k^{-1}+1)(1+m)^2}{2(s_i+1)}+\frac{(k^{-1}-1)(1-m)^2}{2(s_i-1)}-1\equiv C_i \end{aligned}\right\} \tag{7.41}$$

Accordingly, the other two roots $s_\nu(\nu\neq i)$ can be expressed in terms of s_i as

$$B_i+\sqrt{B_i^2-C_i},\ C_i/(B_i+\sqrt{B_i^2-C_i})$$

The field parameter a^2 may be obtained most easily by the following equation derived from the second equation of (7.40)

$$2a^2=m^2-ks_iC_i$$

In actual computations, we can choose s_i in such a way that the amplitude ϕ_i (ϕ_0 for $i=3$) or ϕ^1_i is a round number for rapid use of a table of the elliptic integrals. Since the functions $A(a)$ and $B_j(a)$ are monotonic decreasing functions of a^2 which do not have any inflection points, it is most convenient to plot the functions against a^2 in the interpolations.

8. The Conductance

To begin with, we shall compute the velocity of an ion in a simple electrolytic solution. In the limit of very low concentrations, only the friction of the solvent need be considered, so that the velocity v_j of a j-ion is given by

$$v_j=\omega_je_jX \tag{8.1}$$

In the case of finite concentrations, however, two further effects must be considered, namely, the additional field ΔX_j due to the asymmetric atmosphere and the electrophoretic velocity Δv_j due to the hydrodynamic motion of the medium surrounding a j-ion. Therefore, we have

$$v_j=\omega_je_jX+\omega_je_j\Delta X_j+\Delta v_j \tag{8.2}$$

For a simple electrolyte we have shown in Sec. 4 that $\Delta X_1=\Delta X_2=\Delta X$. Accordingly, the electric current density i is given by

$$i=\sum_{j=1}^{2}n_je_jv_j=X\lambda^\circ\left(1+\frac{\Delta X}{X}+\sum_{j=1}^{2}\frac{\mu_j\Delta v_j}{e_j\bar{\omega}X}\right) \tag{8.3}$$

where λ^0 is the limiting specific conductance and $\bar{\omega}$ is a mean absolute mobility

$$\lambda^\circ=n_1e_1^2\omega_1+n_2e_2^2\omega_2,\ \bar{\omega}=\mu_1\omega_1+\mu_2\omega_2 \tag{8.4}$$

Substituting eq. 4.1 and 5.8 into eq. 8.3, we have the following equation for the specific conductance λ

$$\frac{\lambda^\circ-\lambda}{\kappa\lambda^\circ}=\frac{q|e_1|\ |e_2|}{DkT}A(k,m,a)+\frac{\mu_1\mu_2}{4\pi\eta_0\bar{\omega}}[B_1(k,m,a)+B_2(k,m,a)] \tag{8.5}$$

where $A(k,m,a)$ and $B_j(k,m,a)$ may be computed from eq. 7.26–7.28, but more convenient forms for computation of these functions will be given in the following section.

The equivalent conductance Λ_j for j-ions equals $\mathbf{F}|v_j|/\mathbf{c}^2\times10^{-9}|X|$ (abs. ohm.$^{-1}$ cm.^{2} mole^{-1}) where $\mathbf{F}$ is the Faraday constant (e.s.u.) and $\mathbf{c}$ is the velocity of light in cm./sec. Therefore, from eq. 8.2 we have for Λ_j

$$\Lambda_j=\Lambda^\circ_j-\Lambda^\circ_j\frac{\kappa q|e_1e_2|}{DkT}A(k,m,a)-\frac{\mathbf{F}\kappa|e_1e_2|}{4\pi\mathbf{c}^2\times10^{-9}\eta_0(|e_1|+|e_2|)}B_j(k,m,a) \tag{8.6}$$

where Λ°_j is the limiting equivalent conductance

$$\Lambda^\circ_j=\mathbf{c}^{-2}\times10^9\,\mathbf{F}|e_j|\omega_j(\text{ohm.}^{-1}.\ \text{cm.}^{-2}\ \text{mole}^{-1})$$

Substituting the definition of $\kappa(=\sqrt{4\pi(n_1e_1^2+$

$\overline{n_2e_2^2)/DkT}$ into eq. 8.6, we obtain

$$\Lambda_j = \Lambda^\circ_j - \Lambda^\circ_j \frac{\pi F^3}{5RN_A\sqrt{10\pi R}} \frac{|z_1z_2|q}{(DT)^{3/2}} A(k, m, a)\Gamma^{1/2} - \frac{F^3}{2c^2 \times 10^{-3}N_A\sqrt{10\pi R}} \frac{|z_1z_2|}{(|z_1| + |z_2|)\eta_0(DT)^{1/2}} B_j(k, m, a)\Gamma^{1/2} \quad (8.7)$$

where N_A is the Avogadro number, R the molar gas constant (c.g.s.), D the dielectric constant, T the absolute temperature, η_0 the viscosity coefficient, z_i the ionic valence of i-th ions, and Γ is the ionic strength of the solution defined in terms of the molar concentration, m_i (moles/1000 cm.^{3}), as

$$\Gamma = m_1z_1^2 + m_2z_2^2 \quad (8.8)$$

The Final Results in Practical Units

The parameters k, m and q are dimension-less ratios which do not depend upon the units used. For convenience we restate their definitions, eq. 7.17, 7.19 and 3.15, in terms of the valences and the limiting equivalent conductances

$$k = \frac{|z_2| - |z_1|}{|z_2| + |z_1|} \geqslant 0, \quad m = \frac{|z_1|\Lambda_2^\circ - |z_2|\Lambda^\circ_1}{|z_1|\Lambda^\circ_2 + |z_2|\Lambda^\circ_1}$$

$$q = \frac{1}{2}(1 + km) = \frac{|z_1z_2|}{(|z_1| + |z_2|)} \frac{\Lambda^\circ_2 + \Lambda^\circ_1}{(|z_1|\Lambda^\circ_2 + |z_2|\Lambda^\circ_1)} \quad (8.9)$$

Substituting the recent values[12] for the universal constants the field parameter a becomes (see eq. 3.15 and 2.15)

$$a = \frac{|X|\epsilon}{\kappa kT} q(|z_1| + |z_2|) = 3.2633 \times 10^{-6} \times (|z_1| + |z_2|) q \sqrt{\frac{D}{T}} \frac{V}{\sqrt{\Gamma}} \quad (8.10)$$

where V is the applied field strength expressed in volt/cm., and the final expression (8.7) for the conductance takes the form

$$\Lambda_j = \Lambda^\circ_j - 5.9420 \times 10^6 \frac{|z_1z_2|}{(DT)^{3/2}} A(k, m, a)\Lambda^\circ_j\Gamma^{1/2} - \frac{43.744\,|z_1z_2|}{(|z_1| + |z_2|)\eta_0(DT)^{1/2}} B_j(k, m, a)\Gamma^{1/2} \quad (8.11)$$

The analytical expressions for the functions $A(k, m, a)$ and $B_j(k, m, a)$ $(= H_j(k, m, a) - D_j(k, m, a))$ are given by equations 7.26–7.28. Alternative forms for evaluation by descending power series (for high field intensities) or numerical quadrature (best for low field intensities) will be given by eq. 9.32–9.34 and eq. 9.2–9.4, respectively, in the following section. The descending power series specialized to the ordinary types of simple electrolytes are given in Table I in the appendix.

When $a << 1$, we have from eq. 4.3 and 5.9

$$A(k, m, a) = \frac{1}{3(1 + \sqrt{q})} + O(a^2)$$

$$B_j(k, m, a) = \frac{2}{3(1 - \mu_j)} + O(a^2)$$

Substituting these into (8.11), we obtained

$$\Lambda_j = \Lambda^\circ_j - 1.9807 \times 10^6 \frac{|z_1z_2|}{(DT)^{3/2}} \frac{q}{(1 + \sqrt{q})} \Lambda^\circ_j\Gamma^{1/2} - \frac{29.162\,|z_j|}{\eta_0(DT)^{1/2}} \Gamma^{1/2} + O(a)^2 \quad (8.12)$$

which is the result first obtained by Onsager.[9]

(12) F. D. Rossini, F. T. Gucker, Jr., H. L. Johnston, L. Pauling and G. W. Vinal, *J. Am. Chem. Soc.*, 74, 2699 (1952).

When $a \simeq \infty$, we shall show in the following section that

$$A(k, m, a) = O(a^{-1})$$

$$B_j(k, m, a) = \frac{2\sqrt{\mu_j}}{3(1 - \mu_j)} + a^{-1}\log a + O(a^{-1})$$

Therefore, we obtain the limiting estimate for strong fields

$$\Lambda_j = \Lambda^\circ_j - \frac{29.162}{\eta_0(DT)^{1/2}} |z_j|\sqrt{\mu_j}\,\Gamma^{1/2} + O(a^{-1}\log a) \quad (8.13)$$

9. Convenient Forms for Computations of $A(k, m, a)$ and $B_j(k, m, a)$

Since the analytical expressions for $A(a)$ and $B_j(a)$ contain elliptic integrals of the first and second kind, and the limits of these integrals are determined implicitly by a cubic equation, the numerical quadrature seems simpler for weak fields. We put in the integrals (7.1) and (7.2)

$$\lambda = \sqrt{\gamma}\tan\theta \quad (9.1)$$

where γ is an adjustable constant. Then we easily obtain

$$A(a) = \frac{2\gamma^{3/2}}{\pi a^3} \int_{\sigma=0}^{a} \sigma^2 d\sigma \int_{\theta=0}^{\frac{\pi}{2}} \frac{1}{1 + \sigma^2R^2} \times \frac{\tan^2\theta(\tan^2\theta + 1)}{(\gamma\tan^2\theta + q)(\gamma\tan^2\theta + 1)} d\theta \quad (9.2)$$

$$B_j(a) = \frac{2\sqrt{\mu_j}}{3(1 - \mu_j)} + \frac{2\gamma^{3/2}}{\pi a} \int_{\sigma=0}^{a} \left(1 - \frac{\sigma^2}{a^2}\right) d\sigma \int_{\theta=0}^{\frac{\pi}{2}} \frac{1}{1 + \sigma^2R^2} \times \frac{\tan^2\theta(\tan^2\theta + 1)}{(\gamma\tan^2\theta + \mu_j)(\gamma\tan^2\theta + 1)} d\theta \quad (9.3)$$

where

$$R^2 = \frac{(\gamma\tan^2\theta + \mu_1)(\gamma\tan^2\theta + \mu_2)}{(\gamma\tan^2\theta + q)^2(\gamma\tan^2\theta + 1)}$$

If we integrate over σ, these double integrals can be reduced easily to simple integrals; but the resulting integrands involve $\tan^{-1}(aR)$ which must be obtained from tables—a laborious operation. Accordingly, this short cut is not effective unless the results are wanted only for a few isolated values of the field intensity (a). For the systematic construction of a table we recommend numerical quadrature over θ in (9.2) and (9.3) by the trapezoid rule (because the integrands are periodic and analytic) followed by step-by-step quadrature over σ with end corrections. In order to evaluate the specific conductance, we need $B_1(a) + B_2(a)$

$$\mu_1\mu_2(B_1(a) + B_2(a)) = \frac{2}{3}(\mu_1^{3/2} + \mu_2^{3/2}) + \frac{2\mu_1\mu_2\gamma^{3/2}}{\pi a} \int_{\sigma=0}^{a} \left(1 - \frac{\sigma^2}{a^2}\right) G(\sigma) d\sigma \quad (9.4)$$

where

$$G(\sigma) = \int_{\theta=0}^{\frac{\pi}{2}} \frac{\tan^2\theta(\tan^2\theta + 1)(2\gamma\tan^2\theta + 1)}{(\gamma\tan^2\theta + \mu_1)(\gamma\tan^2\theta + \mu_2)(\gamma\tan^2\theta + 1)} \times \frac{1}{1 + \sigma^2R^2} d\theta$$

The numerical quadrature is not convenient for strong fields. For this case, we shall presently derive convenient series in descending powers of

field strengths. It is awkward to compute a sufficient number of terms from the final analytical formulas for $A(a)$ and $B_j(a)$, because they contain many terms which must be expanded separately. Fortunately, their integral expressions (7.9) and (7.10) are fairly simple. We shall first expand the integrands and integrate to obtain the final results. Since the series obtained from the integrands do not converge over the entire range of the integration, we have to consider the integrals in indefinite forms. The integration constants will be evaluated by another procedure from the analytical formulas of $A(a)$ and $B_j(a)$. For the time being, we shall consider only $A(a)$ and $B_1(a)$, because $B_2(a)$ can be evaluated easily from the final result of $B_1(a)$ by the transformation (7.25).

We shall start from the following indefinite integrals derived from eq. 7.9 and 7.10

$$A(a) = a^{-3}\sum_{\nu=1}^{3}\int^{a}\sigma^2\frac{(\rho_\nu - q)\sqrt{\rho_\nu}}{Q'(-\rho_\nu)}\,d\sigma \quad (9.5)$$

$$B_1(a) = a^{-1}\sum_{\nu=1}^{3}\int^{a}\left(1-\frac{\sigma^2}{a^2}\right)\frac{(\rho_\nu - q)^2\sqrt{\rho_\nu}}{(\rho_\nu-\mu_1)Q'(-\rho_\nu)}\,d\sigma \quad (9.6)$$

where ρ_1, ρ_2, ρ_3 are the roots of the cubic equation 7.5 and satisfy the set of inequality (7.6). In the following computation, we need to know the explicit form of $Q'(-\rho)$

$$Q'(-\rho) = \frac{(\rho - q)}{(\rho-\mu_1)(\rho-\mu_2)}[2(\rho-\mu_1)(\rho-\mu_2)(\rho-1) + (\rho-\mu_1)(\rho-\mu_2)(\rho-q) - (2\rho-1)(\rho-1)(\rho-q)] \quad (9.7)$$

Now we introduce the substitution (7.17), then the cubic equation 7.5 takes the form

$$t = \frac{1}{2\sigma^2} = \frac{(s^2-1)}{(ks-1)(s-m)^2} \quad (9.8)$$

where we have introduced a new parameter t, because we are interested in the large values of σ. When $\sigma \to \infty$; $t \to 0$, the three roots s_1, s_2 and s_3 of eq. 9.8 tend to -1. 1 and ∞, respectively. We put

$$s_0 = \frac{1}{ks_3} \quad (9.9)$$

then s_0 is a root, which tends to zero as $t \to 0$, of the equation

$$t = \frac{s_0(1-k^2s_0^2)}{(1-s_0)(1-kms_0)^2} \quad (9.10)$$

In terms of s_1, s_2 and s_0, the integrals (9.5) and (9.6) take the forms

$$A(a) = \sum_{\nu=1}^{2} a^{-3}\int^{a}\sigma^2\psi_A(s_\nu)d\sigma + a^{-3}\int^{a}\sigma\psi_A(s_0)d\sigma \quad (9.11)$$

$$B_1(a) = \sum_{\nu=1}^{2} a^{-1}\int^{a}\left(1-\frac{\sigma^2}{a^2}\right)\bar{\psi}_B(s_\nu)\,d\sigma + 2a^{-1}\int^{a}\left(1-\frac{\sigma^2}{a^2}\right)\sigma\bar{\psi}_B(s_0)d\sigma \quad (9.12)$$

where

$$\psi_A(s) = \sqrt{2}(s^2-1)\sqrt{1+ks}\,p^{-1}(s) \quad (9.13)$$

$$\psi_B(s) = \sqrt{2}(s-1)(s-m)\sqrt{1+ks}\,p^{-1}(s) \quad (9.14)$$

$$p(s) = 2(s^2-1)(ks-1) + k(s^2-1)(s-m) - 2s(ks-1)(s-m) \quad (9.15)$$

and

$$\bar{\psi}_A(s_0) = \sigma\psi_A(s_3) = (1-kms_0)(1-s_0^2)^{1/2} \times (1-k^2s_0^2)^{1/2}P^{-1}(s_0) \quad (9.16)$$

$$\bar{\psi}_B(s_0) = (2\sigma)^{-1}\psi_B(s_3) = s_0(1-s_0)^{-1/2}(1+s_0)^{1/2} \times (1-ks_0)(1-k^2s_0^2)^{1/2}P^{-1}(s_0) \quad (9.17)$$

$$P(s_0) = k^{-1}s_3^{-3}p(s_3) = 1 + kms_0 - (2m+3k)ks_0^2 + (2+km)k^2s_0^3 \quad (9.18)$$

In order to eliminate the branch point of $\psi(s_3)$ at $s_0 = 0$, we have introduced here $\bar{\psi}(s_0)$ different from $\psi(s_3)$ by a factor σ or $(2\sigma)^{-1}$. Now we shall discuss the analytic properties of these functions, in order to expand them into power series of t. It is clearly seen that the functions $\psi_A(s_\nu)$, $\psi_B(s_\nu)$ ($\nu = 1,2$) and $\bar{\psi}_A(s_0)$, $\bar{\psi}_B(s_0)$ are analytic with respect to s_ν and s_0 in the vicinity of $s_1 = -1$, $s_2 = 1$, and $s_0 = 0$, because the following derivatives are not zero in the same region

$$\frac{\partial t}{\partial s_\nu} = \frac{p(s_\nu)}{(ks_\nu-1)^2(s_\nu-m)^3}, \quad (\nu = 1,2) \quad (9.19)$$

$$\frac{\partial t}{\partial s_0} = \frac{-P(s_0)}{(1-s_0)^2(1-kms_0)^3} \quad (9.20)$$

Accordingly, $\psi_A(s_\nu)$, $\psi_B(s_\nu)$ and $\bar{\psi}_A(s_0)$, $\bar{\psi}_B(s_0)$ are analytic with respect to t in the vicinity of $t = 0$, so that they can be expanded into power series of t. The radius of convergence of the series is determined simply by the singularities of the functions, because $p(s_\nu)$ and $P(s_0)$ are included in the numerators in (9.19) and (9.20) as well as in the denominators of the functions. More explicitly, the radius of convergence is given by the smallest absolute value of $t(s)$ when s is a root of the equation

$$(1-k^2s^2)(1-s^2)p(s) = 0 \quad (9.21)$$

Here we have used the definition of s_0 and the relation between $p(s_3)$ and $P(s_0)$ in eq. 9.18. For the case where $ks = -1$, we obtain

$$|t| = \frac{1-k^2}{2(1+km)^2} \geq \frac{1-k}{2(1+k)} \quad (9.22)$$

because $-1 \leqslant m \leqslant 1$. For $ks = 1$, we have $t = \infty$ which is harmless. The uniformizing substitution $t = 1/2\sigma^2$ takes care of the branch-points at $s^2 = 1$; $t = 0$, so that the two-valued functions of t become one-valued functions of σ. In the appendix we show that the roots of the cubic equation, $p(s) = 0$, are located in a domain where the following inequality holds

$$|t| \geq \frac{1}{8} \quad (9.23)$$

which does not depend upon k or m. Since eq. 9.22 coincides with eq. 9.23 when $k = 3/5$, we obtain the final conclusion that the power series of t for the functions converges uniformly with respect to m in the following domain

$$\left.\begin{aligned} |t| &\leq \frac{1}{8} \quad \text{for } k \leq \frac{3}{5} \\ |t| &< \frac{1-k}{2(1+k)} \quad \text{for } k > \frac{3}{5} \end{aligned}\right\} \quad (9.24a)$$

In terms of σ, this condition becomes

$$\left.\begin{aligned} &\sigma \geq 2 \qquad \text{for } k \leq \frac{3}{5} \\ &\sigma > \sqrt{\frac{1+k}{1-k}} \quad \text{for } k > \frac{3}{5} \end{aligned}\right\} \tag{9.24b}$$

Now it is most convenient to use Lagrange's theorem,[13] in order to obtain the series. We shall first consider $\psi_A(s_1)$ defined by eq. 9.13. The cubic equation 9.8 can be written as

$$s_1 = -1 + t\phi(s_1);\ \phi(s_1) = \frac{(ks_1 - 1)(s_1 - m)^2}{s_1 - 1} \tag{9.25}$$

Then the Lagrange theorem gives

$$\psi_A(s_1) = \psi_A(-1) + \sum_{n=1}^{\infty} \frac{t^n}{n!}\left[\frac{d^{n-1}}{ds^{n-1}}\{\psi'_A(s)\phi^n(s)\}\right]_{s=-1} \tag{9.26}$$

Since $\psi_A(s_1)$ has a factor $s_1 + 1$, we introduce a function $f(s_1)$ by

$$\psi_A(s_1) = (s_1 + 1)f(s_1) \tag{9.27}$$

then eq. 9.26 takes the form

$$\psi_A(s_1) = tf(-1)\phi(-1) + \sum_{n=1}^{\infty} \frac{t^{n+1}}{n!}\left[\frac{d^{n-1}}{ds^{n-1}}\{(f(s)\phi(s))'\phi^n(s)\}\right]_{s=-1} \tag{9.28}$$

It is a simple matter to compute these coefficients in the series. In terms of k, $k' = \sqrt{1-k^2}$, and ω_{ji} which satisfies

$$\omega_{12} \equiv \frac{\omega_1}{\omega_1 + \omega_2} = \frac{1}{2}(1 - m),\ \omega_{21} \equiv \frac{\omega_2}{\omega_2 + \omega_1} = \frac{1}{2}(1 + m)$$

The result is given as

$$\psi_A(s_1) = e_1^{(-1)}t + e_2^{(-1)}t^2 + e_3^{(-1)}t^3 + O(t^4) \tag{9.29}$$

where

$$e_1^{(-1)} = -\sqrt{2}(1-k)^{1/2}\omega_{21}$$

$$e_2^{(-1)} = \sqrt{2}(1-k)^{-1/2}\omega_{21}^2\{3k'^2 - (2 - k + k^2)\omega_{21}\}$$

$$e_3^{(-1)} = -\frac{1}{\sqrt{2}}(1-k)^{-3/2}\omega_{21}^3\{20k'^4 - 10k'^2(3 - 3k + 2k^2)\omega_{21} + (12 - 18k + 5k^2 - 3k^4)\omega_{21}^2\}$$

If we use the symmetry of the function $\psi_A(s)$ and the symmetry of the roots of the cubic eq. 9.8 given by eq. 10.13 in Appendix 1, by applying a transformation $(k, \omega_{21}) \rightarrow (-k, \omega_{12})$ to the above result, we immediately obtain for $\psi_A(s_2)$

$$\psi_A(s_2) = e_1^{(1)}t + e_2^{(1)}t^2 + e_3^{(1)}t^3 + O(t^4) \tag{9.30}$$

where

$$e_1^{(1)} = -\sqrt{2}(1+k)^{1/2}\omega_{12}$$

$$e_2^{(1)} = \sqrt{2}(1+k)^{-1/2}\omega_{12}^2\{3k'^2 - (2 + k + k^2)\omega_{12}\}$$

$$e_3^{(1)} = -\frac{1}{\sqrt{2}}(1+k)^{-3/2}\omega_{12}^3\{20k'^4 - 10k'^2(3 + 3k + 2k^2)\omega_{12} + (12 + 18k + 5k^2 - 3k^4)\omega_{12}^2\}$$

For the case of $\bar{\psi}_A(s_0)$ defined by eq. 9.16 we have to use the cubic equation written in the form (9.10) and Lagrange's original equation like eq. 9.26 because $\bar{\psi}_A(s_0)$ does not have a factor s_0. The result is

$$\bar{\psi}_A(s_0) = e_0^{(0)} + e_1^{(0)}t + e_2^{(0)}t^2 + e_3^{(0)}t^3 + O(t^4) \tag{9.31}$$

where

$$e_0^{(0)} = 1$$

$$e_1^{(0)} = -2km$$

$$e_2^{(0)} = \frac{1}{2}\{12k^2m^2 + 8km - 1 + 5k^2\}$$

$$e_3^{(0)} = -\{20k^3m^3 + 30k^2m^2 + 3km(1 + 7k^2) - 1 + 7k^2\}$$

In the same way the series of $\psi_B(s_1)$, $\psi_B(s_2)$ and $\bar{\psi}_B(s_0)$ can be computed. Since $\psi_B(s)$ does not have such symmetry as $\psi_A(s)$, each series must be computed separately. The results are

$$\psi_B(s_1) = b_0^{(-1)} + b_1^{(-1)}t + b_2^{(-1)}t^2 + b_3^{(-1)}t^3 + O(t^4) \tag{9.29'}$$

$$\psi_B(s_2) = b_1^{(1)}t + b_2^{(1)}t^2 + b_3^{(1)}t^3 + O(t^4) \tag{9.30'}$$

$$\bar{\psi}_B(s_0) = t(b_0^{(0)} + b_1^{(0)}t + b_2^{(0)}t^2 + b_3^{(0)}t^3 + O(t^4)) \tag{9.31'}$$

where the coefficients in the series for $\psi_B(s_1)$ are

$$b_0^{(-1)} = \sqrt{2}(1-k)^{1/2}(1-k)^{-1}$$

$$b_1^{(-1)} = -\sqrt{2}(1-k)^{-1/2}\omega_{21}(2(1-k) - \omega_{21})$$

$$b_2^{(-1)} = \frac{1}{\sqrt{2}}(1-k)^{-3/2}\omega_{21}^2\{12k'^2(1-k) - 8(1-k) \times (2 - k + k^2)\omega_{21} + (6 - 10k + 5k^2 - 3k^3)\omega_{21}^2\}$$

$$b_3^{(-1)} = -\frac{1}{\sqrt{2}}(1-k)^{-5/2}\omega_{21}^3\{40k'^4(1-k) - 30k'^2(1-k)(3 - 3k + 2k^2)\omega_{21} + 6(1-k)(12 - 18k + 5k^2 - 3k^4)\omega_{21}^2 - (20 - 56k + 53k^2 - 22k^3 + 9k^4)\omega_{21}^3\}$$

the coefficients in $\psi_B(s_2)$ are

$$b_1^{(1)} = -\sqrt{2}(1+k)^{1/2}\omega_{12}^2$$

$$b_2^{(1)} = \sqrt{2}(1+k)^{-1/2}\omega_{12}^3(4k'^2 - (3+k)\omega_{12})$$

$$b_3^{(1)} = -\frac{1}{\sqrt{2}}(1+k)^{-3/2}\omega_{12}^4\{30k'^4 - 12k'^2(4 + 3k + k^2)\omega_{12} + (20 + 24k - k^2 - 6k^3 - 5k^4)\omega_{12}^2\}$$

and the coefficients in $\bar{\psi}_B(s_0)$ are

$$b_0^{(0)} = 1$$

$$b_1^{(0)} = -k(3m + 1)$$

$$b_2^{(0)} = \frac{1}{2}\{20k^2m^2 + 10(1-k)km - 1 + 2k + 7k^2\}$$

$$b_3^{(0)} = -\frac{1}{2}\{70k^3m^3 + 42k^2m^2(2+k) + 7(1 + 4k + 9k^2)km + (-2 + k + 18k^2 + 9k^3)\}$$

Now, we substitute eq. 9.29–9.31 into eq. 9.11 and perform the integration using $t = (2\sigma^2)^{-1}$. If we designate the integration constant by i_A which will be derived in Appendix 3, the result is written as

$$\begin{aligned} 2\Lambda(k, m, a) &= e_0^{(0)}a^{-1} + (e_1^{(-1)} + e_1^{(1)})a^{-2} + 2i_Aa^{-3} \\ &\quad + e_1^{(0)}a^{-3}\log a - \frac{1}{2}(e_2^{(-1)} + e_2^{(1)})a^{-4} \\ &\quad - \frac{1}{4}e_2^{(0)}a^{-5} - \frac{1}{12}(e_3^{(-1)} + e_3^{(1)})a^{-6} \\ &\quad - \frac{1}{16}e_3^{(0)}a^{-7} - \cdots \\ &= \sum_{n=1}^{\infty} R_na^{-n} + R_3^*a^{-3}\log a \end{aligned} \tag{9.32}$$

where

$$R_1 = 1$$

$$R_2 = -\sqrt{2(1-k)}\omega_{21} - \sqrt{2(1+k)}\omega_{12}$$

$$R_3^* = -2km$$

$$R_3 = \frac{1}{2}\{1 - K + 2E + 2\left(2 - \log\frac{4}{k'}\right)km - (K - E)m^2\}$$

(13) E. T. Whittaker and G. N. Watson, ref. 10, p. 142.

$$R_4 = -\frac{1}{\sqrt{2}}(1-k)^{-1/2}\omega_{21}^2\{3k'^2-(2-k+k^2)\omega_{21}\}$$
$$-\frac{1}{\sqrt{2}}(1+k)^{-1/2}\omega_{12}^2\{3k'^2-(2+k+k^2)\omega_{12}\}$$

$$R_5 = -\frac{1}{8}\{12k^2m^2+8km-1+5k^2\}$$

$$R_6 = \frac{1}{12\sqrt{2}}(1-k)^{-3/2}\omega_{21}^3\{20k'^4-10k'^2(3-3k+2k^2)\omega_{21}+(12-18k+5k^2-3k^4)\omega_{21}^2\}$$
$$+\frac{1}{12\sqrt{2}}(1+k)^{-3/2}\omega_{12}^3\{20k'^4-10k'^2(3+3k+2k^2)\omega_{12}+(12+18k+5k^2-3k^4)\omega_{12}^2\}$$

$$R_7 = \frac{1}{16}\{20k^3m^3+30k^2m^2+3(1+7k^2)km-1+7k^2\}$$

etc.

In the same way, we obtain from eq. 9.12 and eq. 9.29′–9.31′ for $B_1(k, m, a)$, which contains two integration constants i_H and i_D

$$B_1(k,m,a) = \frac{2}{3}b_0^{(-1)}+b_0^{(0)}a^{-1}\log a+\frac{1}{2}(2i_H-b_0^{(0)})a^{-1}-(b_1^{(-1)}+b_1^{(1)})a^{-2}-\frac{1}{2}b_1^{(0)}a^{-3}\log a-\frac{1}{4}(4i_D+b_1^{(0)})a^{-3}+\frac{1}{6}(b_2^{(-1)}+b_2^{(1)})a^{-4}+\frac{1}{16}b_2^{(0)}a^{-5}+\frac{1}{60}(b_3^{(-1)}+b_3^{(1)})a^{-6}+\frac{1}{96}b_3^{(0)}a^{-7}+\cdots$$
$$=\sum_{n=1}^{\infty}P_{1n}a^{-n}+P^*_{11}a^{-1}\log a+P^*_{13}a^{-3}\log a \qquad (9.33)$$

where

$$P_{10} = \frac{\sqrt{8}}{3}(1-k)^{1/2}(1+k)^{-1}$$

$$P^*_{11} = 1$$

$$P_{11} = \frac{1}{2}\left\{\log\frac{4}{k'}-\frac{k}{1+k}-\frac{E}{1+k}-1+\left(K-\frac{E}{1+k}-\frac{k}{1+k}\right)m\right\}$$

$$P_{12} = \sqrt{2}(1-k)^{-1/2}\omega_{21}\{2(1-k)-\omega_{21}\}+\sqrt{2}(1+k)^{1/2}\omega_{12}^2$$

$$P_{13}^* = \frac{1}{2}k(1+3m)$$

$$P_{13} = \frac{1}{12}\left\{-3+k\left(3\log\frac{4}{k'}+\frac{k^2}{k'^2}\right)+4K-\left(7-\frac{k^2}{k'^2}\right)E\right\}$$
$$+\frac{1}{4}\left\{k\left(3\log\frac{4}{k'}+\frac{k^2}{k'^2}-2\right)+K-\left(1-\frac{k^2}{k'^2}\right)E\right\}m$$
$$+\frac{1}{4}\left\{\frac{k^3}{k'^2}+K-\left(1-\frac{k^2}{k'^2}\right)E\right\}m^2+\frac{1}{12}\left\{\frac{k^3}{k'^2}-2K+\left(2+\frac{k^2}{k'^2}\right)E\right\}m^3$$

$$P_{14} = \frac{1}{6\sqrt{2}}(1-k)^{-3/2}\omega_{21}^2\{12k'^2(1-k)-8(1-k)\times(2-k+k^2)\omega_{21}+(6-10k+5k^2-3k^4)\omega_{21}^2\}$$
$$+\frac{1}{3\sqrt{2}}(1+k)^{-1/2}\omega_{12}^3\{4k'^2-(3+k)\omega_{12}\}$$

$$P_{15} = \frac{1}{32}\{20k^2m^2+10k(1+k)m-1+2k+7k^2\}$$

$$P_{16} = -\frac{1}{60\sqrt{2}}(1-k)^{-5/2}\omega_{21}^3\{40k'^4(1-k)-30k'^2(1-k)(3-3k+2k^2)\omega_{21}+6(1-k)(12-18k+5k^2-3k^4)\omega_{21}^2-(20-56k+53k^2-22k^3+9k^4)\omega_{21}^3\}$$
$$-\frac{1}{60\sqrt{2}}(1+k)^{-3/2}\omega_{12}^4\{30k'^4-12k'^2(4+3k+k^2)\omega_{12}+(20+24k-k^2-6k^3-5k^4)\omega_{12}^2\}$$

$$P_{17} = -\frac{1}{192}\{70k^3m^3+42k^2(2+k)m^2+7k(1+4k+9k^2)m+(-2+k+18k^2+9k^3)\}$$

etc.

Now it is easy to obtain $B_2(k, m, a)$ from $B_1(k, m, a,)$ by the eq. 7.25, *i.e.*

$$B_2(k,m,a) = B_1(-k,-m,a)$$

The result is

$$B_2(k,m,a) = \sum_{n=0}^{\infty}P_{2n}a^{-n}+P^*_{21}a^{-1}\log a+P_{23}{}^*a^{-3}\log a \qquad (9.34)$$

where

$$P_{20} = \frac{\sqrt{8}}{3}(1+k)^{1/2}(1-k)^{-1}$$

$$P_{21}^* = 1$$

$$P_{21} = \frac{1}{2}\left\{\log\frac{4}{k'}+\frac{k}{1-k}-\frac{E}{1-k}-1+\left(K-\frac{E}{1-k}+\frac{k}{1-k}\right)m\right\}$$

$$P_{22} = \sqrt{2}(1+k)^{-1/2}\omega_{12}\{2(1+k)-\omega_{12}\}+\sqrt{2}(1-k)^{1/2}\omega_{21}^2$$

$$P_{23}{}^* = -\frac{1}{2}k(1-3m)$$

$$P_{23} = -\frac{1}{12}\left\{3+k\left(3\log\frac{4}{k'}+\frac{k^2}{k'^2}\right)-4K+\left(7-\frac{k^2}{k'^2}\right)E\right\}$$
$$+\frac{1}{4}\left\{k\left(3\log\frac{4}{k'}+\frac{k^2}{k'^2}-2\right)-K+\left(1-\frac{k^2}{k'^2}\right)E\right\}m$$
$$-\frac{1}{4}\left\{\frac{k^3}{k'^2}-K+\left(1-\frac{k^2}{k'^2}\right)E\right\}m^2+\frac{1}{12}\left\{\frac{k^3}{k'^2}+2K-\left(2+\frac{k^2}{k'^2}\right)E\right\}m^3$$

$$P_{24} = \frac{1}{6\sqrt{2}}(1+k)^{-3/2}\omega_{12}^2\{12k'^2(1+k)-8(1+k)(2+k+k^2)\omega_{12}+(6+10k+5k^2+3k^3)\omega_{12}^2\}$$
$$+\frac{1}{3\sqrt{2}}(1-k)^{-1/2}\omega_{21}^3\{4k'^2-(3-k)\omega_{21}\}$$

$$P_{25} = \frac{1}{32}\{20k^2m^2+10k(1-k)m-1-2k+7k^2\}$$

$$P_{26} = -\frac{1}{60\sqrt{2}}(1+k)^{-5/2}\omega_{12}^3\{40k'^4(1+k)-30k'^2(1+k)(3+3k+2k^2)\omega_{12}+6(1+k)(12+18k+5k^2-3k^4)\omega_{12}^2-(20+56k+53k^2+22k^3+9k^4)\omega_{12}^3\}$$
$$-\frac{1}{60\sqrt{2}}(1-k)^{-3/2}\omega_{21}^4\{30k'^4-12k'^2(4-3k+k^2)\omega_{21}+(20-24k-k^2+6k^3-5k^4)\omega_{21}^2\}$$

$$P_{27} = -\frac{1}{192}\{70k^3m^3 + 42k^2(2-k)m^2 + 7k(1-4k+9k^2)m - (2+k-18k^2+9k^3)\}$$

etc.

According to eq. 9.24, these series converge uniformly with respect to m in the following domain

$$\left.\begin{aligned} a &\geqslant 2 \qquad \text{for } k \leqslant \frac{3}{5} \\ a &\geqslant \sqrt{\frac{1+k}{1-k}} \quad \text{for } k \geqslant \frac{3}{5} \end{aligned}\right\} \tag{9.35}$$

because the series are power series except the first few terms which contain the logarithmic terms, and integration does not change the radius of convergence.

When $a \to \infty$, the relaxation function $A(k, m, a)$ clearly vanishes

$$A(k, m, a) = \frac{1}{2a} + O(a^{-2}) \tag{9.36}$$

while the electrophoretic functions $B_j(k, m, a)$ take the finite values

$$B_j(k, m, a) = \frac{2\sqrt{\mu_j}}{3(1-\mu_j)} + a^{-1}\log a + O(a^{-1}) \tag{9.37}$$

In Table I in the appendix, we shall give the coefficients R_i, P_{ji} specialized for ordinary types of simple electrolytes.

Acknowledgments.—One of us (S.K.K.) wishes to thank the United States Government for a Smith–Mundt Grant and Yale University for a Sheffield Scientific School Fellowship.

10. Appendix I. Reduction of the Elliptic Integrals

In order to reduce the integrals (7.20), (7.23) and (7.24) into the elliptic integrals of the first and second kinds, we introduce the following elliptic substitution

$$s = \mathrm{sn}u \tag{10.1}$$

Then the integrals become

$$\left.\begin{aligned} A(k, m, a) &= -\frac{1}{4a^3}\sum_{n=1}^{2}\int_{u'_n}^{u''_n} du \times \frac{(\mathrm{sn}u - m)^2\mathrm{dn}^2u}{\mathrm{cn}^2u} \\ H_1(k, m, a) &= -\frac{1}{2a}\sum_{n=1}^{2}\int_{u'_n}^{u''_n} du \times \frac{(1+k\mathrm{sn}u)(\mathrm{sn}u - m)}{1+\mathrm{sn}u} \\ D_1(k, m, a) &= -\frac{1}{4a^2}\sum_{n=1}^{2}\int_{u'_n}^{u''_n} du \times \frac{(\mathrm{sn}u - m)^3\mathrm{dn}^2u}{(1-\mathrm{sn}u)\,\mathrm{cn}^2u} \end{aligned}\right\} \tag{10.2}$$

The paths of integrations are shown in Fig. 3 where $\mathrm{sn}u_\nu = s_\nu(\nu = 1, 2, 3)$ are the roots of the cubic equation 7.21. Now it is easy to reduce all the integrals to elliptic integrals of the first and second kinds. Routine procedure yields the following results which are verified easily by differentiation

$$\left.\begin{aligned} 4a^3A(k, m, a) &= A^*(u_2) - A^*(u_1) + A^*(u_3) - A^*(K + iK') \\ 2aH_1(k, m, a) &= H_1^*(u_2) - H_1^*(u_1) + H_1^*(u_3) - H_1^*(K + iK') \\ 4a^3D_1(k, m, a) &= D_1^*(u_2) - D_1^*(u_1) + D_1^*(u_3) - D_1^*(K + iK') \end{aligned}\right\} \tag{10.3}$$

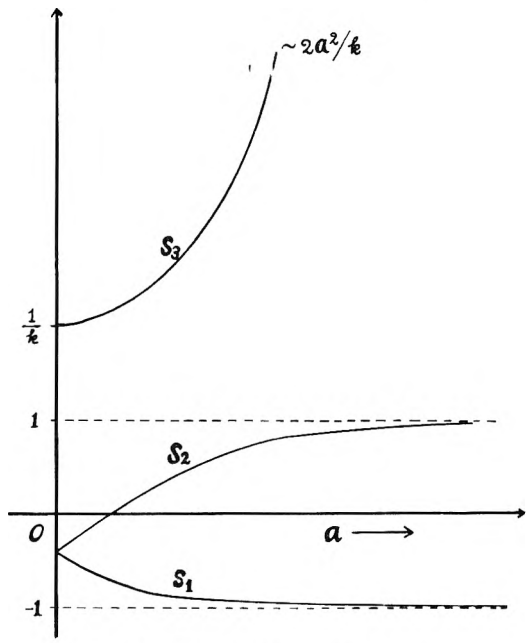

Fig. 2.—The roots s_1, s_2, s_3 *versus* a.

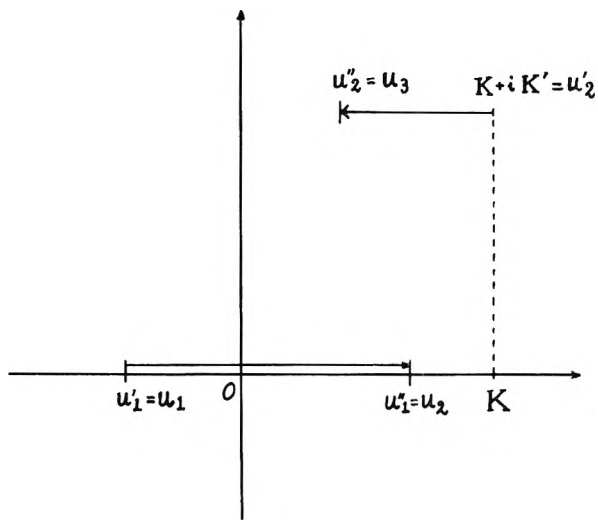

Fig. 3.—The path of the integration in u-plane for the integral (10.2).

where

$$A^*(u) = -(1+m^2)u + (2+m^2)E(u) - mk\log\left(\frac{\mathrm{dc}u + k}{\mathrm{dc}u - k}\right) + (2m - (1+m^2)\mathrm{sn}u)\mathrm{dc}u \tag{10.4}$$

$$H_1^*(u) = mu - \frac{1+m}{1+k}E(u) + \frac{1}{2}\log\left(\frac{\mathrm{dc}u + k}{\mathrm{dc}u - k}\right) - \frac{1+m}{1+k}(1 - \mathrm{sn}u)\mathrm{dc}u \tag{10.5}$$

$$D_1^*(u) = -M_3u + (1 + M_3 - M_1)E(u) - \frac{1}{2}M_2k\log\left(\frac{\mathrm{dc}u + k}{\mathrm{dc}u - k}\right) + \left\{(M_2 - M_1) - (M_3 - M_1)\mathrm{sn}u - M_1(k'/k)^2\frac{1}{1+\mathrm{sn}u}\right\}\mathrm{dc}u \tag{10.6}$$

(in Glaisher's notation: $\mathrm{dc}u = \mathrm{dn}u/\mathrm{cn}u$, etc.) and M_1, M_2, M_3 are defined by eq. 7.30.

These results can be expressed directly by the roots $s_\nu(\nu = 1, 2, 3)$ of the cubic equation 7.21. We

first observe that the cubic equation can be written as

$$\mathrm{dc}u_\nu = a\frac{\sqrt{2(1+ks_\nu)}}{|s_\nu - m|} > 0;\ (\nu = 1, 2, 3) \quad (10.7)$$

If we compare this with the definition of r_ν given by eq. 7.29 we obtain

$$r_1 = -\mathrm{dc}u_1,\ r_2 = \mathrm{dc}u_2,\ r_3 = \mathrm{dc}u_3 \quad (10.8)$$

on account of the inequalities (7.22). We shall next replace the complex variables u_3 by a real one by the transformation

$$u_3 = u_0 + iK' \quad (10.9)$$

Then we have[10]

$$\mathrm{sn}u_0 = \frac{1}{k\mathrm{sn}u_3} = \frac{1}{ks_3} \quad (10.10)$$

and

$$E(u_3) - E(K + iK') = E(u_0) - \mathrm{cn}u_3\,\mathrm{ds}u_3 - E = E(u_0) + (s_3 - s_3^{-1})r_3 - E \quad (10.11)$$

Thus, the terms of the elliptic integrals in eq. 10.3 take the forms

$$\left.\begin{aligned} I &\equiv u_2 - u_1 + u_3 - (K + iK') \\ &= \int_{s_1}^{s_2}(1-s^2)^{-1/2}(1-k^2s^2)^{-1/2}\mathrm{d}s - \int_{(ks_3)^{-1}}^{1}(1-s^2)^{-1/2}(1-k^2s^2)^{-1/2}\,\mathrm{d}s \\ J &\equiv E(u_2) - E(u_1) + E(u_3) - E(K+iK') \\ &= \int_{s_1}^{s_2}(1-s^2)^{-1/2}(1-k^2s^2)^{1/2}\mathrm{d}s - \int_{(ks_3)^{-1}}^{1}(1-s^2)^{-1/2}(1-k^2s^2)^{1/2}\mathrm{d}s + (s_3 - s_3^{-1})r_3 \end{aligned}\right\} \quad (10.12)$$

According to the definitions of the amplitudes given by eq. 7.35, these formulas for I and J coincide with those given by eq. 7.32 and 7.33. Substituting eq. 10.8 and 10.12 into eq. 10.3 we have obtained eq. 7.26 and 7.27.

We shall use eq. 7.25 to obtain eq. 7.28 from eq. 7.27. Since the cubic equation 7.21 is invariant under a transformation, $(s, k, m) \to (-s, -k, -m)$, it is easy to prove that the three roots satisfy the relations

$$\left.\begin{aligned} -s_1(-k, -m, a) &= s_2(k, m, a) \equiv s_2 \\ -s_2(-k, -m, a) &= s_1(k, m, a) \equiv s_1 \\ -s_3(-k, -m, a) &= s_3(k, m, a) \equiv s_3 \end{aligned}\right\} \quad (10.13)$$

Analogous relations hold for r_ν defined by eq. 7.29. Thus the functions I, J and L defined by eq. 10.12 and 7.34 are evidently invariant under the transformation $(k, m, a) \to (-k, -m, a)$. Now it may be easy to obtain eq. 7.28 from eq. 7.27.

Appendix 2. Landen's Transformation

We shall describe briefly the procedure by which we have obtained eq. 7.37. By the Landen transformation (7.36)

$$k_1 = \frac{2\sqrt{k}}{1+k}$$

the elliptic functions transform as[11]

$$u^{\mathrm{I}} = (1+k)u \quad (10.14)$$

$$s_{\mathrm{I}} = \frac{(1+k)s}{1+ks^2},\ c_{\mathrm{I}} = \frac{cd}{1+ks^2},\ d_{\mathrm{I}} = \frac{1-ks^2}{1+ks^2} \quad (10.15)$$

where $s_{\mathrm{I}} = \mathrm{sn}(u^{\mathrm{I}}, k_{\mathrm{I}})$, $s = \mathrm{sn}(u, k)$, etc. The transform of the elliptic integral of the first kind is given by 10.14. To obtain the transform of $E(k, u)$, we shall use the following equation derived from the last equation of (10.15):

$$ks^2 = \frac{1-d_{\mathrm{I}}}{1+d_{\mathrm{I}}}$$

Then

$$E(k,u) = \int_0^u (1-k^2s^2)\mathrm{d}u = \frac{1}{1+k}\times\int_0^{u^{\mathrm{I}}}\left(1 - k\frac{1-d_{\mathrm{I}}}{1+d_{\mathrm{I}}}\right)\mathrm{d}u^{\mathrm{I}}$$

The result of the integration is

$$E(k,u) = \frac{1+k}{2}E(k_{\mathrm{I}}, u^{\mathrm{I}}) + \frac{1-k}{2}u^{\mathrm{I}} - \frac{1+k}{2}\frac{c_{\mathrm{I}}(1-d_{\mathrm{I}})}{s_{\mathrm{I}}} = \frac{1+k}{2}E(k_{\mathrm{I}}, u^{\mathrm{I}}) + \frac{1-k}{2}u^{\mathrm{I}} - k\frac{scd}{1+ks^2} \quad (10.16)$$

where in the last term we have used eq. 10.15. In order to obtain the transforms of the integrals I and J, it is most convenient to use the definitions given by the first parts of eq. 10.12. Substituting 10.14 and 10.16 into eq. 10.12 we have obtained eq. 7.37. We note here that $\sin\phi_\nu^{\mathrm{I}}$ defined by eq. 7.38 is always less than unity so that ϕ_3^{I} is no longer a complex angle.

Appendix 3. The Evaluation of the Integration Constants in the Descending Power Series

In order to obtain the integration constants i_{A}, i_{H} and i_{D} given by eq. 9.32 and 9.33, we need to compare the descending power series with the analytical result (10.3). We shall first transform the complex terms in (10.3) by the transformation (10.9), *i.e.*

$$u_3 = u_0 + iK'$$

In this time we shall express the result in terms of $\mathrm{sn}u_0$ instead of $\mathrm{sn}u_3$ corresponding to equation 9.9 in the computation of the descending power series. Since[10]

$$\mathrm{sn}u_3 = k^{-1}\mathrm{ns}u_0,\ \mathrm{dc}u_3 = k\mathrm{cd}u_0$$

$$E(u_3) - E(K+iK') = E(u_0) - E + \mathrm{ns}u_0\mathrm{cd}u_0 - k^2\mathrm{sn}u_0\mathrm{cd}u_0$$

we obtain

$$A^*(u_3) - A^*(K+iK') = -(1+m^2)(u_0 - K) + (2+m^2)(E(u_0) - E) - mk\log\left(\frac{1+\mathrm{cd}u_0}{1-\mathrm{cd}u_0}\right) + (2mk - (2+m^2)k^2\mathrm{sn}u_0 + \mathrm{ns}u_0)\mathrm{cd}u_0 \quad (10.17)$$

$$H_1^*(u_3) - H_1^*(K+iK') = m(u_0 - K) - \frac{1+m}{1+k}(E(u_0) - E) + \frac{1}{2}\log\left(\frac{1+\mathrm{cd}u_0}{1-\mathrm{cd}u_0}\right) - k\left(\frac{1+m}{1+k}\right)(1 - k\mathrm{sn}u_0)\mathrm{cd}u_0 \quad (10.18)$$

$$D_1^*(u_3) - D_1^*(K+iK') = -M_3(u_0 - K) + (1 + M_3 - M_1)(E(u_0) - E) - \frac{1}{2}M_2\log\left(\frac{1+\mathrm{cd}u_0}{1-\mathrm{cd}u_0}\right) + \left\{(M_2k - M_1k^{-1}) - (1 + M_3 - M_1)k^2\mathrm{sn}u_0 + \mathrm{ns}u_0 + \frac{M_1(k'^2/k)}{1+k\mathrm{sn}u_0}\right\}\mathrm{cd}u_0 \quad (10.19)$$

In view of the indefinite integral (9.5), the integration constant i_{A} is the coefficient of a^{-3} order term in $A(a)$. According to the definition of $H_1(a)$ and

$D_1(a)$ given by eq. 7.14, eq. 9.6 can be written in two pieces

$$H_1(a) = \sum_{\nu=1}^{2} a^{-1} \int^{a} \psi_B(s_\nu)\,d\sigma + 2a^{-1} \int^{a} \sigma\bar{\psi}_B(s_0)d\sigma \tag{10.20}$$

$$D_1(a) = \sum_{\nu=1}^{2} a^{-3} \int^{a} \sigma^2\psi_B(s_\nu)d\sigma + 2a^{-3} \int^{a} \sigma^3\bar{\psi}_B(s_0)d\sigma \tag{10.21}$$

Therefore, the integration constant i_{1I} in the indefinite integral (10.20) is the coefficient of a^{-1} order term in the analytic expression of $H_1(a)$ and the integration constant i_D in the integral (10.21) is the coefficient of a^{-3} order term in $D_1(a)$. It is easy to obtain these terms from the analytical result (10.3) with the aid of eq. 10.17–10.19 if we use the following equations obtained by means of the Lagrange theorem

$$\left.\begin{aligned} &\mathrm{sn}u_1 = s_1 = -1 + \frac{(1+k)(1+m)^2}{4a^2}\left\{1 + \left(\frac{1-k}{2(1+k)} - \frac{2}{1+m}\right)a^{-2} + O(a^{-4})\right\} \\ &\mathrm{dc}u_1 = -r_1 = \frac{\sqrt{2(1-k)}}{1+m}\,a\left\{1 + \left(\frac{k}{2(1-k)} + \frac{1}{1+m}\right)\frac{(1+k)(1+m)^2}{4a^2} + O(a^{-4})\right\} \\ &u_1 = -K + O(a^{-1}) \\ &E(u_1) = -E + O(a^{-1}) \end{aligned}\right\} \tag{10.22}$$

$$\left.\begin{aligned} &\mathrm{sn}u_2 = s_2 = 1 - \frac{(1-k)(1-m)^2}{4a^2} + O(a^{-4}) \\ &\mathrm{dc}u_2 = r_2 = \frac{\sqrt{2(1+k)}}{1-m}\,a + O(a^{-1}) \\ &u_2 = K + O(a^{-1}) \\ &E(u_2) = E + O(a^{-1}) \end{aligned}\right\} \tag{10.23}$$

$$\left.\begin{aligned} &\mathrm{sn}u_0 = s_0 = \frac{1}{2a^2}\left\{1 - (1+2km)\frac{1}{2a^2} + O(a^{-4})\right\} \\ &\mathrm{cd}u_0 = 1 - \frac{k'^2}{8a^4} + O(a^{-6}) \\ &u_0 = \frac{1}{2a^2} + O(a^{-4}) \\ &E(u_0) = \frac{1}{2a^2} + O(a^{-4}) \end{aligned}\right\} \tag{10.24}$$

The results of computations are

$$4i_A = 1 - K + 2E + 2\left(2 - \log\frac{4}{k'}\right)km - (K-E)m^2 \tag{10.25}$$

$$2i_{II} = \log\frac{4}{k'} - \frac{k}{1+k} - \frac{E}{1+k} + \left(K - \frac{E}{1+k} - \frac{k}{1+k}\right)m \tag{10.26}$$

$$\begin{aligned} 12i_D = {} & 3 - k\left(3\log\frac{4}{k'} - 3 + \frac{k^2}{k'^2}\right) - 4K + \left(7 - \frac{k^2}{k'^2}\right)E \\ & - \left\{k\left(3\log\frac{4}{k'} - 5 + \frac{k^2}{k'^2}\right) + K - \left(1 - \frac{k^2}{k'^2}\right)E\right\}3m \\ & - \left\{\frac{k^3}{k'^2} + K - \left(1 - \frac{k^2}{k'^2}\right)E\right\}3m^2 \\ & - \left\{\frac{k^3}{k'^2} - 2K + \left(2 + \frac{k^2}{k'^2}\right)E\right\}m^3 \end{aligned} \tag{10.27}$$

11. Appendix 4. The Location of the Roots of the Cubic Equation, $p(s) = 0$

In the discussion for the convergence of the series in Sec. 9, we postponed to prove that the roots of the cubic equation

$$p(m, s) \equiv 2(s^2-1)(ks-1) - (ks^2 - 2s + k)(s-m) = 0 \tag{11.1}$$

satisfy the inequality (9.23), *i.e.*

$$t(s) \geqslant \frac{1}{8} \tag{11.2}$$

where

$$t(s) = \frac{s^2-1}{(ks-1)(s-m)^2} \tag{11.3}$$

and

$$0 \leqslant k \leqslant 1, \quad -1 \leqslant m \leqslant 1 \tag{11.4}$$

To begin with, when m equals one of its extreme values, -1, the roots of eq. 11.1 are

$$-1,\ 1 \pm i\sqrt{2(1-k)/k} \tag{11.5}$$

When m equals the other extreme value, 1, the roots are

$$1,\ -1 \pm \alpha \tag{11.6}$$

where

$$\alpha \equiv \sqrt{2(1+k)k};\ 2 \leqslant \alpha \leqslant \infty$$

Since $p(m, s)$ is linear with respect to m, $p(m, s)$ can be expressed as a linear combination of the extreme cases, $p(-1, s)$ and $p(1, s)$, *i.e.*

$$2p(m, s) = (1-m)\,p(-1, s) + (1+m)\,p(1, s) \tag{11.7}$$

Thus, it is very easy to prove that

$$\begin{aligned} &p(m, s) < 0 \quad \text{when } s < -1-\alpha \\ &p(m, s) > 0 \quad \text{when } -1 < s < 1 \\ &p(m, s) > 0 \quad \text{when } -1+\alpha < s \end{aligned} \tag{11.8}$$

Therefore, the allowed ranges for the roots on the real axis of the s-plane are

$$-1-\alpha \leqslant s \leqslant -1, \quad -1 \leqslant s \leqslant -1+\alpha \tag{11.9}$$

Moreover, in the first interval of these, there exists one or three roots, while in the second interval there exist none or two roots. From the coefficient of s^2 term of the cubic eq. 11.1, we know that the sum of the three roots equals $-m$ which cannot be less than -1. Accordingly, there exists only one root in the first interval.

We next write the cubic eq. 11.1 as

$$m = \frac{2 - 3ks + ks^3}{2s - k - ks^2} \tag{11.10}$$

This clearly shows that m is a one-valued function of each root of eq. 11.1. Therefore, each root, if it is real, must be a monotonic function of m. Thus, when m varies from -1 to 1, the paths of the three roots s_1, s_2 and s_3 can be represented in the s-plane as shown in Fig. 4. At a point $s = b$, the cubic equation has a double root, *i.e.*, $s_2 = s_3 = b$. Therefore, $s = b$ satisfies the two equations

$$p(m, s) = 0, \quad \frac{dm}{ds} = 0 \tag{11.11}$$

For $s \neq b$, we have the inequalities

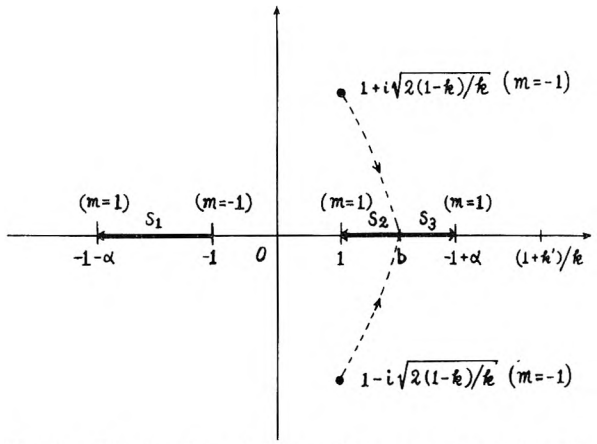

Fig. 4.—The location of the roots s_1, s_2, s_3 in s-plane for $|m| \leq 1$.

$$\left.\begin{aligned} \frac{dm}{ds} &< 0 \quad \text{when } -1-\alpha \leqslant s \leqslant -1 \\ \frac{dm}{ds} &< 0 \quad \text{when } 1 \leqslant s < b \\ \frac{dm}{ds} &> 0 \quad \text{when } b < s \leqslant -1+\alpha \end{aligned}\right\} \quad (11.12)$$

Now we are prepared to obtain the smallest absolute value of $t(s)$ when s is the root of the cubic equation (11.1). Since $(\partial t/\partial s)_m = 0$ from eq. 9.19 and eq. 11.1 we obtain by differentiating eq. 11.3

$$\frac{dt}{ds} = \frac{(ks^2 - 2s + k)^3}{4(ks-1)^4(s^2-1)^2}\frac{dm}{ds} \quad (11.13)$$

where we have eliminated $(s-m)^2$ using eq. 11.1. Since the roots of the equation $ks^2 - 2s + k = 0$ satisfy the following inequalities (see Fig. 4);

$$0 < \frac{1-k'}{k} \leqslant 1, \quad -1+\alpha \leqslant \frac{1+k'}{k} \quad (11.14)$$

eq. 11.11–11.13 yield the inequalities

$$\left.\begin{aligned} \frac{dt}{ds} &< 0 \quad \text{when } -1-\alpha \leqslant s \leqslant -1 \\ \frac{dt}{ds} &> 0 \quad \text{when } -1 \leqslant s < b \\ \frac{dt}{ds} &= 0 \quad \text{when } s = b \\ \frac{dt}{ds} &< 0 \quad \text{when } b < s < -1+\alpha \end{aligned}\right\} \quad (11.15)$$

Therefore, $t(s)$ takes a largest value at $s = -1-\alpha$ in the first interval defined in eq. 11.9 and a maximum at $s = b$ in the second interval. Now, from eq. 11.1 and 11.3, we have

$$t(s) = \frac{(ks^2 - 2s + k)^2}{4(ks-1)^3(s^2-1)} \quad (11.16)$$

This is clearly negative when s is located in the first or second interval. Therefore, in order to obtain the smallest absolute value of $t(s)$, we need to consider only the cases where s equals $-1-\alpha$ or b or the complex roots of eq. 11.1.

When $s = -1-\alpha$ we obtain from equation (11.16)

$$t(-1-\alpha) = -\frac{1}{(\sqrt{1+k} + \sqrt{2k})^2} \quad (11.17)$$

Since $0 \leqslant k \leqslant 1$, we have

$$|t(s_1)| \geqslant \frac{1}{8} \quad (11.18)$$

In order to treat the case of two complex roots, we consider the product $\prod_{i=1}^{3} t(s_i)$. Since $p(m, s) = -k\prod_{i=1}^{3}(s - s_i)$, we have from eq. 11.3

$$\prod_{i=1}^{3} t(s_i) = -k^{-2}\frac{p(m,1)\,p(m,-1)}{p(m,k^{-1})\,p^2(m,m)} = -(1-km)^{-3}(1-m^2)^{-1} \quad (11.19)$$

Using eq. 11.10 and eq. 11.16, this can be written as

$$\frac{1}{t(s_2)t(s_3)} = -\frac{1}{4}\left(\frac{1-km}{1-ks_1}\right)^3 (ks_1^2 + 2ks_1 - 2 - k)(ks_1^2 - 2ks_1 + 2 - k) \quad (11.20)$$

Since $m \geqslant s_1$, we obtain

$$\frac{1-km}{1-ks_1} \leqslant 1 \quad (11.21)$$

The remaining two factors, $|(ks_1^2 + 2ks_1 - 2 - k)|$ and $(ks_1^2 - 2ks_1 + 2 - k)$ take their largest values at $s_1 = -1$ and $s_1 = -1-\alpha$, respectively. Accordingly, we have

$$\left.\begin{aligned} |(ks_1^2 - 2ks_1 - 2 - k)| &\leqslant 2(1+k) \\ (ks_1^2 - 2ks_1 + 2 - k) &\leqslant 4\sqrt{1+k}\,(\sqrt{1+k} + \sqrt{2k}) \end{aligned}\right\} \quad (11.22)$$

Substituting eq. 11.21 and 11.22 into eq. 11.20, we obtain

$$\left|\frac{1}{t(s_2)t(s_3)}\right| < 2(1+k)^{3/2}(\sqrt{1+k} + \sqrt{2k}) \leqslant 16 \quad (11.23)$$

For the case where s_2, s_3 equal b or the complex roots of eq. 11.1, this yields

$$|t(s_2)| = |t(s_3)| > \frac{1}{4} \quad (11.24)$$

because s_2 and s_3 are mutually complex conjugate. From eq. 11.18 and eq. 11.24 we get the required result, eq. 11.2.

Table I

The Descending Power Series for $A(a)$ and $B_j(a)$ Specialized to the Ordinary Types of Simple Electrolytes

The general forms of the descending power series are

$$2A(k, m, a) = \sum_{n=1}^{\infty} R_n a^{-n} + R_3^* a^{-3}\log a$$

$$B_j(k, m, a) = \sum_{n=0}^{\infty} P_{jn} a^{-n} + P_{j1}^* a^{-1}\log a + P_{j3}^* a^{-3}\log a$$

The ordinary types of simple electrolytes are

NaCl-type; $k = 0$, $BaCl_2$-type; $k = 1/3$, $LaCl_3$-type; $k = 1/2$, $Al_2(SO_4)_3$-type; $k = 1/6$, $K_4[FeCN_6]$-type; $k = 3/5$

When $k = 0$

$$R_1 = 1,\ R_2 = -\sqrt{2},\ R_3^* = 0,\ R_3 = \frac{1}{2} + \frac{\pi}{4},$$

$$R_4 = -\frac{\sqrt{2}}{2},\ R_5 = \frac{1}{8},\ R_6 = \frac{\sqrt{2}}{12},\ R_7 = -\frac{1}{16},\ \text{etc.}$$

and $P_{jn} \equiv P_n$, $P_{jn}^* \equiv P_n^*$ where

$$P_0 = \frac{2}{3}\sqrt{2},\ P_1^* = 1,\ P_1 = -\left(\frac{1}{2} + \frac{\pi}{4} - \log 2\right),$$

$$P_2 = \sqrt{2},\ P_3^* = 0,\ P_3 = -\left(\frac{1}{4} + \frac{\pi}{8}\right),$$

$$P_4 = \frac{\sqrt{2}}{6},\ P_5 = -\frac{1}{32},\ P_6 = -\frac{\sqrt{2}}{60},\ P_7 = \frac{1}{96},\ \text{etc.}$$

For the cases of general electrolytes, we express the results in terms of m and ω_{ji}

$$m = \omega_{21} - \omega_{12};\ \omega_{21} = \frac{|z_1|\Lambda^\circ_2}{|z_1|\Lambda^\circ_2 + |z_2|\Lambda^\circ_1},$$

$$\omega_{12} = \frac{|z_2|\Lambda^\circ_1}{|z_1|\Lambda^\circ_2 + |z_2|\Lambda^\circ_1}$$

when $k = {}^1/_3$,

$R_1 = 1$

$$R_2 = -\frac{2}{\sqrt{3}}\omega_{21} - \frac{4}{\sqrt{6}}\omega_{12}$$

$$R_3^* = -\frac{2}{3}m$$

$$R_3 = 1.21752 + 0.18494m - 0.04558_5m^2$$

$$R_4 = -\frac{4}{3\sqrt{3}}\omega_{21}^2(3 - 2\omega_{21}) - \frac{1}{3\sqrt{6}}\omega_{12}^2(12 - 11\omega_{12})$$

$$R_5 = -\frac{1}{18}(-1 + 6m + 3m^2)$$

$$R_6 = \frac{1}{27\sqrt{3}}\omega_{21}^3(80 - 100\omega_{21} + 33\omega_{21}^2) + \frac{5}{216\sqrt{6}}\omega_{12}^3 \times (64 - 152\omega_{12} + 75\omega_{12}^2)$$

$$R_7 = \frac{1}{216}(-3 + 24m + 45m^2 + 10m^3)$$

etc.

$$P_{10} = \frac{1}{\sqrt{3}}$$

$$P_{11}^* = 1$$

$$P_{11} = -0.47473_5 + 0.11136m$$

$$P_{12} = \frac{1}{\sqrt{3}}\omega_{21}(4 - 3\omega_{21}) + \frac{4}{\sqrt{6}}\omega_{12}^2$$

$$P_{13}^* = \frac{1}{6}(1 + 3m)$$

$$P_{13} = -0.46136 + 0.27553m + 0.08090m^2 + 0.00417_6m^3$$

$$P_{14} = \frac{1}{18\sqrt{3}}\omega_{21}^2(48 - 64\omega_{21} + 21\omega_{21}^2) + \frac{1}{9\sqrt{6}}\omega_{12}^3(16 - 15\omega_{12})$$

$$P_{15} = \frac{1}{72}(1 + 10m + 5m^2)$$

$$P_{16} = \frac{-1}{270\sqrt{3}}\omega_{21}^3(320 - 600\omega_{21} + 396\omega_{21}^2 - 99\omega_{21}^3) - \frac{1}{1080\sqrt{6}}\omega_{12}^4(480 - 1104\omega_{12} + 559\omega_{12}^2)$$

$$P_{17} = -\frac{1}{2592}(9 + 105m + 147m^2 + 35m^3)$$

etc.

$$P_{20} = \frac{2}{3}\sqrt{6}$$

$$P_{21}^* = 1$$

$$P_{21} = -0.67206_5 + 0.08597m$$

$$P_{22} = \frac{1}{\sqrt{6}}\omega_{12}(8 - 3\omega_{12}) + \frac{2}{\sqrt{3}}\omega_{21}^2$$

$$P_{23}^* = \frac{1}{6}(-1 + 3m)$$

$$P_{23} = -0.70917 + 0.13456m + 0.06007m^2 + 0.00277m^3$$

$$P_{24} = \frac{1}{72\sqrt{6}}\omega_{12}^2(192 - 352\omega_{12} + 135\omega_{12}^2) + \frac{4}{9\sqrt{3}}\omega_{21}^3(4 - 3\omega_{21})$$

$$P_{25} = \frac{1}{72}(-2 + 5m + 5m^2)$$

$$P_{26} = -\frac{1}{4320\sqrt{6}}\omega_{21}^3(2560 - 9120\omega_{12} + 9000\omega_{12}^2 - 2763\omega_{12}^3) - \frac{1}{135\sqrt{3}}\omega_{21}^4(120 - 168\omega_{21} + 61\omega_{21}^2)$$

$$P_{27} = -\frac{1}{2592}(-9 + 21m - 105m^2 + 35m^3)$$

etc.

When $k = {}^1/_2$,

$R_1 = 1$

$$R_2 = -\omega_{21} - \sqrt{3}\omega_{12}$$

$$R_3^* = -m$$

$$R_3 = 1.12460 + 0.23493m - 0.10915m^2$$

$$R_4 = -\frac{1}{4}\omega_{21}^2(9 - 7\omega_{21}) - \frac{1}{4\sqrt{3}}\omega_{12}^2(9 - 11\omega_{12})$$

$$R_5 = -\frac{1}{32}(1 + 16m + 12m^2)$$

$$R_6 = \frac{5}{96}\omega_{21}^3(36 - 48\omega_{21} + 13\omega_{21}^2) + \frac{1}{288\sqrt{3}}\omega_{12}^3(180 - 600\omega_{12} + 353\omega_{12}^2)$$

$$R_7 = \frac{1}{128}(6 + 33m + 60m^2 + 20m^3)$$

etc.

$$P_{10} = \frac{4}{9}$$

$$P_{11}^* = 1$$

$$P_{11} = -0.39076_5 + 0.18707m$$

$$P_{12} = 2\omega_{21}(1 - \omega_{21}) + \sqrt{3}\,\omega_{12}^2$$

$$P_{13}^* = \frac{1}{4}(1 + 3m)$$

$$P_{13} = -0.29819 + 0.54253m + 0.21853m^2 + 0.01827m^3$$

$$P_{14} = \frac{1}{24}\omega_{21}^2(36 - 56\omega_{21} + 15\omega_{21}^2) + \frac{1}{6\sqrt{3}}\omega_{12}^3(6 - 7\omega_{12})$$

$$P_{15} = \frac{1}{128}(7 + 30m + 20m^2)$$

$$P_{16} = -\frac{1}{240}\omega_{21}^3(180 - 360\omega_{21} + 195\omega_{21}^2 - 49\omega_{21}^3) - \frac{1}{1440\sqrt{3}}\omega_{12}^4(270 - 828\omega_{12} + 491\omega_{12}^2)$$

$$P_{17} = -\frac{1}{1536}(33 + 147m + 210m^2 + 70m^3)$$

etc.

$$P_{20} = \frac{4}{\sqrt{3}}$$

$$P_{21}^* = 1$$

$$P_{21} = -0.7024 + 0.1246m$$

$$P_{22} = \frac{2}{\sqrt{3}}\omega_{12}(3 - \omega_{12}) + \omega_{21}^2$$

$$P_{23}^* = \frac{1}{4}(-1 + 3m)$$

$$P_{23} = -0.7085 + 0.1886m + 0.1352m^2 + 0.00951m^3$$

$$P_{24} = \frac{1}{72\sqrt{3}}\omega_{12}^2(108 - 264\omega_{12} + 101\omega_{12}^2) + \frac{1}{6}\omega_{21}^3(6 - 5\omega_{21})$$

$$P_{25} = \frac{1}{128}(-1 + 10m + 20m^2)$$

$$P_{26} = -\frac{1}{2160\sqrt{3}}\omega_{12}^3(540 - 2700\omega_{12} + 3177\omega_{12}^2 - 1033\omega_{12}^3) - \frac{1}{480}\omega_{21}^4(270 - 396\omega_{21} + 131\omega_{21}^2)$$

$$P_{27} = -\frac{7}{1536}(1 + 5m + 18m^2 + 10m^3)$$

etc.

When $k = {}^1/_5$,

$$R_1 = 1$$

$$R_2 = -\frac{4}{\sqrt{10}}\omega_{21} - \frac{6}{\sqrt{15}}\omega_{12}$$

$$R_3^* = -\frac{2}{5}m$$

$$R_3 = 1.26153 + 0.11866m - 0.01595m^2$$

$$R_4 = -\frac{1}{5\sqrt{10}}\omega_{21}^2(36 - 23\omega_{21}) - \frac{4}{5\sqrt{15}}\omega_{12}^2(9 - 7\omega_{12})$$

$$R_5 = -\frac{1}{50}(-5 + 10m + 3m^2)$$

$$R_6 = \frac{1}{600\sqrt{10}}\omega_{21}^3(2880 - 3720\omega_{21} + 1343\omega_{21}^2) + \frac{1}{225\sqrt{15}}\omega_{12}^3(720 - 1380\omega_{12} + 617\omega_{12}^2)$$

$$R_7 = \frac{1}{1000}(-45 + 48m + 75m^2 + 10m^3)$$

etc.

$$P_{10} = \frac{2}{9}\sqrt{10}$$

$$P_{11}^* = 1$$

$$P_{11} = -0.52788_5 + 0.06220m$$

$$P_{12} = \frac{1}{\sqrt{10}}\omega_{21}(8 - 5\omega_{21}) + \frac{6}{\sqrt{15}}\omega_{12}^2$$

$$P_{13}^* = \frac{1}{10}(1 + 3m)$$

$$P_{13} = -0.55168 + 0.13726m + 0.02625_5m^2 + 0.00078m^3$$

$$P_{14} = \frac{1}{120\sqrt{10}}\omega_{21}^2(576 - 736\omega_{21} + 261\omega_{21}^2) + \frac{8}{15\sqrt{15}}\omega_{12}^3(6 - 5\omega_{12})$$

$$P_{15} = \frac{1}{200}(-2 - 15m + 5m^2)$$

$$P_{16} = -\frac{1}{12000\sqrt{10}}\omega_{21}^3(23040 - 44640\omega_{21} + 32232\omega_{21}^2 - 8405\omega_{21}^3) - \frac{1}{1125\sqrt{15}}\omega_{12}^4(1080 - 2088\omega_{12} + 965\omega_{12}^2)$$

$$P_{17} = -\frac{7}{12000}(-9 + 27m + 33m^2 + 5m^3)$$

etc.

$$P_{20} = \frac{\sqrt{15}}{3}$$

$$P_{21}^* = 1$$

$$P_{21} = -0.64350_5 + 0.05342m$$

$$P_{22} = \frac{1}{\sqrt{15}}\omega_{12}(12 - 5\omega_{12}) + \frac{4}{\sqrt{10}}\omega_{21}^2$$

$$P_{23}^* = \frac{1}{10}(-1 + 3m)$$

$$P_{23} = -0.69374 + 0.08892m + 0.02209m^2 + 0.00061m^3$$

$$P_{24} = \frac{1}{90\sqrt{15}}\omega_{12}^2(432 - 672\omega_{12} + 257\omega_{12}^2) + \frac{1}{15\sqrt{10}}\omega_{21}^3(48 - 35\omega_{21})$$

$$P_{25} = \frac{1}{200}(-7 + 10m + 5m^2)$$

$$P_{26} = -\frac{1}{6750\sqrt{15}}\omega_{12}^3(8640 - 24840\omega_{12} + 22212\omega_{12}^2 - 6545\omega_{12}^3) - \frac{1}{3000\sqrt{10}}\omega_{21}^4(4320 - 6192\omega_{21} + 2375\omega_{21}^2)$$

$$P_{27} = -\frac{1}{12000}(-97 + 49m + 189m^2 + 35m^3)$$

etc.

When $k = {}^3/_5$

$$R_1 = 1$$

$$R_2 = -\frac{1}{\sqrt{5}}(3 - m)$$

$$R_3^* = -\frac{6}{5}m$$

$$R_3 = 1.04272 + 0.23434m - 0.16633m^2$$

$$R_4 = -\frac{2}{5\sqrt{5}}\omega_{21}^2(12 - 11\omega_{21}) - \frac{1}{10\sqrt{5}}\omega_{12}^2(24 - 17\omega_{12})$$

$$R_5 = -\frac{1}{50}(5 + 30m + 27m^2)$$

$$R_6 = \frac{2}{75\sqrt{5}}\omega_{21}^3(160 - 240\omega_{21} + 51\omega_{21}^2) + \frac{1}{2400\sqrt{5}}\omega_{12}^3(1280 - 5520\omega_{12} + 3783\omega_{12}^2)$$

$$R_7 = \frac{1}{1000}(95 + 396m + 675m^2 + 270m^3)$$

etc.

$$P_{10} = \frac{\sqrt{5}}{6}$$

$$P_{11}^* = 1$$

$$P_{11} = -0.32593_5 + 0.24472m$$

$$P_{12} = \frac{1}{4\sqrt{5}}(7 - 10m - m^2)$$

$$P_{12}^* = \frac{3}{10}(1 + 3m)$$

$$P_{13} = -0.15762 + 0.79120m + 0.36696m^2 + 0.03915_5m^3$$

$$P_{14} = \frac{2}{15\sqrt{5}}\omega_{21}^2(24 - 44\omega_{21} + 9\omega_{21}^2) + \frac{1}{30\sqrt{5}}\omega_{21}^3(32 - 45\omega_{21})$$

$$P_{15} = \frac{1}{200}(17 + 60m + 45m^2)$$

$$P_{16} = -\frac{1}{375\sqrt{5}}\omega_{21}^3(640 - 1440\omega_{21} + 612\omega_{21}^2 - 185\omega_{21}^3) - \frac{1}{12000\sqrt{5}}\omega_{12}^4(1920 - 7392\omega_{12} + 5015\omega_{12}^2)$$

$$P_{17} = -\frac{1}{12000}(439 + 1743m + 2457m^2 + 945m^3)$$

etc.

$$P_{20} = \frac{4}{3}\sqrt{5}$$

$$P_{21}^* = 1$$

$$P_{21} = -0.71789_5 + 0.14724m$$

$$P_{22} = \frac{1}{8\sqrt{5}}(31 - 14m - m^2)$$

$$P_{23}^* = \frac{3}{10}(-1 + 3m)$$

$$P_{23} = -0.69667 + 0.22603_3m + 0.19821m^2 + 0.01710m^3$$

$$P_{24} = \frac{1}{480\sqrt{5}}\omega_{12}^2(768 - 2368\omega_{12} + 903\omega_{12}^2) + \frac{2}{15\sqrt{5}}\omega_{21}^3(16 - 15\omega_{21})$$

$$P_{25} = \frac{1}{200}(2 + 15m + 45m^2)$$

$$P_{26} = -\frac{1}{96000\sqrt{5}}\omega_{12}^3(20480 - 132480\omega_{12} + 181584\omega_{12}^2 - 61405\omega_{12}^3) - \frac{2}{375\sqrt{5}}\omega_{21}^4(240 - 384\omega_{21} + 115\omega_{21}^2)$$

$$P_{27} = -\frac{1}{12000}(121 + 483m + 1323m^2 + 945m^3)$$

etc.

THE RELAXATION EFFECTS IN MIXED STRONG ELECTROLYTES*

BY LARS ONSAGER AND SHOON KYUNG KIM†

Contribution No. 1376 from the Sterling Chemistry Laboratory, Yale University, New Haven, Connecticut

Received July 9, 1956

The separation of the Onsager–Fuoss equations for the modification of interionic forces by conduction, diffusion and viscosity in mixed electrolytes is greatly facilitated with the aid of an algebraic device which was invented more recently. The numerical work involved in applying the theory to mixtures is substantially reduced. While further refinement of theory has not been undertaken, helpful intermediate results have been obtained.

I. Introduction

Since the forces acting between the ions in an electrolyte solution are known, it is possible to compute the various physical properties of the system which depend upon these forces. The mathematical difficulties involved were first overcome by Debye and Hückel[1] who introduced the concept of the "ionic atmosphere" and successfully computed the limiting laws for the thermodynamic properties of electrolytes. In addition, they developed a qualitatively correct theory for the electrolytic conduction.[1] Onsager[2,3] perfected their kinetic theory and computed the limiting law for conduction in simple electrolytes. After Jones and Dole[4] had discovered that the viscosities of electrolyte solutions vary linearly with the square root of the concentration (in the limit), Falkenhagen and Dole[5] computed the appropriate coefficient for simple electrolytes. Onsager and Fuoss[6] computed limiting laws for conduction and viscosity in mixtures of arbitrary compositions, and they obtained the corresponding formulas for diffusion in simple and mixed electrolytes.

The general problem for s species of ions involves a system of s linear differential equations in s unknown functions, with a matrix **H** of constant coefficients; some knowledge of the algebraic properties of this matrix is essential to the solution of the equations. For the case of $s = 3$, Onsager and Fuoss[6] obtained explicit results in closed form; for more complicated cases they constructed series expansions and proved convergence with the aid of the general theory of quadratic forms. While the series are convenient for a great variety of cases, they converge none too well in the particularly interesting cases where the ions present exhibit widely different coefficients of diffusion.

Quite some time later, Onsager[7] discovered that the eigen vectors of the matrix **H** have a simple special form. We shall take advantage of this discovery to simplify the analysis as well as the methods of numerical computation.

As a matter of convenience we shall briefly review the derivation of the fundamental equations specialized to conduction and diffusion. We shall then solve the system of differential equations with the aid of appropriate special algebraic methods. While the methods do depend on a knowledge of the eigen vectors of the matrix of coefficients, and we shall clearly exhibit this connection, we shall have no need to assume that the readers know the general theory of eigenwert problems, because all pertinent

* This paper is based on the dissertation submitted by Shoon K. Kim to the Faculty of the Graduate School of Yale University in partial fulfillment of the requirements for the Degree of Doctor of Philosophy.

† Institute for Fluid Dynamics and Applied Mathematics, University of Maryland, College Park, Maryland.

(1) P. Debye and E. Hückel, *Physik. Z.* [I] **24**, 185 (1923); [II] **24**, 305 (1923).

(2) L. Onsager, I, *Physik. Z.*, **27**, 388 (1926).

(3) L. Onsager, *ibid.*, [II] **28**, 277 (1927).

(4) Grinnell Jones and M. Dole, *J. Am. Chem. Soc.*, **51**, 2950 (1929).

(5) H. Falkenhagen and M. Dole, *Z. physik. Chem.*, **6**, 159 (1929); *Physik. Z.*, **30**, 611 (1929); H. Falkenhagen, *ibid.*, **32**, 365, 745 (1931).

(6) L. Onsager and R. M. Fuoss, THIS JOURNAL, **36**, 2689 (1932). A review of this work is available in H. S. Harned and B. B. Owen, "Physical Chemistry of Electrolytic Solutions," Reinhold Publ. Corp., New York, N. Y., 1950, pp. 75–85.

(7) L. Onsager, *Annals of the New York Academy of Science*, Vol. XLVI, pp. 263–264 (1945).

relations are just as easily derived directly by elementary algebra.

Since nothing has been changed in the "electrophoretic effect" worked out by Onsager and Fuoss,[6] we shall confine our attention to the "relaxation effect" in the conductance and in the dissipation function for conduction and diffusion. We shall obtain an integral representation for the forces which arise from the asymmetry of the ionic atmospheres, and prove that the matrix which describes the contribution to the dissipation function from this (relaxation) effect has all positive diagonal elements and all negative off-diagonal elements. We shall devise a method of numerical computation which enables us to deal with systems containing an arbitrary number of species of ions.

Recently Fuoss and Onsager[8] refined the theory of conduction in simple electrolytes to the extent that they included terms of second order in the electric charges and allowed for the finite sizes of the ions. Our methods would facilitate an analogous improvement of the theory for mixtures; because we have obtained reasonably explicit descriptions of the distribution of ions, and we have satisfied ourselves that the Green functions for our systems of differential equations (the first approximation) are readily obtainable.

We have also computed the contribution to the viscosity from the relaxation effect for arbitrary mixtures; the variation of the algebra is trivial. For this problem, any review of the derivation of the fundamental equation first given by Onsager and Fuoss[6] seemed redundant.

II. The Fundamental Equations for the Ionic Atmospheres 2.1. Linearized Equation of Continuity Specialized to Conduction and Diffusion.— We consider a solution containing $n_1, n_2, \ldots n_s$ ions (per cm.^{3}) of species $1, 2, \ldots s$ with charges $e_1, e_2, \ldots, e_s$ (e.s.u. per ion). We confine our attention to any two particular volume elements $dv_1 = dx_1\, dy_1\, dz_1$ and $dv_2 = dx_2\, dy_2\, dz_2$ in the solution located by vectors $\mathbf{r}_1$ and $\mathbf{r}_2$ drawn from an arbitrary origin. Then the relative location may be designated by

$$\mathbf{r}_{21} = \mathbf{r}_2 - \mathbf{r}_1;\ \mathbf{r}_{12} = \mathbf{r}_1 - \mathbf{r}_2 \qquad (2.1.1)$$

If we designate by n_{ji} the time average concentration of i-ions at $\mathbf{r}_{21}$ in the ionic atmosphere of a j-ion located by $\mathbf{r}_1$, we have

$$n_{ji} = n_{ji}(\mathbf{r}_1, \mathbf{r}_{21})$$

Likewise

$$n_{ij} = n_{ij}(\mathbf{r}_2, \mathbf{r}_{12}) \qquad (2.1.2)$$

The (time average) probability of finding simultaneously a j-ion in the volume element dv_1 and an i-ion in the volume element dv_2 equals to $n_j n_{ji}\, dv_1\, dv_2$ or equally well $n_i n_{ij}\, dv_1\, dv_2$. Therefore, we define a symmetric distribution function

$$f_{ji}(\mathbf{r}_1, \mathbf{r}_{21}) \equiv n_j n_{ji}(\mathbf{r}_1, \mathbf{r}_{21}) = n_i n_{ij}(\mathbf{r}_2, \mathbf{r}_{12}) \equiv f_{ij}(\mathbf{r}_2, \mathbf{r}_{12}) \qquad (2.1.3)$$

for ion pairs in the 6-dimensional space $(x_1, y_1, z_1, x_2, y_2, z_2)$. If we designate by v_{ji} the (time average) velocity of an i-ion in the ionic atmosphere of a j-ion, we have in general

$$\mathbf{v}_{ji} = \mathbf{v}_{ji}(\mathbf{r}_1, \mathbf{r}_{21}) \qquad (2.1.4)$$

Likewise

$$\mathbf{v}_{ij} = \mathbf{v}_{ij}(\mathbf{r}_2, \mathbf{r}_{12})$$

Since the number of ions of every species is conserved the average motion of the ion pair (ji) in the 6-dimensional space must satisfy the following equation of continuity

$$-\frac{\partial f_{ji}}{\partial t} = \nabla_1\cdot(f_{ij}\mathbf{v}_{ij}) + \nabla_2\cdot(f_{ji}\mathbf{v}_{ji}) = -\frac{\partial f_{ij}}{\partial t} \qquad (2.1.5)$$

In a steady state, f_{ji} is independent of time so that we obtain the continuity equation specialized for the stationary state

$$\nabla_1\cdot(f_{ij}\mathbf{v}_{ij}) + \nabla_2\cdot(f_{ji}\mathbf{v}_{ij}) = 0 \qquad (2.1.6)$$

In developing the theory of conduction and diffusion we shall assume homogeneous fields of force acting upon the ions in a solution at rest. Then the distribution functions depend only on the relative location $\mathbf{r} = \mathbf{r}_{21} = -\mathbf{r}_{12}$, so that

$$f_{ji}(\mathbf{r}) = f_{ij}(-\mathbf{r}) \qquad (2.1.7)$$

We shall denote by $\psi_j(\mathbf{r})$ the (average) electrostatic potential at a directed distance $\mathbf{r}$ from a j-ion. This potential is related to the distribution functions f_{ji} by Poisson's equation

$$\nabla^2\psi_j = -\frac{4\pi}{D}\sum_{i=1}^{s} f_{ji}e_i/n_j \qquad (2.1.8)$$

where D is the dielectric constant of the medium, and $\nabla = \nabla_2 (= -\nabla_1)$.

If we assume that we may compute the field due to two ions and their joint atmosphere by linear superposition of the separate fields, we have for the force $\mathbf{K}_{ji}(\mathbf{r})$ acting on an i-ion in the atmosphere of a j-ion

$$\mathbf{K}_{ji}(\mathbf{r}) = \mathbf{k}_i + e_i\Delta\mathbf{X}_i - e_i\nabla_2\psi_j(\mathbf{r}) \qquad (2.1.9a)$$

where $\mathbf{k}_i$ is the applied external force, $e_i\Delta\mathbf{X}_i$ is the force due to i-ion's own asymmetric atmosphere caused by the external forces, and $-e_i\nabla_2\psi_j(\mathbf{r})$ is the force exerted by the j-ion and its atmosphere. Likewise

$$\mathbf{K}_{ij}(-\mathbf{r}) = \mathbf{k}_j + e_j\Delta\mathbf{X}_j - e_j\nabla_1\psi_i(-\mathbf{r}) \qquad (2.1.9b)$$

The force $\mathbf{K}_{ji}$ gives the i-ion a velocity $\mathbf{K}_{ji}\omega_i$ where ω_i is the absolute mobility (the reciprocal of the friction constant ρ_i) of an i-ion. According to the generalized equation of Brownian motion, a "concentration gradient" $(\nabla_2 f_{ji})$ produces an average velocity equal to $-(\omega_i kT/f_{ji})\ \nabla_2 f_{ji}$. Combining these two contributions to the velocity $\mathbf{v}_{ji}$ of an i-ion in the atmosphere of a j-ion, we obtain

$$\mathbf{v}_{ji}(\mathbf{r}) = \omega_i\mathbf{K}_{ji}(\mathbf{r}) - \omega_i kT\nabla_2 \log f_{ji}(\mathbf{r}) \qquad (2.1.10a)$$

Likewise

$$\mathbf{v}_{ij}(-\mathbf{r}) = \omega_j\mathbf{K}_{ij}(-\mathbf{r}) - \omega_j kT\nabla_1 \log f_{ij}(-\mathbf{r}) \qquad (2.1.10b)$$

Since we are interested in the limiting law, we have here neglected the hydrodynamic motion of the fluid at dV_2 caused by the presence of a moving j-ion at dV_1. By this approximation we lose terms of the order $c \log c$ (c = concentration) in the final results.[8] Substituting eq. (2.1.9) and (2.1.10) into the equation of continuity (2.1.6) and using the identity $f_{ji}(\mathbf{r}) = f_{ij}(-\mathbf{r})$, we obtain

(8) R. M. Fuoss and L. Onsager, *Proc. Nat. Acad. Sci.*, **41**, No. 5, 274–283 (1955).

$$(\omega_j + \omega_i)kT\nabla^2 f_{ji} + e_i\omega_i\nabla\cdot[f_{ji}\nabla\psi_j(\mathbf{r})] + e_j\omega_j\nabla\cdot[f_{ji}\nabla\psi_i(-\mathbf{r})] = \omega_i(\mathbf{k}_i + e_i\Delta\mathbf{X}_i)\cdot\nabla f_{ji} - \omega_j(\mathbf{k}_j + e_j\Delta\mathbf{X}_j)\cdot\nabla f_{ji} \quad (2.1.11)$$

where we have assumed that the force $\mathbf{k}_j$ is a constant. In order to linearize eq. 2.1.11, we shall assume that the concentration of our system is low. Then, we can neglect[6] terms of the order e_i^2 or e_j^2 compared with terms of the order e_i or e_j. Since

$$\psi_j \sim e_j, \quad \psi_i \sim e_i, \quad f_{ji} - n_j n_i \sim e_j e_i, \quad \text{and } \Delta\mathbf{X}_j \sim e_j, \Delta\mathbf{X}_i \sim e_i$$

we obtain

$$(\omega_j + \omega_i)kT\nabla^2 f_{ji}(\mathbf{r}) + e_i\omega_i n_i n_j\nabla^2\psi_j(\mathbf{r}) + e_j\omega_j n_j n_i\nabla^2\psi_i(-\mathbf{r}) = (\omega_i\mathbf{k}_i - \omega_j\mathbf{k}_j)\cdot\nabla f_{ji}(\mathbf{r}) \quad (2.1.12)$$

This equation and Poisson's equation give us a complete system of linear differential equations. We have not yet imposed any restriction on the magnitude of the force $\mathbf{k}_i$. Equation 2.1.12 is still applicable to the theory of deviations from Ohm's law.

2.2. First-order Perturbation of the Ionic Atmospheres.—Now we shall assume that the applied forces are weak, so that we can treat the problem by the first order perturbation method, and superimpose their effects. Accordingly, we put

$$\left.\begin{aligned}\psi_j(\mathbf{r}) &= \psi^\circ{}_j(r) + \psi'_j(\mathbf{r})\\ \psi_i(-\mathbf{r}) &= \psi^\circ{}_i(r) + \psi'_i(-\mathbf{r})\\ f_{ji}(\mathbf{r}) &= f^\circ{}_{ji}(r) + f'_{ji}(\mathbf{r})\end{aligned}\right\} \quad (2.2.1)$$

Here $\psi^\circ_j(r)$ and $f_{ji}(r)$ are the potential and the distribution function at equilibrium where $\mathbf{k}_j = 0$. These functions were first obtained by Debye and Hückel.[1,2] The results are

$$\psi^\circ{}_j = \frac{e_j}{D}\frac{e^{-\kappa r}}{r} \quad (2.2.2)$$

$$f^\circ{}_{ji} = n_j n_i\left(1 - \frac{e_j e_i}{DkT}\frac{e^{-\kappa r}}{r}\right) \quad (2.2.3)$$

where

$$\kappa \equiv \sqrt{\frac{4\pi\Gamma_0}{DkT}} \quad ; \quad \Gamma_0 \equiv \sum_{i=1}^{s} n_i e_i^2 \quad (2.2.4)$$

It may be easily verified that eq. 2.2.2 and 2.2.3 satisfy the differential system, (2.1.8) and (2.1.12) when $\mathbf{k}_j = 0$. When the applied forces $\mathbf{k}_j$ are small in the sense[9]

$$\frac{|\mathbf{k}_j|}{\kappa kT} << 1 \quad (2.2.5)$$

then the first-order perturbation method is valid; *i.e.*, the additional functions ψ'_j and f'_{ji} are linearly related to the applied forces. In this case we have Ohm's law for the electrolytic conduction. Thus, the general form of ψ'_j and f'_{ji} must be

$$(\mathbf{r}\cdot\mathbf{k})R(r) \quad (2.2.6)$$

where $R(r)$ is a function of the scalar distance r. Accordingly, ψ'_i and f'_{ji} satisfy the following symmetry conditions

$$\psi'_i(-\mathbf{r}) = -\psi'_i(\mathbf{r}), f'_{ji}(-\mathbf{r}) = -f'_{ji}(\mathbf{r}) = -f'_{ij}(-\mathbf{r}) \quad (2.2.7)$$

Without actual loss of generality, we shall assume further that the force $\mathbf{k}_j$ has a component k_j only in the x-direction. Then we have

$$\mathbf{k}_j\nabla f^\circ{}_{ji} = -\frac{n_j n_i e_j e_i}{DkT}k_j\frac{\partial}{\partial x}\left(\frac{e^{-\kappa r}}{r}\right) \quad (2.2.8)$$

If we substitute eq. 2.2.1 into the linearized equation of continuity (2.1.12), those terms on the left which remain in the unperturbed state must cancel each other. The terms of second order on the right can be neglected. Thus, we obtain

$$(\omega_j + \omega_i)kT\nabla^2 f'_{ji}(\mathbf{r}) + e_i\omega_i n_i n_j\nabla^2\psi'_j(\mathbf{r}) - e_j\omega_j n_j n_i\nabla^2\psi'_i(\mathbf{r}) = -\frac{n_j n_i e_j e_i}{DkT}(\omega_i k_i - \omega_j k_j)\frac{\partial}{\partial x}\left(\frac{e^{-\kappa r}}{r}\right) \quad (2.2.9)$$

where we have used eq. 2.2.7 and 2.2.8. The terms on the right-hand side of the equation contain perturbing factors; the terms on the left represent the asymmetric contributions to the potential and the distribution thereby produced. Poisson's eq. 2.1.8 takes the form

$$n_j\nabla^2\psi'_j = -\frac{4\pi}{D}\sum_{i=1}^{s} f'_{ji}e_i \quad (2.2.10)$$

By means of this equation we can eliminate the distribution functions f'_{ji} in eq. 2.2.9 to obtain

$$\nabla^2\nabla^2\psi'_j - \frac{4\pi}{DkT}\sum_{i=1}^{s}\frac{n_i e_i^2\omega_i}{\omega_i + \omega_j}\nabla^2\psi'_j + \frac{4\pi}{DkT}\sum_{i=1}^{s}\frac{n_i e_i e_j\omega_j}{\omega_i + \omega_j}\nabla^2\psi'_i = \frac{4\pi}{(DkT)^2}\sum_{i=1}^{s}\frac{\omega_i k_i - \omega_j k_j}{\omega_i + \omega_j}n_i e_i^2 e_j\frac{\partial}{\partial x}\left(\frac{e^{-\kappa r}}{r}\right) \quad (2.2.11)$$

We shall change this into more convenient form. From Poisson's eq. 2.2.10 and the symmetry property of f'_{ji}, we have

$$\frac{4\pi}{DkT}\sum_{i=1}^{s} n_i e_i e_j\nabla^2\psi'_i = -\frac{(4\pi)^2}{D^2kT}\sum_{j,i=1}^{s} e_j e_i f'_{ji} = -\frac{1}{2}\frac{(4\pi)^2}{D^2kT}\sum_{j,i=1}^{s} e_j e_i(f'_{ij} + f'_{ji}) = 0 \quad (2.2.12)$$

Subtracting this from eq. 2.2.11, we obtain

$$\nabla^2\nabla^2\psi'_j - \frac{4\pi}{DkT}\sum_{i=1}^{s}\frac{n_i e_i^2\omega_i}{\omega_i + \omega_j}\nabla^2\psi'_j - \frac{4\pi}{DkT}\sum_{i=1}^{s}\frac{n_i e_i e_j\omega_i}{\omega_i + \omega_j} \times \nabla^2\psi'_i = \frac{4\pi}{(DkT)^2}\sum_{i=1}^{s}\frac{\omega_i k_i - \omega_j k_j}{\omega_i + \omega_j}n_i e_i^2 e_j\frac{\partial}{\partial x}\left(\frac{e^{-\kappa r}}{r}\right) \quad (2.2.13)$$

which is the Onsager–Fuoss equation for the potential ψ_j'.

It is convenient to define the relative ionic strength μ_i, a mean mobility $\bar{\omega}$, and the limiting transference number t_i

$$\mu_i \equiv n_i e_i^2 \Big/ \sum_{i=1}^{s} n_i e_i^2 \quad (2.2.14)$$

$$\bar{\omega} \equiv \sum_{i=1}^{s}\mu_i\omega_i \quad (2.2.15)$$

$$t_i \equiv n_i e_i^2\omega_i \Big/ \sum_{i=1}^{s} n_i e_i^2\omega_i = \mu_i\omega_i/\bar{\omega} \quad (2.2.16)$$

Then eq. 2.2.13 can be written as

$$\nabla^2\nabla^2(\psi'_j/e_j) - \kappa^2\sum_{i=1}^{s}\frac{\bar{\omega}t_i}{\omega_i + \omega_j}\nabla^2(\psi'_j/e_j) - \kappa^2\sum_{i=1}^{s}\frac{\bar{\omega}t_i}{\omega_i + \omega_j}\nabla^2(\psi'_i/e_i) = -\frac{\kappa^2}{DkT}\left\{k_j - \sum_{i=1}^{s}\frac{\bar{\omega}t_i}{\omega_i + \omega_j}k_j - \sum_{i=1}^{s}\frac{\omega t_i}{\omega_i + \omega_j}k_i'\right\} \times \frac{\partial}{\partial x}\left(\frac{e^{-\kappa r}}{r}\right) \quad (2.2.17)$$

(9) L. Onsager, *J. Chem. Phys.*, **2**, 599 (1934).

Now, we define a function

$$d(\zeta) = \sum_{i=1}^{s} \frac{\tilde{\omega} t_i}{\omega_i + \zeta} \tag{2.2.18}$$

and a matrix **H** with elements

$$h_{ij} = d(\omega_j)\delta_{ji} + \frac{\tilde{\omega} t_i}{\omega_i + \omega_j} \tag{2.2.19}$$

where δ_{ji} is the Kronecker symbol

$$\delta_{ji} = \begin{cases} 1 & \text{for } j = i \\ 0 & \text{for } j \neq i \end{cases}$$

Then eq. 2.2.17 takes the following compact form

$$\nabla^2(\nabla^2\delta_{j\sigma} - \kappa^2 h_{j\sigma})\psi'_\sigma/e_\sigma = -\frac{\kappa^2}{DkT}(\delta_{j\sigma} - h_{j\sigma})k_\sigma \frac{\partial}{\partial x}\left(\frac{e^{-\kappa r}}{r}\right) \tag{2.2.20}$$

(Greek indices always imply summation over 1,2, . . . s).

III. The Solutions of the Differential Equation

3.1. Introduction.—In order to simplify the system of differential eq. 2.2.20 we propose to replace the system by s independent linear combinations of the form

$$\sum_{j=1}^{s} t_j\chi^p{}_j\nabla^2(\nabla^2\delta_{j\sigma} - \kappa^2 h_{j\sigma})\psi'_\sigma/e_\sigma$$

$$= -\frac{\kappa^2}{DkT}\sum_{j=1}^{s} t_j\chi^p{}_j(\delta_{j\sigma} - h_{j\sigma})k_\sigma \frac{\partial}{\partial x}\left(\frac{e^{-\kappa r}}{r}\right) \tag{3.1.1}$$

with the coefficients $t_j\chi^p{}_j$ which satisfy the set of homogeneous equations

$$\sum_{j=1}^{s} (t_j\chi^p{}_j)h_{ji} = q_p(t_i\chi^p{}_i);\ (p = 1, 2, \ldots, s) \tag{3.1.2}$$

If we can find a complete set of such linear combinations, the system becomes simply

$$\nabla^2(\nabla^2 - \kappa^2 q_p)Y_p = A_p \frac{\partial}{\partial x}\left(\frac{e^{-\kappa r}}{r}\right);\ (p = 1, 2, \ldots, s) \tag{3.1.3}$$

where

$$Y_p = t_\sigma\chi^p{}_\sigma\psi'_\sigma/e_\sigma \tag{3.1.4}$$

$$A_p = -\frac{\kappa^2}{DkT}(1 - q_p)(t_\sigma\chi^p{}_\sigma k_\sigma) \tag{3.1.5}$$

The differential eq. 3.1.3, all of the same type, are easily solved to determine $Y_1, Y_2, \ldots Y_s$; the system (3.1.4) of ordinary linear equations then determines the potentials $\psi'_1, \psi'_2, \ldots \psi'_s$. In view of the symmetry

$$t_i h_{ji} = t_j h_{ij} \tag{3.1.6}$$

the homogeneous eq. 3.1.2 may be written in the slightly simpler form

$$\sum_{i=1}^{s} h_{ji}\chi^p{}_i = q_p\chi^p{}_j \tag{3.1.7}$$

According to the general theory of linear equations, (3.1.7) is soluble if and only if the determinant of the coefficients vanishes. This determinant, considered as a function of q_p, is a polynomial of order s, and the condition that it vanishes amounts to an algebraic equation of order s, which is called the secular equation of the matrix $||h_{ji}||$

$$\begin{vmatrix} h_{11} - q & h_{12} & \cdots & h_{1s} \\ h_{21} & h_{22} - q & \cdots & h_{2s} \\ \cdots & \cdots & \cdots & \cdots \\ h_{s1} & h_{s2} & \cdots & h_{ss} - q \end{vmatrix} = 0 \tag{3.1.8}$$

The task before us: to find the roots of a secular equation—and to determine the corresponding "eigen vectors" $(\chi^p{}_j)$; $(p = 1.2 \ldots s' \leqslant s)$—is called an eigenwert problem; problems of this type are very common in applied mathematics.

Eigenvectors which correspond to separate roots of the secular equation form a linearly independent system; further investigation is needed to decide whether the number of appropriate eigen vectors equals the multiplicity of the root. Thanks to the symmetry (3.1.6) and the fact that $t_i > 0$ $(i = 1.2 \ldots s)$, the theory of quadratic forms guarantees a complete system of s independent eigen vectors which are real to boot, as are the roots of the secular equation.[6] Actually, the matrix (h_{ji}) lends itself to a special method of analysis which yields even more detailed information[7]; the case of coincident roots will require separate discussion but no difficulties will arise.

3.2. The Eigen Vectors of the Matrix H.—The s^2 elements of the matrix $||h_{ji}||$ are determined by the ratios of the $2s$ constants $\omega_1, \omega_2, \ldots \omega_s$; $t_1, t_2, \ldots t_s$. Accordingly, the matrix is of a rather special type. We can take advantage of its special properties to simplify the solution of its eigenwert problem.

We first observe the following identity in α

$$\sum_{i=1}^{s} \frac{\tilde{\omega} t_i}{(\omega_i + \omega_j)(\omega_i + \alpha)} = \sum_{i=1}^{s} \frac{\tilde{\omega} t_i}{(-\alpha + \omega_j)(\omega_i + \alpha)} + \frac{\tilde{\omega} t_i}{(\omega_i + \omega_j)(-\omega_j + \alpha)}\Big\} = \frac{d(\alpha)}{\omega_j - \alpha} - \frac{d(\omega_j)}{\omega_j - \alpha} \tag{3.2.1}$$

in the notation (2.2.18), and in view of (2.2.19)

$$\sum_{i=1}^{s} h_{ij}\left\{\frac{1}{\omega_i + \alpha} + \frac{1}{\omega_i - \alpha}\right\} = \frac{d(\alpha)}{\omega_j - \alpha} + \frac{d(-\alpha)}{\omega_j + \alpha} \tag{3.2.2}$$

Now, if we take α equal to one of the roots

$$\alpha_1 = 0, \pm\alpha_2, \ldots, \pm\alpha_s \tag{3.2.3}$$

of the equation

$$0 = d(\alpha_p) - d(-\alpha_p) = -2\tilde{\omega}\alpha_p \sum_{i=1}^{s} \frac{t_i}{\omega_i^2 - \alpha_p^2} \tag{3.2.4}$$

then eq. 3.2.2 becomes simply

$$\sum_{i=1}^{s} h_{ji}\frac{\omega_i}{\omega_i^2 - \alpha_p^2} = d(\alpha_p)\frac{\omega_j}{\omega_j^2 - \alpha_p^2} \tag{3.2.5}$$

and $\omega_j/(\omega_j^2 - \alpha_p^2)$ satisfies the following orthogonality relation

$$(\alpha_p^2 - \alpha_q^2)\sum_{i=1}^{s} \frac{t_i\omega_i^2}{(\omega_i^2 - \alpha_p^2)(\omega_i^2 - \alpha_q^2)} = \alpha_p^2 \sum_{i=1}^{s} \frac{t_i}{\omega_i^2 - \alpha_p^2} - \alpha_q^2 \sum_{i=1}^{s} \frac{t_i}{\omega_i^2 - \alpha_q^2} = 0 \tag{3.2.6}$$

We next define a function

$$\phi(\theta) = \frac{1}{2\tilde{\omega}}\theta^{1/2}(d(+\theta^{1/2}) - d(-\theta^{1/2})) \tag{3.2.7}$$

$$= -\theta\sum_{i=1}^{s} \frac{t_i}{\omega_i^2 - \theta} \tag{3.2.8}$$

$$= 1 - \sum_{i=1}^{s} \frac{t_i\omega_i^2}{\omega_i^2 - \theta} \tag{3.2.9}$$

By construction $\phi(\theta)$ has zeros for $\theta = \alpha_p^2$ ($p = 1,2, \ldots s$), poles for $\theta = \omega_i^2$ ($i = 1,2, \ldots s$) and $\phi(\theta) \to 1$ as $\theta \to \infty$. We may express it accordingly as a quotient of two polynomials, thus

$$\phi(\theta) \equiv \frac{\prod_{p=1}^{s} (\alpha_p^2 - \theta)}{\prod_{i=1}^{s} (\omega_i^2 - \theta)} \qquad (3.2.10)$$

Moreover, we may expand the reciprocal in partial fractions

$$1/\phi(\theta) \equiv 1 + \sum_{p=1}^{s} \frac{N_p^2}{\alpha_p^2 - \theta} \qquad (3.2.11)$$

To determine $N_1^2, N_2^2, \ldots N_s^2$ we observe that

$$1/N_p^2 = \lim_{\theta \to \alpha_p^2} \frac{\phi(\theta)}{(\alpha_p^2 - \theta)} = -\phi'(\alpha_p^2) = \sum_{i=1}^{s} \frac{t_i \omega_i^2}{(\omega_i^2 - \alpha_p^2)^2} \qquad (3.2.12)$$

The whole set of relations is quite symmetrical in ($\omega_1^2, \ldots \omega_s^2$; $t_1\omega_1^2, \ldots t_s\omega_s^2$) *versus* ($\alpha_1^2, \ldots \alpha_s^2$; $N_1^2, \ldots N_s^2$). Accordingly, we need only replace $\phi(\theta)$ by $1/\phi(\theta)$ to obtain

$$(\omega_j^2 - \omega_i^2) \sum_{p=1}^{s} \frac{N_p^2}{(\omega_j^2 - \alpha_p^2)(\omega_i^2 - \alpha_p^2)} = 0 \qquad (3.2.13)$$

as the counterpart of eq. 3.2.6 and

$$1/t_j\omega_j^2 = \sum_{p=1}^{s} \frac{N_p^2}{(\omega_j^2 - \alpha_p^2)^2} \qquad (3.2.14)$$

as the counterpart of eq. 3.2.12 by completely analogous derivations. We get another set of identities from eq. 3.2.9 and eq. 3.2.11

$$\sum_{p=1}^{s} \frac{t_i\omega_i^2}{\omega_i^2 - \alpha_p^2} = 1 \qquad (3.2.15)$$

$$\sum_{p=1}^{s} \frac{N_p^2}{\omega_i^2 - \alpha_p^2} = 1 \qquad (3.2.16)$$

upon using $\phi(\alpha_p^2) = 0$ and $1/\phi(\omega_i^2) = 0$.

This preparation enables us to construct the solution of the homogeneous eq. 3.1.7 explicitly for the case that mobilities $\omega_1, \omega_2, \ldots \omega_s$ are all different. The transference numbers $t_1, \ldots t_s$ are all positive and $\phi(\theta)$ increases from $-\infty$ to $+\infty$ as θ increases from ω_i^2 to ω_{i+1}^2. Accordingly, the zeros of $\phi(\theta)$ interlace with the poles as follows

$$0 = \alpha_1^2 < \omega_1^2 < \alpha_2^2 < \ldots < \alpha_s^2 < \omega_s^2 \qquad (3.2.17)$$

Now, we take

$$\chi^{p}{}_i = \frac{N_p\omega_i}{\omega_i^2 - \alpha_p^2} \qquad (3.2.18)$$

then by virtue of eq. 3.2.6 and 3.2.12 the orthogonality relations

$$\sum_{i=1}^{s} t_i \chi^{r}{}_i \chi^{q}{}_i = \delta_{pq} \qquad (3.2.19)$$

are valid, as are the reciprocal orthogonality relations

$$\sum_{p=1}^{s} t_j \chi^{p}{}_j \chi^{p}{}_i = \delta_{ji} \qquad (3.2.20)$$

by virtue of eq. 3.2.13 and 3.2.14. Finally, according to eq. 3.2.5 $\chi^{p}{}_i$ satisfies the homogeneous eq. 3.1.7

$$\sum_{i=1}^{s} h_{ji}\chi^{p}{}_i = q_p\chi^{p}{}_j$$

where

$$q_p = d(\alpha_p)\, d = (-\alpha_p) = \frac{1}{2}\left\{d(\alpha_p) + d(-\alpha_p)\right\} = \sum_{i=1}^{s} \frac{\tilde{\omega}_i\omega_i}{\omega_i^2 - \alpha_p^2} \qquad (3.2.21)$$

If we observe that $d(0) = 1$ and that $d(\zeta)$ is a decreasing function of ζ for $\zeta \geq 0$, we have

$$1 = q_1 > d(\omega_1) > q_2 > \ldots > q_s > d(\omega_s) > 0 \qquad (3.2.22)$$

For later use we express eq. 3.2.4 and eq. 3.2.21 by the eigen vectors χ^p

$$\sum_{i=1}^{s} \mu_i \chi^{p}{}_i = 0 \quad (p \neq 1) \qquad (3.2.23)$$

$$\sum_{i=1}^{s} t_i \chi^{p}{}_i = N_p q_p/\tilde{\omega} \qquad (3.2.24)$$

3.3. The Eigen Vectors in the Case of Confluence.—Whenever two or several of the absolute mobilities $\omega_1, \omega_2, \ldots \omega_s$ coincide

$$\omega_r = \omega_{r+1} = \ldots = \omega_{r+m} (\equiv \omega_c) \qquad (3.3.1)$$

then the intervals which enclose $\alpha_{r+1}, \ldots \alpha_{r+m}$ according to the condition (3.2.17) shrink to a single point

$$\alpha_{r+1} = \alpha_{r+2} = \ldots = \alpha_{r+m} = \omega_c \qquad (3.3.2)$$

Since the eigen values of a matrix are continuous functions of its elements, we must obtain an m-fold eigen value

$$q_{r+1} = q_{r+2} = \ldots = q_{r+m} = d(\omega_c) \equiv q_c \qquad (3.3.3)$$

For $m = 1$, this eigen value is still simple. It is degenerate for $m > 1$, that is, when at least three absolute mobilities coincide. In view of eq. 3.2.22 this is the only case in which our eigen value problem can have a degenerate solution.

Our formula (3.2.18) becomes indeterminate in the confluence, because the denominators vanish for those components which correspond to ions r, $r+1, \ldots r+m$, and in order to keep these components finite, the normalization factors N_{r+1}, $N_{r+2}, \ldots N_{r+m}$ must vanish too. Therefore, the components χ_i^p of these eigen vectors which correspond to ions not involved in the confluence vanish

$$\chi^{p}{}_i = 0 \quad \text{for } \omega_i \neq \omega_c = \alpha_p \qquad (3.3.4)$$

The remaining components $\chi^{p}{}_r, \chi_r^{p+1}, \ldots, \chi_r^{p+m}$ may be computed by a suitable limiting process, for example, taking $\omega_r = \omega_c$ and

$$\lim_{\omega_{r+m} \to \omega_c} \left(\lim_{\omega_{r+m-1} \to \omega_c} \left(\text{Lim} \ldots \left(\lim_{\omega_{r+2} \to \omega_c} \left(\lim_{\omega_{i+1} \to \omega_c} \frac{N_p\omega_i}{\omega_i^2 - \alpha_p^2} \right) \right) \cdots \right) \right)$$

This yields

$$\chi^{p}{}_r = \chi^{p}{}_{r+1} = \ldots = \chi^{p}{}_{p-1} = -\sqrt{\frac{t_p}{T_{p-1}T_p}},$$

$$\chi^{p}{}_p = \sqrt{\frac{T_{p-1}}{t_p T_p}}, \quad \chi^{p}{}_{p+1} = \chi^{p}{}_{p+2} = \ldots = \chi^{p}{}_{r+m} = 0 \qquad (3.3.5)$$

where

$$T_{p-1} = \sum_{i=r}^{p-1} t_i,\ T_p = \sum_{i=r}^{p} t_i;\ (p = r+1, \ldots r+m) \tag{3.3.6}$$

These eigen vectors satisfy all the relations which we have derived in the case of non-confluence. In the following calculation we only need to know the sum

$$\sum_{p=r+1}^{r+m} t_i \chi^p{}_i \chi^p{}_j = \left(\delta_{ij} - \frac{t_i}{T_{r+m}}\right) \delta(\omega_i, \omega_c)\delta(\omega_j, \omega_c)$$

where

$$T_{r+m} = \sum_{i=r}^{r+m} t_i,\ \delta(\omega_i, \omega_c) = \begin{cases} 0, \text{ for } \omega_i \neq \omega_c \\ 1 \text{ for } \omega_i = \omega_c \end{cases}$$

If confluences occur for more than one value (ω_c, ω_c', . . .) of ω, then each confluence can be dealt with in the same manner, quite independently of the others.

3.4. The Potential ψ'_j.—In order to obtain the potential ψ'_j, at first we have to solve the differential eq. 3.1.3

$$\nabla^2(\nabla^2 - \kappa^2 q_p)\, Y_p = A_p \frac{\partial}{\partial x}\left(\frac{e^{-\kappa r}}{r}\right)$$

where

$$Y_p = \sum_{i=1}^{s} t_i \chi^p{}_i \psi'_i / e_i \tag{3.4.1}$$

$$A_p = -\frac{\kappa^2}{DkT}(1 - q_p)(t_\sigma \chi^p{}_\sigma k_\sigma) \tag{3.4.2}$$

According to eq. 2.2.6 the potentials ψ'_i and their linear combination Y_p are functions of the type $\partial R(r)/\partial x = xR'(r)/r$. With this restriction the most general solution of the differential equation is

$$Y_p = \frac{A_p}{\kappa^2(1 - q_p)} \frac{\partial}{\partial x}\left\{\frac{e^{-\kappa r}}{\kappa^2 r} + B_1 \frac{e^{-\sqrt{q_p}\kappa r}}{r} + B_2 \frac{e^{\sqrt{q_p}\kappa r}}{r} + B_3 r^2 + B_4 \frac{1}{r}\right\}$$

where $B_1, \ldots B_4$ are constants to be determined by the boundary conditions that the potential ψ'_i as well as the charge density $(-\nabla^2\psi_i/D)$ approach zero for r $\cong \infty$ and remains finite for all values of r. Accordingly, our solution becomes

$$Y_p = \frac{1}{DkT}(t_\sigma \chi^p{}_\sigma k_\sigma) \frac{\partial}{\partial x}\left(\frac{1 - e^{-\kappa r}}{\kappa^2 r} - \frac{1 - e^{-\sqrt{q_p}\kappa r}}{q_p \kappa^2 r}\right) \tag{3.4.3}$$

If we multiply eq. 3.4.1 by $\chi^p{}_j$ and sum over $p = (1,2, \ldots s)$, the orthogonality condition of the eigen vector (3.2.20) yields

$$\psi_j' = e_j \sum_{p=1}^{s} \chi^p{}_j Y_p$$

Substituting eq. 3.4.3 into this, we obtain

$$\psi'_j = \frac{e_j}{DkT} \sum_{p=2}^{s} \chi^p{}_j (t_\sigma \chi^p{}_\sigma k_\sigma) \frac{\partial}{\partial x}\left(\frac{1 - e^{-\kappa r}}{\kappa^2 r} - \frac{1 - e^{-\sqrt{q_p}\kappa r}}{q_p \kappa^2 r}\right) \tag{3.4.4}$$

where we have used $q_1 = d(0) = 1$.

For $r \cong 0$, *i.e.*, in the vicinity of the central ion the potential ψ'_j can be described by power series of r

$$\psi'_j = \frac{e_j}{DkT} \sum_{p=2}^{s} \chi^p{}_j (t_\sigma \chi^p{}_\sigma k_\sigma) \left\{\frac{1}{3}(1 - \sqrt{q_p})\kappa x + \frac{1}{8}(1 - q_p)\kappa^2 x r + \kappa x O(\kappa^2 r^2)\right\} \tag{3.4.5}$$

so that the x-component of the field intensity equals

$$-\nabla_x \psi'_j = -\frac{\kappa e_j}{DkT} \sum_{p=2}^{s} (1 - \sqrt{q_p}) \chi^p{}_j (t_\sigma \chi^p{}_\sigma k_\sigma) \left\{\frac{1}{3} + \frac{(1 + \sqrt{q_p})}{8}\kappa r + \frac{(1 + \sqrt{q_p})}{8}\frac{\kappa x^2}{r} + O(\kappa^2 r^2)\right\} \tag{3.4.6}$$

Since κ^2 is proportional to the total concentration of the solution, all terms of the order κr will be small compared to 1 in the vicinity of the origin. Therefore the asymmetric field is fairly homogeneous in the vicinity of the central ion. For $r \cong \infty$, the potential ψ'_j tends to a dipolar potential

$$\psi_j' \cong K \frac{e_j}{DT} O\left(\frac{x}{\kappa^2 r^3}\right) \tag{3.4.7}$$

where K is a constant proportional to the applied force.

An alternative form of ψ'_j is of interest. From eq. 3.2.23 together with $q_1 = 1$, we have

$$\mu_\sigma \chi^p{}_\sigma \frac{\partial}{\partial x}\left(\frac{1 - e^{-\kappa r}}{\kappa^2 r} - \frac{1 - e^{-\sqrt{q_p}\kappa r}}{q_p \kappa^2 r}\right) = 0$$

and accordingly

$$\frac{e_j}{DkT\bar{\omega}} \sum_{p=1}^{s} \chi^p{}_j k_j \omega_j \mu_\sigma \chi^p{}_\sigma \frac{\partial}{\partial x}\left(\frac{1 - e^{-\kappa r}}{\kappa^2 r} - \frac{1 - e^{-\sqrt{q_p}\kappa r}}{q_p \kappa^2 r}\right) = 0$$

Subtracting this from eq. 3.4.4 we obtain

$$\psi'_i = \frac{-e_j}{DkT\bar{\omega}} \sum_{p=1}^{s} \chi^p{}_j \mu_\sigma \chi^p{}_\sigma (k_\sigma \omega_\sigma - k_j \omega_j) \times \frac{\partial}{\partial x}\left(\frac{1 - e^{-\sqrt{q_p}\kappa r}}{q_p \kappa^2 r}\right) \tag{3.4.8}$$

Therefore, if

$$k_1\omega_1 = k_2\omega_2 = \ldots = k_s\omega_s$$

then ψ'_j vanishes. This is an expected result because the perturbation term in eq. 2.2.9 vanishes under the condition.

The force due to the ionic atmosphere upon the central ion is determined by the asymmetric field $-\nabla\psi'_j$ at $r = 0$, which has only an x-component ΔX_j

$$\Delta X_j = -\nabla\psi'_j(0) = -\frac{\kappa e_j}{3DkT} \sum_{p=2}^{s} (1 - \sqrt{q_p}) \chi^p{}_j (t_\sigma \chi^p{}_\sigma k_\sigma) \tag{3.4.9}$$

$$= -\frac{\kappa e_j}{3DkT} \sum_{i=1}^{s} k_i \sum_{p=2}^{s} (1 - \sqrt{q_p}) \chi^p{}_j t_i \chi^p{}_i \tag{3.4.10}$$

Here we note that this field is proportional to the square root of the total concentration c of the system. In the course of the derivation we have, in fact, neglected all effects which would lead to terms of higher order. Equation 3.4.9 can be written in the following form analogous to eq. 3.4.8

$$\Delta X_j = \frac{\kappa e_j}{3DkT\bar{\omega}} \sum_{p=1}^{s} \sqrt{q_p} \chi^p{}_j \mu_\sigma \chi^p{}_\sigma (k_\sigma \omega_\sigma - k_j \omega_j) \tag{3.4.11}$$

3.5. The Distribution Function f'_{ji}.—We shall now compute the distribution function f'_{ji} from eq. 2.2.9

$$\nabla^2 f'_{ji} = \frac{n_j n_i e_j e_i}{kT(\omega_j + \omega_i)} \left\{ \frac{\omega_j}{e_i} \nabla^2 \psi'_i - \frac{\omega_i}{e_j} \nabla^2 \psi'_j - \frac{(\omega_i k_i - \omega_j k_j)}{DkT} \frac{\partial}{\partial x} \left(\frac{e^{-\kappa r}}{r} \right) \right\} \quad (3.5.1)$$

The distribution function f'_{ji} is of the same type as the potential and satisfies the same boundary condition as ψ'_j. Therefore, we immediately obtain

$$f'_{ji} = \frac{n_j n_i e_j e_i}{kT(\omega_j + \omega_i)} \left\{ \frac{\omega_j}{e_i} \psi'_i - \frac{\omega_i}{e_j} \psi_j' + \frac{\omega_i k_i - \omega_j k_j}{DkT} \frac{\partial}{\partial x} \left(\frac{1 - e^{-\kappa r}}{\kappa^2 r} \right) \right\} \quad (3.5.2)$$

Substituting the explicit formulas for the potentials (3.4.4), we have

$$f_{ji}' = \frac{n_j n_i e_j e_i}{D(kT)^2(\omega_j + \omega_i)} \left\{ \sum_{p=2}^{s} (\omega_i \chi^{p_i} - \omega_i \chi^{p_j})(\chi^{p\sigma} t_\sigma k_\sigma) \times \frac{\partial}{\partial x} \left(\frac{1 - e^{-\kappa r}}{\kappa^2 r} - \frac{1 - e^{-\sqrt{q_p}\kappa r}}{q_p \kappa^2 r} \right) + (\omega_i k_i - \omega_j k_j) \frac{\partial}{\partial x} \left(\frac{1 - e^{-\kappa r}}{\kappa^2 r} \right) \right\} \quad (3.5.3)$$

In the case $s = 2$, and in the case of complete confluence ($\omega_1 = \omega_2 = \ldots = \omega_s$), all $\partial/\partial x\ (1/r)$ terms in equation 3.5.3 drop out, but in general for $r \cong \infty$

$$f'_{ji} \cong K \frac{n_j n_i e_j e_i}{D(kT)^2} O\left(\frac{x}{\kappa^2 r^3} \right)$$

where K is a constant proportional to the external force. Thus the ionic atmosphere extends farther than it does in the unperturbed case.

3.6. The Ionic Field Acting on Tracer Ions.—We consider an electrolytic solution which contains ions of species, 1, 2, ... s and l where one of the ionic species, say l, is present in very small concentration so that the transference number of the l-th ion (t_l) is almost zero. This special condition allows an explicit specification of the eigen vector and eigen value corresponding to the ion.

The fundamental eq. 3.2.4 can be written as

$$(\omega_l^2 - \alpha_p^2)\left(\sum_{i=1}^{s} \frac{t_i}{\omega_i^2 - \alpha_p^2} \right) + t_l = 0 \quad (3.6.1)$$

Therefore, if t_l tends to zero, one of the roots, α_p, tends to ω_l and the other roots, α_p, are determined by

$$\alpha_p \sum_{i=1}^{s} \frac{t_i}{\omega_i^2 - \alpha_p^2} = 0$$

as before. We shall denote by α_l the particular root of α_p which tends to ω_l. Then we have from eq. 3.6.1

$$\lim_{t_l \to 0} \frac{t_l}{\omega_l^2 - \alpha_l^2} = -\sum_{i=1}^{s} \frac{t_i}{\omega_i^2 - \omega_l^2} < \infty \quad (3.6.2)$$

where we have assumed $\omega_l \neq \omega_i$ and $i = 1,2,3 \ldots s$. From eq. 3.2.12 the normalization constant of the l-ion is given by

$$\frac{1}{N_l^2} = \frac{t_l \omega_l^2}{(\omega_l^2 - \alpha_l^2)^2} + \sum_{i=1}^{s} \frac{t_i \omega_i^2}{(\omega_i^2 - \alpha_l^2)^2}$$

From this and eq. 3.6.2 we obtain

$$\lim_{t_l \to 0} N_l = 0, \quad \lim_{t_l \to 0} \frac{N_l^2 t_l \omega_l^2}{(\omega_l^2 - \alpha_l^2)^2} = 1$$

Therefore, the eigen vector corresponding to the l-ion satisfies the following condition in the limit of $t_l \to 0$

$$t_l \chi_l{}^l \chi_l{}^l = 1 \quad \chi_i{}^l = 0;\ i = 1, 2, \ldots s \quad (3.6.3)$$

and the eigen value q_l equals $d(\omega_l)$.

We are now ready to compute the potential ψ_l'. Substituting eq. 3.6.3 into eq. 3.4.4 we obtain

$$\psi_l' = \frac{e_l}{DkT} \left\{ k_l \frac{\partial \Phi_l}{\partial x} + \sum_{p=2}^{s} \chi^{p_l} \sum_{i=1}^{s} t_i \chi^{p_i} k_i \frac{\partial \Phi_p}{\partial x} \right\} \quad (3.6.4)$$

where

$$\Phi_n(r) = \frac{1 - e^{-\kappa r}}{\kappa^2 r} - \frac{1 - e^{-\sqrt{q_n}\kappa r}}{q_n \kappa^2 r}$$

$(n = 1, 2, \ldots s \text{ and } l)$

and

$$q_l = d(\omega_l), \quad \chi^{p_l} = \frac{N_p \omega_l}{\omega_l^2 - \alpha_p^2}$$

From eq. 3.4.9, the field acting on an l-ion is given by

$$\Delta X_l = -\frac{\kappa e_l}{3DkT} \left\{ (1 - \sqrt{d(\omega_l)})\, k_l + \sum_{p=2}^{s} (1 - \sqrt{q_p}) \chi^{p_l} \sum_{i=1}^{s} (t_i k_i \chi^{p_i}) \right\} \quad (3.6.5)$$

From eq. 3.5.3 the additional distribution function for the ion pair (l,i) is given by

$$-f'_{il} = f'_{li} = -\frac{n_l n_i e_l e_i}{D(kT)^2(\omega_l + \omega_i)} \left\{ (\omega_l k_l - \omega_i k_i) \frac{\partial}{\partial x} \left(\frac{1 - e^{-\kappa r}}{\kappa^2 r} \right) + \omega_i k_l \frac{\partial \Phi_l}{\partial x} + \sum_{i=1}^{s} k_i \sum_{p=1}^{s} (\omega_i \chi^{p_l} - \omega_l \chi^{p_i}) \frac{\partial \Phi_p}{\partial x} \right\} \quad (3.6.6)$$

Here we note that n_l is very small compared with $n_i (i \neq l)$.

IV. Conduction and Diffusion

4.1. Migration of Ions.—The problem of ions migrating in a general homogeneous field has been discussed completely by Onsager and Fuoss.[6] We shall review briefly the previous work to the extent required for our treatment of the effect due to the asymmetric ionic atmosphere. We designate the homogeneous external forces by $\mathbf{k}_1, \ldots \mathbf{k}_s$ (per ion) acting on ions of species 1,2, ... s, respectively, and a balancing force

$$n_0 \mathbf{k}_0 = -\sum_{i=1}^{s} n_i \mathbf{k}_i \quad (4.1.1)$$

acting on the molecules of the solvent. Then, as has been shown by Onsager and Fuoss on the basis of thermodynamics, such a system of forces is equivalent to a combination of a homogeneous electric field $\mathbf{E} = -\nabla\varphi$ and uniform concentration gradients $\nabla n_1, \nabla n_2, \ldots \nabla n_s$, subject to the restriction of electrical neutrality

$$\sum_{i=1}^{s} e_i \nabla n_i = \nabla \sum_{i=1}^{s} n_i e_i = \nabla(0) = 0 \quad (4.1.2)$$

Denoting the electro-chemical potential of an ion or molecule by μ_j, we can write

$$\mu_j = \mu_j' + e_j\varphi$$

where μ_j' stands for the purely chemical potential. The separation of μ_j into two parts is possible according to molecular theory; but only the sum enters into thermodynamic relations and can be measured by corresponding experiments. We cannot expect to obtain information about the actual static potentials from diffusion experiments. For the purpose of thermodynamics, a non-operational convention about the separation is of course admissible if self-consistent.

Now, the statement of Onsager and Fuoss is as follows: if the forces $\mathbf{k}_j$ equal the electro-chemical forces

$$\mathbf{k}_j = -\nabla\mu_j = -\nabla(\mu_j' + e_j\varphi) \qquad (4.1.3)$$

both forces will cause the same migration of ions. With this extended concept of "the forces" $\mathbf{k}$ we shall treat the conduction and diffusion of ions in one combined scheme.

We shall first compute the velocity of an ion in the solution. In the limit of very low concentrations, only the friction of the solvent need be considered, so that the velocity $\mathbf{v}_j$ of a j-ion is given by

$$\mathbf{v}_j = \mathbf{k}_j/\rho_j = \omega_j\mathbf{k}_j \qquad (4.1.4)$$

In the case of finite concentrations, however, two further effects must be considered, namely, the additional field ($\Delta\mathbf{X}_j$) due to the asymmetric atmosphere caused by the force $\mathbf{k}_j$ and the electrophoretic flow $\Delta\mathbf{v}_j$ of the medium surrounding a j-ion. Therefore, we have

$$\mathbf{v}_j = \omega_j(\mathbf{k}_j + e_j\Delta\mathbf{X}_j) + \Delta\mathbf{v}_j \qquad (4.1.5)$$

The electrophoretic effect was first recognized by Debye and Hückel[1] and discussed completely by Onsager and Fuoss.[6] The result of Onsager and Fuoss is

$$\Delta\mathbf{v}_j = -\frac{2e_j}{3\eta\kappa DkT}(n_\sigma e_\sigma \mathbf{k}_\sigma) \qquad (4.1.6)$$

where we have omitted terms of order higher than the square root of the total concentration in view of other comparable approximations.

In the case of $s = 2$, the condition for pure diffusion is

$$0 = \mathbf{i} = n_1e_1\mathbf{v}_1 + n_2e_2\mathbf{v}_2$$

and the electro-neutrality condition is

$$n_1e_1 + n_2e_2 = 0$$

Therefore, we have

$$\mathbf{v}_1 = \mathbf{v}_2$$

That is, all ions move with the same velocity so that the asymmetric ionic atmosphere should vanish ($\psi'_j = 0$). This can also be seen from eq. 3.4.8. In this case, the diffusion problem was treated more elaborately by Onsager and Fuoss[6] using the more precise expression for $\Delta\mathbf{v}_j$.

4.2. Electrical Conductance in a Mixed Electrolyte.—The pure electrical conduction is characterized by the condition that there are no concentration gradients. Therefore, $\nabla\mu_i'$ vanishes and the force $\mathbf{k}_j$ equals $e_j\mathbf{X}$ where $\mathbf{X}$ is the applied electric field. Thus we have from eq. 4.1.5 and 4.1.6

$$\mathbf{v}_j = \mathbf{X}\left(e_j\omega_j - \frac{\kappa e_j}{6\pi\eta} + e_j\omega_j\frac{\Delta X_j}{X}\right) \qquad (4.2.1)$$

Accordingly, the electric current density $\mathbf{i}$ is given by

$$\mathbf{i} = \sum_{j=1}^{s} n_je_j\mathbf{v}_j = \mathbf{X}\lambda^\circ\left(1 - \frac{\kappa}{6\pi\eta\bar{\omega}} + \sum_{j=1}^{s}\frac{t_j\Delta X_j}{X}\right)$$

where λ^0 is the limiting specific conductance

$$\lambda^0 = \sum_{j=1}^{s} n_je_j^2\omega_j$$

Substituting eq. 3.4.9 for ΔX_j we have for the contribution ($\Delta\lambda$) to the specific conductivity from the asymmetric atmosphere

$$\Delta\lambda/\lambda^\circ = \sum_{j=1}^{s} t_j\Delta X_j/X =$$

$$-\frac{\kappa}{3DkT}\sum_{p=2}^{s}(1-\sqrt{q_p})\left(\sum_{i=1}^{s}e_it_i\chi^p{}_i\right)^2 \qquad (4.2.2)$$

The mobility $\bar{u}_j = |v_j|/|X|$ is given by

$$\bar{u}_j = \bar{u}_j^\circ\left(1 - \frac{\kappa}{6\pi\eta\omega_j} + \frac{\Delta X_j}{X}\right) \qquad (4.2.3)$$

where $\bar{u}_j^\circ$ is the limiting mobility for infinite dilution equal to $|e_j|\omega_j$ in electrostatic units or $|e_j|\omega_j/300$ in practical units (cm.^{2}/sec. volt). Since the equivalent conductance Λ_j equals 96500 $\bar{u}_j$ in practical units (ohm^{-1} cm.^{2} mole^{-1}), we have

$$\Lambda_j = \Lambda_j^\circ - \frac{965\kappa|e_j|}{18\pi\eta} + \Lambda_j^\circ\frac{\Delta X_j}{X} \qquad (4.2.4)$$

where Λ_j° is the limiting equivalent conductance of j-ions

$$\Lambda_j^\circ = \frac{965}{3}|e_j|\omega_j$$

Substituting the explicit formula of ΔX_j, eq. (3.4.9), and the definition of κ into eq. 4.2.4, we obtain

$$\Lambda_j = \Lambda_j^\circ - \left\{\frac{965}{18}\frac{N_A\epsilon^2}{\sqrt{250\pi R}}\frac{|z_j|}{\eta(DT)^{1/2}} + \right.$$

$$\left.\Lambda_j^\circ\sqrt{\frac{\pi}{250R}}\frac{N_A{}^2\epsilon^3}{3R}\frac{z_j}{(DT)^{3/2}}\sum_{p=2}^{s}(1-\sqrt{q_p})\chi^p{}_j(z_\sigma l_\sigma\chi^p{}_\sigma)\right\}\Gamma^{1/2} \qquad (4.2.5)$$

where N_A is the Avogadro number, R the molar gas constant (c.g.s.), ϵ the absolute electronic charge (e.s.u.), z_i the positive or negative valence of i-th ions, and Γ is the ionic strength of the solution defined in terms of the molar concentration m_i (moles/1000 cm.^{3}) as

$$\Gamma = \sum_{i=1}^{s} m_iz_i^2$$

Using Birge's[10] values of the physical constants we have the following final result

$$\Lambda_j = \Lambda_j^\circ - \left\{\frac{29.16|z_j|}{\eta(DT)^{1/2}} + \right.$$

$$\left.\Lambda_j^\circ\frac{1.981\times10^6}{(DT)^{3/2}}z_j\sum_{p=2}^{s}(1-\sqrt{q_p})\chi^p{}_j(z_\sigma l_\sigma\chi^p{}_\sigma)\right\}\Gamma^{1/2} \qquad (4.2.6)$$

4.3. The Dissipation Function for a Mixed Electrolyte.—The phenomenological law for conduction and diffusion in an electrolytic solution may be expressed as

(10) R. T. Birge, *Rev. Mod. Phys.*, **13**, 233 (1941).

$$\mathbf{J}_j = -\sum_{i=1}^{s} \Omega_{ji}\nabla\mu_i \qquad (4.3.1)$$

where $\mathbf{J}_j$ is the flow (ions/cm.^{2}) of j-ions and $-\nabla\mu_i = \mathbf{k}_i$ is the electrochemical force acting on an i-ion. The matrix of coefficients $||\Omega_{ji}||$ satisfies Onsager's reciprocal relation[6,11]

$$\Omega_{ji} = \Omega_{ij} \qquad (4.3.2)$$

This relation was derived from the assumption of microscopic reversibility. To obtain a simple formulation of laws for combined conduction and diffusion, it is convenient to express the "forces" in terms of the flow as

$$\mathbf{k}_j = -\nabla\mu_j = \sum_{i=1}^{s} R_{ji}\mathbf{J}_i \qquad (4.3.3)$$

where the matrix of coefficients $||R_{ji}||$ is the reciprocal matrix of $||\Omega_{ji}||$. On account of the symmetry of the latter, $||R_{ji}||$ also satisfies the symmetry relation

$$R_{ji} = R_{ij} \qquad (4.3.4)$$

Thanks to this symmetry, we need only know the dissipation-function

$$2F(\mathbf{J}\cdot\mathbf{J}) = \sum_{j,i=1}^{s} R_{ji}(\mathbf{J}_j\cdot\mathbf{J}_i) \qquad (4.3.5)$$

and eq. 4.3.3 can be written in the form

$$\mathbf{k}_j = -\nabla\mu_j = \frac{\partial F}{\partial \mathbf{J}_j} \qquad (4.3.6)$$

We shall obtain the explicit formula for R_{ji}. Since the flow J_j equals $n_j\mathbf{v}_j$, in the limit of very low concentration we have from eq. 4.1.4

$$-\nabla\mu_j = \mathbf{k}_j = \frac{1}{n_j\omega_j}\mathbf{J}_j = \frac{\rho_j}{n_j}\mathbf{J}_j \qquad (4.3.7)$$

In this case the matrix $||R_{ji}||$ is diagonal. At finite concentration, we have from eq. 4.1.5

$$-\nabla\mu_j = \mathbf{k}_j = (\rho_j/n_j)\mathbf{J}_j - \rho_j\Delta\mathbf{v}_j - e_j\Delta\mathbf{X}_j \qquad (4.3.8)$$

where the terms on the right represent, in the order given, the friction of the ion against the solvent, and the electrophoretic velocity and the ionic field at the center of the atmosphere. Since we have neglected the terms of order higher than $c^{1/2}$ in $\Delta\mathbf{v}_j$ and $\Delta\mathbf{X}_j$, it is sufficient to substitute the zeroth order approximation (4.3.7) for the forces $\mathbf{k}_j$ in $\Delta\mathbf{v}_j$ and $\Delta\mathbf{X}_j$. Therefore, we obtain from eq. 4.1.6

$$-\rho_j\Delta\mathbf{v}_j = \frac{2}{3\eta\kappa D\bar{k}T}\sum_{i=1}^{s} e_jc_i\rho_j\rho_i\mathbf{J}_i \equiv \sum_{i=1}^{s} R'_{ji}\mathbf{J}_i \qquad (4.3.9)$$

and from eq. 3.4.10

$$-e_j\Delta\mathbf{X}_j = \frac{\kappa}{3\lambda^\circ D\bar{k}T}\sum_{i=1}^{s}\left(\sum_{p=2}^{s}(1-\sqrt{q_p})\chi^{p}_{j}\chi^{p}_{i}\right)e_j^2e_i^2\mathbf{J}_i \equiv \sum_{i=1}^{s} R''_{ji}\mathbf{J}_i \qquad (4.3.10)$$

Thus, we obtain for R_{ji}

$$R_{ji} = (\rho_j/n_j)\delta_{ji} + R'_{ji} + R''_{ji} \qquad (4.3.11)$$

and for the "force"

$$-\nabla\mu_j = \mathbf{k}_j = \sum_{i=1}^{s} R_{ji}\mathbf{J}_i = \sum_{i=1}^{s}((\rho_j/n_j)\delta_{ji} + R'_{ji} + R''_{ji})\mathbf{J}_i \qquad (4.3.12)$$

(11) L. Onsager, *Phys. Rev.*, **37**, 405 (193).

Here we point out that the matrix $||R_{ji}||$ is symmetric as required by equation 4.3.4, since the first term in eq. 4.3.11 is diagonal and R'_{ji} and R''_{ji} are both symmetric. Now, the dissipation function takes the form

$$2F(\mathbf{J}\cdot\mathbf{J}) = \sum_{j=1}^{s}\sum_{i=1}^{s} R_{ji}\mathbf{J}_j\mathbf{J}_i = (\rho_\sigma/n_\sigma)\mathbf{J}_\sigma^2 + \frac{2}{3\eta\kappa D\bar{k}T}(e_\sigma\rho_\sigma\mathbf{J}_\sigma)^2 + \frac{\kappa}{3\lambda^\circ D\bar{k}T}\sum_{p=2}^{s}(1-\sqrt{q_p})(\chi^{p}_{\sigma}e^2_\sigma\mathbf{J}_\sigma)^2 \qquad (4.3.13)$$

We note that the three terms on the right are all positive ($1 \geqslant q_p$). Therefore, all three effects consume the free energy of the system because the dissipation function is equal to $T\dot{S}$ where T is the temperature of the system and $\dot{S}$ is the rate of creation of entropy per unit volume so that the dissipation function equals the rate of dissipation of free energy at constant temperature.

We shall next prove that the ionic contribution to the dissipation function $2F'' = \sum_{j,i} R''_{ij}\mathbf{J}_j\cdot\mathbf{J}_i$ vanishes when the velocities of all ions are equal

$$\mathbf{J}_1/n_1 = \mathbf{J}_2/n_2 = \ldots = \mathbf{J}_s/n_s = \mathbf{v}_1 = \mathbf{v}_2 = \ldots = \mathbf{v}_s \qquad (4.3.14)$$

This is what we should expect, because a simultaneous displacement of all ions will not disturb the ionic atmosphere (eq. 3.4.8). We shall express $2F''$ in terms of the velocities of the ions. Substituting $\mathbf{J}_i = n_i\mathbf{v}_i$ into $2F''$ we obtain

$$2F'' = \sum_{j=1}^{s} R_{ji}''n_jn_i\mathbf{v}_j\cdot\mathbf{v}_i = \frac{\kappa^3}{12\pi\tilde{\omega}}\sum_{p=2}^{s}(1-\sqrt{q_p})\left(\sum_{i=1}^{s}\chi^{p}_{i}\mu_i\mathbf{v}_i\right)^2 \qquad (4.3.15)$$

From eq. 3.2.23 and $q_1 = 1$, we have

$$\sum_{p=1}^{s}(1-\sqrt{q_p})\chi^{p}_{j}\sum_{i=1}^{s}\chi^{p}_{i}\mu_i = 0$$

and accordingly

$$\sum_{i=1}^{s} R''_{ji}n_i = \sum_{i=1}^{s} n_iR''_{ji} = 0 \qquad (4.3.16)$$

By means of this equation $2F''$ can be written as

$$2F'' = -\sum_{j>i}^{s} R''_{ji}n_jn_i(\mathbf{v}_j - \mathbf{v}_i)^2 = \frac{\kappa^3}{12\pi\tilde{\omega}}\sum_{j>i}^{s}\sum_{p=1}^{s}\sqrt{q_p}\chi^{p}_{j}\chi^{p}_{i}\mu_j\mu_i(\mathbf{v}_j - \mathbf{v}_i)^2 \qquad (4.3.17)$$

This clearly vanishes when the velocities of all ions are equal. We shall show in V that non-diagonal elements of the matrix R''_{ji} are all negative, (whereas the diagonal elements are all positive.)

We point out here that in the dissipation function $F(\mathbf{J}\cdot\mathbf{J})$ the friction of the solvent yields the term of order c, and the electrophoretic effect and relaxation effect yield the term of order $c^{3/2}$ where c is the total concentration of the system.

V. Integral Representation of the Matrix R''

5.1. Introduction.—If we know the matrix $[\lambda\mathbf{E} - \mathbf{A}]^{-1}$ where λ is an arbitrary constant, $\mathbf{E}$ is the unit matrix, and $\mathbf{A}$ is the matrix which has eigen

values $\alpha_1^2, \alpha_2^2, \ldots \alpha_s^2$ corresponding to the eigen vectors $\chi^1, \chi^2 \ldots \chi^s$, respectively, then the matrix $[\sqrt{\mathbf{H}} - \mathbf{E}]$, where $\mathbf{H}$ is the matrix with eigen values q_p corresponding to the eigen vectors χ^p, can be expressed by the integral

$$[\sqrt{\mathbf{H}} - \mathbf{E}] = \frac{1}{2\pi i} \oint_c (\sqrt{d(z^{1/2})} - 1)[z\,\mathbf{E} - \mathbf{A}]^{-1} dz$$

where C is a contour to be specified presently.

We shall see in the following that

$$R''_{ji} = -\frac{\kappa}{3\lambda^\circ DkT} \frac{e_j^2 e_i^2}{t_i} [\sqrt{\mathbf{H}} - \mathbf{E}]_{ji}$$

where R''_{ji} is the matrix elements defined by eq. 4.3.10. Therefore, if we can evaluate the contour integral we can obtain the dissipation function completely.

5.2. Functions of the Matrix H.—A function of the matrix $\mathbf{H}$ is defined by

$$f(\mathbf{H})\chi^p = f(q_p)\chi^p, (p = 1, 2, \ldots s) \quad (5.2.1)$$

where $f(t)$ is a single-valued but otherwise a general function of t. It is easy to prove that the matrix $f(\mathbf{H})$ commutes with $\mathbf{H}$ and conversely that all of the matrices which commute with $\mathbf{H}$ must be functions of $\mathbf{H}$ if $\mathbf{H}$ has a non-degenerate set of eigen values.

According to the orthogonality relation, (3.2.20), for the eigen vectors χ^p, the matrix $f(\mathbf{H})$ satisfies the following expansion formula

$$f(\mathbf{H})_{ji} = \sum_{\nu=1}^{s} f(\mathbf{H})_{j\nu}\delta_{\nu i} = \sum_{p=1}^{s}\sum_{\nu=1}^{s} f(\mathbf{H})_{j\nu}\chi^{p}{}_{\nu} t_i \chi^{p}{}_{i} = \sum_{p=1}^{s} f(q_p)\chi^{p}{}_{j} t_i \chi^{p}{}_{i} \quad (5.2.2)$$

From this, we have the symmetry relation

$$t_j f(\mathbf{H})_{ji} = t_i f(\mathbf{H})_{ij} \quad (5.2.3)$$

which is analogous to eq. 3.1.6.

If we substitute the expression for the eigen vectors χ^p

$$\chi^{p}{}_{j} = \frac{N_p \omega_j}{\omega_j^2 - \alpha_p^2} \quad (5.2.4)$$

into eq. 5.2.2 and expand into partial fractions, we immediately see that the off-diagonal elements of $f(\mathbf{H})$ take the following simple forms

$$f(\mathbf{H})_{ji} = -\omega_j \omega_i t_i \frac{\beta_j - \beta_i}{\omega_j^2 - \omega_i^2}; (j \neq i) \quad (5.2.5)$$

where

$$\beta_j = \sum_{p=1}^{s} f(q_p) N_p^2/(\omega_i^2 - \alpha_p^2)$$

The diagonal elements of the matrix $f(\mathbf{H})$ can be expressed in terms of off-diagonal elements. From eq. 3.2.23, we have

$$\sum_{p=1}^{s}\sum_{i=1}^{s} \{f(q_p) - f(1)\}\chi^{p}{}_{j}\mu_i \chi^{p}{}_{i} = \sum_{i=1}^{s} \frac{\bar{\omega}}{\omega_i} [f(\mathbf{H}) - f(\mathbf{E})]_{ji} = 0$$

and accordingly

$$[f(\mathbf{H}) - f(\mathbf{E})]_{jj} = -\sum_{i \neq j}^{s} \frac{\omega_j}{\omega_i} f(\mathbf{H})_{ji} \quad (5.2.6)$$

We are particularly interested in the matrix, $||R''_{ji}||$, whose elements are given by eq. 4.3.10, *i.e.*

$$R''_{ji} = \frac{\kappa}{3\lambda^\circ DkT} \sum_{p=1}^{s} (1 - \sqrt{q_p})\chi^{p}{}_{j}\chi^{p}{}_{i} e_i^2 e_i^2$$

If we compare this with eq. 5.2.2, we immediately obtain

$$R''_{ji} = -\frac{\kappa}{3\lambda^\circ DkT} \frac{e_j^2 e_i^2}{t_i} [\sqrt{\mathbf{H}} - \mathbf{E}]_{ji} \quad (5.2.7)$$

In order to determine the explicit formula of the matrix $[\sqrt{\mathbf{H}} - \mathbf{E}]$ we need to know the matrix elements of $\mathbf{A}$ and $[\lambda\mathbf{E} - \mathbf{A}]^{-1}$ defined in (5.1).

(1) **A Matrix A.**—According to the expansion formula (5.2.2), the elements of the matrix $\mathbf{A}$ which has the set of eigen values α_p^2 $(p = 1, 2, \ldots s)$ corresponding to the eigen vectors χ^p are given by

$$a_{ji} = \sum_{p=1}^{s} \alpha_p^2 \chi^{p}{}_{j} t_i \chi^{p}{}_{i} \quad (5.2.8)$$

We substitute the expressions for $\chi^{p}{}_{j}$, then with the aid of the orthogonality relations for the eigen vectors and the identity (3.2.16) we may obtain

$$a_{ji} = \omega_j^2 \delta_{ji} - \omega_j \omega_i t_i \quad (5.2.9)$$

This admits a "β-representation" according to eq. 5.2.5, with

$$\beta_j - \beta_i = \omega_j^2 - \omega_i^2$$

(2) **The Matrix $[\lambda\mathbf{E} - \mathbf{A}]^{-1}$.**—We shall next compute the elements of the matrix $[\lambda\mathbf{E} - \mathbf{A}]^{-1}$ where λ is an arbitrary constant and $\mathbf{E}$ is a unit matrix. From the expansion formula (5.2.2), we obtain

$$\|[\lambda\,\mathbf{E} - \mathbf{A}]^{-1}\|_{ji} = \sum_{p=1}^{s} \frac{1}{(\lambda - \alpha_p^2)} \chi^{p}{}_{j} t_i \chi^{p}{}_{i} \quad (5.2.10)$$

Using the relation

$$\frac{1}{(\lambda - \alpha_p^2)} \chi^{p}{}_{j} = \frac{N_p \omega_j}{(\lambda - \alpha_p^2)(\omega_j^2 - \alpha_p^2)} = \frac{N_p \omega_j}{(\lambda - \alpha_p^2)(\omega_j^2 - \lambda)} + \frac{N_p \omega_j}{(\lambda - \omega_j^2)(\omega_j^2 - \alpha_p^2)} \quad (5.2.11)$$

the orthogonality relation for χ^p and eq. 3.2.8, 3.2.16, we obtain

$$\|[\lambda\mathbf{E} - \mathbf{A}]^{-1}\|_{ji} = \frac{\delta_{ji}}{(\lambda - \omega_j^2)} - \frac{\omega_j \omega_i t_i}{(\lambda - \omega_j^2)(\lambda - \omega_i^2)\phi(\lambda)} \quad (5.2.12)$$

The only singularities of this expression are poles at the zeros, $\lambda = \alpha_1^2, \alpha_2^2, \ldots \alpha_s^2$, of $\phi(\lambda)$. According to the explicit description for $\phi(\lambda)$ given by eq. 3.2.10, the apparent poles at $\lambda = \omega_j^2$, $\lambda = \omega_i^2$ are cancelled by poles of $\phi(\lambda)$ whenever $j \neq i$, and even when $j = i$, a detailed calculation reveals that the apparent pole of order two is no singularity at all.

5.3. Integral Representation of the Matrix R''.—We consider the function $d(\zeta)$ (equation 2.2.18) of the complex variable ζ, which is analytic at all points except the points $\zeta = -\omega_1, -\omega_2, \ldots -\omega_s$. Since $q_p = d(\alpha_p)$, we have by means of Cauchy's theorem

$$\sqrt{q_p} - 1 = \frac{1}{2\pi i} \oint_c \frac{\sqrt{d(z^{1/2})} - 1}{(z - \alpha_p^2)} dz \quad (5.3.1)$$

$$(p = 1, 2, \ldots s)$$

where C is a contour entirely to the right of the

imaginary axis surrounding the points α_2^2, α_3^2. . . . α_s^2, which are all greater than ω_1^2 (*cf.* Fig. 1), and we take the principal values of $\sqrt{d(z^{1/2})}$. Since $d(0) = q_1 = 1$, it does not matter that the point $z = \alpha_1 = 0$ is outside of the contour C, eq. (5.3.1) is valid for $p = 1$ as well. According to eq. 5.2.2, we have for the elements of the matrix $[\sqrt{\mathbf{H}} - \mathbf{E}]$

$$[\sqrt{\mathbf{H}} - \mathbf{E}]_{ji} = \sum_{p=1}^{s} (\sqrt{q_p} - 1)\chi^{p}{}_{j} t_i \chi^{p}{}_{i} \quad (5.3.2)$$

Substituting eq. 5.3.1 into this, we obtain

$$[\sqrt{\mathbf{H}} - \mathbf{E}]_{ji} = \frac{1}{2\pi i}\oint_C \sqrt{d(z^{1/2})} - 1)\left(\sum_{p=1}^{s} \frac{1}{z - \alpha_p{}^2}\, \chi^{p}{}_{j} t_i \chi^{p}{}_{i}\right) dz = \frac{1}{2\pi i}\oint_C (\sqrt{(d(z^{1/2})} - 1)\left(\frac{\delta_{ji}}{z - \omega_j{}^2} - \frac{\omega_j\omega_i t_i}{(z - \omega_j{}^2)(z - \omega_i{}^2)\phi(z)}\right)dz \quad (5.3.3)$$

where we have used eq. 5.2.10 and 5.2.12.

We first consider the off-diagonal elements. Substituting $z = \zeta^2$ into eq. (5.3.3) we have for $j \neq i$

$$(\sqrt{\mathbf{H}})_{ji} = -\frac{\omega_j\omega_i t_i}{2\pi i}\oint_C \frac{2\zeta(\sqrt{d(\zeta)} - 1)}{(\zeta^2 - \omega_j{}^2)(\zeta^2 - \omega_i{}^2)\phi(\zeta^2)} d\zeta$$

where the contour C can be taken as before. We note that as $|\zeta| \to \infty$

$$\phi(\zeta^2) \to 1,\ d(\zeta) \to 0$$

and as $\zeta \to 0$

$$\phi(\zeta^2) = O(\zeta^2),\ \sqrt{d(\zeta)} - 1 = O(\zeta)$$

Therefore, we can deform the contour to obtain the following integral

$$(\sqrt{\mathbf{H}})_{ji} = \frac{\omega_j\omega_i t_i}{2\pi i}\int_{-i\infty}^{i\infty} \frac{2\zeta(\sqrt{d(\zeta)} - 1)}{(\zeta^2 - \omega_j{}^2)(\zeta^2 - \omega_i{}^2)\phi(\zeta^2)} d\zeta \quad (5.3.4)$$

From eq. 3.2.7, we have

$$\phi(\zeta^2) = \frac{\zeta}{2\bar{\omega}}(d(\zeta) - d(-\zeta))$$

We substitute this into eq. 5.3.4 and put $\zeta = iy$. Then, observing that

$$2iy\,(\sqrt{d(iy)} - 1) + (-2iy)(\sqrt{d(-iy)} - 1) = 2iy(\sqrt{d(iy)} - \sqrt{d(-iy)})$$

we easily obtain

$$(\sqrt{\mathbf{H}})_{ji} = (2\bar{\omega}\omega_j\omega_i t_i/\pi)\int_0^{\infty} \frac{dy}{(y^2 + \omega_j{}^2)(y^2 + \omega_i{}^2)(\sqrt{d(iy)} + \sqrt{d(-iy)})} = (\bar{\omega}\omega_j\omega_i t_i/\pi)\int_0^{\infty} \frac{dy}{(y^2 + \omega_j{}^2)(y^2 + \omega_i{}^2)R(y)\cos\Theta} \quad (5.3.5)$$

where

$$R(y) = \left[\left(\frac{(\bar{\omega}\omega_\sigma t_\sigma}{\omega_\sigma{}^2 + y^2}\right)^2 + y^2\left(\frac{\bar{\omega}t_\sigma}{\omega_\sigma{}^2 + y^2}\right)^2\right]^{1/4} \quad (5.3.6)$$

$$\Theta(y) = \frac{1}{2}\tan^{-1}\left[y\left(\frac{t_\sigma}{\omega_\sigma{}^2 + y^2}\right)\Big/\left(\frac{\omega_\sigma t_\sigma}{\omega_\sigma{}^2 + y^2}\right)\right];\ 0 \leqslant \Theta \leqslant \frac{\pi}{4} \quad (5.3.7)$$

Since $\cos\Theta > 0$ in the range $0 \leqslant \Theta \leqslant \pi/4$, the off-diagonal elements of the matrix $\sqrt{\mathbf{H}}$ are clearly positive. Accordingly, from eq. 5.2.7, the off-diagonal elements of $||R_{ji}''||$ are negative. Their values can be obtained by numerical quadrature of eq. 5.3.5 (caution: the branch point at ∞ should be mapped out by a suitable substitution, for example, $y = \omega \tan^4 u$). The symmetry relation

$$t_j[\sqrt{\mathbf{H}} - \mathbf{E}]_{ji} = t_i[\sqrt{\mathbf{H}} - \mathbf{E}]_{ij}$$

required by eq. 5.2.3 is evidently satisfied by the integral (5.3.5). If we expand the integrand into partial fractions, we obtain

$$(\sqrt{\mathbf{H}})_{ji} = -\omega_j\omega_i t_i \frac{\beta_j{}^* - \beta_i{}^*}{\omega_j{}^2 - \omega_i{}^2} \quad (5.3.8)$$

where

$$\beta_j{}^* = \frac{\bar{\omega}}{\pi}\int_0^{\infty} \frac{dy}{(y^2 + \omega_j{}^2)R(y)\cos\Theta} \quad (5.3.9)$$

In view of eq. 5.3.6 and 5.3.7, this integral clearly converges. Equation 5.3.8 is nothing else but the "β-representation," eq. 5.2.5.

According to the general eq. 5.2.6, the diagonal elements of the matrix $[\sqrt{\mathbf{H}} - \mathbf{E}]$ are given in terms of the off-diagonal elements

$$[\sqrt{\mathbf{H}} - \mathbf{E}]_{jj} = -\sum_{i \neq j}^{s} \frac{\omega_j}{\omega_i}(\sqrt{\mathbf{H}})_{ji} \quad (5.3.10)$$

Since $[\sqrt{\mathbf{H}}]_{ji}$ are positive for $j \neq i$, these are clearly negative.

Thus, the matrix $[\sqrt{\mathbf{H}} - \mathbf{E}]$ has negative diagonal elements and positive off-diagonal elements. In view of eq. 5.2.7, the dissipation matrix $||[R_{ji}'']||$ due to the relaxation effect has positive diagonal elements and negative off-diagonal elements. This is the result which we have promised to prove in 4.3.

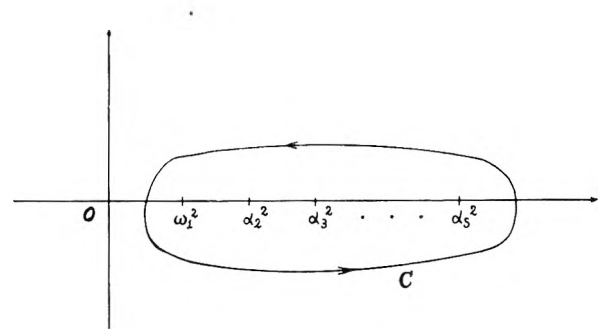

Fig. 1.—The contour C of the integral (5.3.1).

VI. The Method of Computation

6.1. Introduction.—In obtaining numerical values from the results which we have derived, computational difficulties arise only in the evaluation of the "characteristic mobilities" for the system under consideration, *i.e.*, the roots of the algebraic eq. (3.2.4). One of the roots is always zero, *i.e.*, $\alpha_1 = 0$, while the other roots (α_2^2, α_3^2, . . ., α_s^2) are determined by

$$\sum_{i=1}^{s} \frac{t_i}{(\omega_i{}^2 - \theta)} = 0 \quad (6.1.1)$$

This formula is equivalent to an ordinary algebraic equation of degree $s - 1$

$$\theta^{s-1} - c_1\theta^{s-2} + c_2\theta^{s-3} + \ldots + (-)^i c_i\theta^{s-i-1} + \ldots + (-1)^{s-1} c_{s-1} = 0 \quad (6.1.2)$$

where (in view of $\Sigma t_i = 1$) the coefficients c_1, . . . c_{s-1} have the following values

$$c_1 = \sum_{i<1}^{s} \alpha_i{}^2 = \sum_{i=1}^{s} (1 - t_i)\omega_i{}^2 \quad (6.1.3)$$

$$c_2 = \sum_{1 < k_1 < k_2}^{s} \alpha_{k_1}{}^2\alpha_{k_2}{}^2 = \sum_{1 \le k_1 < k_2}^{s} (1 - t_{k_1} - t_{k_2})\omega_{k_1}{}^2\omega_{k_2}{}^2$$

$$\cdots \qquad (6.1.4)$$

$$c_i = \sum_{1 < k_1 < k_2 < \ldots < k_i}^{s} \alpha_{k_1}{}^2\alpha_{k_2}{}^2 \ldots \alpha_{k_i}{}^2 =$$

$$\sum_{1 \le k_1 < k_2 < \ldots < k_i}^{s} (1 - t_{k_1} - t_{k_2} - \ldots - t_{k_i})\omega_{k_1}{}^2\omega_{k_2}{}^2 \ldots$$

$$\cdots \times \omega_{k_i}{}^2 \qquad (6.1.5)$$

$$c_{s-1} = \prod_{i \ne 1}^{s} \alpha_i{}^2 =$$

$$\sum_{1 \le k_1 < k_2 < \ldots < k_{s-1}} (1 - t_{k_1} - t_{k_2} - \ldots - t_{k_{s-1}})\omega_{k_1}{}^2\omega_{k_2}{}^2 \ldots$$

$$\times \omega^2{}_{k_{s-1}} = \prod_{i=1}^{s} \omega_i{}^2 \sum_{j=1}^{s} t_j/\omega_j{}^2 \qquad (6.1.6)$$

For $s = 2$, *i.e.*, when the system contains only two species of ions, eq. 6.1.3 or 6.1.6 yields

$$\alpha_2{}^2 = t_2\omega_1{}^2 + t_1\omega_2{}^2 \qquad (6.1.7)$$

In particular, for a binary electrolytes α_2 becomes the geometric mean of the absolute mobilities of two constituent ions. For $s = 3$, we have from eq. 6.1.3 and 6.1.6

$$\alpha_2{}^2 = B - \sqrt{B^2 - C}$$
$$\alpha_3{}^2 = B + \sqrt{B^2 - C} \qquad (6.1.8)$$

where

$$2B \equiv (1 - t_1)\omega_1{}^2 + (1 - t_2)\omega_2{}^2 + (1 - t_3)\omega_3{}^2$$
$$C \equiv \omega_1{}^2\omega_2{}^2\omega_3{}^2\left(\frac{t_1}{\omega_1{}^2} + \frac{t_2}{\omega_2{}^2} + \frac{t_3}{\omega_3{}^2}\right)$$

Now, for $s = 4$ or 5, we can still get the explicit formulas for $\alpha_i{}^2$ from eq. 6.1.2 by well-known algebraic methods, but the expressions become much more complicated. We prefer a procedure which quite clearly exhibits the general dependence of $\alpha_p{}^2$ on the composition, and can be applied to a system which contains any number of species of ions.

6.2. The Location of the Roots of the Fundamental Equation.—More often than not, questions pertaining to mixtures need to be answered for a series of compositions obtained by linear interpolation between two given extreme compositions. In such cases it is convenient to invert the problem; for eq. 6.1.1 determines the mixing ratio as a simple explicit function of θ. Reasonably accurate values of $\alpha_2{}^2, \ldots \alpha_s{}^2$ which belong to any specified mixing ratio can be obtained by graphical interpolation, and these are easily improved to any required degree by Newton's method.

We describe the extreme compositions I and II by the transference numbers t_{Ii}, t_{IIi} $(i = 1,2, \ldots s)$; some of these may vanish but $t_{Ii} + t_{IIi} > 0$. The mixing ratio may be described by the Roman-numbered transference numbers $t_I, t_{II} = 1 - t_I$, so that the transference number of species i equals

$$t_i = t_I t_{Ii} + t_{II} t_{IIi} \qquad (6.2.1)$$

Then eq. 6.1.1 takes the form

$$t_I/t_{II} = -\sum_{i=1}^{s} \frac{t_{IIi}}{\omega_i{}^2 - \theta} \Big/ \sum_{i=1}^{s} \frac{t_{Ii}}{\omega_i{}^2 - \theta} \qquad (6.2.2)$$

Now we designate the characteristic mobilities corresponding to two extreme compositions I and II by $\alpha_{Ip}{}^2$ and $\alpha_{IIp}{}^2$ $(p = 1,2, \ldots s)$ which satisfy the following relation according to eq. 3.2.17

$$0 = \alpha_{II}{}^2 = \alpha_{III}{}^2 < \omega^2{}_1 \le \ldots \le \omega^2{}_{p-1} \le \frac{\alpha_{Ip}{}^2}{\alpha_{IIp}{}^2} < \omega_p{}^2$$
$$\le \ldots \le \omega_s{}^2 \qquad (6.2.3)$$

Here the equality sign must obviously be taken in all cases of confluence. Moreover, whenever a species of ions, *e.g.*, j, is absent in one of the limiting compositions either α_j and α_{j+1} will equal ω_j in the limit, as we have shown in our discussion of tracer ions (3.6). At the intermediate composition the p-th root $(\alpha_p{}^2)$ of the eq. 6.2.2 must be located between two extreme values $\alpha_{Ip}{}^2$ and $\alpha_{IIp}{}^2$

$$\alpha_{Ip}{}^2 \gtrless \alpha_p{}^2 \gtrless \alpha_{IIp}{}^2 \qquad (6.2.4)$$

because t_I/t_{II} is a single-valued function of $\theta = \alpha_p{}^2$, so that conversely, $\alpha_p{}^2$ is a monotonic function of t_I/t_{II} in every range of continuity.

If but two or three kinds of ions are present at either end (I,II) of the mixing range, the corresponding extreme values of $\alpha_p{}^2$ are easily determined from the formulas given for those simple cases together with the rule for tracer ions. In other cases it may be more convenient to rely entirely on graphs and successive approximations, supplemented by the rule for tracer ions where applicable. If we plot t_I or t_{II} by giving to θ in eq. 6.2.2 a suitable series of values belonging to each allowed range of $\alpha_p{}^2$, we obtain curves as shown in Fig. 2.

The extreme characteristic mobilities, $\alpha_{Ip}{}^2$, $\alpha_{IIp}{}^2$ may be determined in the process, possibly with the aid of a point or two outside the required interval $0 \le t_I = 1 - t_{II} \le 1$. The values of $\alpha_2{}^2, \ldots \alpha_s{}^2$ belonging to any specified composition within this range may be read from the completed graphs. We should point out that the ratio $(\alpha_p{}^2 - \omega_{p-1}{}^2)/(\omega_p{}^2 - \alpha_p{}^2)$ must be determined with adequate precision. The number of required decimals in α_p may exceed the number of significant figures in the measured ω_p! Accordingly, if $\omega_p{}^2 - \omega_{p-1}{}^2$ is small, the graph for $\alpha_p{}^2$ should be drawn on a large scale.

If the initial values of $\alpha_2{}^2, \ldots, \alpha_s{}^2$ obtained from the graphs are not accurate enough, they can be easily improved to any required degree by Newton's approximation formula

$$\alpha_p{}^2 \cong \beta_p{}^2 - \left[\sum_{i=1}^{s} \frac{t_i}{(\omega_i{}^2 - \beta_p{}^2)} \Big/ \sum_{i=1}^{s} \frac{t_i}{(\omega_i{}^2 - \beta_p{}^2)^2}\right]$$

where $\beta_p{}^2$ is the approximate value of $\alpha_p{}^2$. The relations (6.1.3) and (6.1.6) may be used to determine the last two roots of the fundamental 6.2.2 once the others are known, or they may serve as over-all checks on the computation of a set.

6.3. The Numerical Values of $\alpha_p{}^2$ and the Relaxation Term in Equivalent Conductance for a Mixed Electrolyte.—We consider a mixed electrolytic solution of ions of group-I ($NaNO_3$) and group-II (x_{LiCl} LiCl + x_{KCl} KCl), where x_{LiCl} and x_{KCl} are the mole fractions of LiCl and KCl. We shall choose the composition of group-II ions in such a way that one of $\alpha_p{}^2$ for pure group-II solution equals $\omega_{Na}{}^2$. This choice is interesting because in the limit of $t_I = 0$, two adjoint curves of $\alpha_p{}^2$ coin-

cide as it has been shown by the point A in Fig. 2. We use Harned and Owen's[12] values for limiting equivalent conductances, Λ^0_j, which are shown below. Then the above choice yields

$$x_{LiCl} = 0.7618_5,\ x_{KCl} = 1 - x_{LiCl} = 0.2381_5$$

Therefore, two extreme compositions x_{Ii} and x_{IIi} expressed in mole fractions are

	Li^+	Na^+	NO_3^-	K^+	Cl^-
x_{Ii}	$1/2 \times 0.7618_5$	0	0	$1/2 \times 0.2381_5$	$1/2$
x_{IIi}	0	$1/2$	$1/2$	0	0
Λ_j° (at 25°)	38.69	50.11	70.44	73.52	76.34

Since the eigen values, q_p and eigen vectors, χ_{jp} are dimensionless, we can use $\Lambda^\circ_j/|z_j|$ in the place of ω_j. Then, the resulting numerical values for "α_p" are $\bar{\alpha}_p = (965/3)\ \epsilon\alpha_p$(ohm^{-1}, cm.^{2}, mole^{-1}), which has been given in Table I. Substituting these values into the relaxation term $\Delta\Lambda_j$

$$\Delta\Lambda_j \equiv \Lambda_j^\circ \frac{1.981 \times 10^6}{(DT)^{3/2}} z_j \sum_{p=2}^{s} (1 - \sqrt{q_p})\chi^p{}_j(z_\sigma t_\sigma \chi^p{}_\sigma)\Gamma^{1/2}$$

in eq. 4.2.6 we have obtained the numerical values given in Table II.

TABLE I

THE NUMERICAL VALUES OF $\bar{\alpha}_p$'(OHM^{-1} CM.^{2} MOLE^{-1}) FOR $x_{NaNO_3}NaNO_3 + (1 - x_{NaNO_3})(0.7618_5$ LiCl $+ 0.2381_5$ KCl) AT 25°

x_{NaNO_3}	0.0000	0.2000	0.4000	0.6000	0.8000	1.0000
$\bar{\alpha}_1^2$	0	0	0	0	0	0
$\bar{\alpha}_2^2$	2511.0	2018.6	1832.6	1697.4	1588.7	(1496.9)
$\bar{\alpha}_3^2$	(2511.0)	3031.2	3236.0	3380.9	3491.9	3579.9
$\bar{\alpha}_4^2$	(5103.7)	5196.6	5283.7	5341.0	5386.1	(5405.2)
$\bar{\alpha}_5^2$	5486.2	5503.1	5536.8	5600.9	5701.9	(5827.8)

TABLE II

THE NUMERICAL VALUES OF $\Delta\Lambda_j/(\Lambda^0_j\sqrt{\Gamma})$ FOR A SOLUTION $x_{NaNO_3}NaNO_3 + (1 - x_{NaNO_3})(0.7618_5$ LiCl $+ 0.2381_5$ KCl) AT 25° ($D = 78.57$)[13]

x_{NaNO_3}	0.0000	0.2000	0.4000	0.6000	0.8000	1.000
Li^+	.148	.146	.144	.142	.140	....
Na^+	....	.170	.168	.166	$.16_4$	0.162
NO^-_3	....	.157	.158	.159	$.16_1$	.162
K^+	.211	.207	.205	.203	$.20_2$	....
Cl^-	.163	.164	.165	.166	$.16_7$	....

VII. Viscosity

7.1. Introduction.—The viscosity coefficient of an electrolyte is composed of two parts

$$\eta = \eta_0 + \eta^* \qquad (7.1.1)$$

where η_0 is the viscosity of the solvent and η^* is the increment of viscosity due to the electrostatic interaction between the ions. In an undisturbed electrolyte, an ion is surrounded by a spherically symmetric atmosphere. A velocity gradient in the liquid will deform every sphere into an ellipsoid, and the ionic atmosphere will remain somewhat deformed because of the finite time of relaxation. The increment η^* is the part due to this deformation of the ionic atmospheres.

Onsager and Fuoss[6] expressed η^* by a set of functions $\xi_j(r)$

(12) H. S. Harned and B. B. Owen, "Physical Chemistry of Electrolytic Solutions," Reinhold Publ. Corp., New York, N. Y., 1950, Table 6-8-2, p. 172.

(13) F. H. Drake, G. W. Pierce and M. R. Dow, *Phys. Rev.*, 35, 613 (1930).

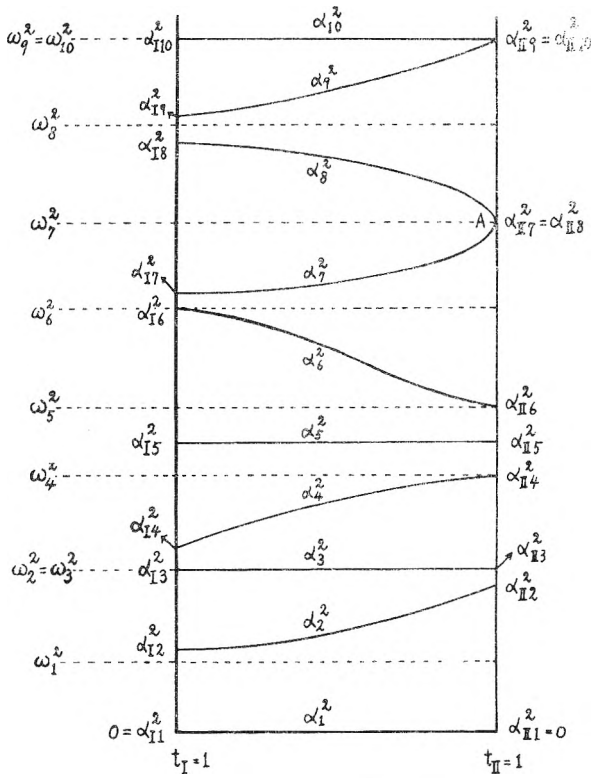

Fig. 2.—The location of the roots α_p^2 of the fundamental eq. 6.1.1 *versus* the mixing ratio $t_I(=1-t_{II})$.

$$\eta^* = \frac{1}{15} \sum_{j=1}^{s} n_j e_j \nabla^2 \xi_j(0) \qquad (7.1.2)$$

which satisfy a system of differential equations

$$\nabla^2\nabla^2\xi_j - \frac{4\pi}{DkT} \sum_{i=1}^{s} \frac{n_i e_i{}^2 \omega_i}{\omega_i + \omega_j} \nabla^2\xi_j - \frac{4\pi}{DkT} \sum_{i=1}^{s} \frac{n_i e_i e_j \omega_j}{\omega_i + \omega_j} \times \nabla^2\xi_i = -\frac{4\pi}{(DkT)^2} \frac{e^{-\kappa r}}{\kappa} \sum_{i=1}^{s} \frac{n_i e_i{}^2 e_j}{\omega_i + \omega_j} \qquad (7.1.3)$$

and are subject to the boundary conditions that $\xi_j(r)$ and $\nabla^2\xi_j(r)$ are finite everywhere and tend to zero as $r \to \infty$.

Their derivation of eq. 7.1.3 corresponds closely to the computation which leads to eq. 2.2.13 in the case of conduction and diffusion and the approximations are similar. We shall outline briefly the assumptions and procedure for a simple case where the bulk velocity $\mathbf{v}$ in the solution has a constant velocity gradient $a^1{}_2$

$$\mathbf{v}(\mathbf{r}_2) = \mathbf{v}(\mathbf{r}_1) + a^1{}_2 y\mathbf{i} \qquad (7.1.4)$$

where $\mathbf{r}_1$ and $\mathbf{r}_2$ are defined in section 2.1 and $\mathbf{i}$ is a unit vector in the x-direction. In this case the distribution function f_{ji} and the potential ψ_j depend only upon the relative location $\mathbf{r} = \mathbf{r}_2 - \mathbf{r}_1$. The only difference from the conduction-diffusion problem is the fact that the velocity $\mathbf{v}_{ji}(\mathbf{r})$ and $\mathbf{v}_{ij}(-\mathbf{r})$ in eq. 2.1.10 contain the bulk velocities $\mathbf{v}(\mathbf{r}_2)$ and $\mathbf{v}(\mathbf{r}_1)$, respectively, and instead the applied external forces $\mathbf{k}_j$ are zero. Therefore, if we make appropriate approximations for low concentrations, the equation of continuity will be linearized to yield

$$(\omega_j + \omega_i)kT\nabla^2 f_{ji}(\mathbf{r}) + e_i\omega_i n_i n_j \nabla^2\psi_j(\mathbf{r}) + e_j\omega_j n_j n_i \nabla^2\psi_i(-\mathbf{r}) = a^1{}_{2y}\frac{\partial}{\partial x} f_{ji} \quad (7.1.5)$$

Content to compute the Newtonian viscosity, we regard the velocity gradient $a^1{}_2$ as a first-order perturbation, and neglect the second-order perturbation terms which arise from the disturbance. Then the right member of eq. 7.1.5 becomes

$$a^1{}_{2y}\frac{\partial}{\partial x} f_{ji}^{\circ} = a^1{}_2 \frac{n_j n_i e_j e_i}{DkT\kappa}\frac{\partial^2}{\partial x \partial y} e^{-\kappa r} \quad (7.1.6)$$

The perturbations of the distribution function $f_{ji}(\mathbf{r})$ and the potential $\psi_j(\mathbf{r})$ are proportional to the velocity gradient; thanks to the principle of superposition, they must exhibit a corresponding variation with the direction

$$f_{ji}(\mathbf{r}) = f_{ji}^{\circ}(\mathbf{r}) + a^1{}_2\frac{\partial^2}{\partial x \partial y}\varphi_{ji}(r)$$
$$\psi_j(\mathbf{r}) = \psi_j^{\circ}(\mathbf{r}) + a^1{}_2\frac{\partial^2}{\partial x \partial y}\xi_j(r) \quad (7.1.7)$$

By means of Poisson's equation, the "distribution functions" $\varphi_{ji}(r)$ are eliminated from eq. 7.1.5; then the boundary condition for $\xi_j(r)$ leads to eq. 7.1.3.[14] By computing the total transport of electrostatic force perpendicular to the y-axis defined in eq. (7.1.4), Onsager and Fuoss obtained eq. 7.1.2.

7.2. The Increment η^* of Viscosity.—If we introduce the notations defined by (2.2.14) to (2.2.16) eq. 7.1.3 can be written as

$$\nabla^2\nabla^2(\xi_j/e_j\omega_j) - \kappa^2\sum_{i=1}^{s}\frac{\bar{\omega}t_i}{\omega_i + \omega_j}\nabla^2(\xi_j/e_j\omega_j) - \kappa^2\sum_{i=1}^{s}\frac{\bar{\omega}t_i}{\omega_i + \omega_j}\nabla^2(\xi_i/e_i\omega_i) = -\frac{\kappa}{DkT}\sum_{i=1}^{s}\frac{\bar{\omega}t_i}{(\omega_i + \omega_j)\omega_i\omega_j}e^{-\kappa r} \quad (7.2.1)$$

In terms of the matrix $\mathbf{H}$, this takes the following compact form

$$\nabla^2(\nabla^2\delta_{j\sigma} - \kappa^2 h_{j\sigma})\phi_\sigma = -\frac{\kappa\bar{\omega}}{DkT}\sum_{i=1}^{s}\frac{t_i}{(\omega_i + \omega_j)\omega_i\omega_j}e^{-\kappa r} \quad (7.2.2)$$

where $\phi_j(r)$ are defined by

$$\phi_j(r) = \xi_j/e_j\omega_j; \quad (j = 1, 2, \ldots s) \quad (7.2.3)$$

From eq. 7.1.2, $\phi_j(r)$ are related to η^* as follows

$$\eta^* = \frac{\Gamma_0\bar{\omega}}{15}\sum_{j=1}^{s} t_j\nabla^2\phi_j(0) \quad (7.2.4)$$

Now we shall solve the differential system (7.2.2) in the same way as we have solved the system (2.2.20). Multiplying $t_j\chi^p{}_j$ and summing over $j = 1,2, \ldots s$, we obtain

$$\nabla^2(\nabla^2 - \beta_p{}^2)Z_p(r) = b_p\frac{\partial}{\partial\kappa}\left(\frac{e^{-\kappa r}}{r}\right) \quad (7.2.5)$$

where

$$\beta_p = \kappa\sqrt{q_p} \quad (7.2.6)$$

(14) The natural boundary conditions for the potential $\psi_j(\mathbf{r})$ do not uniquely determine those for $\xi_j(\mathbf{r})$: in as much as an additional term of the form

$$c_1 r^2 + c_2$$

will not affect the potentials at all. To that extent the choice $\xi_j = 0$ for $r = \infty$ is arbitrary; it is preferred because it simplifies the subsequent analysis.

$$Z_p(r) = \sum_{j=1}^{s} t_j\chi^p{}_j\phi_i(r) \quad (7.2.7)$$

$$b_p = \frac{\kappa\bar{\omega}N_p}{DkT}\sum_{j,i=1}^{s}\frac{t_j t_i}{(\omega_i^2 - \alpha_p{}^2)(\omega_j + \omega_i)\omega_i} \quad (7.2.8)$$

In the last equation we have substituted the explicit form for $\chi_j{}^p$. To simplify this rather complicated formula we exchange j and i and take the mean. The result is

$$b_p = \frac{\kappa\bar{\omega}N_p}{2DkT}\left[\left(\sum_{j=1}^{s}\frac{t_j}{\omega_j^2 - \alpha_p{}^2}\right)^2 - \alpha_p{}^2\left(\sum_{j=1}^{s}\frac{t_j\omega_j}{(\omega_j^2 - \alpha_p{}^2)\omega_j{}^2}\right)^2\right] \quad (7.2.9)$$

When $p = 1$, $\alpha_1 = 0$. Accordingly

$$b_1 = \frac{\kappa N_1}{2DkT}\frac{\bar{\rho}^2}{\bar{\omega}}; \quad \bar{\rho} = \sum_{i=1}^{s}\mu_i/\omega_i = \sum_{i=1}^{s}\mu_i\rho_i \quad (7.2.10a)$$

When $p \geqq 2$, the first term in eq. 7.2.9 is zero from eq. 3.2.4. If we expand the second term into partial fractions and use the expression for q_p, (3.2.21), we easily obtain

$$b_p = -\frac{\kappa N_p(1 - q_p)^2}{2DkT\bar{\omega}\alpha_p{}^2}; \quad (p = 2, \ldots s) \quad (7.2.10b)$$

Now, the most general solution of eq. 7.2.5 is

$$Z_p(r) = b_p\frac{\partial}{\partial\kappa}\left[\frac{1}{(\kappa^2 - \beta_p{}^2)}\left(\frac{e^{-\kappa r}}{\kappa^2 r} + A_1\frac{e^{-\beta_p r}}{r} + A_2\frac{1}{r} + A_3\frac{e^{\beta_p r}}{r} + A_4\right)\right]$$

where β_p is kept constant in the differentiation with respect to κ. The integration constants $A_1, \ldots, A_4$ are determined by the boundary condition that $Z_p(r)$ and $\nabla^2 Z_p(r)$ are finite everywhere and tend to zero as $r \to \infty$. The result is

$$Z_p(r) = b_p\frac{\partial}{\partial\kappa}\left[\frac{1}{(\kappa^2 - \beta_p{}^2)}\left(\frac{e^{-\kappa r} - 1}{\kappa^2 r} - \frac{e^{-\beta_p r} - 1}{\beta_p{}^2 r}\right)\right]$$

In order to compute η^* we need to know $\nabla^2 Z_p(0)$

$$\nabla^2 Z_p(0) = b_p\operatorname*{Lim}_{r\to 0}\frac{\partial}{\partial\kappa}\left(\frac{e^{-\kappa r} - e^{-\beta_p r}}{(\kappa^2 - \beta_p{}^2)r}\right) = \frac{b_p}{(\kappa + \beta_p)^2}$$

Substituting eq. 7.2.6 and 7.2.10 into this, we obtain

$$\nabla^2 Z_p(0) = \frac{N_p}{2DkT\kappa\bar{\omega}}\begin{cases}\dfrac{(\bar{\rho})^2}{4} & (p = 1)\\ -\dfrac{1}{\alpha_p{}^2}(1 - \sqrt{q_p})^2 & (p \geqq 2)\end{cases} \quad (7.2.11)$$

By means of the orthogonality relations for the eigen vectors χ^p, we can solve eq. 7.2.7 to obtain

$$\phi_j(r) = \sum_{p=1}^{s}\chi^p{}_j Z_p(r)$$

and accordingly

$$\nabla^2\phi_j(0) = \sum_{p=1}^{s}\chi^p{}_j\nabla^2 Z_p(0)$$

Substituting this into eq. 7.2.4 we get

$$\eta^* = \frac{\Gamma_0\bar{\omega}}{15}\sum_{p=1}^{s}\nabla^2 Z_p(0)\sum_{j=1}^{s} t_j\chi^p{}_j$$

With the aid of eq. 7.2.11 and 3.2.24 we finally obtain

$$\eta^* = \frac{\kappa}{480\pi}\left(\bar{\rho} - 4\sum_{p=2}^{s} N_p{}^2 q_p (1 - \sqrt{q_p})^2 \alpha_p{}^{-2}\right) \quad (7.2.12)$$

where we have used $N_1 = \bar{\omega}/\bar{\rho}$. This is clearly proportional to the square root of the total concentration of the solution.

For the case of complete confluence, *i.e.*, $\omega_1 = \omega_2 = \ldots = \omega_s = \omega$ we have proved that

$$N_2 = N_3 = \ldots = N_s = 0$$

which leads to the result previously obtained by Onsager and Fuoss[6]

$$\eta^* = \frac{\kappa}{460\pi\omega} \quad (7.2.13)$$

Acknowledgments.—One of us (S.K.K.) wishes to thank the United States Government for a Smith-Mundt Grant and Yale University for a Sheffield Scientific School Fellowship.

Appendix 1. Successive Reduction of the Fundamental Equation

If we know one of the roots of the algebraic eq. 6.1.1 we can reduce the degree of the equation by one. Denoting by $\alpha_k{}^2$ the known root we have from eq. 6.1.1

$$0 = \sum_{i=1}^{s} \frac{t_i}{(\omega_i{}^2 - \theta)} \frac{(\omega_k{}^2 - \theta)}{(\alpha_k{}^2 - \theta)}$$

$$= \sum_{i=1}^{s} \frac{t_i}{(\omega_i{}^2 - \theta)} \frac{\omega_k{}^2 - \omega_i{}^2}{(\alpha_k{}^2 - \omega_i{}^2)} + \sum_{i=1}^{s} \frac{t_i}{(\omega_i{}^2 - \alpha_k{}^2)} \frac{\omega_k{}^2 - \alpha_k{}^2}{\alpha_k{}^2 - \theta}$$

$$= \sum_{i \neq k}^{s} \frac{t_i}{(\omega_i{}^2 - \theta)} \frac{\omega_k{}^2 - \omega_i{}^2}{(\alpha_k{}^2 - \omega_i{}^2)} \quad (1)$$

where we have used

$$\sum_{i=1}^{s} \frac{t_i}{(\omega_i{}^2 - \alpha_k{}^2)} = 0$$

Now, we introduce a set of pseudo-transference numbers $t^*{}_i$ defined by

$$t_i{}^* \equiv t_i \frac{\omega_k{}^2 - \omega_i{}^2}{\alpha_k{}^2 - \omega_i{}^2} \quad (2)$$

then, $t^*{}_i$ may be positive or negative but still are normalized to unity as

$$\sum_{i \neq \kappa}^{s} t_i{}^* = \sum_{i=1}^{s} t_i + \sum_{i=1}^{s} \frac{t_i}{\alpha_k{}^2 - \omega_i{}^2} \underbrace{(\omega_k{}^2 - \alpha_k{}^2)}_{=1} \quad (3)$$

Thus, eq. 6.1.1 becomes

$$\sum_{i \neq k}^{s} \frac{t_i{}^*}{\omega_i{}^2 - \theta} = 0 \quad (4)$$

which is the required result. We repeat the procedure until we reach a quadratic equation.

STABILITY CONSTANTS OF PICOLINIC AND QUINALDIC ACID CHELATES OF BIVALENT METALS

BY KEINOSUKE SUZUKI, MOTOO YASUDA AND KAZUO YAMASAKI

Contribution from Chemical Institute, Faculty of Science, Nagoya University, Nagoya, Japan

Received July 9, 1956

Stability constants of picolinates of nickel, zinc, cadmium and lead were determined by the *p*H method and also that of copper picolinate by the photometric method. The values of log *K* found were Cu 16.0, Ni 11.9, Zn 9.42, Pb 7.88 and Cd 7.54. Many metals form precipitates with quinaldic acid; the stability constants of only lead and nickel were determined by *p*H method.

The chelates of picolinic acid and copper or iron were first reported by Weidel,[1] followed by Ley's studies[2] on chelates of chromium and cobalt. Recently Shinra[3] determined the absorption spectra of ferrous chelate and applied the results to colorimetric determination of iron. He also found that quinaldic acid forms colored complexes with iron. The present study is concerned with the stability constants of picolinic acid chelates, formed by bivalent metals such as Ni, Zn, Cd, Pb which were determined by the *p*H method and also the stability constants of copper picolinate, determined by the spectrophotometric method. While many metals form precipitates with quinaldic acid, stability constants of only lead and nickel can be determined by the *p*H method.

Experimental

(1) Reagents.—Picolinic acid was prepared by oxidation of α-picoline.[4] Quinaldic acid[5] was prepared by hydrolysis of ω-tribromoquinaldine, formed by bromination of quinaldine. Metal nitrates of reagent grade were used.

(2) Procedure of the *p*H Method.—Solutions containing the following concentrations of nitrates of the respective metals and picolinic or quinaldic acid were prepared and were titrated with standard NaOH or HNO_3 at 25°: $Cd(NO_3)_2$, 0.0013 *M*; $Pb(NO_3)_2$, 0.0010–0.0020 *M*; $Zn(NO_3)_2$, 0.0013 *M*; $Ni(NO_3)_2$, 0.0006–0.0011 *M*; picolinic acid, 0.001–0.01 *M*; quinaldic acid, 0.0005–0.005 *M*. The ionic strength of the solutions was maintained at 0.1 by adding KNO_3. A glass electrode combined with an electronic amplifier was employed for the determination of *p*H and standardized against standard buffers.

For the first acid dissociation constant of picolinic acid, the value of pK_1 1.60 reported by Jellinek and Urwin[6] was used, and for quinaldic acid we adopted the results of Wen-

(1) H. Weidel, *Ber.*, **12**, 1989 (1879).
(2) H. Ley and K. Ficken, *ibid.*, **50**, 1123 (1917).
(3) K. Shinra, K. Yoshikawa, T. Kato and Y. Nomizo, *J. Chem. Soc. Japan, Pure Chem. Sect.*, **75**, 44 (1954).
(4) A. W. Singer and S. M. McElvain, *Org. Syntheses*, **20**, 79 (1940).
(5) D. L. Hammick, *J. Chem. Soc.*, **123**, 2882 (1923).
(6) H. H. G. Jellinek and J. R. Urwin, THIS JOURNAL, **58**, 548 (1954).

TABLE I

TITRATION DATA OF THE NICKEL CHELATE OF PICOLINIC ACID

Temp. = 25°, μ = 0.1, γ_H = 0.83,[a] A = picolinate ion.

pH	C_{Ni}, M	C_A, M	C_{Cu}, M	$\bar{n}$	p-[A]
2.77	0.0011	0.0010	0.00237	0.63	6.29
2.69	.0011	.0010	.00285	.57	6.30
2.63	.0011	.0010	.00323	.56	6.36
2.58	.0011	.0010	.00363	52	6.37
2.91	.00056	.0014	.00221	1.27	5.80
2.97	.00056	.0014	.00198	1.31	5.75
3.08	.00056	.0014	.00166	1.36	5.65
3.17	.00056	0014	.00141	1.46	5.60
3.39	.00056	.0014	.00101	1.58	5.43

[a] J. Kielland, *J. Am. Chem. Soc.*, 59, 1675 (1937).

TABLE II

SPECTROPHOTOMETRIC DATA OF THE COPPER CHELATE WITH PICOLINIC ACID

μ = 0.1[a], γ_H = 0.83

	λ	ϵ_{Cu}	ϵ_{CuA}	E_1
pH 1.12, a_1 = 0.017 M, C_A = 0.0127 M				
	760	10.3	23.1	0.330
	750	9.8	23.5	.330
k_1	740	9.1	23.3	.327
	730	8.4	23.4	.322
	720	7.6	23.2	.318
	λ	ϵ_{CuA}	ϵ_{CuA_2}	E_2
pH 1.93, a_2 = 0.00378 M, C_A = 0.00800 M				
	670	19.1	40.5	0.137
	660	17.5	41.1	.138
k_2	650	16.2	41.4	.137
pH 2.70, a_2 = 0.00367 M, C_A = 0.00777 M				
	670	19.1	40.5	0.143
	630	17.5	41.1	.145
	650	16.2	41.4	.145

[a] In the determination of k_1 ionic strength was kept at about 0.1 by copper nitrate itself, while in the determination of k_2 KNO_3 was added to maintain ionic strength at 0.1.

ger[7] who found that the first step of the acid dissociation was nearly complete.

The second acid dissociation constants of both acids were determined by the titration of their solutions with alkali, and the pK_2 values found for picolinic and quinaldic acids are 5.44 and 4.49, respectively.

By the use of both acid dissociation constants and the results of pH titration of solutions containing metal ion and chelating agent, the formation curves were drawn by the method of Bjerrum and thus stability constants were calculated. The data on nickel chelate are shown in Table I.

(3) **Procedure of the Spectrophotometric Method.**—The stability constant of copper picolinate chelate was determined by the spectrophotometric method because the high acidity caused by the strong chelation between copper and picolinate ions made the pH method practically impossible.

(a) **Determination of Extinction Coefficient.**—First we determined the extinction coefficients of CuA (A for picolinate ion). The solutions used contained an excess of copper ion compared to picolinic acid (about 2-fold) and it was assumed that the appreciably colored species in these solutions were Cu and CuA alone.[8] By subtracting the extinction of Cu from the observed value, the molar extinction coefficient of CuA (ϵ_{CuA}) can be obtained.

Then the extinction coefficients of CuA_2 were determined. The solutions which contained an excess of picolinic acid as compared to copper ion (about 4-fold), were used. As it was assumed that in these solutions the colored species was CuA_2 alone,[9] the observed data gave the value of ϵ_{CuA_2}. The values actually found are ϵ_{CuA} = 16.2–23.5 for 650–760 mμ and ϵ_{CuA_2} = 40.5–41.4 for 670–650 mμ.

(b) **Calculation of Stability Constant.**—In the determination of the extinction coefficients of complexes, the solutions of higher pH were used. But for the measurements of the stability constants, we used the solutions of lower pH for the purpose of controlling the complex formation. Calculation of stability constants are as follows.

The extinction E_1 of the solution containing 0.0171–0.0189 M of copper and 0.0127–0.0140 M picolinic acid was first determined at pH 1.12–1.65. If the concentrations of total copper and free copper ions are expressed by a_1 and x_1, respectively, the following equation holds, thickness of the cells being 1 cm.

$$E_1 = \epsilon_{Cu}\, x_1 + \epsilon_{CuA}\,(a_1 - x_1) \qquad (1)$$

Then the extinction (E_2) of the solution containing copper (0.0038 M) and an excess of picolinic acid (0.008 M) was determined at pH 1.95–2.73. In the same way as for (1), equation (2) holds

$$E_2 = \epsilon_{CuA}\, x_2 + \epsilon_{CuA_2}\,(a_2 - x_2) \qquad (2)$$

where a_2 and x_2 mean concentrations of total copper ion, and CuA chelate. From these two equations x_1 and x_2 are calculated. Concentrations of free picolinic acid in these solutions were calculated by use of acid dissociation constants, and by combining these values the stability constants, k_1 and k_2, for the chelates CuA and CuA_2 were calculated. Experimental data used for calculation of stability constants are given in Table II.

Results and Discussion

The stability constants of chelates formed between picolinic acid and Cu, Ni, Zn, Pb and Cd are given in Table III. The constants of following equilibria 3 and 4 are expressed by k_1 and k_2, respectively

$$\mathrm{M} + \text{picolinate ion} \overset{k_1}{\rightleftarrows} \mathrm{M(picolinate)} \qquad (3)$$

$$\mathrm{M(picolinate)} + \text{picolinate ion} \overset{k_2}{\rightleftarrows} \mathrm{M(picolinate)_2} \qquad (4)$$

and K is the over-all stability constant (*i.e.*, $K = k_1k_2$).

TABLE III

Metal	log k_1	log k_2	log K
Copper	8.6	7.4	16.0
Nickel	6.4	5.5	11.9
Zinc	5.12	4.30	9.42
Lead	4.82[10]	3.06	7.88
Cadmium	4.36	3.18	7.54

During the course of this study, a report by Holmes and Crimmin[11] on the stabilities of picolinates was

(7) P. E. Wenger, D. Monnier and L. Epars, *Helv. Chim. Acta*, **35**, 396 (1952).

(8) This assumption is based upon the following facts. $\bar{n}$ values of the testing solutions which were calculated from the pH measurement (pH 4.5) were nearly equal to 0.5, the ratio of the total picolinic acid concentration to the total copper ion concentration. This indicates that picolinic acid coördinates almost completely to copper and therefore we supposed that the free picolinic acid was negligible. On the other hand, we supposed that CuA_2 was not appreciably present, since the free copper ions were present large excessively–$\bar{n}$ is small. This assumption was strengthened by the fact that these solutions have only one absorption maximum in the vicinity of 740 mμ in the visible region.

(9) This assumption is based on the following facts. $\bar{n}$ values of the testing solutions which were calculated from the pH measurements (pH 4.5), nearly equal to 2. This indicates that copper ions added formed almost perfectly CuA_2. Therefore it was assumed that the free copper ion and CuA were negligible small. This assumption was strengthened by the fact that these solutions have only one absorption maximum near the 640 mμ in the visible region. So we assumed this absorption maximum may be due to CuA_2.

(10) It is known that lead forms a complex $Pb(NO_3)^+$ in the nitrate medium and the correction of this complex was made for the value of k_1 of Pb chelate. *Cf.* V. L. Hughes and A. E. Martell, THIS JOURNAL, **57**, 694 (1953).

(11) F. Holmes and W. R. Crimmin, *J. Chem. Soc.*, 1175 (1955).

TABLE IV

		log K					
	pK_2	Cu	Ni	Zn	Pb	Cd	$\left(\frac{\log K}{pK_2}\right)_{Ni}$ $\left(\frac{\log K}{pK_2}\right)_{Zn}$
Picolinic acid	5.44	16	11.9	9.42	7.88	7.54	2.19 1.73
Proline[15]	10.6	16.8	11.3	10.2	..	8.7	1.07 0.96
Glycine[11]	9.78	15.59	11.14	9.96	8.86	8.1	1.14 1.02

published wherein they gave the following values for the stability constants of copper and nickel chelates, determined by the pH method

	log k_1	log k_2	log K
Cu	..	6.0	..
Ni	5.9	5.4	11.3

Their value for copper picolinate chelate is smaller than ours, probably because the methods of determination used are different. We used the spectrophotometric method, since the pH method did not give reproducible values in highly acidic solutions.

The constants we determined for nickel chelate by the pH method are somewhat larger than their values. They carried out their determinations in solutions of ionic strength of 0.02, while we carried out ours in solutions of 0.1. In general, stability constants determined in the solutions of lower ionic strength are larger than those determined in higher ionic strength. Therefore our values might be considered to be smaller than these of Holmes and Crimmin, but the result is opposite. This difference may be due to errors in pH measurements of highly acidic medium.

It is clear from Table I that the stability of metal picolinates decreases in the order

$$Cu > Ni > Zn > Pb > Cd$$

This order is in agreement with the following order reported by various authors[12-14]

$$Cu > Ni > Co > Zn > Fe, Mn$$

for the stability of bivalent metals with various chelating agents.

The stability constants and the values of log K/pK_2 (K over-all stability constant; K_2 second acid dissociation constant) of chelates of picolinic acid, proline and glycine are given in Table IV. These compounds have in common the same chelating group $\rangle N-\underset{|}{C}-COOH$.

The values log K/pK_2 for Zn and Ni picolinates are larger than those for glycine and proline chelates. This is true for other metals though not given in Table IV. It is reasonable to say that this effect is due to the fact that resonance in the pyridine ring stabilizes the chelate of picolinate, while no such resonance occurs in glycine and proline chelates.

For quinaldic acid, since Cu, Zn and Cd form precipitates with this chelating agent, only nickel and lead chelates were studied by the pH method, the same as used for picolinate chelates. Even for those two metals, only the first stability constants could be found.

$$M + \text{quinaldate ion} \overset{k_1}{\rightleftharpoons} M(\text{quinaldate})$$

The values of log k_1 for nickel chelate was 4.19 and for lead chelate was 4.0.

(12) K. Sone and K. Yamasaki, *Nature*, **166**, 998 (1950).
(13) C. B. Monk, *Trans. Faraday Soc.*, **47**, 297 (1951).
(14) D. P. Mellor and L. Maley, *Nature*, **159**, 370 (1947).
(15) A. Albert, *Biochem. J.*, **47**, 531 (1950).

THE MOLECULAR POLARIZATIONS AND APPARENT DIPOLE MOMENTS OF TITANIUM TETRACHLORIDE, TIN TETRACHLORIDE AND TIN TETRAIODIDE IN NON-POLAR SOLVENTS

BY A. R. TOURKY AND H. A. RIZK

Department of Chemistry, Faculty of Science, University of Cairo, Egypt

Received July 20, 1956

Titanium tetrachloride and tin tetraiodide are found to be non-polar whereas tin tetrachloride is found to be polar, irrespective of the solvent used. The former two halides apparently possess tetrahedral structures with the metal atom at the center of the grouping, whereas tin tetrachloride has pyramidal structure with tin at the apex. The total polarization of each of the three halides at infinite dilution whether obtained from Debye's or modified equations varies with the solvent. The ratio of the polarization at infinite dilution calculated from any modified equation to that calculated from Debye's equation is invariable with the solvent and appears to be higher for a polar than for a non-polar halide. From such calculations it seems likely that substances of near apparent dipole moment values should possess nearly the same ratio.

Introduction

Tetravalent metal halides now are attracting the attention of many investigators due to their use as starting materials for the production of the metals. It is, therefore, of theoretical and practical interest to obtain information regarding the structure of these halides. In spite of its importance as an effective tool in elucidating molecular structures, the method of dipole moment scarcely has been applied to these metal halides and the results obtained were either varying or fortuitous where agreement has been attained. Tin tetrachloride, for example, was found by Ulich and co-workers[1] to be polar in benzene and non-polar in carbon

(1) H. Ulich, E. Hertel and N. Nespital, *Z. physik. Chem.*, **B17**, 369 (1932).

tetrachloride whereas Bergmann, *et al.*,[2] found it to be polar in carbon tetrachloride. Although the experimental procedure of the latter authors was criticized by the former ones, they both arrived at the same structure for titanium tetrachloride when using the solvent carbon tetrachloride. These authors applied Debye's equation, which was then modified by others[3] to account for the mutual interaction between molecular dipoles.

The object of the present investigation was to determine the dipole moments of the tetravalent halides: titanium and tin tetrachloride and tin tetraiodide by carrying out dielectric constant measurements in non-polar solvents such as benzene and carbon tetrachloride, and to examine the feasibility of the assumption of the non-solvent effect by using modified equations.

Experimental

Materials.—Chemically pure titanium and tin tetrachlorides were subjected four times to vacuum distillation following a method similar to that given in Archibald.[4] Tin tetraiodide was crystallized three times from carbon tetrachloride, well-dried and then subjected to the same treatment as the chlorides. Benzene, carbon tetrachloride and nitrobenzene of grade "AnalaR" were rigorously dried and purified according to recommended procedures.[5]

Measurements.—The dielectric constant ϵ was measured using a resonance circuit in which a frequency of 10^6 cycles per second was fixed by a quartz crystal. The silvered Sayce–Briscoe measuring cell[5] could not be applied because of chemical interaction with the halides and therefore a specially designed cylindrical platinum cell was used. It was rigidly fixed in a jacket that could be connected to an ultra-thermostat. The air capacity of the cell was 30 $\mu\mu F$, the range over which ϵ could be measured was 1.9–3.1 and the volume required to fill the annulus was 8 cc. In the calibration of the apparatus only liquids of reliable dielectric constants were used, thus

	Benzene[7,8]	Carbon tetrachloride[7]	Nitrobenzene in benzene[9,10]		
ϵ at					
25°	2.2725	2.2270	2.2925	2.3000	2.3325
		f_2 =	0.0008707	0.001197	0.002612

The uncertainty in ϵ was ±0.0005.

The density was measured by a pycnometer of the Sprengel–Ostwald type that was filled by the method of Smyth and Morgan[11] and Miller.[12] The refractive index for the sodium-D line was directly measured by means of a Hilger–Abbe refractometer. The concentration was determined using Dorfman and Hildebrand's method.[13] All measurements were made at 25.0 ± 0.002°.

Results

The total molecular polarization of the halide P_2 at different concentrations was calculated using the modified Clausius–Mosotti–Debye equation[14,15] applicable to solutions. The polarization at infinite dilution $P_{2\infty}$ was graphically and mathematically determined. In the latter case, the Hedestrand method[16] and the Palit–Banerjee method[17] were used. The mean of the values of $P_{2\infty}$ as deduced by the three methods was then taken. The part of the molecular polarization arising from induced dipoles R_2 was calculated from measurements of n_D using the modified form of Lorenz–Lorentz equation[18] applicable to solutions and then corrected by means of the dispersion formula $(1 - \lambda^2_0/\lambda^2)R_2$, where λ_0 = 1013 Å.[12] and λ = 5896 Å.[19] so as to get the molecular refraction for infinite wave length $R_{2\infty}$ which is identical with the electronic polarization E^{P_2}. The deformation polarization D^{P_2} was taken as 1.10 $R_{2\infty}$[20] and the dipole moment μ was obtained by the refractivity method.[21]

The modified formulas of Henriquez, Kirkwood and Newton[22] were also used in evaluating the polarization at infinite dilution for studying the solvent effect.

The results obtained are summarized together with these of previous workers in Table I.

Discussion

Titanium Tetrachloride.—The electronic polarization value is in better agreement with Ulich's value[1] than with that of Bergmann.[2] The orientation polarization is zero in carbon tetrachloride and 3.29 cc. in benzene. Thus, titanium tetrachloride is a dipole-free halide and may be considered as a tetrahedral grouping around Ti in agreement with previous results arrived at by different methods.[24,25]

Tin Tetrachloride.—The electronic polarization value is very near to Ulich's value but appreciably lower than that of Bergmann. The atomic polarization of this halide was determined by the former author as the difference between its total polarization in the solid state and its electronic polarization. The value obtained was 8–10 cc. in agreement with the value 10.8 cc. obtained by Smyth[26] by the same method. Jenkins,[27] considering that atomic polarizations higher than 7 cc. do not exist, ascribed those in the neighborhood of 10 cc. to the hygroscopic nature of the halide. The dipole moment of this halide when determined in carbon tetrachloride is 0.86 *D*, thus agreeing with Bergmann's value of 0.80 *D* and deviating from that of Ulich which is zero. Although the total polarization as deter-

(2) E. Bergmann and L. Engel, *Z. physik. Chem.*, **B13**, 232 (1931).

(3) (a) P. C. Henriquez, *Rec. trav. chim.*, **54**, 574 (1935); (b) R. Newton, *cf. J. Franklin Inst.*, **224**, 583 (1937); *Trans. Faraday Soc.*, **47**, 1304 (1951); (c) J. G. Kirkwood, *J. Chem. Phys.*, **7**, 911 (1939).

(4) E. H. Archibald, "The Preparation of Pure Inorganic Substances," John Wiley & Sons, Inc., New York, N. Y., 1932, pp. 184, 212.

(5) A. Weissberger and E. Proskauer, "Organic Solvents, Physical Constants and Methods of Purification," 1935, pp. 105, 107, 163.

(6) L. A. Sayce and H. Briscoe, see R. J. W. Le Fèvre,[7] "Dipole moments," Methuen, London, 1948, p. 32.

(7) R. J. W. Le Fèvre, *Trans. Faraday Soc.*, **34**, 1129 (1938).

(8) L. Hartshorn and D. A. Oliver, *Proc. Roy. Soc. (London)*, **123A**, 664 (1929).

(9) H. G. Jenkins, *J. Chem. Soc.*, 382 (1934).

(10) C. G. Le Fèvre and R. J. W. Le Fèvre, *ibid.*, **49**, 1136 (1936).

(11) C. P. Smyth and S. O. Morgan, *J. Am. Chem. Soc.*, **50**, 1547 (1928).

(12) G. Miller, *ibid.*, **56**, 2360 (1934).

(13) M. E. Dorfman and J. H. Hildebrand, *ibid.*, **49**, 729 (1927).

(14) R. Clausius and O. F. Mosotti, R. J. W. Le Fèvre, ref. 6, p. 7.

(15) P. Debye, *Handbuch Radiol.*, **6**, 600 (1925).

(16) G. Hedestrand, *Z. physik. Chem.*, **B2**, 428 (1929).

(17) S. R. Palit and B. C. Banerjee, *Trans. Faraday Soc.*, **47**, 1299 (1951).

(18) L. Lorenz and H. A. Lorentz, See R. J. W. Le Fèvre[7]; ref. 6, p. 11, 17.

(19) C. B. Allsopp and H. F. Willis, *Proc. Roy. Soc. (London)*, **153**, 379 (1936).

(20) C. I. Zahn and J. B. Miles, *Phys. Rev.*, **32**, 497 (1928).

(21) R. J. W. Le Fèvre, "Dipole Moments," Methuen, 1928, p. 12.

(22) J. W. Smith and L. B. Witten, *Trans. Faraday Soc.*, **47**, 1315 (1951).

(23) J. W. Williams and R. J. Allgeier, *J. Am. Chem. Soc.*, **49**, 2416 (1927).

(24) P. Wierl, *Ann. Physik*, [5] **8**, 521 (1931).

(25) B. Trumpy, *Z. Physik*, **66**, 790 (1930).

(26) C. P. Smyth, *Phil. Mag.*, **50**, 361 (1925).

(27) H. O. Jenkins, *Trans. Faraday Soc.*, **30**, 739 (1934).

TABLE I

Solvent	t, ° C.	$P_{2\infty}$ Debye, cc. Graphical	Hedestrand	Palit-Banerjee	Mean value	α[a]	β[b]	EP_2, cc.	AP_2, cc.	$\mu R \times 10^{18}$	$P_{2\infty}$ modified formulas, cc. Henriquez	Kirkwood	Newton	Ref. (TP, this paper)
Titanium tetrachloride														
Benzene	14.7–20.0	44–45	...	...	...	...	...	37.8	2.7	0	...	...	...	1
	25.0	43.93	44.27	44.09	44.10	0.5611	0.9400	n_∞ 37.10	3.71	0	48.32	53.95	68.03	TP
Carbon tetrachloride	15.0–18.0	40–41	...	...	...	...	...	37.8	2.7	0	...	...	...	1
	19.8	43.2	...	...	...	...	...	43.23	...	0	...	...	...	2
	25.0	40.31	40.33	40.34	40.33	0.5591	0.1992	n_∞ 36.86	3.69	0	44.02	49.18	62.07	TP
Tin tetrachloride														
Benzene	14.7–20.0	58	...	...	...	...	...	n_∞ 35.2	8–10	0.80	...	...	...	1
	25.0	56.65	56.79	56.50	56.64	1.3502	1.7015	n_∞ 34.26	3.43	0.96	63.35	72.24	92.88	TP
Carbon tetrachloride	15.0–18.0	43–45	...	...	...	...	...	n_∞ 35.2	8–10	0	...	...	...	1
	17.7	52.5	...	...	...	...	...	38.91	...	0.80	...	...	...	2
	25.0	53.45	53.50	53.32	53.42	1.1453	0.7248	n_∞ 34.42	3.44	0.86	59.31	67.26	86.14	TP
Tin tetraiodide														
Benzene	25.0	26.70	...	...	...	...	...	...	30	0	...	...	...	23
	25.0	26.50	26.62	26.84	26.65	0.5967	6.4226	n_∞ 24.74	2.47	0	29.60	33.67	43.20	

[a] $\alpha = d\epsilon_{12}/df_2$, where ϵ_{12} is the dielectric constant of the solution and f_2 is the mole fraction of the solute ($\epsilon_{12} = \epsilon_1 + \alpha f_2$). [b] $\beta = d_{12}/df_2$, where d_{12} is the density of the solution ($d_{12} = d_1 + \beta f_2$). α and β are determined by the method of least squares.

mined in carbon tetrachloride is quite comparable with that of Bergmann and higher than that of Ulich, yet it could not be ascribed to the probable presence of water as was inferred by Ulich when discussing Bergmann's data, firstly because the total polarization of this halide when determined in benzene was found to be very near to that of Ulich and secondly, because there is no reason to assume that the presence of water should have a detrimental effect greater in carbon tetrachloride than in benzene since the solubility of HCl in the former solvent is less than that in the latter.[28] This compound may accordingly be conceived to possess a pyramidal structure with Sn located at the apex so as to account for the presence of an electric doublet in the molecule detectable in the different non-polar solvents.

The higher polarization values at infinite dilution in benzene than in carbon tetrachloride for the two halides may be attributed to the higher dissociating power of the former solvent.[29]

Tin Tetraiodide.—Measurements on tin tetraiodide show that this compound is non-polar. This agrees with previous work carried out by Williams and Allgeier[23] and with the conclusion drawn by Hildebrand[13,30] from solubility determinations in different organic solvents. This halide may, therefore, be considered in analogy to titanium tetrachloride to possess a tetrahedral structure with tin at the center of the grouping.

Application of Modified Formulas.—The modified formulas of Henriquez, Kirkwood and Newton applicable to solutions[22] were applied for calculating $P_{2\infty}$ and the values obtained are shown in Table II. From this table it can be seen that $P_{2\infty}$ for one halide varies with the solvent thus indicating that even equations which are based on a modified field theory do not satisfactorily account for the solvent effect. The effect of the solvent on the ratio between $P_{2\infty}$ obtained from each modified formula and that obtained from Debye's formula, and the dependence of this ratio on the polarity of the substance has been traced. The data shown in Table III reveal that the ratio for one halide is nearly the same in the two different solvents and that the increase in polarity is accompanied by a slight increase in the ratio. This result can be further supported when similar calculations are made on the Smith and Witten data.[22] One can, therefore, predict that substances of near dipole moment values should be of the same ratio. However, further work is necessary to substantiate this prediction.

TABLE II

$t = 25°$

Halide	Solvent	$P_{2\infty}$, cc. Kirkwood	Henriquez	Newton	Debye
$TiCl_4$	C_6H_6	53.95	48.32	68.03	44.10
	CCl_4	49.18	44.02	62.07	40.33
$SnCl_4$	C_6H_6	72.24	63.35	92.88	56.64
	CCl_4	67.26	59.31	86.14	53.42
SnI_4	C_6H_6	33.67	29.60	43.20	26.65

TABLE III

$t = 25°$

Halide	Solvent	$\frac{P_{2\infty}K}{P_{2\infty}D}$	$\frac{P_{2\infty}H}{P_{2\infty}D}$	$\frac{P_{2\infty}N}{P_{2\infty}D}$	$\mu_R \times 10^{18}$
$TiCl_4$	C_6H_6	1.22	1.09	1.54	0
	CCl_4	1.22	1.09	1.54	0
$SnCl_4$	C_6H_6	1.27	1.11	1.64	0.95
	CCl_4	1.26	1.11	1.61	0.86
SnI_4	C_6H_6	1.27	1.11	1.62	0

(28) F. Fairbrother, *J. Chem. Soc.*, 43 (1932).

(29) A. E. Van Arkel and S. L. Snoek, *Rec. trav. chim.*, **52**, 719 (1933).

(30) J. H. Hildebrand, "Solubility," Reinhold Publishing Corporation, New York, N. Y., 1924, Chap. 14.

VOLUME–TEMPERATURE RELATIONSHIPS IN MAGNESIUM–CADMIUM ALLOYS. I. THERMAL EXPANSIVITIES IN THE ORDER–DISORDER RANGE[1,2]

By R. A. Flinn,[3] W. E. Wallace and R. S. Craig

Department of Chemistry, University of Pittsburgh, Pittsburgh 13, Pa.

Received August 7, 1956

The cadmium-rich magnesium–cadmium alloys are known to contain an exceptionally large number of vacant lattice sites. Thermal expansivities of $MgCd_3$ were measured to try to ascertain the factors responsible for the abundance of vacancies. The measurements were then extended to the compositions MgCd and Mg_3Cd. Expansivities in each case show the expected maximum near the order–disorder Curie point. There is in the main good agreement between the present results and expansivities obtained by the X-ray method and volume expansivities computed from measured linear expansivities of bulk samples. This indicates that the fraction of vacant lattice sites is virtually independent of temperature. The implications of this finding as regards the mechanism of vacancy formation, particularly the energy requirements, are presented.

Introduction

Magnesium–cadmium alloys have been studied extensively[1] in this Laboratory in recent years. In alloys containing 75 to 90 atomic % cadmium Schottky defects (vacant lattice sites) were found[4–6] to be exceptionally numerous, ranging up to a maximum of about 2%. The present measurements involving $MgCd_3$ were undertaken in hopes that the factors responsible for the large number of vacancies in this substance might be revealed and clarified. Once facilities were available it was decided to extend the measurements to include Mg_3Cd and MgCd, which, in addition to $MgCd_3$, are known to exist as a single phase at room temperature.

Experimental Details

Apparatus and Materials.—All the measurements were made using a dilatometer consisting of a cylindrical chamber filled with a fluid in which the sample in rod form was immersed. A glass capillary was sealed into the chamber and the increase in volume of the sample caused a displacement of the meniscus in the capillary of several centimeters. The displacement was read with a cathetometer.

The dilatometer was of simple design. The sample was a rod about 2 cm. in diameter and 3 cm. long. The dilatometer chamber was made of stainless steel rod, drilled out to an internal diameter about 2 mm. greater than the sample diameter. A 1 mm. diameter capillary tube about 60 cm. long was attached to the top by a glass–Kovar seal, the Kovar end being hard soldered to the dilatometer chamber. The chamber was loaded from the bottom and was closed by a machined and polished plate which fit onto a polished seal. This arrangement was backed up by a lead gasket to eliminate leakage. The dilatometer fluid was a chlorinated biphenyl compound sold under the trade name of "Aroclor." Preliminary tests showed the alloys to be chemically inert to this fluid.

The cross-sectional area of the capillary was established by determining the length of a mercury thread of known weight at various places along the tube. A measuring microscope was used to measure these lengths. The cross-sectional area was constant to ± 0.0001 cm.^{2} and averaged 0.00641 ± 0.00006 cm.^{2}. Thus, by reading the position of the meniscus to 0.01 cm. a volume change of the sample corresponding to 0.001% could be observed. A fiducial mark was inscribed on the capillary and its position periodically observed to guarantee that the relative positions of the cathetometer and dilatometer had not changed.

Samples for study were prepared and analyzed by techniques which have been described.[7,8] They were homogenized at 300° for at least two weeks prior to use. Compositions studied were 74.58 ± 0.09, 50.09 ± 0.04 and 24.93 ± 0.03 atomic % cadmium which are referred to as $MgCd_3$, MgCd and Mg_3Cd, respectively.

Procedure in the Expansivity Measurements.—The usual experimental procedure was to raise the temperature of the apparatus to the uppermost value desired and allow the system to equilibrate at this point for about 15 hours. The temperature was then reduced by 10-degree intervals, allowing the meniscus to come to a steady level before proceeding with the next reduction. Generally, the waiting period between reductions was about $^1/_2$ hour, although the system had usually adjusted to the next temperature within 15 min. In the case of $MgCd_3$, where the ordering and disordering proceeded rather slowly, much longer waiting periods were necessary, sometimes extending to several days. This will be discussed in more detail in the following paper dealing with the kinetics of this reaction. When the measurements had been completed down to room temperature, they were repeated, using rising temperatures with similar increments and waiting periods.

The above procedure was reversed in the case of the MgCd sample. The order–disorder transition temperature in this alloy is at about 250°, requiring measurements up to 270°. A cottonseed oil-bath was used for temperatures above 100° and this proved to be rather unsatisfactory above 200°. Measurements in the range above this had to be made as rapidly as possible. Since allowing the sample to equilibrate for any extended period of time at an elevated temperature was not feasible, measurements were made starting at about 30° and increasing the temperature by 10° increments.

When the temperature of the dilatometer was changed, several things combined to give the observed displacement of the meniscus. Let us consider the effect of increasing the temperature from T to T'. First, the volume of the dilatometer chamber increases; this lowers the meniscus. Second, the specific volume of the Aroclor increases, raising the meniscus. Third, the sample expands, raising the meniscus. Fourth, these changes expelled from the bath to the capillary a certain volume of liquid whose temperature was lowered. This reduces the height of the meniscus. Finally, a very small rise in the meniscus is caused by the slight increase in temperature of the fluid contained in the capillary.

To evaluate the volume increase of a sample from the observed displacement of the meniscus it is necessary to know the expansivities of the dilatometer and the Aroclor. These were determined in calibration experiments in which the dilatometer was first used without a sample, and second

(1) This work was supported by the U. S. Atomic Energy Commission.

(2) From a thesis submitted by R. A. Flinn to the Graduate School, University of Pittsburgh, June, 1954.

(3) Dow Chemical Company Fellow during the academic year 1953–54.

(4) L. W. Coffer, R. S. Craig, C. A. Krier and W. E. Wallace, *J. Am. Chem. Soc.*, **76**, 241 (1954). This paper gives references to the earlier studies of this system.

(5) J. M. Singer and W. E. Wallace, This Journal, **52**, 999 (1948).

(6) D. A. Edwards, W. E. Wallace and R. S. Craig, *J. Am. Chem. Soc.*, **74**, 5256 (1952).

(7) C. B. Satterthwaite, R. S. Craig and W. E. Wallace, *ibid.*, **76**, 232 (1954).

(8) F. A. Trumbore, W. E. Wallace and R. S. Craig, *ibid.*, **74**, 132 (1952).

TABLE I

EXPANSIVITIES OF MAGNESIUM–CADMIUM ALLOYS, $(1/V)(dV/dT) \times 10^4$

T, °C.	$MgCd_3$ Falling temp.	$MgCd_3$ Rising temp.	Mg_3Cd Falling temp.	Mg_3Cd Rising temp.	MgCd Rising temp.
25.0	1.50	1.50	0.91	0.91	1.21
35.0	1.50	1.50	.92	.92	1.22
45.0	1.50	1.50	.94	.94	1.23
55.0	1.66	1.57	.96	.96	1.23
65.0	2.73	2.00	.98	.98	1.24
70.0	4.65 (max.)				
75.0	1.62	2.75	1.01	1.01	1.25
77.5		2.77 (max.)			
80.0	1.25				
85.0	1.22	2.57	1.06	1.06	1.26
95.0	1.20	1.28	1.12	1.12	1.27
105.0	1.20	1.20	1.21	1.21	1.29
115.0	1.20	1.20	1.33	1.33	1.30
125.0	1.20		1.55	1.55	1.32
135.0	1.20		2.14	2.14	1.34
145.0	1.20			3.45	1.36
146.0			4.89 (max.)		
149.0				3.67 (max.)	
150.0			2.45		
155.0	1.20		1.40	1.85	1.38
160.0				1.24	
165.0	1.20		1.15	1.15	1.40
175.0	1.20		1.15	1.15	1.42
185.0	1.20		1.15		1.44
195.0	1.20		1.15		1.47
205.0	1.20		1.15		1.50
215.0	1.20		1.15		1.57
225.0					1.72
235.0					2.00
245.0					5.25
249.0					9.22 (max.)
255.0					2.75
260.0					1.00

with a sample of magnesium, whose expansivity is known.[9] Calculations of the Aroclor and dilatometer expansivities from these series of determinations and the alloy expansivities from the other measurements involve some straightforward but tedious algebra which will not be given here since the details can be found elsewhere.[10]

The volume of the sample was computed from its weight and the known densities of these alloys.[5] Temperatures were measured using a copper–constantan thermocouple which had been calibrated at the freezing points of lead and tin and at the boiling point of water.

Discussion of Results

Observed Results.—Measured results are given in Table I. Hysteresis in the expansivities was found near the order–disorder Curie points for $MgCd_3$ and Mg_3Cd but not for MgCd. With both Mg_3Cd and $MgCd_3$ the extra expansivity due to the transformation extends over a wider temperature range for rising than for falling temperatures. The hysteresis is most pronounced with $MgCd_3$ as would be expected from the low transformation temperature for this alloy.

Temperature Dependence of the Number of Schottky Defects in $MgCd_3$.—To ascertain the effect of temperature on the number of vacancies in $MgCd_3$ one intercompares the volume increments measured macroscopically with those measured using the X-ray method. If the macroscopically measured expansivity exceeds that measured by the X-ray method, one concludes that the fraction of vacant lattice sites is increasing with rising temperature. Since the expansivity is dependent on history at temperatures in the vicinity of the transformation, it is not possible to make a meaningful comparison of expansivities at these temperatures. The volume change for the transformation is, however, almost the same for rising or falling temperatures and so one can make an appropriate intercomparison of the integrated volume changes over an extended temperature interval covering the range in which the transformation occurs. The volume of $MgCd_3$ at 140° relative to that at 25° was found by the X-ray method[6] to be 1.0178 as compared to 1.0186 obtained from the present results. Corresponding quantities for 215° are 1.0262 and 1.0270. Hirabayashi has measured[11] linear expansivities of single crystals of $MgCd_3$ from which one can compute the ratio of volumes at 25 and 140° to be 1.0165. This is in reasonably good agreement with the results obtained in the present study. These data indicate that on increasing the temperature from 25 to 140° the percentage of vacant lattice

(9) H. Esser and H. Eusterbrook, *Arch. Eisenhutten w.*, **14**, 341 (1941).

(10) R. A. Flinn, Ph.D. Dissertation, University of Pittsburgh, 1954.

(11) M. Hirabayashi, *J. Jap. Inst. Metals (Sendai)*, **15**, No. 2 (1951).

sites increases by 0.08% if the present data are employed, or decreases by 0.13% if one makes use of Hirabayashi's measurements. Thus there is little if any variation of the fraction of lattice sites which are vacant on going from the ordered to the disordered state. The further increase in Schottky defects on going from 140 to 215° is 0.00%.

Inferences about the Energy of Vacancy Formation in $MgCd_3$.—When a lattice site in a pure solid is vacated, both the energy and the entropy of the solid increase. For a small number of vacancies the entropy effect on the free energy is dominant and the solid contains under equilibrium conditions a fraction of vacancies sufficient to minimize its free energy. Experiment has shown that the percentage of vacancies in pure metals is small, being of the order of 0.1% at temperatures approaching their melting points. The existence of 2% vacancies in $MgCd_3$ at 25° would suggest that if they originate in the same way as in pure solids, the energy of vacancy formation is unusually small—roughly 2.5 kcal./mole of vacancies. If the energy of vacancy formation were really so small, one would expect approximately a fourfold increase in vacancy concentration on increasing the temperature from 25 to 200°. The measurements presented in this paper exclude this as a possibility. It therefore appears that some other mechanism must be responsible for the defects in $MgCd_3$.

Elsewhere it has been pointed out that extensive vacancies also occur in certain alkali halide solid solutions.[12,13] The idea has been advanced[13] that in solid solutions wherein particles of unequal size must be arranged on a common lattice, stresses develop and these may be relieved by omitting an occasional particle. For example, when a small amount of KCl is dissolved in solid NaCl, the first neighbors of the potassium ion are so crowded that the energy of the system may actually be lowered by creating vacancies. In this way one may account for the abundance of vacancies in the KCl-rich NaCl–KCl system[13] and similarly in the cadmium-rich magnesium–cadmium alloys. In each case a solvent ion is replaced by a larger ion as the solution is formed and considerable stresses must be developed. It is to be noted that these ideas imply that in certain solid solutions vacancies are formed *exothermally*. For this reason in such systems vacancies are not expected to become significantly more numerous as the temperature is raised.

There is an alternative possibility to the effect that the introduction of the first 1 to 2% vacancies is accomplished with a very small expenditure of energy per vacancy (due to the simultaneous relief of strains) after which the energy increases very rapidly. One would expect in this case a large number of vacancies but a small temperature coefficient. To distinguish between these two possibilities it would be necessary to study the effect of temperature on the number of defects at lower temperatures. It is possible that this approach might further clarify the factors responsible for the large number of vacancies, although increasing difficulties in attaining equilibrium conditions at reduced temperatures might obscure the interpretation of results obtained in this way.

(12) W. T. Barrett and W. E. Wallace, *J. Am. Chem. Soc.*, **76**, 366 (1954).

(13) W. E. Wallace and R. A. Flinn, *Nature*, **172**, 681 (1953).

VOLUME–TEMPERATURE RELATIONSHIPS IN MAGNESIUM–CADMIUM ALLOYS. II. KINETICS OF THE ORDER–DISORDER TRANSFORMATION IN $MgCd_3$[1,2]

BY R. A. FLINN,[3] W. E. WALLACE AND R. S. CRAIG

Department of Chemistry, University of Pittsburgh, Pittsburgh 13, Pa.

Received August 7, 1956

The rates of ordering and disordering of $MgCd_3$ have been determined by a dilatometric method. The transformation appears to occur in two stages both of which are, within the limit of error, first-order processes. Rate constants at a number of temperatures are presented. It has been found that the kinetic behavior of the system is not uniquely determined by temperature but depends on thermal history as well.

Introduction

Thermal expansivities of $MgCd_3$ at temperatures covering the order–disorder Curie point have been measured and reported in the preceding paper[4] (hereinafter referred to as I). While these measurements were being made, it became apparent that some interesting information pertaining to the velocity of the order–disorder transformation in $MgCd_3$ was emerging. This paper contains an account of studies of the kinetics of ordering and disordering in $MgCd_3$ as determined dilatometrically.

Experimental Details

Measurements were made in the dilatometer described in paper I. Three types of measurements were performed. In the type A experiments temperature was decreased in intervals of about 10° and the rate of ordering observed by watching the fall in the meniscus of the dilatometric liquid. This gave information covering the rate of attainment of the equilibrium amount of order characteristic of various temperatures in the region below the critical temperature. In the type B experiments the sample was quenched to

(1) This work was supported by the U. S. Atomic Energy Commission.

(2) From a thesis submitted by R. A. Flinn to the Graduate School, University of Pittsburgh, June, 1954.

(3) Dow Chemical Company Fellow during the academic year 1953–1954.

(4) R. A. Flinn W. E. Wallace and R. S. Craig, THIS JOURNAL, **61**, 234 (1957).

various temperatures below the critical temperature from a single temperature (83 to 84°). This gave information concerning the rate of the transition as a function of the degree of undercooling. The type C experiments were similar to the type A experiments except that in the former case the temperature was increased at intervals of about 10° and the kinetics of disordering were determined.

The sample of $MgCd_3$ was the same as that used in paper I.

Experimental Results and Treatment of Data

The variation of meniscus height relative to the final position of the meniscus for the three types of rate studies is shown in Figs. 1, 2 and 3, which give data for the A, B and C types of experiment. Numerical values are given elsewhere.[5] Since these data all seemed to indicate an exponential approach to h_f, the final meniscus position, an attempt was made to fit the data to an equation of the form $h - h_f = ce^{-kt}$. A plot of log $(h - h_f)$ *versus* time showed in all cases linearity beyond a time t' but in most cases there was a positive departure from the straight line at times smaller than t'. A typical example of this is represented in Fig. 4 which shows the time variation of log $(h - h_f)$ at 54.6° for a sample of $MgCd_3$ quenched from 65.3°. The nature of this plot suggests that the transformation in $MgCd_3$ occurs in two stages the first of which is the more rapid. Thus the $MgCd_3$ transformation seems to follow the customary pattern, since most investigations of the kinetics of ordering have led to the conclusion that these processes occur in two stages.[6-9] We shall now examine the data in detail to see if they are indeed consistent with the notion of two consecutive processes with differing rate constants.

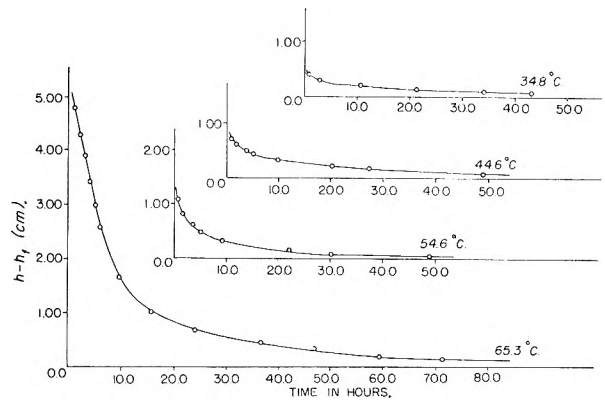

Fig. 1.—Dilatometrically measured rate of ordering of $MgCd_3$ at successively lower temperatures (Type A experiment).

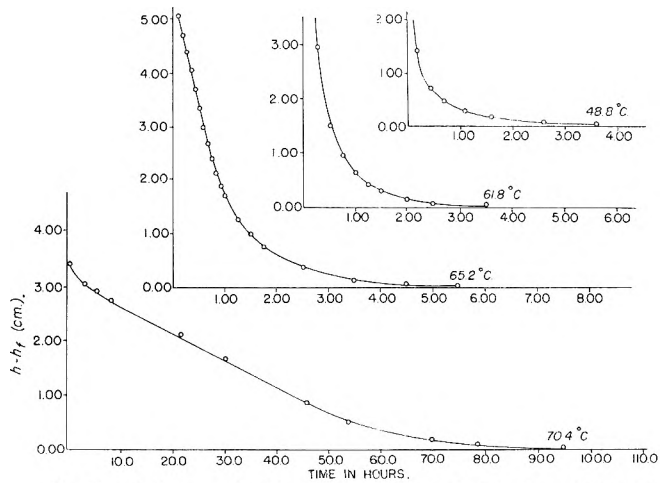

Fig. 2.—Dilatometrically measured rate of ordering of $MgCd_3$ when quenched from a common temperature, 84° (Type B experiments).

Let us denote the transformation from the disordered to the ordered state as

$$A \longrightarrow B \longrightarrow C \qquad (1) \text{ and } (2)$$

It will be assumed that each of these processes is first order kinetically with rate constants k_1 and k_2 for the first and second stages, respectively. As indicated above the first stage is faster and hence k_1 is larger than k_2.

Let us first consider the meniscus displacement (m.d.) due to the second process. $\Delta h''$ will represent the m.d. from the final position due to process 2 and is of course a function of time. The m.d. in the time interval dt due to process 2 is

$$dh = -c_2 \frac{dC}{dt} dt \qquad (3)$$

where c_2 is a positive constant and dC/dt is the rate of formation of C from B. Since the rate of formation of C is first order with respect to the concentration of B, equation 3 may be rewritten as

$$\frac{dh}{dt} = -c_2 k_2 B \qquad (4)$$

In such a reaction sequence as shown in (2) when both steps are first order, the concentration of the intermediate substance is given by the expression

$$B = \frac{k_1 A_0}{k_1 - k_2} (e^{-k_2 t} - e^{-k_1 t}) \qquad (5)$$

A_0 is the initial concentration of A. Substituting

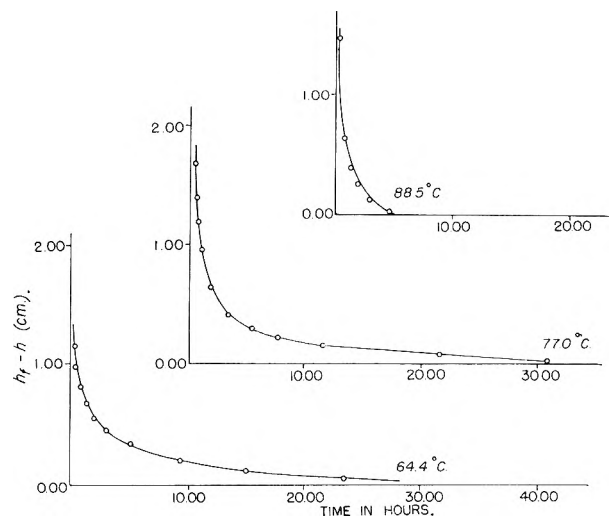

Fig. 3.—Dilatometrically measured rate of disordering of $MgCd_3$ at successively higher temperatures (type C experiments).

(5) R. A. Flinn, Ph.D. Thesis, University of Pittsburgh (1954).

(6) C. Sykes and H. Evans, *Proc. Roy. Soc.* (*London*), **A157**, 213 (1936).

(7) C. Sykes and F. W. Jones, *J. Inst. Metals*, **58**, 225 (1936).

(8) G. Borelius, L. E. Larsen and H. Selberg, *Arkiv. Fysik*, **2**, 161 (1950).

(9) N. W. Lord, *J. Chem. Phys.*, **21**, 692 (1953).

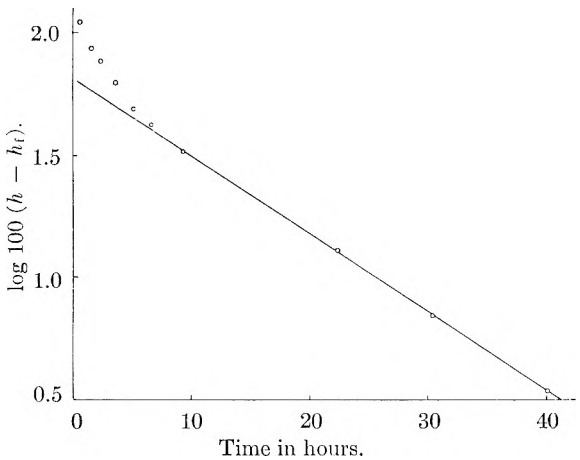

Fig. 4.—Dilatometrically measured rate of ordering in $MgCd_3$ at 54.6°.

eq. 5 into 4 and integrating from infinite time to time t one obtains

$$\Delta h'' = \beta k_2 \left(\frac{e^{-k_2 t}}{k_2} - \frac{e^{-k_1 t}}{k_1} \right) \qquad (6)$$

where $\beta = c_2 k_1 \Delta_0/(k_1 - k_2)$. Since $k_1 > k_2$, the second term in the parentheses becomes negligible at large values of t and $\Delta h'' = \beta e^{-k_2 t}$. The constants β and k_2 are readily evaluated by plotting log $(h - h_f)$ against time. For times near the completion of the reaction $h - h_f = \Delta h''$, the first stage being so nearly complete as to make a negligible effect on the displacement of the meniscus. After β and k_2 have been obtained, it is then possible to obtain k_1, the rate constant for the more rapid first stage.

Let us denote by $\Delta h_0''$ the total m.d. due to the second process. $\Delta h_0''$ can, of course, be evaluated by setting $t = 0$ in eq. 6. Call h_f' the final position which the meniscus would have reached if only process 1 had occurred.

$$h_f' = h_f + \Delta h_0'' \qquad (7)$$

To obtain the m.d. from h_f' due solely to process 1 for $t < t'$ it is necessary to correct the observed meniscus position h for the displacement due to process 2 during the interval from 0 time up to time t. Let us call this corrected meniscus position h'.

$$h' = h + \Delta h_0'' - \Delta h'' \qquad (8)$$

Now the m.d. associated with the conversion of the alloy in state A to state B is $h' - h_f' = h - h_f - \Delta h''$. Since the rate of the conversion of A into B is assumed to obey first-order kinetics

$$h' - h_f' = C' e^{-k_1 t} \qquad (9)$$

C' is a constant, the initial value of the m.d. due to process 1. We thus see that

$$h - h_f - \Delta h'' = C' e^{-k_1 t} \qquad (10)$$

which with eq. 6 gives the relationship

$$h - h_f - \beta e^{-k_2 t} = \alpha e^{-k_1 t} \qquad (11)$$

Where $\alpha = C' - \beta k_2/k_1$. We thus have the complete expression for the variation of $h - h_f$, the position of the meniscus relative to its final position

$$h - h_f = \alpha e^{-k_1 t} + \beta e^{-k_2 t} \qquad (12)$$

α and k_1 may be evaluated by plotting log $(\Delta h')$ against time for times less than t', where $\Delta h' = h - h_f - \beta e^{-k_2 t}$.

Treatment of the disordering process leads to an equation of the same form as eq. 12 and the evaluation of constants is accomplished in the same way.

Examination of the data for the early stages of the transformation shows that in the main log $\Delta h'$ is linear with time within the limit of experimental error. Two representative cases are shown in Fig. 5. In those cases where there is departure from linearity simple explanations can be provided. For the type A experiment at 34.8° and the type C experiment at 88.5° there is clear evidence for a faster process in the earlier stages but the $\Delta h'$ values are too small and too few in number to confirm the exponential dependence on time. In the type B experiments at 61.8 and 48.8° the data suggest the possibility of a two stage process, the first being the rapid one. However, at these temperatures the entire reaction occurs so rapidly that if there is a first stage, it occurs for the most part in the first half hour during which thermal contraction is very important and is mainly responsible for the m.d. The rapid variation of meniscus position seemed to persist for a longer time than one would expect for the attainment of thermal equilibrium but one cannot regard the existence of a fast first process as established in these cases. The existence of a rapid first stage and the exponential variation of $\Delta h'$ with time were found for the type A experiments at 54.6 and 44.6°, the type C experiments at 64.4 and 77.0° and after 5 hours for the type A experiment at 65.3. The rates during the first 5 hours in this latter experiment were abnormally slow. It seems likely that during this period nucleation was either rate controlling or at least reducing the rate of reaction, since this temperature is only slightly below the transformation temperature. The existence of an induction period during which nuclei are being formed and the rate is extremely slow is very noticeable in the type B experiment at 70.4°. Here the plot of log $(h - h_f)$ *versus* time shows at first glance no evidence of a rapid process for small values of t. The plot is linear for large values of t but for times less than 50 hr. the log $(h - h_f)$ points fall well below the extension of the straight line. Again it seems reasonable to ascribe the small rate of the reaction in the early stages to the slow formation of nuclei. It is possible that here too there is a rapid first stage but that its presence is masked by the growing number of nuclei and the resulting opportunity for acceleration of the transformation as time elapses. This tendency combined with the dying away of the rapid first stage process may be responsible for the rather odd linear variation of $h - h_f$ with time from $t = 5$ hr. to $t = 45$ hr. (see Fig. 2).

The opposing effects of nucleation and a rapid first process are also apparent in the type B experiment at 65.2°. In that case they so nearly cancel that the log $(h - h_f)$ is almost linear over the entire duration of the experiment.

The values of the constants α, β, k_1 and k_2 are shown in Table I together with the time beyond which eq. 12 is applicable.

Discussion of Results

The data are consistent with the notion that the ordering or disordering of $MgCd_3$ occurs in two

TABLE I

CONSTANTS FOR EQ. 12 IN TEXT

Temp., °C.	α, cm.	β, cm.	k_1, hr.$^{-1}$	k_2, hr.$^{-1}$	Applicable beyond hr.
		Type A experiments			
65.3	6.64	1.660	0.271	0.0370	5
54.6	0.570	0.621	.401	.0675	1
44.6	.319	.470	.360	.0368	1
34.8	.16	.328	.80	.0400	1
		Type B experiments			
70.4	...	22.4	...	0.0703	0.55
65.2	...	6.84	...	1.142	2.5
61.8	...	2.580	...	1.508	1.25
48.8	...	0.728	...	0.835	1
		Type C experiments			
64.4	−0.583	−0.562	0.744	0.113	0.9
77.0	−1.022	− .382	.753	.0801	0.8
88.5	...	− .977	...	.724	1.25

stages, a fast first stage followed by a slower second stage, although in some cases the first stage is masked by other effects—attainment of thermal equilibrium or nucleation. Like most studies of the kinetics of order–disorder transformations the present study provides no information as to the nature of the two stages. It has been suggested[6,7,9] that the first stage may be the growth of domains from existing nuclei until impingement occurs and the second stage consists in the coalescence of antiphase domains. Another notion[10] is that the ordering of the first stage leaves the alloy in a strained condition and the order parameter which is adopted is characteristic of the strained alloy. The second stage is then ascribed to the disappearance of strains and subsequent relaxation of the order parameter to the value characteristic of the alloy in its equilibrium state. Neither of these suggested explanations is of such a nature as to be amenable to illumination by dilatometric work.

The general features of the data suggest that the transformation in $MgCd_3$ occurs by a nucleation and growth mechanism. The two stage process under discussion above, of course, applies only to the growth stage. The existence of something in the nature of an induction period in the ordering process which was at temperatures just below the transformation point is of course characteristic of processes initiated by nucleation. In this connection the difference between the kinetic behavior in the type A experiment at 65.3° and the type B experiment at 65.2° are significant. The over-all rate of the former was very much less than that of the latter. The thermal histories of the sample differed markedly in the two cases In the type A experiment the sample was held at 207° for 15 hr. and subsequently reduced to temperature over a period of several days while expansivities between 207 and 65.3° were being measured. In the other experiment the sample was held at 120° for 10 hr., cooled to 84°, held there an hour and quenched to 65.2°. Avrami[11] has advanced the notion that there are precursors to the actual nuclei. He has called these precursors "germ nuclei." He has further maintained that the number of "germ nuclei" are reduced progressively with the amount and length of superheating above the transition point. Thus, he expects the number of nuclei formed on subsequent cooling, and hence the transformation rate, to be sensitive to the thermal history of the sample. Perhaps Avrami's germ nuclei are lattice defects of some sort which are conducive to nucleation and which are annealed out at elevated temperature. Whatever the cause, the effect of thermal history is clearly apparent in the two experiments under discussion. This sensitivity to thermal history does not, of course, establish that the ordering in $MgCd_3$ requires nucleation but it can be most easily rationalized in terms of a nucleation and growth mechanism.

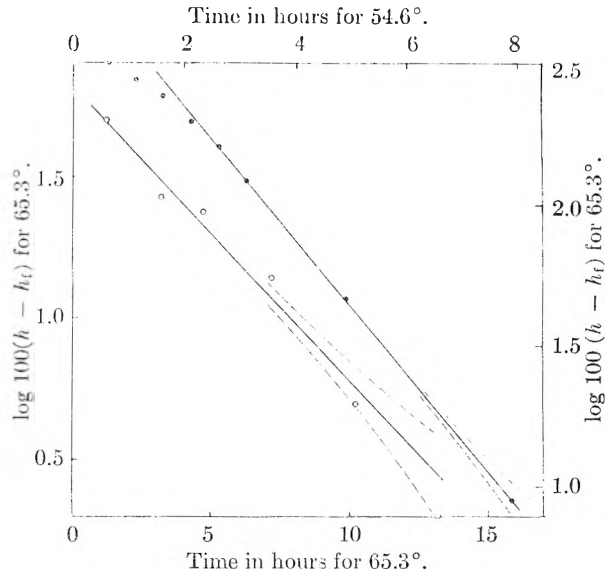

Fig. 5.—Dilatometrically measured rates of ordering in $MgCd_3$: ○, at 54.6°; ●, at 65.3°. Dotted lines show effect of ±0.01 cm. in meniscus position.

(10) G. Borelius, C. H. Johansson and J. O. Linde, *Ann. Physik*, **86**, 291 (1928).

(11) M. Avrami, *J. Chem. Phys.*, **7**, 1103 (1939).

VAPOR PRESSURES AND CRYOSCOPIC DATA FOR SOME ALIPHATIC DINITROXY AND TRINITROXY COMPOUNDS

BY M. D. KEMP, S. GOLDHAGEN AND F. A. ZIHLMAN

Contribution from the Research and Development Department of the U. S. Naval Powder Factory,[1] *Indian Head, Md.*

Received August 27, 1956

Vapor pressures of nine aliphatic dinitroxy and trinitroxy compounds were determined at 20, 30 and 40° by use of the transportation method. Heats of vaporization were calculated by means of the Clausius–Clapeyron equation. Freezing curves on 0.2 to 0.5 g. samples were used to determine purity, heats of fusion and freezing points for zero impurity for six compounds which froze at an appreciable rate. Refractive indices of the liquids are given.

Introduction

As a part of a series of studies of physical properties of compounds containing explosive groups, vapor pressures were determined at 20, 30 and 40° for six aliphatic dinitroxy and three aliphatic trinitroxy compounds by means of a transpiration method. Heats of vaporization were calculated by means of the Clausius–Clapeyron equation.

Freezing curve techniques, modified for use with small amounts of explosive material, were used to determine purity, heats of fusion and freezing points corrected to zero impurity. This technique was applicable to six compounds which froze at an appreciable rate.

Experimental

Materials Used.—1,3-Dinitroxypropane, nitroglycerin I, nitroglycerin II, 1,3-dinitroxybutane, 1,4-dinitroxybutane, 1,2,4-trinitroxybutane, 1,5-dinitroxypentane, 2,4-dinitroxypentane, 1,2,5-trinitroxypentane and 2,5-dinitroxyhexane were prepared and purified by Louis Silberman.[2] Nitroglycerin I was prepared by nitrating glycerol with sulfuric acid and nitric acid; nitroglycerin II was prepared by use of nitric acid alone in the nitration. The remaining compounds were prepared by mixed acid nitration of the alcohols. After purification by repeated washings, distillations and crystallizations the compounds were dried in an Abderhalden drier (boiling methylene chloride and phosphoric anhydride) and aerated for 24 to 48 hours with dry metered air to a constant rate of loss in weight.

Methods Used for Freezing Points, Purity and Heats of Fusion.—The freezing curve apparatus is arranged in a manner similar to that of Glasgow, Streiff and Rossini.[3] The sample tube and cryostat were reduced to a size more suitable for use with samples of from 0.2 to 0.5 g. Temperature measurements were made with a No. 36 gage copper-constantan thermocouple in conjunction with a Leeds and Northrup K-2 potentiometer and a high sensitivity mirror type galvanometer. The thermocouple was calibrated from a deviation curve for the region below 0° by the determination of the e.m.f.'s at the freezing point of mercury (−38.87°) and the normal sublimation point of carbon dioxide (−78.51°), and drawing a line through the points and the origin (0°). An accuracy better than +2 μv. may be obtained in this manner. Using an equation of the Antoine type, $\log_{10} p = B - A/t + c$ ($c = 273.16$), the temperature of the carbon dioxide was computed from the equation

$$\log_{10} p = 9.81137 \frac{-1349}{t + 273.16}$$

where the constants were obtained from the data of Myers and Van Dusen.[4]

For the region above 0°, the thermocouple was calibrated at the boiling point of water the melting point of methylnaphthalene (33.62°) and naphthalene (79.81°) previously compared with a platinum resistance thermometer at these points.

The freezing points were determined and the heats of fusion and purity were calculated from the time–temperature freezing curves according to the method first described by White[5] as modified by Schwab and Wichers.[6]

The purity was calculated from the relationship

$$\frac{x}{\Delta T_x} = \frac{x + a}{\Delta T_{x+a}}$$

in which x is the mole fraction of minor component, a is the mole fraction of added impurity, and ΔT_x and ΔT_{x+a} represent the decrease in temperature between two timed corresponding stages of freezing for the sample and the sample plus added impurity, respectively. In the determination of purity by this method, it is essential that the conditions of freezing including the rate of freezing be substantially reproduced between the sample and the sample plus the added impurity. The nitroxyesters were added to each other as impurities.

The heats of fusion and freezing point for zero impurity were calculated in the manner

$$-\ln(1 - x) = \frac{\Delta H_{f_0}(T_0 - T_1)}{RT^2_{f_0}} = \frac{\Delta H_{f_0} T_0}{RT^2_{f_0}} - \frac{\Delta H_{f_0} T_1}{RT^2_{f_0}} \quad (1)$$

$$-\ln(1 - x - a) = \frac{\Delta H_{f_0}(T_0 - T^*)}{RT^2_{f_0}} = \frac{\Delta H_{f_0} T_0}{RT^2_0} - \frac{\Delta H_{f_0} T^*}{RT^2_0} \quad (2)$$

Subtracting eq. 2 from eq. 1

$$\ln \frac{(1 - x - a)}{(1 - x)} = \frac{\Delta H_{f_0} T^*}{RT^2_0} - \frac{\Delta H_{f_0} T_1}{RT^2_0} = \frac{\Delta H_{f_0}(T^* - T_1)}{RT^2_0} \quad (3)$$

then

$$\frac{\Delta H_{f_0}}{T^2_0} = \frac{R}{(T^* - T_1)} \ln \frac{(1 - x - a)}{(1 - x)} \quad (4)$$

but from eq. 1

$$\frac{\Delta H_{f_0}}{T^2_0} = \frac{-R \ln(1 - x)}{(T_0 - T_1)} \quad (5)$$

T_0, T_1 and T^* are the freezing points of the pure substance, the substance with x mole fraction of impurity and with $x + a$ mole fraction of impurity, respectively.

The quantity $\Delta H_{f_0}/T^2_0$ was calculated from experimental data by eq. 5.

For systems which approach ideal solutions such as benzene–toluene and naphthalene–methylnaphthalene, this procedure was found to give values of x within about 2% of the known values.

Nitrogen determinations by means of a nitrometer were made, and the relation between experimental nitrogen and theoretical nitrogen is included for comparison of the purity determinations.

Method Used in Vapor Pressure Measurements.—The vapor pressures were determined by the transpiration

(1) Published with permission of the Bureau of Ordnance, Navy Department. The opinions and conclusions are those of the authors.

(2) Picatinny Arsenal, Dover, New Jersey.

(3) A. R. Glasgow, Jr., A. J. Streiff and F. D. Rossini, *J. Research Natl. Bur. Standards*, **25**, 355 (1945).

(4) C. H. Myers and M. S. Van Dusen, *J. Research Natl. Bur. of Standards*, **10**, 381 (1933). R.P. 538 (See also reference No. 6, p. 212).

(5) W. P. White, THIS JOURNAL, **24**, 292 (1920).

(6) "Temperature, Its Measurement and Control in Science and in Industry," Reinhold Publishing Corp., New York, N. Y., 1941, p. 256.

TABLE I

FREEZING POINTS, PURITY ESTIMATES AND HEATS OF FUSION OF SELECTED NITRATE ESTERS

Compound	Cor. f.p. (°C.)	% Nitrogen based on Theory	% Nitrogen based on Nitrometer	% theor. nitrogen	Mole % purity by freezing curves	Heats of fusion Cal./g.	Heats of fusion Kcal./mole
1,3-Dinitroxypropane	−29.49	16.87	16.82	99.70	>97 (est.)	..	..
Nitroglycerin (mixed acid nitration)	12.83	18.51	18.47	99.78	99.71	25.0	5.68
Nitroglycerin (straight acid nitration)	12.86	18.51	18.48	99.84	100.00	28.1	6.36
1,3-Dinitroxybutane	−19.78	15.55	15.55	100.00	99.81	22.2	4.00
1,4-Dinitroxybutane	12.3	15.55	15.55	100.00	99.98	35.4	6.38
1,2,4-Trinitroxybutane	−11.34	17.43	17.42	99.94	>97 (est.)	..	...
1,5-Dinitroxypentane	−16.59	14.43	14.41	99.86	99.69	19.1	3.70
2,4-Dinitroxypentane	−18.48	14.43	14.38	99.65	99.81	29.8	5.79
1,2,5-Trinitroxypentane	...	16.47	16.46	99.94	....	..	...
2,5-Dinitroxyhexane	50.37	13.46	13.38	99.41	99.68	63.4	13.2

method as used by Crater[7] and modified by Brandner.[8] The measured amount of dry air passed through liquid samples contained in two absorption bulbs by siphoning water from a calibrated 50-liter container and the loss in weight of the sample was determined on a semi-micro balance. The solid was contained in long narrow tubes with sintered-glass discs to prevent mechanical loss of the sample. A mercury manometer near the Geissler bulbs was used to measure the pressure developed due to resistance to flow of the air passing through the system. Constant temperature was maintained to ±0.1°. If the change in the weight of the second bulb exceeded 1% of that in the first bulb, the determination was discarded. From 6 to 8 valid determinations in total were made for each compound except for the solid, 2,5-dinitroxyhexane, in which case 20 determinations were made.

Assuming that the ideal gas laws hold and that Dalton's law of partial pressure is applicable, the following expression is used to calculate the vapor pressures

$$P_x = \frac{V_x(H_0 - P_c)}{V_0 + V_x}$$

where

P_x = vapor pressure of sample (mm.)
V_x = vol. of vapor found (ml. S.T.P.)
H_0 = barometer pressure (cor., mm.)
V_0 = vol. of air drawn through (S.T.P.)
P_c = corrn. for head of liquid in Geissler bulb and resistance to air flow in drying train for the inflowing air

Experimentally, it is assumed that 1 mole of vapor occupies 22,400 ml. and V_x = 22,400 (wt. of material volatilized/mol. wt.) and

$$V_0 = V\frac{(H_0 - p - b)}{760} \times \frac{273}{t + 273}$$

where

p = corrn. to barometric pressure due to head of liquid in bulbs and the resistance to air flow of drying trains
b = vapor pressure of water at t°C.
t = final temp. of aspirator °C.
V = vol. of water run out of aspirator in ml.

The heats of vaporization were computed by a least squares treatment of the vapor pressures at the three temperatures using the Clausius–Clapeyron equation. The procedure was as follows[9]

$$E = \Sigma(\ln p)^2 - \frac{\Sigma(\ln p^2)}{n} - b^2\left(\Sigma\left(\frac{1}{T}\right)^2 - \frac{(\Sigma 1/T)^2}{n}\right)$$

where E is the sum of the squares of the deviations of ln p from the least squares equation of slope b, and n is the number of measurements. The variance of the slope was computed from

$$\sigma^2 = \frac{\frac{E}{n-2}}{\Sigma\left(\frac{1}{T}\right)^2 - \frac{(\Sigma 1/T)^2}{n}}$$

and the appropriate coefficient for a 95% confidence interval was then applied.

Results and Discussions

Freezing Curve Results.—Table I presents the freezing points corrected to zero impurity, the purity as determined from freezing curves, the per cent. theoretical nitrogen measured and the heats of fusion. 1,3-Dinitroxypropane and 1,2,4-trinitroxybutane could be made to freeze but at a very slow rate. For 1,2,4-trinitroxybutane a freezing point could also be obtained between 9 and 10°. This is analogous to the two forms of nitroglycerin which freeze at 12.86 and 1.9–2.2°.[10]

The 1,2,5-trinitroxypentane could not be made to freeze but the nitrogen analysis is included because the vapor pressure was determined for that sample.

Because the purity determinations by freezing curves are more reliable than those by the nitrometer for small quantities of impurity, a comparison with the nitrometer determinations is of interest. A comparison with the results of the two methods for 1,4-dinitroxybutane and nitroglycerin II, 99.98 and 100.00 mole % pure, respectively, would eliminate ambiguity due to possible nitrate impurities. In these cases the nitrometer is 0.02% high and 0.16% low, respectively. These results are within the precision (about 2 parts in 1500) obtained with the potassium nitrate used in calibration. The heats of fusion for the two nitroglycerin samples, are 5.68 and 6.38 kcal./mole, respectively. It is not believed that this difference is due to difference in mole % purity as determined by freezing curve methods but indicates uncertainty that might be expected in applying these semi-micro methods to the determination of purity. Small errors in the freezing point depression could cause large errors in the heat of fusion.

Vapor Pressure Results.—The vapor pressure results are given in Table II. The vapor pressures of nitroglycerin agree reasonably well with those obtained by Marshall and Peace[11] and with those obtained by Ernsberger, *et al.*[12]

(7) W. C. Crater, *Ind. Eng. Chem.*, **21**, 674 (1929).

(8) J. D. Brandner, *Ind. Eng. Chem.*, **30**, 681 (1938).

(9) C. A. Bennett and N. L. Franklin, "Statistical Analysis in Chemistry and Chemical Industry," John Wiley and Sons, Inc., New York, N. Y., 1954, p. 38.

(10) T. L. Davis, "Chemistry of Powder and Explosives," John Wiley and Sons, Inc., New York, N. Y., 1943, p. 207.

(11) A. Marshall and G. Peace, *J. Chem. Soc.*, **109**, 298 (1916).

(12) U. S. Naval Ordnance Test Station: NAVORD Report No. 1184 Part I, by F. M. Ernsberger, J. G. Wyllie and A. L. Olsen, Sept. 28, 1949.

Table II

Vapor Pressures and Heats of Vaporization of Selected Nitrate Esters

Compound	Vapor pressure (μ) 20°	30°	40°	Heat of vaporization (kcal./mole)
1,3-Dinitroxypropane	17, 16	41, 42	118, 114, 116	17.9 ± 1.1
Nitroglycerin I	0.21, 0.23, 0.18	0.82, 0.82, 0.80	3.4, 3.3, 3.0	25.1 ± 1.4
Nitroglycerin II	0.20, 0.20	1.0, 1.1, 1.2	3.8, 3.5, 3.4	26.0 ± 2.7
1,3-Dinitroxybutane	23, 21	50, 52	142, 137, 151	17.2 ± 1.7
1,4-Dinitroxybutane	9.1	20, 20, 20	41, 41	13.7 ± 0.2
1,2,4-Trinitroxybutane	1.2, 1.0	2.8, 2.2	5.2, 5.4	14.4 ± 2.7
1,5-Dinitroxypentane	4.3, 5	14.1, 13.3	36.8, 36.2	18.8 ± 1.4
2,4-Dinitroxypentane	30, 27, 30	73, 71	143, 137	14.5 ± 1.4
1,2,5-Trinitroxypentane	0.16	0.27, 0.30, 0.29	0.46, 0.50	10.0 ± 0.5
2,5-Dinitroxyhexane	0.98, 1.23, 1.33	6.1, 7.2, 7.6	24, 27, 26	26.2 ± 3.8[a]
	1.28	9.4, 7.4, 7.0	28, 28, 37	(13.0)[b]
		8.7, 7.4	25, 31, 19	

[a] Heat of sublimation. [b] Heat of vaporization computed by subtracting heat of fusion.

Marshall and Peace obtained the vapor pressure of nitroglycerin by air saturation techniques. The air was passed through ground cordite. (Composition: guncotton 37, mineral jelly 5, nitroglycerin 58.) The ground surface of the cordite served as saturators. Ernsberger, *et al.*, obtained their values with a modification of Knudsen's effusion cell.

The heat of vaporization of nitroglycerin is considerably higher than those of the other compounds. The viscosity of nitroglycerin and also the rate of change of viscosity with temperature have been reported to be considerably higher than for 1,3-dinitroxypropane, 1,3-dinitroxybutane and 1,4-dinitroxybutane.[13-15]

This would be consistent with a higher heat of vaporization for nitroglycerin.

(13) J. M. Peterson, *J. Am. Chem. Soc.*, **52**, 3669 (1930).
(14) L. J. De Kreuk, *Rec. trav. chim.*, **61**, 819 (1942).
(15) B. Jacques and M. Thomas, *Mem. Poudres*, **33**, 155 (1951).

X-RAY STUDIES ON THE FORMATION OF COPPER–NICKEL ALLOYS FROM THE PRECIPITATED BASIC CARBONATES

By W. Keith Hall and Leroy Alexander[1]

Contribution from the Multiple Fellowship of Gulf Research & Development Company, Mellon Institute, Pittsburgh, Pa.

Received August 31, 1956

The formation of copper–nickel alloys by the low temperature reduction of the mixed oxides with hydrogen has been studied. It has been shown that even when two oxidic phases are present, on reduction a single metallic phase is formed in which compositional variations, if present at all, cannot exceed 3%. The oxidic phases formed by the method used in this study appear to be pure CuO and an NiO phase in which up to 35% of the Ni atoms have been substituted by Cu.

A number of years ago, Long, Fraser and Ott[2] demonstrated that the copper–nickel (and a number of other) alloy systems could be formed beginning with the coprecipitation of the metals as the hydroxide from solutions of the mixed ions; these were then reduced to metal with hydrogen. The measured lattice parameters were found to be identical with those determined for the corresponding alloys prepared by melting the metals together. The correctness of this work was confirmed by several other workers[3,4] and has been verified again in the present study.

The reason for the effectiveness of the alloying process just described is not immediately apparent. Although a random distribution of metal atoms is to be expected in the freshly precipitated basic carbonates, subsequent conversion to the oxides by means of thermal treatment should result in segregation of the CuO and NiO crystallites because of their different crystal systems, *viz.*, monoclinic and cubic, respectively. Furthermore, segregation should persist when the oxides are then reduced at relatively low temperatures (200 to 450°) because the inter-diffusion of copper and nickel among adjacent pure crystallites would be expected to be too slow at such low temperatures to produce a significant amount of solid solution. Thus homogeneous alloy systems would not be anticipated on the basis of the foregoing arguments. With these considerations in mind, it was decided to repeat once again this alloying procedure over a wide range of composition, examining both the oxide and alloy phases by X-ray diffraction.

Preparation of the samples of the basic carbonates followed quite closely the modification of the method of Long, Fraser and Ott[2] used by Best and Russell.[4] Analytical reagent grade reagents including Fisher's nickelous nitrate labeled "Low in cobalt" were used, and the precipitation was carried out using ammonium bicarbonate. Tests on

(1) Department of Chemical Physics, Mellon Institute.
(2) J. H. Long, J. C. W. Fraser and E. Ott, *J. Am. Chem. Soc.*, **56**, 1101 (1934).
(3) P. H. Emmett and Nis Skau, *ibid.*, **65**, 1029 (1943).
(4) R. J. Best and W. W. Russell, *ibid.*, **76**, 838 (1954).

the samples for iron using SCN^- were all negative.

These samples were first heated to 400° for four hours in air to convert them to the oxides. At this stage, they were analyzed for copper and for nickel by standard analytical techniques, and it is from these data that the compositions of the reduced materials are calculated. At this stage also, their X-ray patterns were obtained; they were next heated for an additional two hours to 750° and the X-ray patterns were again determined; finally, samples which had first been heated to 400° were reduced in hydrogen and a third series of patterns were prepared. One-hour exposures were made with copper Kα radiation in a Debye–Scherrer camera of 57.3 mm. radius.

The identity and composition of the various oxidic samples and the nature of their diffraction patterns are listed in the accompanying table. The samples that had been heated to only 400° are listed in columns 3 and 4. In general, two phases were found, a face-centered cubic phase and a monoclinic phase. All lines of both phases were more or less broadened, indicating a small crystallite size. With up to 27.5 mole % copper substituted for nickel, no evidence of a copper oxide phase appeared, although the pattern of catalyst VI showed a small expansion of the lattice parameter of about 0.4%.

For catalysts VII, IX and X, the observed intensities of the copper oxide lines were markedly less than would correspond to the actual proportions of copper and nickel, assuming no mutual solubility of the two oxide phases. Semi-quantitative estimates of these deficiencies in the copper oxide intensities indicated that about 35% of the nickel atoms in the cubic phase had been replaced by copper. These particular samples also yield patterns that indicate the NiO lattice to be highly defective; as copper replaces nickel in the NiO lattice, a progressive broadening and doubling of the diffraction lines occurs. The nature of the effects is such as to denote a tetragonal distortion of the NiO lattice, one cubic cell edge expanding and the other two contracting. The modification of the diffraction pattern is most pronounced for these same catalysts (VII, IX and X) with the axial ratio, c/a, approaching a maximum value of about 1.1.

When the same samples were further sintered at 750°, the patterns (columns 5 and 6) of the two phases became much sharper and the line abnormalities largely disappeared. This showed that the higher temperature treatment had caused further growth in the crystallites and an "ironing out" of lattice imperfections. Intensity measurements now showed by difference that the copper oxide deficiencies were consistent with a composition of the face-centered cubic phase of approximately 13% copper and 87% nickel oxide.

These data suggested the possibility that too stringent sintering conditions may be undesirable. Our observations indicate that the amount of copper substituted in the cubic NiO phase decreases as the sintering temperature increases. Hence, it may be supposed that the distribution of the copper and nickel ions is more uniform in the coprecipitated basic carbonates than in the oxides formed from them. Whether or not this factor is important in the formation of homogeneous alloys on reduction with hydrogen is not well defined as a result of the present investigation. The authors were, however, able to show that fairly homogeneous alloys were obtained from samples heated to 400°. Although the desirability of further work along these lines is evident, the authors have not had occasion to extend the data as presented herewith.

TABLE I

DATA OBTAINED IN X-RAY EXAMINATION OF THE CATALYSTS IN OXIDE FORM

(1) Catalyst no.	(2) Mole % Ni in catalyst (reduced basis)	(3) Intensity of patterns after 400° sintering CuO	(4) Intensity of patterns after 400° sintering NiO	(5) Intensity of patterns after 750° sintering CuO	(6) Intensity of patterns after 750° sintering NiO
VIII	100.0	..	s	..	s
V	84.8	..	s	..	s
VI	72.4	..	ms	w+	s
VII	53.8	vw	m[a]	mw	ms
IX	45.5	w	m[a]	m	ms
X	34.3	mw	mw[a]	m	m
IV	20.6	m	mw	ms	m
XI	14.7	ms	w	s	mw
III	7.8	s	vw	s	w
II	0.0	s	..	s	..
I	0.0	s	..	s	..

[a] Lines distorted; certain of the NiO lines are abnormal in shape and intensity, indicating lattice imperfections; vw, very weak; w, weak; mw, medium weak; m, medium; ms, medium strong; s, strong.

Samples similar to those used in studies of the 400° treatment were reduced to the metals at 350° for periods of from 16 to 48 hours, and tests were made of their activities toward the hydrogenation of benzene and the hydrogenation of ethylene at temperatures not exceeding 220°. These results will be reported elsewhere[5,6] the above-mentioned information serving to indicate that these treatments were mild and that little annealing would be expected. After this work, surface area measurements were made by the standard BET method, and then the catalysts were evacuated for several more hours at 350° and sealed off under vacuum in the reaction vessels. These tubes were then broken under benzene and Debye–Scherrer powder specimens were prepared.

The positions of the lines of the patterns were determined with a precision film-measuring instrument and these were converted into a_0 values. The edge length of the face-centered cubic unit cell was in each instance determined by extrapolation of the calculated values of a_0 against the Taylor–Sinclair[7] angular correction function to $\theta = 90°$ where absorption and geometrical errors theoretically vanish. These data are plotted against composition as points (in kX. units) in Fig. 1 for the purpose of comparing them (catalysts that had not been heated above 350°) with the more accurate values of Owen and Pickup[8] given as the solid line (alloys that had been prepared by melting). The accuracy of the

(5) W. K. Hall and P. H. Emmett, to be published.
(6) W. K. Hall and P. H. Emmett, to be published.
(7) A. Taylor and H. Sinclair, *Proc. Phys. Soc.*, **57**, 108 (1945).
(8) E. A. Owen and L. Pickup, *Z. Krist.*, **88**, 116 (1935).

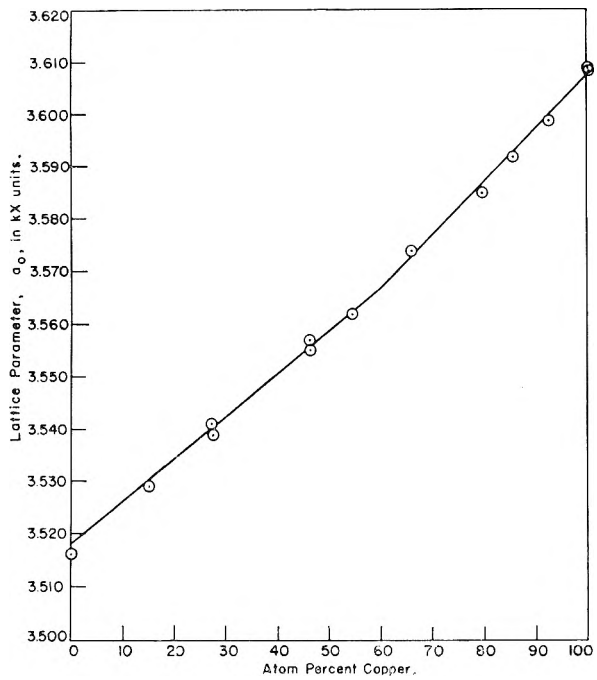

Fig. 1.—Experimental lattice parameters of copper–nickel alloys. Solid line represents data of Owen and Pickup.[8]

lattice constants determined in the present work is estimated to be ±0.002 kX.

The excellent agreement obtained between the two sets of data indicate that alloys prepared by the method of Long, Fraser and Ott must be fairly homogeneous. It was observed that the X-ray diffraction lines obtained from all samples were noticeably broadened. This phenomenon may be attributed either to small crystallite size or to inhomogeneity in composition of the individual crystallites. On the basis of the first hypothesis, the crystallite dimensions fall in the range of 100 to 400 Å. On the other hand, if the line broadening were entirely the result of inhomogeneity, the experimental uncertainty in the lattice constant determinations limits the variation in composition to 3%. The fact that the extent of line broadening is approximately the same for the pure nickel and the pure copper samples, however, may be taken as evidence that much of the effect is due to small crystallite size. On the other hand, the fact that the specific surface areas calculated from the line broadening measurements were from 10 to 50 times the BET nitrogen areas (16.2 Å.²/molecule) might be taken to imply larger crystallite dimensions and hence that small fluctuations in composition occurred in the alloys. That compositional variations, if present at all, could not have exceeded 3%, seems somewhat surprising to the authors in view of the fact that in most instances the oxides studied here existed in at least two (and probably more) phases. This may be taken as an indication of the probability that many additional alloy systems could be prepared by this method. The proposition deserves more attention than it has heretofore received.

The authors wish to acknowledge the efforts of Mr. G. G. Sumner in measuring the diffraction patterns and computing the lattice constants.

EXCHANGE DIFFUSION OF IONS OF SIMILAR MOBILITY

BY L. G. LONGSWORTH

Contribution from the Laboratories of the Rockefeller Institute for Medical Research, New York, N. Y.

Received September 7, 1956

At 25° the limiting mobilities, and hence the ion diffusion coefficients at zero concentration, of chloride and iodide ions in aqueous solution differ by only 0.7%. The exchange diffusion of these ions at a boundary between dilute equimolar solutions of KI and KCl, for example, thus approaches closely the so-called self-diffusion of these species. With the aid of Rayleigh interference optics this diffusion process has been studied and the results for the concentration range from 0.01 to 1 mole per liter are presented with both potassium and sodium as the common ion. With increasing dilution the coefficients approach the Onsager limiting slope for ion diffusion from above as do the electric mobilities in the same concentration range. Also in agreement with the theory is the observation that in the presence of potassium the Cl–I exchange diffusion is slightly more rapid than in the presence of sodium. Improvements in experimental procedure and sources of boundary "skewing" also are presented.

In a recent paper Adamson[1] has assembled the available data on the self diffusion of ions in aqueous solutions of electrolytes, as measured with the aid of isotopes by the porous diaphragm and capillary tube methods, and has concluded that they are not sufficiently accurate to establish the concentration dependence of this property in dilute solutions. It appears desirable, therefore, to investigate the possibility of adapting the refractometric methods to this problem.

Although actual practice usually deviates somewhat, the ideal process in self diffusion is the exchange in position of a tagged ion with its untagged isotope, the solution being otherwise homogeneous. Except for the isotopes of hydrogen the small differences in the refractive increments of those of the other elements preclude their use in a method depending on this property. Insofar, however, as the hydrodynamic properties of an ion are adequately described by its limiting mobility the exchange diffusion of two species having the same mobility should approximate, in sufficiently dilute solution, the self diffusion of either species. At 25° the limiting mobilities, and hence the ion diffusion coefficients at infinite dilution, of chloride and iodide ions differ by less than 0.7%. The equivalent refractions of these two species are quite different, however, and the spreading, with time, of a boundary with KI below at a concentration, c, of 0.1 mole per liter of solution and 0.1 c KCl above, for example, can be measured accurately. It is the purpose

(1) A. W. Adamson, THIS JOURNAL, 58, 514 (1954).

of this paper to report the results of such measurements over the concentration range from 0.01 to 1 *c* with both sodium and potassium as the common ion and to describe improvements in experimental procedure and interpretation that have been incorporated in this work.

Experimental

The method employed is that of free diffusion from an initially sharp boundary between the two solutions, the spreading of the boundary with time being followed with the aid of Rayleigh interference fringes.[2] Over the interval from 0.01 to 1 *c* the difference in refractive index, Δn, between equimolar solutions of iodide and chloride varies from 0.000117 to 0.0119. This variation is approximately linear with concentration and nearly independent of the coion if this is sodium or potassium. In a channel of 1 cm. depth, *a*, and with mercury green light for which $\lambda = 5461$ Å. this corresponds to a path difference, $J = a\Delta n/\lambda$, of 2 fringes at 0.01 *c* and 218 fringes at 1 *c*. Electrophoresis cells having channel depths of 1 and 2.5 cm., respectively, and modified to facilitate the formation of Rayleigh fringes, have served as diffusion cells. In work with concentrated solutions in deep channels, *e.g.*, Table II, blurring of the fringes due to excessive path differences has been avoided by enclosing the comparison channel so that it can be filled with liquid other than the thermostat fluid. This has been accomplished with the aid of a new center section with a twin channel, access to both portions of which is provided by adjacent 3 × 25 mm. slots in the horizontal plates.

Since the precision decreases with the number, *J*, of diagonal fringes the dilute solutions have been studied in the cell for which $a = 2.5$ cm. with reflection of the light back through the channel, thus obtaining 10 fringes at the lowest concentration. To this end the optical system has been provided with a second light source in the focal plane of the second schlieren lens and a removable, first surface mirror. In some instances a boundary has been studied in the conventional manner after which the cell has been shifted toward the camera so that the mirror could be inserted in its object plane, the second light source turned on, the boundary resharpened with the capillary siphoning used throughout this work for that purpose and a second set of patterns obtained, this time with twice the number of diagonal fringes as in the first experiment. In the case of Rayleigh fringes, where a vertically extended source is used, the light incident on the mirror and that reflected therefrom can be kept more nearly "on axis" if this light is brought in from the side instead of from above as suggested in another application.[3]

The recording of the diffusion process has been made automatic with the aid of two devices, a timer and a switching cam, each of which is driven by a synchronous motor. The timer may be set to close a switch momentarily ten times in a period not exceeding 10^5 seconds, *i.e.*, 28 hours, with a deviation of less than 1 second from the predetermined time for each closure, provided that the local a.c. frequency control is correspondingly close. This is checked at intervals against signals from the National Bureau of Standards station WWV. Except that they must be multiples of 100 seconds, no restriction is placed on the intervals between closures. This flexibility is an advantage in free diffusion where the boundary spread is proportional to the square root of the time and increasing intervals between exposures are essential for representative sampling of the fringe separations. Each closure activates the switch cam to make the exposure, advance the photographic plate and then reset itself preparatory for the next impulse.

The solutions have been prepared from weighed quantities of salt and water, the concentrations being expressed as moles per liter of solution at 25° with the aid of the density data in the International Critical Tables. Reagent grade salts have been used without further purification except for drying to constant weight at 120°.

Since the average deviation of the values of the diffusion coefficient, *D*, for individual exposures from the mean value for all patterns is not necessarily a measure of accuracy some additional precautions that can be taken for the elimination of systematic errors may be mentioned. (1) The zero-time correction obtained on minimizing the average deviations should agree with that computed from the photographs of the boundary during sharpening.[2] Failure to obtain such agreement frequently can be traced to disturbances resulting from movement of the boundary on isolation of the bottom section of the Tiselius cell and withdrawal of the capillary. (2) As will be described later in the paragraph on non-Gaussian boundaries, symmetrical pairing of the fringes is useful in detecting errors in the comparator readings and misalignment of the pattern in that instrument. (3) A deviation plot of the number, *J*, of diagonal fringes, *e.g.*, J/ac *vs.* *c*, is useful in detecting errors in *J*, especially if small values of *J* are involved since *D* then becomes quite sensitive to the value assigned to *J*. If the fractional part of *J* is obtained from the patterns recorded during sharpening, as is usually the case, the capillary should be hidden completely by the double slit mask. (4) Although not a serious problem with aqueous solutions, evaporation of solute or solvent and solubility of the grease used in assembling the cell can be troublesome with other liquids. Any shift, during the diffusion period, of the vertical fringes conjugate to the homogeneous columns of fluid on either side of the boundary with respect to the reference fringes is a serious source of error. (5) If the variation of concentration through the boundary is not Gaussian and the deviations are due to the concentration dependence of the diffusion coefficient, the ratio, D_1/D_2, of its values at the edges of the boundary, as estimated from the skewness, should agree with that from a plot of *D vs.* *c* as obtained in a series of experiments at different mean concentrations.

Non-Gaussian Boundaries

Although the variation of the refractive index through a boundary has been approximately Gaussian at the lower concentrations appreciable skewness has been observed above 0.2 *c*. Since skewness can arise from sources other than a variation in the diffusion coefficient with the mixing ratio $c_{Cl}/(c_{Cl} + c_I)$ it is essential to consider these departures from the Gauss distribution. One such source, the so-called Wiener skewness, has been studied in detail by Svensson[4] and may be described with the aid of Fig. 1. Here a light ray enters the channel normally at a level near the center of the boundary where the refractive index is changing rapidly with the height. For the case most frequently encountered, namely, the denser solution having the higher refractive index, the ray is deflected downward following an approximately parabolic path into solution of higher refractive index than at the entrance level. The tangent to the path at exit intersects the center of the channel at the entrance level and it is from this level that the ray appears to come if the camera is focussed on the plane at $a/2$. Owing both to the curvature of the ray and to the fact that it moves progressively into regions of higher refractive index the retardation along the actual path is greater than if the ray traversed the channel without deflection and corresponds to the retardation along a path parallel to the axis but at a level slightly below the entrance level. Svensson has shown that this is the level at which the exit tangent intersects a plane $a/3$ distant from the front wall. Consequently if the camera is focussed on the plane at $a/3$ a plot of the fringe number *versus* fringe position gives the refractive index accurately as a function of the height in the channel. If, on the other hand, the camera is focussed on the center of the channel at $a/2$ the maximum gradient in a sharp Gaussian boundary will appear to be displaced to the solvent side, an

(2) L. G. Longsworth, *J. Am. Chem. Soc.*, **74**, 4155 (1952).

(3) L. G. Longsworth, *Anal. Chem.*, **25**, 1074 (1953).

(4) Harry Svensson, *Optica Acta*, **1**, 25 (1954); **2**, 90 (1954).

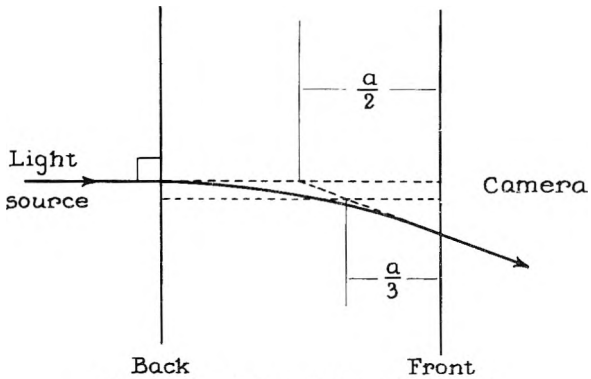

Fig. 1.—The light path through the cell.

effect that may be described as the Wiener skewness. It should be noted, however, that this skewness disappears as the boundary spreads whereas that due to a variation of the diffusion coefficient with the mixing ratio is invariant with time.

With the vertically extended light source that is essential for short exposures, the Rayleigh fringes are most sharply defined when the plane at $a/2$ is in focus and it is in this plane that the scale must be placed in determining the camera magnification. The choice, then, is to focus at $a/2$ and obtain sharp fringes with Wiener skewing in the early patterns or to focus at $a/3$ and get less sharply defined fringes without this skewing. With the method of computation used the Wiener skewing is not a source of error in the evaluation of a mean diffusion coefficient for the experiment. Consequently the author has focussed on the center of the channel but has refrained from using the early photographs in the determination of the variation in that coefficient from the boundary skewness.

The procedure for sharpening the boundary initially also introduces its own distortion, the dissipation of which requires time. Guggenheim[5] has estimated this time to be a small multiple of letter l^2/D, where l is half the breadth of the initial boundary. In typical cases encountered in this research l is of the order of 0.04 cm. and $l^2/D = 80$ seconds. Thus patterns obtained after diffusion for 300 seconds, say, should not be seriously affected by the initial distortion. In work with serum albumin, on the other hand, Hoch[6] found it necessary to focus at $a/8$, Fig. 1, in order to obtain normalized distributions that were invariant with time, a result that may be due to the slowness with which the initial distortion of the protein boundary was dissipated.

It is more difficult to distinguish skewness due to concentration dependence of D from that arising from a variation in the specific refraction $n' = dn/dc$, since both are time independent.[7,8] In evaluating D from the spacing of the fringes in a pattern these are paired to avoid locating the center of the boundary. In order to include the central ones and also to assign approximately equal weight to all comparator readings, x, the fringes are paired unsymmetrically, *e.g.*, in a 50-fringe pattern fringe number $j_k = 2$ is paired with $j_l = 26$, 4 with 28, ... and 24 with 48. Owing to the uncertainty in their location, fringes 1 and $J - 1$ are seldom used. If D and n' are constant over the concentration interval, Δc, across the boundary the value of $(\Delta x/\Delta z)_{kl} = (x_l - x_k)/(z_l - z_k)$ for each pair is constant. Here z_k is the argument[9] of the error integral H for $H_k = (2j_k - J)/J$, etc. If, however, either or both of these coefficients is concentration dependent the values of $(\Delta x/\Delta z)_{kl}$ shift with the fringe pair and the nature of the dependence frequently can be inferred from this variation. Several possibilities may be mentioned.

(a) If n' is constant but D varies linearly with c, and neither this variation nor Δc is too large, the ratio D_1/D_2 of the diffusion coefficient at the edges of the boundary can be computed from the slope, m, of the straight line that is obtained on plotting $(\Delta x/\Delta z)_{kl}/\overline{(\Delta x/\Delta z)}$ *versus* $(\Delta R/\Delta z)_{kl}$. Here $\overline{\Delta x/\Delta z}$ is the average of all values of $(\Delta x/\Delta z)_{kl}$ for a given pattern, R is the function obtained by Creeth,[10] *i.e.*, $R = (1 - H^2 - zHH_1 - {}^1/_2H_1^2)/2H_1$ where $H_1 = dH/dz$ and $D_1/D_2 = (1 - m)/(1 + m)$.

(b) If D is constant and n' a linear function of c the values of $(\Delta x/\Delta z)_{kl}/\overline{(\Delta x/\Delta z)}$ should be plotted against $(\Delta U/\Delta z)_{kl}$ where U is the function obtained by Creeth[10] for this case. A plot *versus* $(\Delta R/\Delta z)_{kl}$ is also linear, however, and unless D is known to be constant the skewness could be misinterpreted as due to a variation in this coefficient. If n' is known as a function of c this information can be used to convert the reduced "concentration" on the n-scale, *i.e.*, $(2j - J)/J$, to the concentration or c-scale before interpolation for z. On the c-scale $(\Delta x/\Delta z)_{kl}$ is then constant.

(c) If both D and n' are linear in c a plot of $(\Delta x/\Delta z)_{kl}/\overline{(\Delta x/\Delta z)}$ *versus* $(\Delta R/\Delta z)_{kl}$ is also linear but its slope gives the wrong value for D_1/D_2 unless the skewness due to the concentration dependence of n' has been eliminated by conversion of the reduced concentrations to the c-scale. Without this conversion the value of D_1/D_2 would not agree with that from a graph of D *versus* c. This affords a useful clue as to the origin of the skewness.

Since the deviations from the Gauss distribution due to a linear dependence of D and n' on c are even functions of z the resultant skewing may be described as "symmetrical" and does not become evident if the fringes are paired symmetrically,[10] *i.e.*, 2–48, 4–46, ...,24–26 for $J = 50$. In the cases considered thus far symmetrical pairing of the fringes gives a constant $(\Delta x/\Delta z)_{kl}$ on either the n- or c-scale and is useful in checking the alignment of the pattern in the comparator and the readings on that instrument. The constant value thus obtained is identical with $\overline{\Delta x/\Delta z}$ from the unsymmetrical pairing but it is only the mean value on the c-scale that may be substituted in the relation $D = \overline{(\Delta x/\Delta z)}^2/4M^2t$ if the differential diffusion coef-

(5) E. A. Guggenheim, *J. Am. Chem. Soc.*, **52**, 1315 (1930).
(6) Hans Hoch, *Arch. Biochem. Biophys.*, **53**, 387 (1954).
(7) L. G. Longsworth, *J. Am. Chem. Soc.*, **75**, 5705 (1953).
(8) L. G. Longsworth, "Electrochemistry in Biology and Medicine," Chap. 12, T. Shedlovsky, editor, John Wiley and Sons, New York, N. Y., 1955.
(9) Federal Works Agency—Works Project Administration, Supt. of Documents, Washington, D. C. (1941).
(10) J. M. Creeth, *J. Am. Chem. Soc.*, **77**, 6428 (1955).

ficient at the mean concentration $\bar{c}$ is desired. Here M is the camera magnification and t the time after correction for the initial breadth of the boundary. If the comparator is provided with a graduated cross-axis movement Creeth[10] has shown how this may be used quite simply to obtain accurately symmetrical pairing when J is not an integer.

(d) If additional terms, *i.e.*, quadratic, are needed to represent the concentration dependence of either D or n', or if Δc is too large, a plot of $(\Delta x/\Delta z)_{KI}/\overline{(\Delta x/\Delta z)}$ *versus* $(\Delta R/\Delta z)_{KI}$ is no longer linear and symmetrical pairing of the fringes does not give a constant $(\Delta x/\Delta z)_{KI}$. This situation, which may be designated as "unsymmetrical skewing," has been encountered by the author in dilute aqueous methanol but not in the present research.

Results

A by-product of this research has been the determination of the concentration dependence of the refractive index differences between the solutions forming a boundary. Figure 2 is a deviation plot of these differences for all pairs of solutions that have been studied. Here J/ac is plotted as ordinate *versus* the concentration c as abscissa. The data of this figure may be represented by the empirical relations

$$J/ac = 214.20 + 2.12c \quad \text{for the potassium salts}$$

and

$$J/ac = 214.20 + 3.00c \quad \text{for the sodium salts}$$

with an average deviation of the computed values of J from those observed of 0.04. Although the scatter of the points in Fig. 2 is greatest in the dilute solutions where J is small the largest deviations actually occur in the concentrated solutions where channel depths of 1 cm. are used. Readjustment of the a values by as little as 4 μ materially reduces the average deviation noted above. This adjustment corresponds to one division on the scale of the microscope vernier that is used in the determination of a and suggests the need for a refinement in this procedure. It may also be noted that the identity of the intercepts in the two empirical relations given above affords confirmation, with a differential interferometric method, of the additivity of ionic refractions at infinite dilution.

The results of the diffusion measurements are presented in Table I and plotted as ordinates in Fig. 3 with the square root of the concentration as abscissa. Where more than one experiment was done at a given concentration the entries in columns 2 and 4 of Table I are mean values whereas those in the adjoining columns 3 and 5 are the average deviations from these means. In Fig. 3 the straight lines are the limiting slopes computed with the aid of Gosting and Harned's adaptation[11] of the Onsager theory. The intercept at zero concentration is $(D_{Cl}^0 + D_I^0)/2$, where D_{Cl}^0 (2.0324×10^{-5}) and D_I^0 (2.0457×10^{-5}) have been computed from the conductance and transference data of Harned and Owen[12] with the aid of the relation $D^0 = RT\lambda^0/F^2$.

(11) L. J. Gosting and H. S. Harned, *J. Am. Chem. Soc.*, **73**, 159 (1951).

(12) H. S. Harned and B. B. Owen, "The Physical Chemistry of Electrolytic Solutions," 2nd ed., Reinhold Publ. Corp., New York, N. Y. 1950. p. 590.

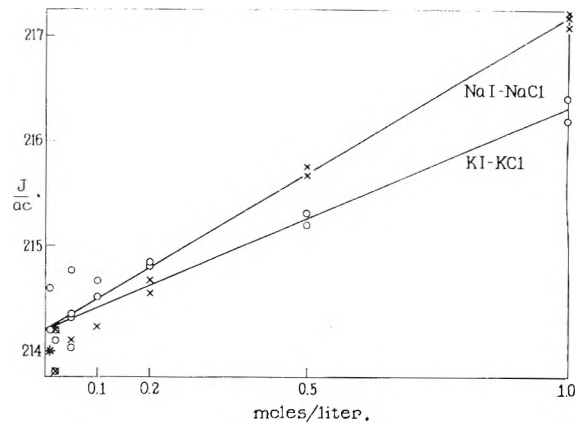

Fig. 2.—The variation, with concentration, of the refractive index difference between equimolar chloride and iodide solutions.

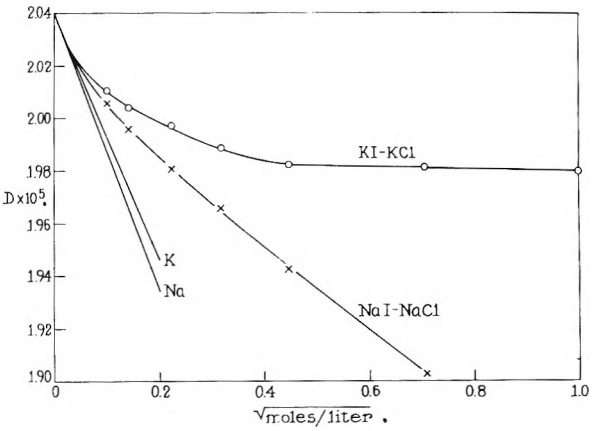

Fig. 3.—The variation, with concentration, of the Cl-I exchange diffusion coefficient with different common ions.

TABLE I

EXCHANGE DIFFUSION COEFFICIENTS, D, OF CHLORIDE AND IODIDE IONS IN AQUEOUS SOLUTIONS AT 25°

Concn., moles/l.	$D \times 10^5$, cm.²/sec. KI–KCl	Av. dev., %	NaI–NaCl	Av. dev., %
0.01	2.0109	0.24	2.0056	0.09
.02	2.0041	.05	1.9960	.29
.05	1.9971	.11	1.9808	..
.1	1.9888	.01	1.9656	..
.2	1.9825	.04	1.9426	.04
.5	1.9815	.05	1.9027	.02
1.0	1.9800	.06	1.8440	.02

The 0.7% difference in D_{Cl}^0 and D_I^0 might be expected to introduce a small variation of the diffusion coefficient with the ratio $c_{Cl}/(c_{Cl} + c_I)$ in a boundary and hence a slight departure from the ideal, *i.e.*, Gaussian, distribution. In dilute solutions, where this variation would not be complicated by other factors, the values of J were so small, however, that skewness of this magnitude was lost in the uncertainty with which the fringes could be located. At 0.05 and 0.1 c the boundaries were essentially Gaussian. Above 0.2 c, on the other hand, the boundaries were definitely skew and the results of Table II were obtained as an aid in interpreting this non-ideal behavior. The data of this table refer to a total concentration of 1 c but the mixing ratio varied across the boundary

from 0.0 to 0.1 in one pair of experiments and from 0.9 to 1.0 in the second pair, whereas the 1 molar data of Table I refer to a variation in this ratio from 0 to 1.

TABLE II

DATA FOR THE INTERPRETATION OF SKEW BOUNDARIES

Upper soln.		Lower soln.		$D \times 10^5$	
c_I	c_{Cl}	c_I	c_{Cl}	KI–KCl	NaI–NaCl
0.0	1.0	0.1	0.9	1.9463	1.8116
0.9	0.1	1.0	0.0	2.0244	1.8903
				$\Delta = 0.0781$	0.0787

Discussion

As is shown in Fig. 3 the D values in the dilute solutions approach the limiting slopes from above, as do the electric mobilities in the same concentration range. Moreover, the values in the presence of sodium are less than for potassium, differences that persist at concentrations sufficiently low for a viscosity effect to be negligible. This, again, is in qualitative accord with the Onsager theory. Although the diffusion coefficients of the ions of KCl and KI differ only slightly, in dilute solutions, from the salt coefficients, this is not true of D_{Cl}^0 or D_I^0 and D_{NaCl}^0 or D_{NaI}^0. Thus, the results with the sodium salts indicate clearly that the process is not one of salt diffusion. This emphasizes the approximate nature of the computation made by MacInnes and Longsworth[13] when they adopted the suggestion of Guggenheim[6] that the electrolytes in a boundary between 0.1 c HCl and 0.1 c KCl be assumed to diffuse independently.

Although the results presented here cannot be interpreted as establishing the validity of the limiting law for ion diffusion they suggest that if the measurements could be extended to more dilute solutions that law would be obeyed. Although Mills and Kennedy[14] did not interpret their data as supporting this law their values for the self diffusion of I in KI agree with those of Table I for the KI–KCl solutions up to 0.2 c with an average deviation of 0.3%.

It is not possible at present to interpret quantitatively the results in concentrated solutions. In Table II it will be noted that the differences Δ are essentially independent of the common ion, suggesting that an additive property of these solutions, *e.g.*, the viscosity, contributes to the variation of D with the mixing ratio. If the data of Table II, together with those of Table I for 1 c solutions, are plotted against the mean mixing ratio in the boundary, short extrapolations then give D_{Cl} (1 c KI) = 2.030, D_I (1 c KCl) = 1.943, D_{Cl} (1 c NaI) = 1.896 and D_I (1 c NaCl) = 1.809 $\times 10^5$. Here the subscript is the ion species whose concentration approaches zero on extrapolation. It is uncertain whether or not these values can be identified as the corresponding ion diffusion coefficient in the solution in parentheses, and the only tracer datum available for comparison is 1.991×10^{-5} for iodide ion in 1 c KCl.[15] A simple viscosity factor overcorrects somewhat, giving D_{Cl}(1 c KI) = 1.900, D_{Cl}(1 c NaI) = 1.953 and D_I(1 c KCl) = 1.937, D_I(1 c NaCl) = 1.982 $\times 10^{-5}$. Two additional factors have, however, been neglected. One is the difference in the diffusion mobility of chloride and iodide ions, about which little is known at 1 c. The other is the variation in the activity coefficient γ with the mixing ratio, which for 1 *molal* solutions is γ(NaI) − γ(NaCl) = 0.081 and γ(KI) − γ(KCl) = 0.041.[12]

It is of interest, however, that if D is assumed to vary linearly with the mixing ratio in the 0.5 and 1 c boundaries of Table I this variation, expressed as the ratio, D_1/D_2, of the coefficient in the two solutions forming the boundary, may then be computed from the skewness. For KI–KCl at 1 c the value of D_1/D_2 thus obtained is 0.962 whereas the extrapolations mentioned above give 0.957. For NaI–NaCl at 1 c the values are 0.960 and 0.954, respectively. At 0.5 c the skewness is about one-half of that at 1 c, *i.e.*, $D_1/D_2 = 0.980$, suggesting a proportionality between this property and the concentration.

Acknowledgment.—The author is grateful to Josef Blum and Nils Jernberg of the Rockefeller Institute Instrument Shop for many of the details in the design and for the construction of the exposure devices and to Emil Meier of the Pyrocell Mfg. Co. for the twin channel cell. It is also a pleasure to acknowledge the care with which D. A. MacInnes has reviewed this manuscript and to express appreciation to J. M. Creeth for a copy of his recent paper in advance of its publication.

(13) D. A. MacInnes and L. G. Longsworth, *Cold Spring Harbor Symposia on Quantitative Biology*, **4**, 18 (1936).

(14) R. Mills and J. W. Kennedy, *J. Am. Chem. Soc.*, **75**, 5896 (1953).

(15) A. M. Friedman and J. W. Kennedy, *ibid.*, **77**, 4499 (1955).

NOTES

SOME ISOTOPIC EXCHANGE REACTIONS OF IODINE CYANIDE

By F. E. Jenkins and G. M. Harris

Contribution from the Department of Chemistry of the University of Buffalo, Buffalo, New York

Received September 7, 1956

Iodine cyanide is a well-defined molecular compound, but recent studies have pointed up its chemical peculiarities, both as regards some of its reactions in solution[1-3] and its ability to form molecular complexes.[4,5] It was considered of interest to examine the nature of the various isotopic exchange reactions possible with this compound in an attempt to throw additional light on its chemistry. The reactions studied were

$$ICN + I^{131-} \rightleftharpoons I^{131}CN + I^- \quad (1)$$

$$ICN + C^{14}N^- \rightleftharpoons IC^{14}N + CN^- \quad (2)$$

$$ICN + I^{131}I \rightleftharpoons I^{131}CN + I_2 \quad (3)$$

Experimental

A. Preparation of Materials.—Iodine cyanide was synthesized from iodine and sodium cyanide by the usual procedure.[6] It was purified by recrystallization from chloroform/heptane solvent followed by vacuum sublimation. Dioxane was purified by the method of Hess and Frahm,[7] omitting the freezing step. Acetone was purified by treatment with $KMnO_4$ and ignited K_2CO_3, followed by fractional distillation. Commercial *n*-heptane was purified by passage through a 30-inch silica-gel column. Other reagents were of analytical grade and were used without further treatment. Radiocyanide and radioiodide were obtained from commercial suppliers. Radioiodine was prepared by the exchange reaction between aqueous radioiodide and solid iodine.[8]

B. Procedure.—For reactions 1 and 2, accurately weighed portions of iodine cyanide (*ca.* 0.5 g.) were dissolved in 20 ml. of solvent and thermostated at the desired temperature (to within ±0.1°); 5 ml. of solution of radioactive potassium iodide or cyanide of accurately known concentration (*ca.* 0.159 g. of KI or 0.100 g. of KCN per 5-ml. aliquot) were added rapidly with constant stirring. In most cases, satisfactory separations were achieved by direct precipitation of the iodide or cyanide in 1-ml. portions of the mixture with silver nitrate. In the pure organic solvents, however, silver iodide precipitation is incomplete, and in these instances the separations were made on Amberlite MB-1 resin. On shaking a 1-ml. aliquot of reaction mixture with 200 mg. of resin, all iodide ion was adsorbed within 30 sec. together with a small constant fraction of the iodine cyanide. The adsorbed iodide was eluted from the resin with concentrated aqueous KNO_3 and precipitated as before. The precipitates were centrifuged down, washed and transferred to weighed steel planchets in the form of alcohol slurry. After drying under an infrared lamp, the weighed samples were counted by conventional end-window G/M tube technique.

Reaction 3 was studied in *n*-heptane solution only. Weighed amounts of iodine cyanide (*ca.* 0.03 g.) were dissolved in 25 ml. of heptane, brought to temperature and 0.2-ml. portions of a heptane solution of radioiodine added with vigorous stirring. Two-ml. portions were withdrawn and shaken with an equal volume of water for 10 sec.; a 1-ml. aliquot from each layer was then assayed for radioactivity in a small erlenmeyer flask placed reproducibly over an inverted end-window G/M tube. From a knowledge of the distribution coefficients of iodine cyanide and iodine between heptane and water,[9] the relative acitivity of the two reactants was readily obtainable.

Chemical concentrations of the reactants were determined in all needed cases by titration with dilute thiosulfate. Spectra were obtained as desired on a Beckmann DK-2 spectrophotometer.

Results and Discussion

Even in non-aqueous media and at very low temperatures, all three reactions were found to have gone to completion within the few minutes required for separation. Table I summarizes the experimental conditions. There is the possibility that all

Table I

Iodine Cyanide Exchange Reactions

Reaction	Medium	Temp., °C.	Separation method
(1)	Water	0, 30.2	AgI pptn.
	Water–dioxane (20, 40, 60 and 80% dioxane)	0, 30.2	AgI pptn.
	Acetone	−78, 30.2	Resin adsorption
	Ethanol	−78, 30.2	Resin adsorption
(2)	Water	30.2	AgCN pptn.
	Water–dioxane (20, 40, 60 and 80% dioxane)	30.2	AgCN pptn.
(3)	Heptane	0, 30.2	Extraction with water

the exchanges are separation-induced; this possibility is greatest for the resin-adsorption separation. Since exchange was complete in every experiment, there is no way of investigating the roles of the various separation procedures. However, it seems reasonable to assume that a rapid homogeneous reaction is responsible for at least some of the exchange. Yost and Stone[10] have confirmed the existence of relatively stable complex ions of the types I_2CN^- and ICN_2^-. Logical mechanisms for reactions 1 and 2 are therefore offered by the equilibria

$$ICN + I^{*-} \rightleftharpoons I^*_2CN^- \rightleftharpoons I^*CN + I^-$$

$$ICN + C^*N^- \rightleftharpoons I(C^*N)_2^- \rightleftharpoons IC^*N + CN^-$$

Extremely rapid reaction is possible, since exchange may occur at almost every encounter of iodine cyanide molecule with iodide or cyanide ion. Evidence for this is offered for the first case by the almost instantaneous development of the well-known I_3^- spectrum when solutions of ICN and I^- are mixed; this must result from the rapid occurrence of the series of equilibria $ICN + I^- \rightleftarrows I_2CN^- \rightleftarrows I_2 + CN^-$ and $I_2 + I^- \rightleftarrows I_3^-$.

(1) L. E. Bodnar and A. B. VanCleave, *Can. J. Chem.*, **31**, 923 (1953).

(2) F. Fairbrother, *J. Chem. Soc.*, 180 (1950).

(3) A. A. Woolf, *ibid.*, 4121 (1953); 252 (1954); G. Lord and A. A. Woolf, *ibid.*, 2546 (1954).

(4) R. N. Haszeldine, *ibid.*, 4145 (1954).

(5) D. L. Glusker and H. W. Thompson, *ibid.*, 471 (1955).

(6) *Org. Syntheses*, **32**, 29(1952).

(7) K. Hess and H. Frahm, *Ber.*, **71B**, 2627(1938).

(8) L. R. Darbee and G. M. Harris, This Journal, **61**, 111 (1957).

(9) Values for $K_D = C_{heptane}/C_{water}$ at 25° are 53 and 0.075 for I_2 and ICN, respectively.

(10) Don M. Yost and W. E. Stone, *J. Am. Chem. Soc.*, **55**, 1889 (1933).

Mixtures of ICN and CN^- solutions show a very rapid development of faint yellowish color; the spectrum of such a solution is very similar to that of a dilute cyanogen solution in which partial polymerization has occurred. Apparently the reactions $CNI + CN^- \rightleftarrows I(CN)_2^- \rightleftarrows I^- + (CN)_2$ are also very fast. The mechanism for reaction 3 is similarly most likely one of molecular association, though the spectroscopic evidence is inconclusive; the spectrum of an I_2/ICN mixture in heptane is almost exactly the sum of the spectra of the separate constituents, showing only a very slight increase in absorption in the near ultraviolet.

Support of this research by the U. S. Atomic Energy Commission under Contract No. AT(30-1)-1578 is gratefully acknowledged.

THERMODYNAMICS OF THE FORMATION OF THE SILVER DITHIOSULFATE COMPLEX ION

By Henri Chateau, Bernadette Hervier and Jacques Pouradier

Research Laboratories, Kodak-Pathé S.A., Vincennes, France

Received August 27, 1956

The equilibrium $Ag^+ + 2S_2O_3^{--} \rightleftarrows Ag(S_2O_3)_2^{3(-)}$ was studied by potentiometry between 25 and 70°.[1] To obtain these measurements, it was necessary to determine first the normal potential of the silver electrode[2] and the potential of the reference calomel electrodes[3,4] in that interval of temperature.

As a function of the temperature, the dissociation constant of the silver dithiosulfate complex varies according to the equation

$$\log K = -\frac{4166}{T} + 0.510$$

T being the absolute temperature.

From this result we obtained, at 25°, for the heat of formation of the complex from the ions, the free energy and the molal entropy, the values

$$\Delta H^\circ = -19.05 \pm 0.5 \text{ kcal./mole}$$
$$\Delta G^\circ = -18.35 \pm 0.5 \text{ kcal./mole}$$
$$\Delta S^\circ = -2.3 \pm 2 \text{ cal./mole degree}$$

Heat of Formation.—Only a few investigations of the heat of formation of the complex $Ag(S_2O_3)_2^{3(-)}$ have been reported. Fogh[5] made the first measurements in 1890. He used the calorimetric method and found that the heat of formation of sodium silver thiosulfate from solutions of sodium thiosulfate and silver nitrate is 20 kcal. This comparatively old value is slightly higher than the one we obtained. Fogh's experiments cannot give an exact result, for the sodium thiosulfate concentrations he studied were too high, so that, apart from the complex $Ag(S_2O_3)_2^{3(-)}$, a substantial amount of the complex $Ag(S_2O_3)_3^{5(-)}$ was formed.[6] It is unlikely that the heat of formation of the latter is identical with that of the complex $Ag(S_2O_3)_2^{3(-)}$. Generally, the heat of formation is greater for the higher complexes having a large number of complexing groups per complexed atom. The silver bromide complexes provide an example.[2] This point might explain the slight difference between the value we found and that obtained by Fogh.

In their studies on silver bromochloride mixed crystals, Eastman and Milner[7] have determined the heat of solution of silver bromide and silver chloride in a solution of 0.73 M sodium thiosulfate containing little silver. Under these conditions, according to our study,[6] there is as much $Ag(S_2O_3)_3^{5(-)}$ complex as $Ag(S_2O_3)_2^{3(-)}$ complex. Therefore, the value of the heat of formation of the complex deduced from the Eastman and Milner measurements must be slightly high. Actually, 20 kcal. was obtained, which confirms our estimate.

The heat of formation in solution of the complex $Ag(S_2O_3)_2^{3(-)}$ calculated from the values published by the National Bureau of Standards[8] is −19.3 kcal. This value, which was also cited by Williams,[9] is in good agreement with the −19.05 ± 0.5 kcal. value obtained from our own results.

Entropy.—To explain the stability of the complex ions, Williams[9] considered the entropy. According to him, the change in entropy in the course of the reaction $Ag^+ + 2S_2O_3^{--} \rightarrow Ag(S_2O_3)_2^{3(-)}$ would be −26 cal./deg. This high negative value disagrees with our own results.

Moreover, the value of −26 cal./deg. for the change of molal entropy of the reaction of formation of the complex leads to an abnormally high value of the dissociation constant of the complex

$$\log_{10} K = \frac{\Delta G^\circ}{4.572T} = \frac{\Delta H^\circ - T\Delta S^\circ}{4.572T}$$

The calculations made with $\Delta S^\circ = -26$ cal./deg. and $\Delta H^\circ = -19.3$ kcal. give $\log_{10} K = -8.51$, or $K = 3.1 \times 10^{-9}$. Such a value does not agree with the results published by the various authors who have studied this complex[10] (see results and bibliography, ref. 6).

Nevertheless, in a recent study, Bent[11] used the value published by Williams to calculate the "unitary entropy" of the complex. This has been defined as being the difference between the molal entropy and the configurational entropy. The latter entropy is equal to 8 times the change in the number of ions in the course of the reaction. The unitary entropy of the complex $Ag(S_2O_3)_2^{3(-)}$ would be $-26 + (8 \times 2) = -10$ cal./deg. Bent tried to explain this extremely rare example of negative "unitary entropy" by a spatial configuration quite peculiar to that complex ion.

The value of the molal entropy used by Bent being too small, it is interesting to calculate the "unitary entropy" of the complex from the exact value.

(1) H. Chateau, B. Hervier and J. Pouradier, *J. chim. phys.*, to be published.

(2) J. Pouradier, A. M. Venet and H. Chateau, *ibid.*, **51**, 375 (1954).

(3) J. Pouradier and H. Chateau, *Compt. rend.*, **237**, 711 (1953).

(4) H. Chateau, *J. chim. phys.*, **51**, 590 (1954).

(5) J. Fogh, *Ann. chim. phys.*, **21**, 43 (1890).

(6) H. Chateau and J. Pouradier, *Sci. et inds. phot.*, [2] **24**, 129 (1953).

(7) E. D. Eastman and R. T. Milner, *J. chim. phys.*, **1**, 444 (1933).

(8) "Selected Values of Chemical Thermodynamic Properties," Natl. Bur. of Standards, Circular 500, Washington, D. C., 1952.

(9) R. J. P. Williams, This Journal, **58**, 121 (1954).

(10) The value $K = 3.1 \times 10^{-9}$ is comparatively close to the value $K = 1.5 \times 10^{-9}$ corresponding to the dissociation constant of the complex $AgS_2O_3^-$.[6,12] One might think that the constant of this last complex has been wrongly attributed to the complex $Ag(S_2O_3)_2^{3(-)}$.

(11) H. A. Bent, This Journal, **60**, 123 (1956).

According to our measurements, the molal entropy is $\Delta S^\circ = -2.3$ cal./deg., and the configurational entropy of the complex is equal to -16 cal./deg. With these two values, the "unitary entropy" must be $+13.7$ cal./deg.

It is thus shown that the silver dithiosulfate complex has a positive "unitary entropy" and consequently behaves like all the mineral complexes mentioned by Bent. Therefore, the hypothesis of an exceptional spatial configuration for the silver dithiosulfate is not required.[12]

(12) H. Chateau and J. Pouradier, *Compt. rend.*, **240**, 1882 (1955).

THERMODYNAMIC FUNCTIONS FOR NITROGEN DIOXIDE AND NITROUS ACID

BY A. P. ALTSHULLER

Robert A. Taft Sanitary Engineering Center, U. S. Public Health Service, Cincinnati, Ohio

Received August 23, 1956

The nitrogen oxides and oxy-acids are of both practical and theoretical interest. In recent years these compounds have been of great interest in such diverse fields as air pollution and rocket fuel applications. It is of importance that accurate thermodynamic data on these compounds are available for use. Recent structural and spectroscopic measurements on nitrogen dioxide and nitrous acid permit the statistical calculation of the thermodynamic functions for NO_2 and HNO_2.

The dimensions of the nitrogen dioxide have been determined by electron diffraction,[1] infrared spectroscopy[2] and microwave spectroscopy.[3] These measurements fix the r(N–O) distance at 1.19 Å. and the valence angle at 134° ± 15′. The infrared spectrum has been studied recently by several investigators[2,4,5] with values for the vibrational frequencies in good agreement with an earlier measurement of the ultraviolet spectrum.[6] The vibrational frequencies are $\nu_1 = 1322$ cm.$^{-1}$, $\nu_2 = 750$ cm.$^{-1}$ and $\nu_3 = 1616$ cm.$^{-1}$. The nitrogen dioxide molecule exists in a $^2\Sigma$ ground state so the electronic degeneracy p_e is 2. The symmetry number is two. The moments of inertia are $I_a = 3.486 \times 10^{-40}$ g. cm.^{2}, $I_b = 63.76 \times 10^{-40}$ g. cm.^{2}, $I_c = 67.25 \times 10^{-40}$ g. cm.^{2} and $I_aI_bI_c = 1.495 \times 10^{-116}$ g.^{3} cm.^{6}.

The thermodynamic functions for NO_2 as an ideal gas at one atmosphere calculated to the rigid rotator harmonic oscillator approximation are given in Table I.

Giauque and Kemp[7] determined the entropy of NO_2–N_2O_4 equilibrium mixtures calorimetrically and combined thermochemical data with an approximate statistical thermodynamic calculation to arrive at an entropy at 298.1°K. for nitrogen dioxide of 57.47 e.u. This value is 0.15 e.u. higher than the entropy value calculated in this work. The $-(F^0 - H_0^0)/T$ functions for nitrogen dioxide calculated formerly[7] were obtained by combining thermochemical data with early spectroscopic data. The values of $-(F^0 - H_0^0)/T$ reported herein are 0.06 e.u. lower at 298.1°K. and 0.16 e.u. lower at 900°K. than the values reported formerly.[7,7a]

TABLE I

THERMODYNAMIC FUNCTIONS FOR NITROGEN DIOXIDE IN CAL./DEG./MOLE

T, °K.	C_p^0	$\frac{H^0 - H_0^0}{T}$	$-\frac{F^0 - H_0^0}{T}$	S^0
100	7.95	7.95	40.40	48.35
200	8.23	8.00	45.92	53.92
250	8.53	8.07	47.71	55.78
275	8.70	8.12	48.48	56.60
298.16	8.87	8.18	49.14	57.32
300	8.89	8.18	49.19	57.37
325	9.07	8.24	49.85	58.09
350	9.27	8.31	50.46	58.77
400	9.66	8.45	51.58	60.03
500	10.40	8.77	53.50	62.27
600	11.04	9.09	55.13	64.22
700	11.55	9.41	56.56	65.97
800	11.95	9.71	57.83	67.54
900	12.27	9.97	58.99	68.96
1000	12.53	10.22	60.05	70.27
1100	12.73	10.43	61.04	71.47
1200	12.89	10.63	61.96	72.59
1300	13.03	10.81	62.81	73.62
1400	13.14	10.98	63.62	74.60
1500	13.23	11.12	64.38	75.50

The thermodynamic properties for the reaction $NO(g) + {}^1/_2\,O_2(g) \rightleftarrows NO_2(g)$ are given in Table II. The thermodynamic functions for NO(g) and O_2(g) are taken from the literature.[8–11] The major uncertainty lies in the H_0^0 value for the reaction.

The thermodynamic properties for the reaction $NO(g) + O_3(g) \rightleftarrows NO_2(g) + O_2(g)$ are given in Table III. This reaction is of particular interest because of its kinetic aspects especially in air pollution problems. The thermodynamic functions for ozone used in computing the values in Table III were recalculated using the microwave values for the moments of inertia.[12–14] The values for S^0 and and $-(F^0 - H_0^0)/T$ are 0.25 e.u. higher than those formerly calculated.[15]

The infrared spectra of nitrous acid indicates that the acid exists in a *cis* and *trans* form.[16,17]

(1) S. Claesson, J. Donohue and V. Schomaker, *J. Chem. Phys.*, **16**, 207 (1948).

(2) G. E. Moore, *J. Opt. Soc. Amer.*, **43**, 1045 (1953).

(3) G. R. Bird, *J. Chem. Phys.*, **25** 1040 (1956).

(4) M. K. Kent and R. M. Badger, *Phys. Rev.*, **76**, 473 (1949).

(5) F. L. Keller and A. H. Nielsen *J. Chem. Phys.*, **24**, 636 (1956).

(6) L. Harris, G. W. King, W. S. Benedict and R. W. B. Pearse, *ibid.*, **8**, 765 (1940).

(7) W. F. Giauque and J. D. Kemp, *ibid.*, **6**, 40 (1938).

(7a) The thermodynamic functions for NO_2 between 298.16 and 1000°K. have been given recently by V. P. Morozov, *Ukrain. Khim. Zhur.*, **21**, 554 (1955). His values for S^0 and $-F^0 - H_0^0/T$ are about 0.1 e.u. higher because of the use of somewhat different molecular dimensions.

(8) F. D. Rossini, *et al.*, Selected Values of Properties of Hydrocarbons, NBS Circular C461, Nov., 1947.

(9) H. L. Johnston and A. T. Chapman, *J. Am. Chem. Soc.*, **55**, 153 (1933).

(10) H. L. Johnston and M. K. Walker, *ibid.*, **55**, 172 (1933).

(11) H. W. Woolley, *J. Research Natl. Bur. Standards*, **40**, 163 (1948).

(12) R. Trambarulo, *et al.*, *J. Chem. Phys.*, **21**, 851 (1953).

(13) L. Pierce, *Phys. Rev.*, **99**, 666 (1955).

(14) R. H. Hughes, *J. Chem. Phys.*, **24**, 131 (1956).

(15) M. J. Klein, E. F. Cleveland and A. G. Meister, *ibid.*, **19**, 1068 (1951).

(16) L. H. Jones, R. M. Badger and G. E. Moore, *ibid.*, **19**, 1599 (1951).

(17) L. D'or and P. Tarte, *Bull. Soc. Roy. Sci.*, **Lg**, 178 (1951).

TABLE II

THERMODYNAMIC PROPERTIES FOR THE REACTION NO + $^1/_2O_2 \rightleftarrows NO_2$

$\Delta H_0^\circ = -12.715$ kcal./mole

T, °K.	$-\left(\frac{H^\circ - H_0^\circ}{T}\right)$, cal./deg./mole	$\left(\frac{F^\circ - H_0^\circ}{T}\right)$, cal./deg./mole	ΔH°, kcal./mole	ΔF°, kcal./mole	log K_{eq}	K_{eq}
200	2.927	13.754	−13.30	−9.964	10.89	7.76×10^{10}
250	2.804	14.388	−13.42	−9.118	7.971	9.35×10^{7}
298.16	2.663	14.869	−13.51	−8.282	6.070	1.17×10^{6}
300	2.656	14.889	−13.51	−8.248	6.017	1.04×10^{6}
350	2.509	15.286	−13.59	−7.365	4.598	3.96×10^{4}
400	2.346	15.613	−13.65	−6.470	3.534	3.42×10^{3}
500	2.046	16.104	−13.74	−4.663	2.038	1.09×10^{2}
600	1.776	16.454	−13.78	−2.843	1.036	1.09×10^{1}
700	1.543	16.709	−13.80	−1.019	0.318	2.08
800	1.344	16.905	−13.79	+0.809	−0.221	0.601
900	1.180	17.056	−13.78	2.635	− .640	.229
1000	1.041	17.173	−13.76	4.458	− .974	.106
1100	0.922	17.268	−13.73	6.280	−1.248	5.65×10^{-2}
1200	.823	17.344	−13.70	8.098	−1.474	3.36×10^{-2}
1300	.736	17.407	−13.67	9.914	−1.667	2.15×10^{-2}
1400	.663	17.454	−13.64	11.721	−1.830	1.48×10^{-2}
1500	.601	17.502	−13.62	13.538	−1.972	1.07×10^{-2}

TABLE III

THERMODYNAMIC PROPERTIES FOR THE REACTION NO + $O_3 \rightleftarrows NO_2 + O_2$

$\Delta H_0^\circ = -47.35$ kcal./mole

T, °K.	$-\left(\frac{H^\circ - H_0^\circ}{T}\right)$, cal./deg./mole	$\left(\frac{F^\circ - H_0^\circ}{T}\right)$, cal./deg./mole	ΔH°, kcal./mole	ΔF°, kcal./mole	log K_{eq}	K_{eq}
200	0.536	0.362	−47.46	−47.27	51.65	4.47×10^{51}
250	.521	.469	−47.48	−47.22	41.29	1.95×10^{41}
298.16	.525	.570	−47.51	−47.17	34.57	3.72×10^{34}
300	.524	.575	−47.51	−47.17	34.36	2.29×10^{34}
350	.551	.659	−47.54	−47.11	29.42	2.63×10^{29}
400	.567	.730	−47.58	−47.05	25.70	5.01×10^{25}
500	.604	.862	−47.65	−46.91	20.50	3.16×10^{20}
600	.615	.977	−47.72	−46.76	17.03	1.07×10^{17}
700	.611	1.067	−47.78	−46.60	14.55	3.55×10^{14}
800	.593	1.152	−47.83	−46.42	12.68	4.79×10^{12}
900	.571	1.222	−47.87	−46.24	11.23	1.70×10^{11}
1000	.546	1.282	−47.90	−46.06	10.07	1.17×10^{10}
1100	.522	1.335	−47.93	−45.88	9.115	1.30×10^{9}
1200	.498	1.380	−47.95	−45.69	8.320	2.09×10^{8}
1300	.473	1.418	−47.97	−45.50	7.648	4.45×10^{7}
1400	.451	1.452	−47.98	−45.31	7.074	1.19×10^{7}
1500	.430	1.483	−48.00	−45.12	6.573	3.74×10^{6}

The approximate molecular dimensions for the *cis* and *trans* isomers also have been given.[16] The *cis* and *trans* isomers both take the following interatomic distances: $r_{OH} = 0.98$ Å., $r_{ON} = 1.46$ Å., $r_{NO} = 1.20$ Å. The *cis* isomer has an HON angle of 103° and an ONO angle of 114°. The *trans* isomer has an HON angle of 105° and an ONO angle of 118°. The vibrational frequencies of the *cis* and *trans* isomers which have been determined are given in Table IV.

TABLE IV

VIBRATIONAL FREQUENCIES FOR NITROUS ACID (cm.$^{-1}$)

No.	Discription	D'or and Tarte *cis*	D'or and Tarte *trans*	Jones, *et al.* *cis*	Jones, *et al.* *trans*
ν_1	O–H stretching	~3425	~3590	3462	3590
ν_2	N=O stretching	1639	1700	<1696	1696
ν_3	O–H bending	~1370	1267	~1292	1260
ν_4	O–N stretching	855	793	856	794
ν_5	O–N–O bending	525	598	598 (?)	598
ν_6	H out of plane	638	545 (?)	637	543

The moments of inertia of the *cis* form are $I_a = 10.13 \times 10^{-40}$ g. cm.^{2}, $I_b = 68.4 \times 10^{-40}$ g. cm.^{2}, $I_c = 78.5 \times 10^{-40}$ g. cm.^{2} and of the *trans* form are $I_a = 7.83 \times 10^{-40}$ g. cm.^{2}, $I_b = 75.2 \times 10^{-40}$ g. cm.^{2}, $I_c = 83.0 \times 10^{-40}$ g. cm.^{2}. Both p_e and σ for HNO_2 are equal to one.

The agreement in the vibrational frequencies of the *trans* form in the two investigations[16,17] is very good. D'or and Tarte[17] appear to have been able to fix ν_2 and ν_5 for the *cis* form. In the thermodynamic calculations, ν_3 for the *cis* form is taken as the average of the values given, $\nu_3 = 1330$ cm.$^{-1}$.

The thermodynamic functions for *trans*-HNO_2 and *cis*-HNO_2 as ideal gases at one atmosphere pressure calculated to the rigid rotator-harmonic oscillator approximation are given in Tables V and VI.

The energy difference between the *trans* and *cis* isomers is about 500 cal./mole.[16] From ΔE and ΔS

TABLE V

THERMODYNAMIC FUNCTIONS FOR *trans*-NITROUS ACID IN CAL./DEG./MOLE

T, °K.	C_p^0	$\frac{H^0 - H_0^0}{T}$	$\frac{-F^0 - H_0^0}{T}$	S^0
100	8.03	7.96	41.65	49.61
200	9.33	8.27	47.23	55.50
250	10.21	8.57	49.10	57.67
275	10.63	8.74	49.93	58.67
298.16	11.00	8.90	50.64	59.54
300	11.03	8.91	50.70	59.61
325	11.42	9.09	51.42	60.51
350	11.78	9.27	52.10	61.37
400	12.44	9.62	53.36	62.98
500	13.55	10.30	55.58	65.88
600	14.42	10.92	57.51	68.43
700	15.11	11.47	59.24	70.71
800	15.68	11.96	60.80	72.76
900	16.15	12.40	62.24	74.64
1000	16.55	12.80	63.56	76.36

TABLE VI

THERMODYNAMIC FUNCTIONS FOR *cis*-NITROUS ACID IN CAL./DEG./MOLE

T, °K.	C_p^0	$\frac{H^0 - H_0^0}{T}$	$\frac{-F^0 - H_0^0}{T}$	S^0
100	8.03	7.96	41.75	49.71
200	9.24	8.25	47.33	55.58
250	10.07	8.53	49.19	57.72
275	10.48	8.69	50.02	58.71
298.16	10.84	8.84	50.73	59.57
300	10.87	8.85	50.79	59.64
325	11.25	9.02	51.50	60.52
350	11.61	9.20	52.17	61.37
400	12.28	9.54	53.42	62.96
500	13.42	10.20	55.63	65.83
600	14.32	10.82	57.54	68.36
700	15.05	11.37	59.25	70.62
800	15.64	11.87	60.80	72.67
900	16.14	12.32	62.22	74.54
1000	16.56	12.72	63.55	76.27

for the equilibrium *trans*-$HNO_2 \rightleftarrows$ *cis*-HNO_2, the ratio of the concentrations of *trans* to *cis* isomers has been computed approximately. The values of the equilibrium ratios are as follows: 100°K., 13; 200°K., 3.6; 250°K., 2.8; 275°K., 2.5; 298.16°K., 2.3; 300°K., 2.3; 325°K., 2.2; 350°K., 2.1; 400°K., 1.9; 500°K., 1.7; 600°K., 1.5; 700°K., 1.4; 800°K., 1.4; 900°K. 1.3; 1000°K., 1.3. The entropy of mixing of the *cis* and *trans* forms contributes R ln 2 to the entropy and free energy function. The thermodynamic functions for the equilibrium mixtures of *trans*- and *cis*-HNO_2 are given in Table VII.

TABLE VII

THERMODYNAMIC FUNCTIONS FOR EQUILIBRIUM MIXTURES OF *trans*- AND *cis*-NITROUS ACID IN CAL./DEG./MOLE

T, °K.	C_p^0	$\frac{H^0 - H_0^0}{T}$	$\frac{-F^0 - H_0^0}{T}$	S^0
100	8.03	7.96	43.04	51.00
200	9.31	8.27	48.63	56.90
250	10.17	8.56	50.50	59.06
275	10.59	8.72	51.34	60.06
298.16	10.95	8.88	52.05	60.93
300	10.98	8.89	52.11	61.00
325	11.37	9.07	52.82	61.89
350	11.73	9.25	53.50	62.75
400	12.38	9.59	54.76	64.35
500	13.50	10.26	56.98	67.24
600	14.38	10.88	58.90	69.78
700	15.08	11.45	60.62	72.05
800	15.66	11.92	62.18	74.10
900	16.15	12.37	62.61	74.98
1000	16.55	12.76	64.94	77.70

The only previous values for the thermodynamic functions of nitrous acid given are for the entropy of the *trans*, *cis* and equilibrium mixture at 298°K.[16] These values differ from those calculated in the present work, but a recalculation by the authors[18] gave values in agreement with those given in this paper.[19]

(18) Private communication from Dr. G. E. Moore.

(19) After this paper was submitted for publication, Dr. Ann Palm graciously sent a copy of her manuscript entitled "Potential Constants of Nitrous Acid" to be published in the *J. Chem. Phys.* Her calculations favor a value of 1370 cm.$^{-1}$ for ν_2 of the *cis*-form of HNO_2. If this frequency is used instead of 1330 cm.$^{-1}$, then at 1000°K. S° is decreased by 0.05 e.u. and the other functions are decreased by 0.02 to 0.03 e.u. for the *cis*-HNO_2.

THE ANALYSIS OF THE NEAR ULTRAVIOLET ABSORPTION SPECTRUM OF CS_2[1]

BY JEROME W. SIDMAN[2]

Department of Chemistry, University of Rochester, Rochester 20, N. Y.

Received June 7, 1956

It is the purpose of this note to call attention to some earlier and largely neglected data on the ultraviolet absorption spectrum of CS_2. Rodloff has studied the absorption spectrum of crystalline CS_2 at 20°K.[3] The theoretical interpretations of Mulliken[4,5] and of Walsh[6] have concentrated almost exclusively on the vapor absorption spectrum of CS_2.[7]

The weak, long wave length absorption transition (λ 3500 Å. system) has been interpreted as $^1B_2 - {}^1\Sigma_g^+$. The $^1B_2$ state is one of the components of the $^1\Delta_u$ state which arises from the $(\pi_g)^3$ (π_u) configuration.[6] The orbital degeneracy is removed by the change in the equilibrium nuclear point group, since the molecule is linear in the ground state but is strongly bent in the upper state.[4-7] The absorption spectrum of solid CS_2 shows weak, sharp bands in this region, and the 0-0 band is probably in the vicinity of 28170 cm.$^{-1}$.[3] It does not yet appear possible to give a complete vibrational analysis of these bands, although long progressions of the bending frequency (ν_2) have been identified in the vapor spectrum.[7]

An examination of the absorption spectrum of solid CS_2 at low temperature reveals that a dis-

(1) Supported by the Office of Ordnance Research of the United States Army, under Contract DA-30-115 ORD-728 with the University of Rochester.

(2) Post-doctoral fellow, Shell Chemical Co., 1955-1956. Department of Theoretical Chemistry, Cambridge University, England.

(3) G. Rodloff, *Z. Physik*, **91**, 51 (1934).

(4) R. S. Mulliken, *Phys. Rev.*, **60**, 506 (1941).

(5) R. S. Mulliken, *Rev. Mod. Phys.*, **14**, 204 (1942).

(6) A. D. Walsh, *J. Chem. Soc.*, 2266 (1953).

(7) L. N. Liebermann, *Phys. Rev.*, **59**, 106 (1941); **60**, 496 (1941).

tinctly different electronic transition overlaps the $^1B_2 - {}^1\Sigma_g^+$ transition at its short wave length end. This is most clearly seen in Figs. 6 to 9 of ref. 3. The bands of this transition are more intense than those of the λ 3500 Å. transition and are also broader. A progression of a vibrational frequency of 600 cm.$^{-1}$ is prominent, starting from the band D at 30300 cm.$^{-1}$.[3] This is clearly a progression in ν_1 (657 cm.$^{-1}$ in the ground state). The upper state must be linear, or very nearly so, since progressions of ν_2 (401 cm.$^{-1}$ in the ground state) are absent.

A possible assignment for this transition is $^1\Pi_g - {}^1\Sigma_g^+$, with the upper state arising from the $(\pi_g)^3(\bar{\sigma}_g)$ configuration.[5] The assignment as a forbidden transition is consistent with the low intensity of these bands (λ 3300 Å. system), although the transition from which the intensity might be stolen has not yet been identified. Another possible assignment is $^1\Pi_u - {}^1\Sigma_g^+$, with the upper state arising from the $(\pi_g)^3(\bar{\sigma}_u)$ configuration.[5] This transition is allowed by symmetry. An unequivocal assignment is not possible on the basis of the existing data.

The intense band system at λ 1970 Å. has been assigned as $^1\Sigma_u^+ - {}^1\Sigma_g^+$ ($^1B_2 - {}^1\Sigma_g^+$ if the upper state is bent[4,6]). The upper state of this transition arises from the same $(\pi_g)^3(\bar{\pi}_u)$ configuration which gives rise to the λ 3500 Å. band system.

On the basis of the analysis of the vapor absorption spectrum, Ramasastry[8] has also found evidence for two transitions in the λ 3600–2800 Å. region of the CS_2 spectrum.

I am much indebted to Professor R. S. Mulliken for several helpful criticisms.

(8) Ramasastry, *Proc. Natl. Inst. Sci. India*, **18**, 177, 621 (1952).

LEAST-SQUARES REFINEMENT OF THE STRUCTURE OF TETRAMETHYLPYRAZINE[1]

BY DON T. CROMER

University of California, Los Alamos Scientific Laboratory, Los Alamos New Mexico

Received August 15, 1956

A number of years ago the crystal structure of tetramethylpyrazine (TMP) was determined by Cromer, Ihde and Ritter.[2] Because of the limited computing facilities at that time, this structure was not refined as far as it might have been. In particular, no series termination correction was made. The present author now has access to the Maniac, a high-speed electronic computer at the Los Alamos Scientific Laboratory, and has carried out several least-squares refinements of crystal structures. Relatively small modifications of an existing program permitted a least-squares refinement of TMP to be computed with a minimum of effort. This program simultaneously refines the atomic coördinates, an isotropic temperature factor for each crystallographically different atom and the scale factor. The off-diagonal terms are omitted from the normal equations.

The results of the previous determination were used as a starting point for the calculations. Those reflections with $F_{obs} = 0$ were omitted as well as the reflections 002, 102, 111, 200 and 202 which were evidently strongly influenced by extinction. The other reflections were weighted equally. The McWeeny[3] form factors were used for carbon and nitrogen and the contribution of the hydrogen atoms was neglected. The results are listed in Table I along with the previous ones for comparison. The final value for R is 16.1%. It is interesting to note that the temperature factors for the ring atoms are all about the same while while the methyl groups have a significantly larger thermal motion.

The standard deviations have been determined by the usual method of least-squares except that the reciprocals of the diagonal terms of the normal equations were used as an approximation to the diagonal terms of the inverse matrix. Experience in this Laboratory has shown that for an orthogonal cell this approximation is accurate to within 1% in the estimation of the standard deviations of atomic coördinates, but underestimates by about 25% the standard deviations of the temperature factors. The terms $\Sigma(\partial F/\partial B_i)^2$ in the normal equations are comparable in size to many of the off-diagonal terms. Because the diagonal terms for the temperature factors are not large, it is necessary to scale

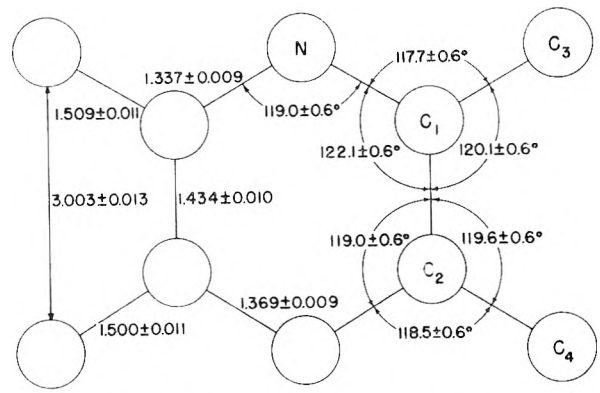

Fig. 1.—Molecular parameters of TMP.

down the computed ΔB_i in the first few cycles or the problem may not converge. The standard deviations given must be considered as lower limits because the least-squares method does not account for systematic errors.

The molecular parameters are given in Fig. 1. Within experimental error the molecule is planar. If the least-squares plane is passed through the origin and the five atoms of the asymmetric unit, the average deviation of the atoms from this plane is 0.008 Å. and the maximum deviation is 0.017 Å. The closest intramolecular distances between methyl groups are 3.74 ± 0.013 and 3.85 ± 0.013 Å.

Tables of observed and calculated structure factors are available from the author.

(1) Work done under the auspices of the Atomic Energy Commission.

(2) D. T. Cromer, A. J. Ihde and H. L. Ritter, *J. Am. Chem. Soc.*, **73**, 5587 (1951).

(3) R. McWeeny, *Acta Cryst.*, **4**, 513 (1951).

TABLE I

RESULTS OF THE LEAST-SQUARES ANALYSIS OF TMP AND COMPARISON WITH PREVIOUS FOURIER ANALYSIS

Atom	Fourier analysis X	Y	Z	Least-squares analysis X	Y	Z	Standard dev. of position, A.	$B \times 10^{16}$ cm.
N	0.092	0.096	−0.069	0.0956 ± 0.0004	0.0961 ± 0.0004	−0.0693 ± 0.0003	0.006	3.56 ± 0.18
C_1	.010	.139	.032	.0080 ± .0005	.1403 ± .0004	.0326 ± .0004	.007	3.11 ± .20
C_2	− .090	.041	.104	− .0869 ± .0005	.0419 ± .0004	.1054 ± .0004	.007	3.26 ± .20
C_3	.020	.297	.067	.0205 ± .0006	.2956 ± .0005	.0710 ± .0005	.009	4.78 ± .28
C_4	− .181	.088	.220	− .1802 ± .0006	.0883 ± .0005	.2202 ± .0005	.009	4.51 ± .25

GALVANIC CELL MEASUREMENTS IN THE COPPER–SILVER SYSTEM[1]

BY RUSSELL K. EDWARDS, JAMES H. DOWNING AND DANIEL CUBICCIOTTI

Contribution from the Department of Chemistry, Illinois Institute of Technology, Chicago, Illinois

Received August 30, 1956

The thermodynamics of the liquid Cu–Ag system have been reported by Edwards and Downing,[2] based on vapor pressure measurements by the effusion method. Previously we had conducted an investigation by the galvanic cell method in view of the potentially greater precision often realized by this method. After considerable exploration our confidence in the method was lessened with regard to its applicability for the study of the Cu–Ag system; however, the results were generally supporting to those of Edwards and Downing[2] and are here reported in that connection.

The limiting factors involved in obtaining reliable galvanic cell measurements are sometimes to a degree inverted as one proceeds to the high temperatures required for the present study. Firstly, the attainment of true equilibrium between the electrode interior and surface is certainly more favorable for the case of liquid metal electrodes as compared to solid metal electrodes. However, the problem of selecting a suitable electrolyte and conducting species becomes often formidable. The electrolyte must (a) be sufficiently non-corrosive toward the container and of sufficiently low volatility to permit observation of the cell behavior over a period of time, (b) provide a medium toward which one of the electrode components is appreciably more noble in behavior than is the other component, and (c) must not display electronic conduction in addition to the ionic conduction required in the cell reaction.

The two types of electrolytes chosen for use were (1) CuCl dissolved in liquid KCl and (2) Cu_2O dissolved in a liquid oxide solution. The desired electrode reactions are

Anode	Cathode
$Cu_{(liquid,\ pure)} = Cu^+ + e^-$	$Cu^+ + e^- = Cu_{(CuAg,\ liquid)}$

The chloride electrolyte suffers from the probability of permitting a simultaneous opposing reaction involving the transfer of Ag from the Cu–Ag electrode to the electrolyte solution and to the Cu electrode. Thus, one may calculate from the data listed by Brewer, *et al.*,[3] that the equilibrium Cu + AgCl = Ag + CuCl lies to the right as is required, but that the equilibrium constant is only about 3 at 1428°K. The chloride electrolyte might become reasonably satisfactory for the cells involving Cu–Ag electrodes more dilute in Ag, where the activity of Ag would be reduced. In this general regard, the oxide electrolyte is much to be preferred for one can estimate from the oxide thermodynamic properties given by Brewer[4] that the comparable equilibrium is overwhelmingly toward the Cu_2O. However, Cu_2O at low temperatures is known to be an excess oxygen semiconductor.[4,5] Presumably this effect might well be minimized by working with a dilute solution of Cu_2O in a liquid oxide solvent at high temperatures and subjected to the reducing action of the liquid Cu electrode.

Experimental

Tungsten wires were used to connect the electrodes to a Brown Electronik recording potentiometer or a Rubicon Portable Precision potentiometer. The tungsten lead wires were isolated from the electrolyte by porcelain protection tubes. The electrolytes were dried and fused under vacuum, but the runs were made in an argon atmosphere to minimize electrolyte volatilization loss from the hot zone. The several different types of cells are noted below for identification later with the figure presenting the results obtained.

Cell Type A.—The anode and cathode were simply contained in small porcelain crucibles separated from each other and within the main porcelain container. The crucibles were spaced from each other by a graphite holder.

Cell Type B.—The anode was concentric with the cathode and separated only by the alumina or zirconia crucible which contained the central anode.

Cell type C.—A Vycor cell of conventional "H" cell design was used.

Cell Type D.—The cell consisted of a porcelain tube which had been fabricated to simulate an "H" cell in that it had legs to separate the anode and cathode compartments.

The KCl electrolyte with about 5% CuCl was used with cells A, B, and C. Several different oxide mixtures were used for the electrolyte in cell D. Most of them were too corrosive toward the porcelain container so that the activity results in these cases do not warrant reporting. One mixture with which activity results were obtained consisted of 60 g. of borax with 55 g. of soft glass, and the liquid mixture was saturated with porcelain at the intended operating temperature of the cell. Then 15 g. of Cu_2O was dissolved in the oxide mixture to constitute the electrolyte. This electrolyte, having been presaturated with porcelain, was much less corrosive to the porcelain container and permitted cell observations for several hours.

A Pt–Pt(10% Rh) thermocouple was used to obtain the cell temperatures. The voltage of the galvanic cell was followed as a function of time until it arrived at a steady state value or failed due to excessive volatilization of the electrolyte or corrosion by the electrolyte. Runs of five to

(1) (a) This work was supported by the U. S. Office of Naval Research, U. S. Navy, through Contract N7-onr-329, Task Order II, and Contract NONR 1406, Task Order II. (b) Based on part of a thesis by J. H. Downing, submitted to the Illinois Institute of Technology in partial fulfillment of the requirements for the Ph.D. degree, May, 1954.

(2) R. K. Edwards and J. H. Downing, *J. Phys. Chem.*, **60**, 108 (1956).

(3) L. Brewer, L. A. Bromley, P. W. Gilles and N. L. Lofgren, Paper 6, National Nuclear Energy Series, Vol. 19B, edited by L. L. Quill, McGraw-Hill Book Company, Inc., New York, N. Y., 1950.

(4) L. Brewer, *Chem. Revs.*, **52**, 10, 36 (1953).

(5) N. F. Mott and R. W. Gurney, "Electronic Processes in Ionic Crystals," 2nd Ed., University Press, Oxford, 1948.

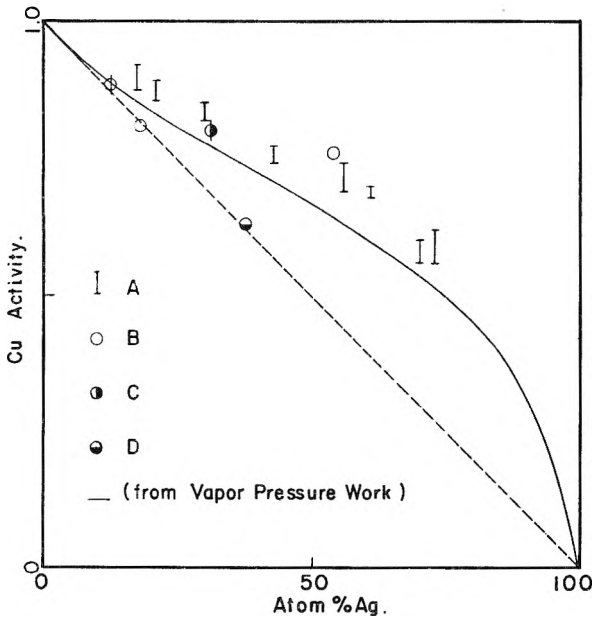

Fig. 1.—Activity of Cu in liquid solutions at 7.0×10^{-4} 1/°K. (1428°K.).

eight hours were obtained in several cases. One of the disturbing features of the voltage behavior was that it generally continuously oscillated about a mean value with an amplitude of about one to two millivolts and a frequency of up to 30 oscillations per minute, even when the so-called steady state was reached. It appeared that periodic polarization was taking place. Purposeful polarization away from the steady state values was generally followed by a rapid return of the cell to its steady state reading, although still accompanied by the usual oscillating behavior. Cells which had larger electrode–electrolyte interface areas usually showed decreased oscillation amplitudes and frequencies. Cells employing the oxide electrolyte were much less subject to this type of disturbance.

Examination of the copper anodes after extended runs using the chloride electrolyte showed that some silver had been transferred from the alloy electrode in line with the factors discussed in the introductory paragraphs.

Results and Discussion

The results are shown in Fig. 1 where observed activities are plotted for the temperature 1428°K. and are compared with the experimental curve of Edwards and Downing[2] for the same temperature. The present results were in general obtained at slightly different temperatures but have been recalculated to the temperature 1428°K. by use of the temperature coefficient data of Edwards and Downing.[2] In several cases the thermocouple protection tube, and consequently the thermocouple, failed during the course of the run and it was necessary to estimate the temperature thereafter. The uncertainties shown in Fig. 1 are ample to cover such temperature errors, and also the oscillation error for the particular cells involved. The dashed line in the figure is the "ideal solution" reference.

For one rather well behaved cell (54 atom % Ag alloy), it was possible to make observations at several temperatures. From these data a relative partial molar enthalpy for Cu of 1,610 calories was obtained.

The galvanic cell activity data are seen to lend general support to the vapor pressure activity data in that they, too, indicate that the liquid Cu–Ag solutions show positive deviation from ideal solution behavior. If a correction could be made for the contribution of the competitive silver reaction, the effect would be such as to bring these activities into closer agreement with the vapor pressure results. It is also to be noted that the effect of the competitive silver reaction should likely decrease at higher silver dilutions in the alloys, and such seems to be observable in Fig. 1.

In spite of the limitations as to the quality of the cell, the relative partial molar enthalpy for Cu obtained in the one case is in good agreement with the work of Edwards and Downing.[2]

COMMUNICATIONS TO THE EDITOR

CRYSTALLOGRAPHIC EVIDENCE FOR THE TRIHYDRATE OF ALUMINUM FLUORIDE

Sir:

Dr. Benjamin Post has pointed out that, in the absence of single crystal evidence to the contrary, the $\sin^2 \theta$ values which I recently reported[1] for $AlF_3 \cdot 3H_2O$ may be equally well fitted to a tetragonal unit cell with c half the value which I assigned. His comments are quite valid. Therefore, until single crystal data for $AlF_3 \cdot 3H_2O$ are presented, the unit cell dimensions should be taken as a = 7.734 Å. and c = 3.665 Å., the l values of the planar indices[2] should be halved, and the space group assignment is not yet definite.

(1) R. D. Freeman, THIS JOURNAL, **60**, 1152 (1956).

DEPARTMENT OF CHEMISTRY
OKLAHOMA A. AND M. COLLEGE ROBERT D. FREEMAN
STILLWATER, OKLAHOMA

RECEIVED JANUARY 7, 1957